

AN *IN VITRO* NHBE MODEL OF THE HUMAN BRONCHIAL EPITHELIUM FOR TOXICOLOGICAL TESTING

ZOË PRYTHERCH



A thesis presented for the degree of Doctor of Philosophy

CARDIFF UNIVERSITY
PRIFYSGOL CAERDYDD

April 2010

Cardiff School of Biosciences
Cardiff University
Museum Avenue
CARDIFF
CF10 3AX

UMI Number: U585361

All rights reserved

INFORMATION TO ALL USERS

The quality of this reproduction is dependent upon the quality of the copy submitted.

In the unlikely event that the author did not send a complete manuscript and there are missing pages, these will be noted. Also, if material had to be removed, a note will indicate the deletion.



UMI U585361

Published by ProQuest LLC 2013. Copyright in the Dissertation held by the Author.
Microform Edition © ProQuest LLC.

All rights reserved. This work is protected against
unauthorized copying under Title 17, United States Code.



ProQuest LLC
789 East Eisenhower Parkway
P.O. Box 1346
Ann Arbor, MI 48106-1346

CONTENTS

CONTENTS	i
ACKNOWLEDGEMENTS	x
DECLARATION	xi
PUBLICATIONS AND COMMUNICATIONS	xii
ABBREVIATIONS	xiv
ABSTRACT	xvii

1 INTRODUCTION	1
1.1 INTRODUCTION	2
1.2 THE HUMAN RESPIRATORY SYSTEM	2
1.2.1 GENERAL OVERVIEW	2
1.2.2 STRUCTURE AND FUNCTION OF THE RESPIRATORY SYSTEM	3
1.3 CELLS OF THE RESPIRATORY LINING	6
1.3.1 PRINCIPAL BRONCHIAL EPITHELIAL CELLS	6
1.3.1.1 CILIATED CELLS	7
1.3.1.2 GOBLET CELLS	8
1.3.1.3 BASAL CELLS	8
1.3.1.4 CLARA CELLS	9
1.3.1.5 EPITHELIAL SEROUS CELLS	10
1.3.1.5 INTERMEDIATE CELLS	11
1.4 PROTECTIVE MECHANISMS	11
1.4.1 PHYSICAL AND NON-IMMUNOLOGICAL DEFENCE MECHANISMS	11
1.4.1.1 CELL JUNCTIONS IN THE BRONCHIAL EPITHELIUM	12
1.4.1.2 MUCIN AND THE MUCO-CILIARY ESCALATOR	14
1.4.2 IMMUNOLOGICAL DEFENCE MECHANISM	16
1.4.2.1 INNATE IMMUNE SYSTEM	16
1.4.2.2 ADAPTIVE IMMUNE SYSTEM	17
1.5 INVESTIGATIVE MODELS OF PULMONARY TOXICITY	19
1.5.1 ANIMAL MODELS	19
1.5.1.1 WHOLE ANIMALS	19
1.5.1.2 PERFUSED ORGANS	20

1.5.2	MONOLAYER CELL CULTURE MODELS	21
1.5.2.1	CARCINOMA-DERIVED	21
1.5.2.2	VIRUS-TRANSFORMED CELL LINES	22
1.5.2.3	PRIMARY CELL LINES	23
1.5.3	HUMAN TISSUE EQUIVALENT MODELS	23
1.5.3.1	MATTEK EPIAIRWAY™ TISSUE MODEL	24
1.5.3.2	NHBE CELLS	25
1.6	VALIDATION OF A 'NEW' RESPIRATORY MODEL	26
1.6.1	BIOCHEMISTRY AND MORPHOLOGY	26
1.6.1.1	BIOCHEMISTRY	27
1.6.1.2	MORPHOLOGY	27
1.6.2	EXPOSURE TO CLASSICAL PULMONARY TOXICANTS	28
1.6.2.1	BACTERIAL DERIVED LIPOPOLYSACCHARIDE	28
1.6.2.2	CADMIUM	30
1.6.2.3	PARAQUAT	31
1.6.2.4	AMIODARONE	33
1.6.2.5	CIGARETTE SMOKE	35
1.6.3	BLIND-EXPOSURE TO POSSIBLE PULMONARY TOXICANTS	36
1.7	RESEARCH HYPOTHESIS, AIMS AND OBJECTIVES	37
1.7.1	HYPOTHESIS	37
1.7.2	SPECIFIC PROJECT AIMS AND OBJECTIVES	37
2	TISSUE-ENGINEERING OF HUMAN LUNG CONSTRUCTS	39
2.1	INTRODUCTION	40
2.2	MATERIALS AND STOCK SOLUTIONS	41
2.2.1	MATERIALS	41
2.2.2	STOCK SOLUTIONS	42
2.2.3	EQUIPMENT	43
2.3	METHODS	43
2.3.1	CELL CULTURE	43
2.3.1.1	INITIAL SEEDING AND CULTURE TO CONFLUENCE OF NHBE CELLS	43
2.3.1.2	SECOND PASSAGE	44
2.3.1.3	SEEDING INTO CELL CULTURE INSERTS	44

2.3.1.4	CONFLUENT INSERT CULTURES	45
2.3.2	PHASE CONTRAST LIGHT MICROSCOPY	45
2.3.3	TRANS-EPITHELIAL ELECTRICAL RESISTANCE	46
2.3.4	BRADFORD ASSAY	47
2.4	RESULTS	48
2.4.1	CELL CULTURE AND PHASE CONTRAST LIGHT MICROSCOPY	48
2.4.2	TRANS-EPITHELIAL ELECTRICAL RESISTANCE	51
2.4.3	BRADFORD ASSAY	53
2.5	DISCUSSION	54
2.5.1	CELL CULTURE	55
2.5.2	TRANS-EPITHELIAL ELECTRICAL RESISTANCE	56
2.5.3	BRADFORD ASSAY	56
2.6	CONCLUSIONS	57
3	CHARACTERISATION OF MORPHOGENESIS IN THE NHBE MODEL	59
3.1	INTRODUCTION	60
3.2	MATERIALS AND STOCK SOLUTIONS	61
3.2.1	MATERIALS	61
3.2.2	STOCK SOLUTIONS	61
3.2.3	EQUIPMENT	62
3.3	METHODS	62
3.3.1	LIGHT MICROSCOPY: TOLUIDINE BLUE	62
3.3.1.1	TISSUE PROCESSING	63
3.3.1.2	STAINING	63
3.3.1.3	DEHYDRATION	63
3.3.1.4	RESIN INFILTRATION	63
3.3.1.5	RESIN EMBEDDING	64
3.3.1.6	SEMI-THIN SECTIONING	64
3.3.2	TRANSMISSION ELECTRON MICROSCOPY	64
3.3.2.1	TISSUE PROCESSING	65
3.3.2.2	ULTRA-THIN SECTIONING	65
3.3.2.3	COUNTER STAINING	65
3.3.3	SCANNING ELECTRON MICROSCOPY	65
3.3.3.1	TISSUE PROCESSING	65

3.3.3.2	CRITICAL POINT DRYING	66
3.3.3.3	MOUNTING	66
3.3.3.4	SPUTTER COATING	67
3.3.4	LIGHT MICROSCOPY: <i>IN VIVO-IN VITRO</i> CORRELATIONS	67
3.3.4.1	TISSUE PROCESSING	67
3.3.4.2	PARAFFIN EMBEDDING	68
3.3.4.3	SECTIONING	69
3.3.4.4	DE-WAXING	69
3.3.4.5	HAEMATOXYLIN AND EOSIN STAINING	69
3.3.4.6	DEHYDRATION	70
3.4	RESULTS	70
3.4.1	LIGHT MICROSCOPY: TOLUIDINE BLUE	70
3.4.1.1	DAYS 1 – 6	70
3.4.1.2	DAYS 15 – 30	71
3.4.1.3	DAYS 36 – 42	71
3.4.2	TRANSMISSION ELECTRON MICROSCOPY	75
3.4.2.1	DAYS 1 – 9	75
3.4.2.2	DAYS 12 – 21	75
3.4.2.3	DAYS 30 – 33	76
3.4.2.4	DAYS 36 – 42	76
3.4.3	SCANNING ELECTRON MICROSCOPY	84
3.4.3.1	DAYS 1 – 12	84
3.4.3.2	DAYS 15 – 33	84
3.4.3.3	DAYS 36 – 42	85
3.4.4	LIGHT MICROSCOPY: <i>IN VIVO-IN VITRO</i> CORRELATION	95
3.4.5	CORRELATION OF BIOCHEMICAL AND MORPHOLOGICAL DATA	95
3.5	DISCUSSION	98
3.5.1	LIGHT MICROSCOPY: TOLUIDINE BLUE	98
3.5.2	TRANSMISSION ELECTRON MICROSCOPY	98
3.5.3	SCANNING ELECTRON MICROSCOPY	101
3.5.4	<i>IN VITRO-IN VIVO</i> CORRELATION	102
3.6	CONCLUSIONS	103

4	DEVELOPMENTAL HISTOLOGY OF THE NHBE MODEL	104
4.1	INTRODUCTION	105
4.2	MATERIALS AND STOCK SOLUTIONS	106
4.2.1	STOCK SOLUTIONS	106
4.2.2	EQUIPMENT	107
4.3	METHODS	108
4.3.1	TISSUE PROCESSING FOR LIGHT MICROSCOPY	108
4.3.2	IMMUNOHISTOCHEMISTRY: CYTOKERATIN 5/6	108
4.3.3	IMMUNOHISTOCHEMISTRY: CC10	109
4.3.4	PERIODIC-ACID SCHIFF STAINING	110
4.3.5	IMMUNOHISTOCHEMISTRY: P63	110
4.3.6	DEHYDRATION AND ADDITION OF COVER-SLIPS	111
4.3.7	STATISTICAL ANALYSIS	112
4.3.8	CONFOCAL MICROSCOPY: TIGHT JUNCTIONS	112
4.3.8.1	INITIAL CULTURE PROCESSING FOR CONFOCAL MICROSCOPY	112
4.3.8.2	INCUBATION WITH FIRST PRIMARY AND SECONDARY ANTIBODIES	112
4.3.8.3	INCUBATION WITH SECOND PRIMARY AND SECONDARY ANTIBODIES	113
4.3.8.4	COUNTERSTAINING, MOUNTING AND DETECTION	113
4.4	RESULTS	113
4.4.1	CYTOKERATIN 5/6: EPITHELIAL CELLS	114
4.4.2	CC10: CLARA CELLS	117
4.4.3	PERIODIC-ACID SCHIFF: GOBLET CELLS	120
4.4.4	P63: BASAL/PROGENITOR CELLS	123
4.4.5	TIGHT JUNCTION PROTEINS	126
4.5	DISCUSSION	129
4.5.1	CYTOKERATIN 5/6: EPITHELIAL CELLS	129
4.5.2	CC10: CLARA CELLS	130
4.5.3	PERIODIC-ACID SCHIFF: GOBLET CELLS	132
4.5.4	P63: BASAL/PROGENITOR CELLS	132
4.5.5	TIGHT JUNCTION PROTEINS	133
4.5.5.1	ZO-1	134

4.5.5.2	OCCLUDIN	135
4.5.5.3	CLAUDIN-1	136
4.6	CONCLUSIONS	137
5	RESPONSE OF THE NHBE MODEL TO CLASSICAL PULMONARY TOXINS	138
5.1	INTRODUCTION	139
5.2	MATERIALS AND STOCK SOLUTIONS	139
5.2.1	MATERIALS	139
5.2.2	STOCK SOLUTIONS	140
5.2.3	EQUIPMENT	140
5.3	METHODS	141
5.3.1	DOSING	141
5.3.1.1	LIPOPOLYSACCHARIDE	141
5.3.1.2	CADMIUM	141
5.3.1.3	PARAQUAT	142
5.3.1.4	AMIODARONE	142
5.3.1.5	CIGARETTE SMOKE EXPOSURE	142
5.3.2	TRANS-EPITHELIAL ELECTRICAL RESISTANCE	144
5.3.3	ATP ASSAY	144
5.3.4	LIGHT MICROSCOPY: TOLUIDINE BLUE	144
5.3.5	SCANNING ELECTRON MICROSCOPY	145
5.3.6	CYTOKINE ARRAY	145
5.3.6.1	PREPARATION OF SAMPLES	145
5.3.6.2	BLOCKING AND INCUBATION	145
5.3.6.3	DETECTION	146
5.3.6.4	ANALYSIS OF RESULTS	146
5.4	RESULTS	146
5.4.1	NHBE RESPONSE TO LIPOPOLYSACCHARIDE	147
5.4.1.1	CULTURE VIABILITY AND TRANS-EPITHELIAL ELECTRICAL RESISTANCE	147
5.4.1.2	LIGHT MICROSCOPY: TOLUIDINE BLUE	148
5.4.1.3	SCANNING ELECTRON MICROSCOPY	150

5.4.2	NHBE RESPONSE TO CADMIUM	151
5.4.2.1	CULTURE VIABILITY AND TRANS-EPITHELIAL ELECTRICAL RESISTANCE	151
5.4.2.2	LIGHT MICROSCOPY: TOLUIDINE BLUE	152
5.4.2.3	SCANNING ELECTRON MICROSCOPY	152
5.4.3	NHBE RESPONSE TO PARAQUAT	154
5.4.3.1	CULTURE VIABILITY AND TRANS-EPITHELIAL ELECTRICAL RESISTANCE	154
5.4.3.2	LIGHT MICROSCOPY: TOLUIDINE BLUE	155
5.4.3.3	SCANNING ELECTRON MICROSCOPY	157
5.4.4	NHBE RESPONSE TO AMIODARONE	158
5.4.4.1	CULTURE VIABILITY AND TRANS-EPITHELIAL ELECTRICAL RESISTANCE	158
5.4.4.2	LIGHT MICROSCOPY: TOLUIDINE BLUE	159
5.4.4.3	SCANNING ELECTRON MICROSCOPY	159
5.4.5	NHBE RESPONSE TO CIGARETTE SMOKE	159
5.4.5.1	CULTURE VIABILITY AND TRANS-EPITHELIAL ELECTRICAL RESISTANCE	159
5.4.5.2	LIGHT MICROSCOPY: TOLUIDINE BLUE	163
5.4.5.3	SCANNING ELECTRON MICROSCOPY	166
5.4.6	NHBE CYTOKINE RESPONSE TO LIPOPOLYSACCHARIDE	168
5.5	DISCUSSION	170
5.5.1	NHBE RESPONSE TO LIPOPOLYSACCHARIDE	170
5.5.1.1	CULTURE VIABILITY AND TRANS-EPITHELIAL ELECTRICAL RESISTANCE	170
5.5.1.2	MORPHOLOGICAL CHANGES	171
5.5.1.3	CYTOKINE CHANGES	172
5.5.2	NHBE RESPONSE TO CADMIUM	175
5.5.2.1	CULTURE VIABILITY AND TRANS-EPITHELIAL ELECTRICAL RESISTANCE	175
5.5.2.2	MORPHOLOGICAL CHANGES	175
5.5.3	NHBE RESPONSE TO PARAQUAT	176
5.5.3.1	CULTURE VIABILITY AND TRANS-EPITHELIAL ELECTRICAL RESISTANCE	176
5.5.3.2	MORPHOLOGICAL CHANGES	177

5.5.4	NHBE RESPONSE TO AMIODARONE	178
5.5.4.1	CULTURE VIABILITY AND TRANS-EPITHELIAL ELECTRICAL RESISTANCE	178
5.5.4.2	MORPHOLOGICAL CHANGES	179
5.5.5	NHBE RESPONSE TO CIGARETTE SMOKE	179
5.5.5.1	CULTURE VIABILITY AND TRANS-EPITHELIAL ELECTRICAL RESISTANCE	179
5.5.5.2	MORPHOLOGICAL CHANGES	180
5.6	CONCLUSIONS	181
6	BLIND-EXPOSURE OF NHBE MODEL TO AZ COMPOUNDS	183
6.1	INTRODUCTION	184
6.2	MATERIALS AND STOCK SOLUTIONS	185
6.2.1	MATERIALS	185
6.2.2	STOCK SOLUTIONS	185
6.3	METHODS	186
6.3.1	DOSING	186
6.3.2	TRANS-EPITHELIAL ELECTRICAL RESISTANCE	187
6.3.3	ATP ASSAY	187
6.3.4	BRADFORD ASSAY	187
6.3.5	LIGHT MICROSCOPY: TOLUIDINE BLUE	188
6.3.6	CORRELATION OF <i>IN VIVO</i> DATA WITH <i>IN VITRO</i> STUDIES	188
6.4	RESULTS	188
6.4.1	PHYSICOCHEMICAL PROPERTIES OF AZ COMPOUNDS	188
6.4.2	BIOCHEMICAL IRRITANCY OF AZ COMPOUNDS	189
6.4.3	MORPHOLOGICAL ANALYSIS OF AZ COMPOUNDS	192
6.5	DISCUSSION	194
6.6	CONCLUSIONS	197
7	GENERAL DISCUSSION	199
7.1	OVERVIEW	200
7.2	CONCLUSIONS	202
7.3	FUTURE WORK	205

7.3.1	GENERAL NHBE PARAMETERS	205
7.3.2	TOXICOLOGICAL EXPOSURE	206
7.3.3	FUTURE DIRECTIONS	206
7.4	ULTIMATE CONCLUSION	207
REFERENCES		208 – 234

ACKNOWLEDGEMENTS

Firstly, I would like to thank AstraZeneca for funding this research and all those up in Loughborough who have been so generous with their time and knowledge throughout this project, a big thank you.

I would like to say a huge thank you to Dr. Kelly BéruBé and Dr Victor Oreffo for firstly giving me the opportunity to undertake this PhD project. Your continuous support and encouragement has no limits. Thank you both for all the time and energy you have spent on me, I hope you are pleased with the end product and I am eternally grateful.

Thanks to everyone in 'the cattleshed' for giving me the excuse to have a break, discuss the rugby and set the world to rights. I would like to especially thank Keith, for being my go-to-guy for any kind of thesis or lab emergency and keeping me sane, especially since I moved into the 'windowless box', without you, it would have been so difficult. Lata, thank you for being there with a cup of tea and occasionally snacks, when I needed to get away. You can have your people skills back now, I think I'm done with them. Tracy, thanks for showing me the ropes and to you and Claire for making endless hours in the cell culture room enjoyable.

Thank you to all my friends who have had to take a back-seat in my life for the last 3 years. You have always been there whenever I needed, now I can repay that debt and catch up with you, I can't wait!!

Finally I would like to thank my family for all their love, support and faith in me, I couldn't have done it without you. Mam, Dad, Bryn, Cara, Rhys, Tomos, Evan, Oliver, Nana and all my family thank you for always understanding and being there, I hope I made you proud. Lastly and by no means least, Vince, you have been my rock, without you I would not have made it.

DECLARATION

This work has not previously been accepted for any degree and is not concurrently submitted in candidature for any degree.

Signed *ZUPythend* (candidate)

Date *01/06/2010*

STATEMENT 1

This thesis is the result of my own investigations, except where otherwise stated. Other sources are acknowledged by footnotes giving explicit references. A bibliography is appended.

Signed *ZUPythend* (candidate)

Date *01/06/2010*

STATEMENT 2

I hereby give consent for my thesis, if accepted, to be made available for photocopying and for inter-library loan, and for the title and summary to be made available to outside organisations.

Signed *ZUPythend* (candidate)

Date *01/06/2010*

PUBLICATIONS

BéruBé, K. A., Prytherch, Z., Job, C. and Hughes, T. (2010). Human Primary Lung Cell Constructs: The New Respiratory Model. *Toxicology. (In Press)*

PUBLICATIONS (IN PREPARATION)

Prytherch, Z., Hughes, T., Job, C., Marshall, H., Oreffo, V., Foster, M. and BéruBé, K. Extensive Characterisation of an NHBE Model: a Respiratory Toxicological Test-System.

Prytherch, Z., Oreffo, V., Foster, M. and BéruBé, K. Response of an NHBE Model to LPS, Cadmium Chloride, Paraquat and Amiodarone.

PUBLISHED ABSTRACTS

BéruBé, K. A., Hughes, T., Prytherch, Z., Balharry, D., Sexton, K., Koshy, L. and Jones, T. (2008). *In vitro* Human Tissue Equivalent Model of Respiratory Epithelia for Toxicological Screening of Inhaled Nanoparticles. *In: Nanotechnology: towards reducing animal testing.* The Royal Society, London. *Institute of Nanotechnology, Post-Event Proceedings, CD-ROM.*

COMMUNICATIONS

***In Vitro* Human Tissue Culture Model of Lung Epithelia for Safety Evaluation of Candidate Respiratory Disease.** *AstraZeneca Local Science Day, Alderly Edge, UK. 2007. Poster Presentation.*

Human Lung Constructs: A New Respiratory Model. *AstraZeneca Local Science Day, Alderly Edge, UK. 2008. Poster Presentation - 1st Prize.*

A New Respiratory Model. *Institute for Science and Health, Aerosol Dynamics and Health: Strategies to Reduce Exposure and Harm, Cardiff University, Cardiff, UK. 2008. Poster Presentation.*

Human Lung Constructs: A New Respiratory Model. *AstraZeneca Local Science Day, Alderly Edge, UK. 2009. Platform Presentation - 1st Prize.*

A New Respiratory Model. *8th CITER Annual Meeting, Cardiff University, Cardiff, UK. 2009. Platform Presentation.*

ABBREVIATIONS

1°	Primary
2°	Secondary
AIPT	Amiodarone-Induced Pulmonary Toxicity
ALI	Air-Liquid Interface
Am	Amiodarone
AMR	ATP Monitoring Reagent
APC	Antigen Presenting Cells
ATP	Adenosine Triphosphate
ATSDR	Agency for Toxic Substances and Disease Registry
AZ	AstraZeneca
BEBM [®]	Bronchial Epithelium Basal Medium
BEGM [®]	Bronchial Epithelium Growth Medium
BSA	Bovine Serum Albumin
cAMP	Cyclic Adenosine Monophosphate
CC10	10kDa Clara Cell Specific Protein
CdCl	Cadmium Chloride
CK	Cytokeratin
CO ₂	Carbon Dioxide
COPD	Chronic Obstructive Pulmonary Disease
CPD	Critical Point Drying
CPT	Classical Pulmonary Toxicant
CS	Cigarette Smoke
Da	Daltons
DAB	Diaminobenzidine
DC	Dendritic Cell
dH ₂ O	Deionised Water
DMEM	Dulbecco's Modified Eagle's Medium
DMSO	Dimethyl Sulfoxide
DNA	Deoxyribonucleic Acid
ECM	Extracellular Matrix
EDTA	Ethyl Diamine Tetraacetic Acid
ENA	Epithelial-Derived Neutrophil-Activating Peptide

EVOM	Epithelial Voltohmeter
FCS	Foetal Calf Serum
FRAME	Fund for the Replacement of Animals in Medical Experiments
G-CSF	Granulocyte Colony-Stimulating Factor
GM-CSF	Granulocyte-Macrophage Colony-Stimulating Factor
h	Hours
H ₂ O ₂	Hydrogen Peroxide
HBSS	Hank's Balanced Salt Solution
H&E	Haematoxylin and Eosin
HRP	Horseradish Peroxidase
IARC	International Agency for Research on Cancer
Ig	Immunoglobulin
IKK	Inhibitor of Kappa-B Kinase
IL	Interleukin
IFN	Interferon
JAM	Junctional Adhesion Molecule
LM	Light Microscopy
logD	Octanol-Water Distribution Coefficient at pH 7.4
logP	Octanol-Water Partition Coefficient
LPS	Lipopolysaccharide
MHC	Major Histocompatibility Complex
MRC	Medical Research Council
<i>n</i>	Number of replicates
NADP	Nicotinamide Adenine Dinucleotide Phosphate
NHBE	Normal Human Bronchial Epithelial
NHTBE	Normal Human Tracheal/Bronchial Epithelial
PAS	Periodic-Acid Schiff
PBS	Phosphate Buffered Saline
PDE4	Phosphodiesterase-4
Pq	Paraquat
PSA	Polar Surface Area
RANTES	Regulated on Activation of Normal T-cell, Expressed and Secreted
ROS	Reactive Oxygen Species

RT	Room Temperature
RTE	Rat Tracheal Epithelium
SCF	Stem Cell Factor
SEM	Scanning Electron Microscopy
SP	Surfactant Protein
TCR	T-Cell Receptor
TD ₅	Dose to cause 5% decrease in culture viability
TD ₂₀	Dose to cause 20% decrease in culture viability
TEER	Trans-Epithelial Electrical Resistance
TEM	Transmission Electron Microscopy
TGF	Transforming Growth Factor
T _H	T-Helper Cell
TNF	Tumour Necrosis Factor
TPO	Thrombopoietin
UA	Uranyl Acetate
v/v	Volume to Volume
v/w	Volume to Weight
WHO	World Health Organisation
ZO	Zonula Occluden Protein

ABSTRACT

The respiratory tract is the primary site of exposure to inhaled substances. A growing need exists for high throughput *in vitro* models of the respiratory epithelium, which can provide rapid, reliable safety and effective screening in preclinical drug development applications. Normal human bronchial epithelial (NHBE) cells were cultured at an air-liquid interface in order to produce an *in vitro* model of the respiratory epithelium for toxicological testing.

Extensive biochemical and morphological characterisation during construct development revealed that the NHBE model formed a pseudo-stratified, fully-differentiated culture of muco-ciliary phenotype. Histochemical and immunohistochemical techniques allowed the identification of basal, Clara, goblet and ciliated cells. Developmental characterisation revealed a toxicological dosing window of 7 days, where the model was deemed to be fully-established.

Fully-developed NHBE cultures were then exposed to classical pulmonary toxicants (CPT); Lipopolysaccharide, cadmium chloride, paraquat, Amiodarone and cigarette smoke. Conventional toxicology techniques (culture viability, trans-epithelial electrical resistance [TEER] and morphology) were utilised to monitor the NHBE response to each CPT. The NHBE model responded with both general and toxicant-specific defence/irritancy mechanisms, observed to take place in the human bronchial epithelium and as such, reflective of *in vivo* toxicity.

The *in vitro* model was finally challenged with candidate respiratory drugs (AstraZeneca [AZ]) to test the utility of the cell system as a drug pre-screening tool. Blind-exposure of AZ compounds were characterised (physicochemical/biochemically/morphologically) in the *in vitro* model and compared to AZ *in vivo* (rat) parallel exposure, focusing on irritancy end-points. A comparison of *in vitro* to *in vivo* exposures resulted in a 76.9 – 85% correlation of irritancy responses.

CHAPTER 1:

INTRODUCTION

1.1 INTRODUCTION

The respiratory tract is the primary site of exposure to airborne compounds, resulting in a growing need for high throughput *in vitro* models of this region. This project involved the investigation of normal human bronchial epithelial (NHBE) cells as a viable *in vitro* model to study injury, repair and disease mechanisms by providing a controlled system for the study of toxicological consequences *in vitro*, which may be predictive of *in vivo* toxicity.

1.2 THE HUMAN RESPIRATORY SYSTEM

1.2.1 GENERAL OVERVIEW

The term 'respiration' is used to describe two different but related processes: 1) cellular respiration; and 2) mechanical respiration. Survival and energy production in most tissues of the body require a supply of oxygen, with subsequent removal of carbon dioxide; this is known as cellular respiration. Mechanical respiration or ventilation is the mechanical process involved in drawing air into and expelling waste gases out of the lungs. In multicellular organisms two types of respiration exist; internal and external. Internal respiration is concerned with the exchange of oxygen and carbon dioxide between the blood (transported via haemoglobin) and the cells in the body (Shier *et al.*, 2004). Cellular respiration is a part of internal respiration, involving the generation of energy (ATP) from glucose; carbon dioxide is produced as a by-product of this process (Lodish *et al.*, 2001). External respiration is the process of exchanging oxygen and carbon dioxide between the atmosphere and the blood, via the lungs (Fox, 2004).

Inhalation exposes the lung to a variety of substances, including, inert, non-pathological and xenobiotic particles, pathogenic organisms and toxic/inert gases. The ability to remove these particles without causing unnecessary inflammation, which could result in permanent damage, is essential (Berne *et al.*, 2004). Deposition of such inhaled materials throughout the respiratory tract is mainly dependent on size (diameter) (West, 2003). Particles greater than 20µm in

diameter will not be inhaled beyond the conducting airways and those with diameters less than $0.05\mu\text{m}$ can behave as gases and can therefore, be exhaled before deposition. Particles with diameters between these two size fractions (i.e. $0.05 - 20\mu\text{m}$) will by-pass the conducting airways and deposit (initially) in the pulmonary region (Brody, 1984). However, many factors influence particle deposition, including, density, shape, solubility and charge of the particle, along with tidal volume (volume of inspired/expired air during normal respiration) and nasal versus mouth breathing (Stuart, 1984).

Numerous protective mechanisms within the lung enable removal of foreign debris. These protective mechanisms (Section 1.4) involve the innate/adaptive immune responses, muco-ciliary clearance system and barrier functions (Berne *et al.*, 2004). Impairment of these defence and/or repair mechanisms causes either transient or permanent damage, sometimes irreparably, resulting in permanent tissue remodelling with severe adverse effects (Wong and Shanley, 2001).

1.2.2 STRUCTURE AND FUNCTION OF THE RESPIRATORY SYSTEM

The respiratory tract can be divided into the upper, lower and distal respiratory tracts (Figure 1.1). The upper respiratory tract includes the nose, nasal passages, paranasal sinuses and pharynx. The trachea, bronchi and bronchioles form the lower respiratory tract, with the respiratory bronchioles and alveoli being the principle structures of the distal tract (Shier *et al.*, 2004).

The two zones of the respiratory system are the conducting and the respiratory zones. The conducting zone includes all anatomical structures that the air passes (i.e. conducts) en-route to the respiratory zone, it contains no alveoli and can not participate in gaseous exchange and as such, is known as the anatomical dead space (Levitzky, 2003). The respiratory epithelium lines the conducting zone and functions to warm, humidify, filter and clean inspired air, as well as forming the protective barrier (Berne *et al.*, 2004). The respiratory zone is the region participates in gas exchange; between the alveoli and pulmonary capillaries. Respiratory bronchioles, alveolar ducts and the alveoli constitute the respiratory zone, or the so-called pulmonary region (Gardner, 2006; Levitzky, 2003).

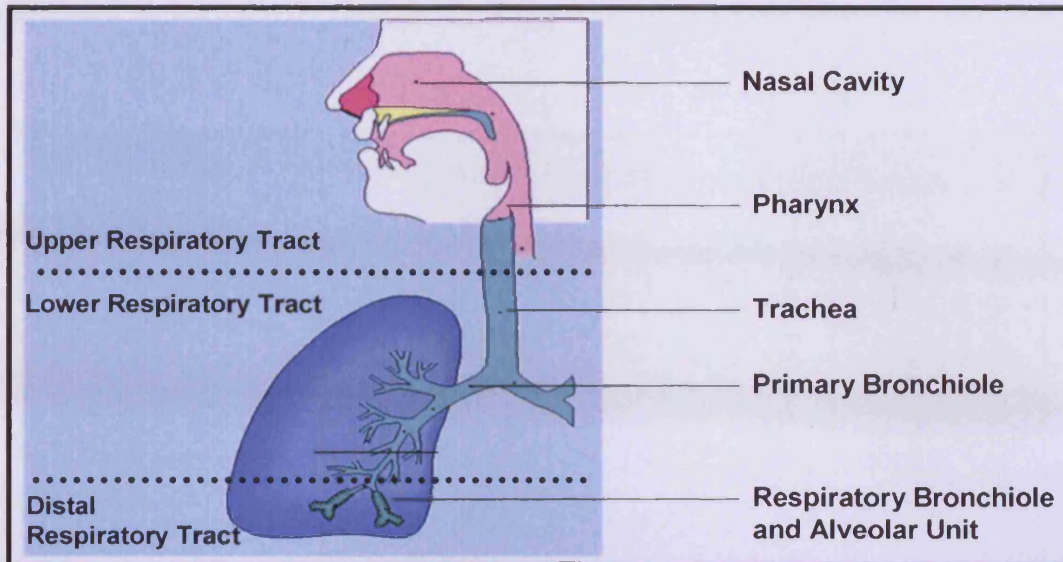


Figure 1.1 Image of the respiratory system, indicating separation between upper, lower and distal respiratory tracts (Adapted from Stevens and Lowe, 2005).

Functionally, the human respiratory system can be divided into three main regions: 1) the extrathoracic region; nose/mouth and larynx; 2) the tracheobronchial region; trachea, bronchi and bronchioles; and 3) the pulmonary region; respiratory bronchioles and all alveolar regions involved with gas exchange (Gardner, 2006). An overview of key structural and functional aspects of the human respiratory system is presented in Table 1.1.

Anatomically, the lungs consist of five lobes, with the right lung consisting of three and the left of two lobes. Initially, the trachea divides into the left and right primary bronchi, supplying the left and right lungs, respectively. The primary bronchus branches into the secondary or lobar bronchi which supply each of the five lobes. The bronchi continue to divide until they become bronchioles, which lack the cartilaginous aspect found in the bronchi and trachea. Numerous divisions of the bronchioles occur until they become the terminal bronchioles, denoting the end of the conducting zone. Subsequent divisions of the terminal bronchioles results in the formation of respiratory bronchioles, marking the beginning of the respiratory zone. Further divisions of the respiratory bronchioles create the alveolar ducts, which eventually terminate in alveolar sacs (Hasleton and Curry, 2006).

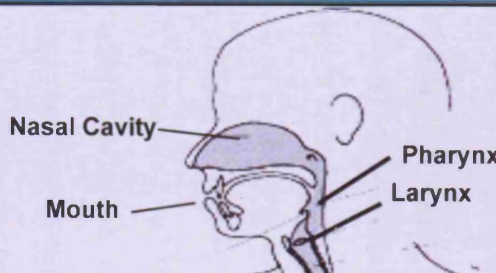
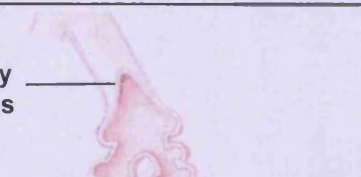
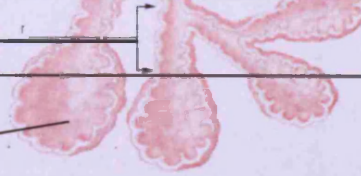
LOCATION	ZONE	FUNCTIONS	ANATOMY	EPITHELIAL TYPES
EXTRATHORACIC	CONDUCTING	<ul style="list-style-type: none"> • Raising air temperature to body temperature • Humidifying the air • Filtering the air • Particle clearance (muco-ciliary escalator) • Air conduction 	 <p>Nasal Cavity</p> <p>Mouth</p> <p>Pharynx</p> <p>Larynx</p>	<ul style="list-style-type: none"> ➤ Squamous epithelium ➤ Pseudo-stratified columnar epithelium ➤ Transitional epithelium ➤ Olfactory epithelium ➤ Muco-ciliary epithelium
			Trachea	
Main Bronchi				
Bronchi				
Bronchioles				
Terminal Bronchioles	<ul style="list-style-type: none"> ➤ Pseudo-stratified columnar epithelium ➤ Ciliated epithelium 			
ALVEOLAR	PULMONARY	<ul style="list-style-type: none"> • Air conduction • Gas exchange • Particle clearance 	 <p>Respiratory Bronchioles</p>	<ul style="list-style-type: none"> ➤ Pseudo-stratified columnar epithelium ➤ Ciliated epithelium
		<ul style="list-style-type: none"> • Gas exchange • Particle clearance 	 <p>Alveolar Ducts</p> <p>Alveolar Sacs</p>	<ul style="list-style-type: none"> ➤ Squamous epithelia (Type I pulmonary cells) ➤ Cuboidal epithelia (Type II pulmonary cells)

Table 1.1 Table showing an overview of the human respiratory tract (Drawn by Z. Prytherch, Cardiff University, 2007)

Generally the lining of the airways from the nasal cavity to the terminal bronchioles consists of ciliated, goblet and basal cells (Section 1.3.1). However, gradual changes in populations of cell types occur as the airways move from conducting to respiratory, e.g. the replacement of goblet with Clara cells (Section 1.3.1.4), which begins in the bronchioles. The pseudo-stratified columnar epithelium eventually presents as a simple, cuboidal, non-ciliated epithelium, with the alveoli consisting of Type I and II pneumocytes (Fox, 2004; Hasleton and Curry, 1996).

1.3 CELLS OF THE RESPIRATORY LINING

1.3.1 PRINCIPAL BRONCHIAL EPITHELIAL CELLS

In larger airways the conducting zone is lined with a pseudo-stratified epithelium containing ciliated cells, mucus-secreting goblet cells and along the basement membrane, a layer of basal cells. Intermediate or transitional cells are located above the basal cells, but do not reach the apical region as the ciliated and goblet cells do. These are undifferentiated cells of the respiratory epithelium, undergoing differentiation into specific cell types, followed by migration to their correct location. Further down the respiratory tract, in the bronchioles, the goblet cells become less frequent and become gradually replaced by another type of cell, the Clara cell. (Breeze and Wheeldon, 1977; Fox, 2004; Levitzky, 2003). This replacement of goblet with Clara cells is due to the fact that Clara cells do not produce mucin, which would impair gaseous exchange in the alveoli (Breeze and Wheeldon, 1977).

With respect to this PhD research project, the principle site of investigation was the bronchial epithelium, which contains ciliated, Clara, goblet, intermediate and basal cells (Figure 1.2).

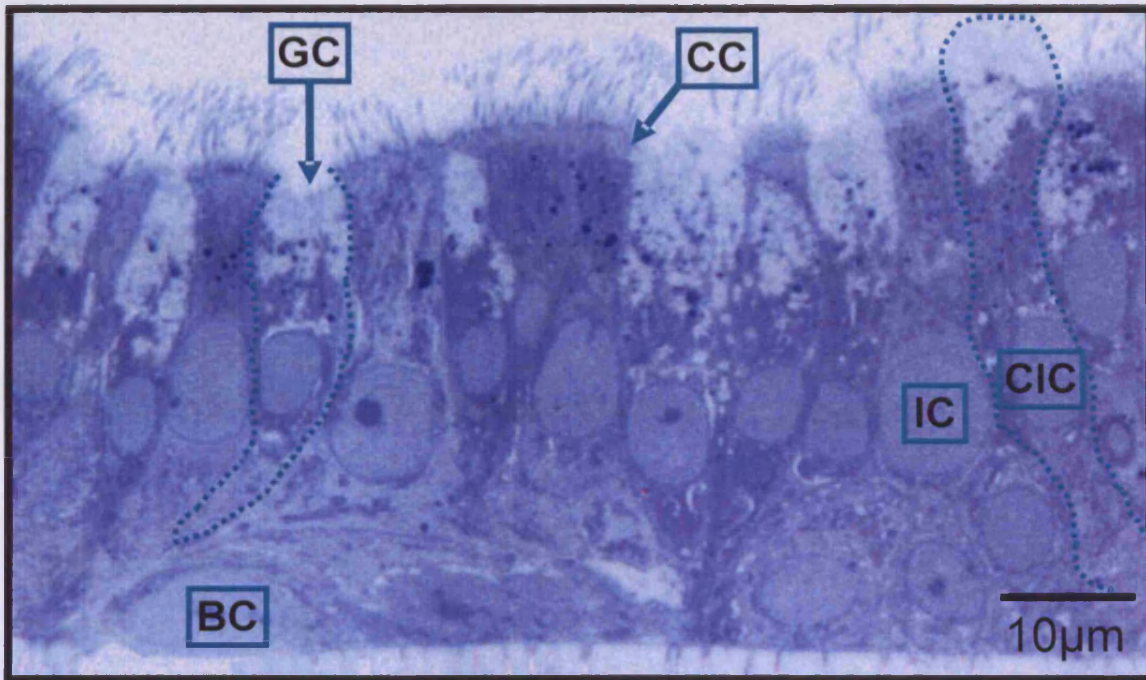


Figure 1.2 The characteristic pseudo-stratified, muco-ciliary bronchial epithelium: NHBE culture. Displaying: GC = goblet cell (delineated); CC = ciliated cell; CIC = Clara Cell (delineated); BC = basal cell and IC = intermediate cell (Image by Z. Prytherch, Cardiff University, 2010).

1.3.1.1 CILIATED CELLS

The ciliated cells are the most prevalent in the tracheobronchial epithelium, approximately 5 to every 1 mucous secreting cell (Rhodin, 1966). Morphologically, ciliated cells are roughly columnar, i.e. 20 μm in height, 7 μm in width, tapering to a width of 2 μm at the basal end of the cell, where they attach to the basement membrane (Breeze and Wheeldon, 1977). The ciliated cell has an oval nucleus located towards the tapered (basal) end (Rhodin, 1966).

Cilia are present on the luminal (apical) surface of ciliated cells (Figure 1.2); their length and number varying according to the maturity of the cell. There are approximately 250 cilia (~6 μm in length and 0.3 μm in width) per cell (Rhodin, 1966). An array of longitudinal microtubules are located inside the cilia, which form a '9 + 2 array'; consisting of 9 peripheral doublet microtubules surrounding 2 central singular microtubules; the microtubules emerge from the basal bodies located just inside the apical region of the ciliated cells (Karp, 2005). Numerous mitochondria are located in the apical portion of the cell, surrounding the basal

bodies. These mitochondria generate the energy (ATP) required for the cilia to beat and therefore move the mucus (Satir, 1989). Interspersed among the cilia are microvilli, which can extend to 2µm in height and 0.1µm in width and are particularly abundant on the apical surface of the ciliated cells; especially on immature cells (Breeze and Wheeldon, 1977). Actin filament bundles cross-linked by myosin, villin and fimbrin proteins constitute the internal structure of the microvilli (Karp, 2005).

1.3.1.2 GOBLET CELLS

Goblet cells are located throughout the conducting airways (Rogers, 2003). Their prevalence decreases as the lower respiratory tract becomes the distal respiratory tract (i.e. between the 5th and 12th bronchial division), beyond which they normally disappear (Berne *et al.*, 2004).

The term 'goblet' cell arose due to the cells typical 'drinking cup' (i.e. goblet) shape, which is a result of the accumulation of secretory mucous granules within the apical portion of the cell (Rhodin, 1966). However, immature goblet cells are generally more columnar in comparison (Breeze and Wheeldon, 1977). The nucleus is oval and found towards the base of the cell. The characteristic shape is also due to the basal portion of the cell tapering and occasionally appearing to twist around intermediate and basal cells, before contacting the basement membrane (Figure 1.2) (Rhodin, 1966). The main function of goblet cells is the production (and release) of mucopolysaccharides, which form the protective mucus barrier (Section 1.4.1.2) (Chilvers and O'Callaghan, 2000).

1.3.1.3 BASAL CELLS

Basal cells form along the basement membrane of the respiratory tract and have long been regarded as the progenitor cells of the adult bronchial epithelium (Ayers and Jeffery 1988; Baldwin, 1994; Breeze and Wheeldon, 1977; Inyama *et al.*, 1988). The basal cells contribute to a decreasing proportion of total epithelial cells along increasing airway generations. The mean percentage of basal cells, in epithelia of airways with diameters greater than 4mm, is approximately 31%

(Boers *et al.*, 1998). The epithelia of airways with diameters less than 0.5mm consists of roughly 6% basal cells (Boers *et al.*, 1998). Under normal conditions the basal cells are the dominant (>50%) cell type in the proliferative compartment (actively proliferating cells), in airways with diameters greater than or equal to 0.5mm (Boers *et al.*, 1998).

Apart from locality, basal cells have a distinct, well-characterised morphology; being relatively small in size, round in shape and large nucleus-to-cytoplasm ratio (Figure 1.2) In addition, very few cytoplasmic organelles or granules are contained within these cells (Baldwin, 1994). Basal cell attachment to the basal lamina is mediated via hemidesmosomes (Section 1.4.1.1) (Boers *et al.*, 1998).

1.3.1.4 CLARA CELLS

Further down the respiratory tract, in the bronchioles, the goblet cells become less frequent and are replaced by Clara cells. They are predominantly located in terminal (11% of total epithelium) and respiratory bronchioles (22% of total epithelium) (Widdicombe, 2002). Clara cells are non-ciliated, non-mucus, dome-shaped, secretory epithelial cells. Their apical surface contains some microvilli and is characteristically dome-shaped (Figure 1.3). Electron-dense proteinaceous granules are found within the Clara cells apical cytoplasm. Clara cells are renowned for being metabolically very active and contain numerous mitochondria for this purpose (Boers *et al.*, 1999).

Although not all of the Clara cells functions are fully understood, their major roles include, secretion of the periciliary sol (Section 1.4.1.2), production of Clara cell specific proteins, cell renewal and metabolism of xenobiotics (Boers *et al.*, 1999; Singh and Katyal, 2000; Widdicombe, 2002). Boers and co-workers (1999), concluded that in concordance with Clara cells in animal lungs, where present in human lungs, they contribute to cell renewal in normal conducting airway epithelium. However, in response to injury, Clara cells have been known to be replaced by goblet cells (Widdicombe, 2002).

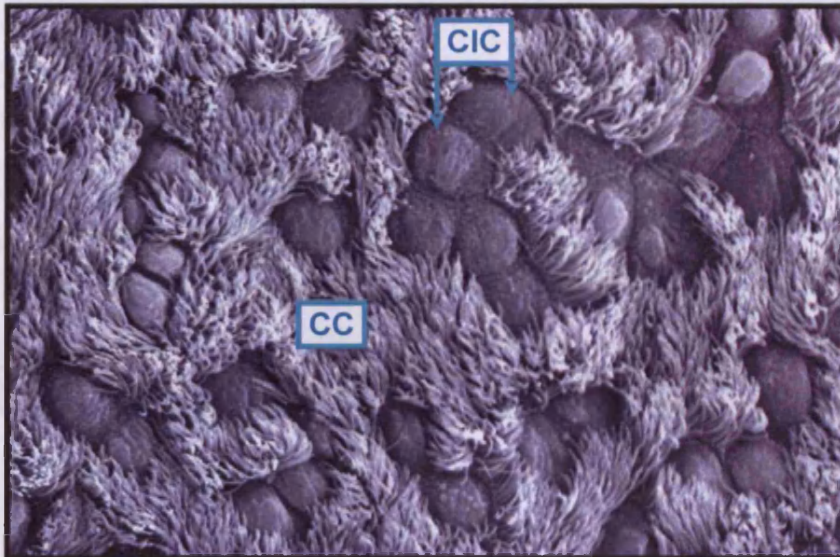


Figure 1.3 Scanning electron micrograph of the surface of a respiratory bronchiole from normal rat lung. Shows Clara cells (CIC) interspersed among ciliated epithelium (CC) (Image taken by D. Balharry and M. Hicks, Cardiff University, 2004).

Clara cells are known to secrete a variety of proteins: 10-kDa protein (CC10 or CCSP); 55-kDa protein; tryptase, β -galactoside-binding lectin; Surfactant proteins A, B and D (SpA, SpB and SpD); and phospholipase. CC10 is one of the most prevalent proteins in the airway lining fluid (Berne *et al.*, 2004; Watson *et al.*, 2001) with its main actions is thought to be, anti-inflammatory and immunosuppressive (Singh and Katyal, 2000).

1.3.1.5 EPITHELIAL SEROUS CELLS

Morphologically, the epithelial serous cell has an irregularly outlined nucleus, a relatively electron-dense cytoplasm and highly electron-dense, membrane-bound secretory granules. The number of secretory granules varies between cells, and are principally situated at the cell apex, where a few microvilli also protruded (Jeffery and Reid, 1975). The serous cells main role is innate airway protection and they produce and secrete numerous protective proteins, including, lysozyme, lactoferrin, peroxidase and anti-leukoprotease (Basbaum *et al.*, 1990). The airway serous cells are predominantly located in the airway submucosal glands (Basbaum *et al.*, 1990), however, they are also located as part of the respiratory epithelium (Bals *et al.*, 1998; Young and Heath, 2000).

1.3.1.6 INTERMEDIATE CELLS

Intermediate cells are so-called because of their 'intermediate' location, with their nucleus above the basal cells, but not reaching the apical surface of the epithelium. These cells are basal cells that have begun, but not completed the process of differentiation into a ciliated, Clara, goblet or secretory cell (Breeze and Wheeldon, 1977).

1.4 PROTECTIVE MECHANISMS

The lungs have developed many protective mechanisms against the inhalation of debris. Efficient removal of foreign material, without causing unnecessary inflammation, is essential in maintaining lung function. Initial protection is generally provided by mechanical barriers and components of the innate immune system (Section 1.4.2.1). Failure of the innate immune system to eliminate an inhalation hazard will result in the activation of the adaptive immune system (Section 1.4.2.2) (Janeway *et al.*, 2005). These protective mechanisms are not mutually exclusive and work together to protect the lung. These systems can be divided into, physical/non-immunological and immunological mechanisms.

1.4.1 PHYSICAL AND NON-IMMUNOLOGICAL DEFENCE MECHANISMS

Structurally, the lungs have to balance between protection and function; ensuring adequate gaseous exchange to survive, whilst protecting from airborne debris and noxious gases. Initial, non-immunological mechanisms, which form part of the baseline protection and encompass both reflexive (e.g. sneezing) and non-reflexive (e.g. humoral defence) responses.

Hairs of the nasal mucosa are the initial filtering system, trapping the vast majority of particulate matter over 20 μ m in diameter and as much as 50% of particles above 5 μ m in diameter, from progressing into the respiratory tract. In addition, mouth breathing prevents most particles over 10 μ m in diameter from translocating beyond the trachea (Berne *et al.*, 2004). Deposition of inhaled particles (90% of those above 2 μ m in diameter), which have by-passed the initial filters,

collect on the mucus lining and are removed from the respiratory tract (via the muco-ciliary escalator) and ingested (Section 1.4.1.2) (Korpáš and Honda, 1996).

Many reflex processes within the respiratory system execute an extremely rapid (milliseconds), defensive response to foreign inhalants. For instance, chemical irritants can cause rapid, shallow breathing, thereby preventing its access to the pulmonary region. Laryngo- and broncho-constriction cause an increase in airflow turbulence (compared to normal laminar flow), thereby increasing impaction and trapping of particles onto the mucus lining. Sneezing and coughing both violently expel contaminated air, with coughing also aiding in the expulsion of mucus and its associated detritus (Korpas and Honda, 1996). Muco-ciliary clearance is considered a non-immunological function, although, many mucus components are, in fact, immunological (Section 1.4.2).

1.4.1.1 CELL JUNCTIONS IN THE BRONCHIAL EPITHELIUM

One of the major functions of the respiratory epithelium is its ability to 'maintain a protective barrier' between the airway lumen and the internal milieu. The cell junctions in vertebrate epithelial cells play a vital role in managing the structural integrity of an epithelial barrier and are defined as: 1) cell-cell junctions; tight junction, adherens junction and desmosomes, which collectively form the 'junctional complex', as well as the gap junction and; 2) cell-matrix junctions; hemidesmosomes (Alberts *et al.*, 2002) (Figure 1.4). With respect to this PhD research project the focus will be on the junctional complex, specifically tight junctions.

Tight junctions (or zonulae occludens) are the most apically located of all epithelial junctions (Farquar and Palade, 1963) and are essential in maintaining the barrier properties of epithelial sheets. The main functions of tight junctions are three-fold: 1) to establish a semi-permeable barrier for the paracellular transport of ions and solutes; 2) confer apico-basal polarity within the epithelium; and 3) coordinate signalling and trafficking molecules involved in cellular differentiation, proliferation and gene expression (Chiba *et al.*, 2008; Guillemot *et al.*, 2008). In the bronchial epithelium, in particular, the regulatory role the tight junctions play in

the paracellular transport of ions is of particular importance. This regulation helps maintain the level and limit the viscosity of the periciliary sol, which in itself enables the efficient removal of mucus along the muco-ciliary escalator (Section 1.4.1.2) (Chilvers and O'Callaghan, 2000).

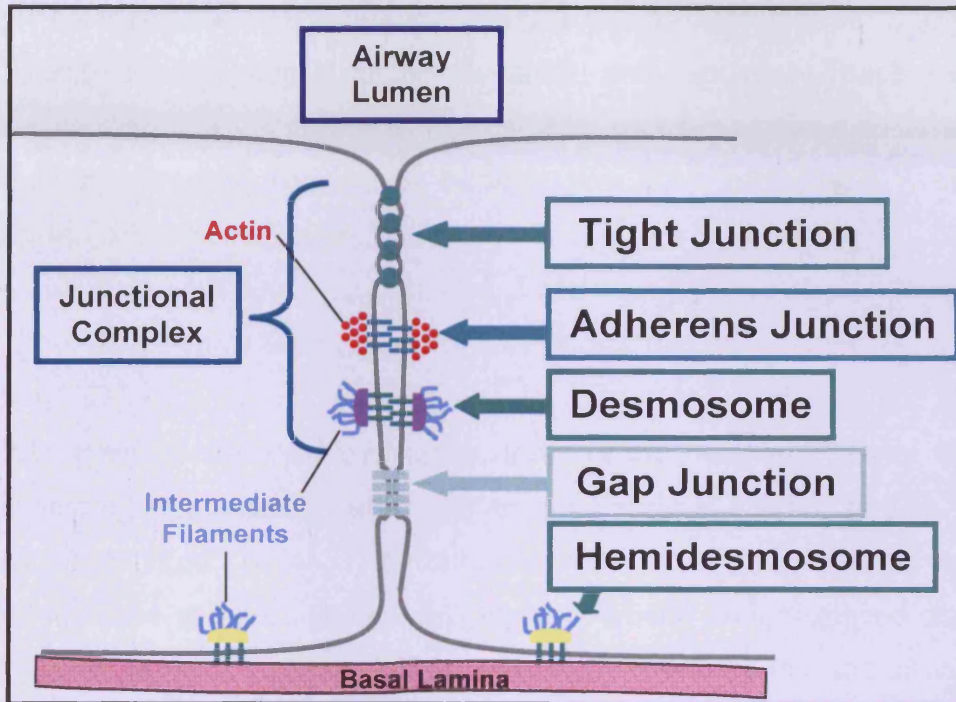


Figure 1.4 Schematic diagram of the various epithelial cell junctions. Tight junctions: essential in maintaining the barrier properties of epithelial sheets. Adherens junctions: associated with actin filaments, usually form an adhesion belt around the cells. Desmosomes: form cell-cell contacts and are associated with intermediate filaments. Gap Junctions: allows passage of small water-soluble ions and molecules. Hemidesmosomes: resemble half a desmosome, form contacts between the cell and the extracellular matrix of the basal lamina (Adapted from Alberts *et al.*, 2002; drawn by Z. Prytherch, 2009).

Freeze fracture transmission electron microscopy (TEM) observations of epithelial tight junctions, reveals a series of lateral intra-membrane strands (Godfrey, 1997). Claude (1978) discovered that the trans-epithelial electrical resistance (TEER) across an epithelium increases exponentially with the number of these strands, with TEER now considered a valid measurement for cell culture junctional formation (Gardner *et al.*, 1997).

Each adjacent epithelial cell contains a series of specific transmembrane proteins which interact with each other to confer its barrier role. The integral transmembrane proteins involved in mammalian tight junctions are occludin, claudins, junctional adhesion molecules and tricellulin (Chiba *et al.*, 2008). The cytoplasmic ends of the tight junctions transmembrane proteins interact with a variety of proteins; the most common being the zonula occludens (ZO) proteins. The ZO proteins are integral to the formation and regulatory functions of tight junctions, as they link the transmembrane proteins to the actin cytoskeleton and also mediate signalling responses through the ZO-1 associated nucleic acid binding protein (Guillemot *et al.*, 2008).

1.4.1.2 MUCIN AND THE MUCO-CILIARY ESCALATOR

The upper airways are lined by mucus, forming an important barrier to inhaled particles, aiding opsonisation and clearance of various foreign bodies from the respiratory tract (Fox, 2004). The major macromolecular constituents present in airway mucus are mucins. Mucins are high molecular weight glycoproteins ($2 - 20 \times 10^5$ Da; Rose and Voynow, 2006), which upon release into the airway lumen combine with other lipid, protein and glycoconjugate compounds to produce a dilute aqueous solution, in the form of mucus (Rogers, 2003). Mucins can be membrane-bound (tethered), which are integrated into the cellular membrane or secretory, which are released apically in response to secretagogues (Rose and Voynow, 2006).

The general composition of mucus is; water (95%), glycoproteins (2%), lipids (1%), proteins (1%) and salts (1%) (Samet and Cheng, 1994). Mucus contains a comprehensive array of compounds essential for the protection of the respiratory epithelia. These compounds form part of the innate immune system (Section 1.4.2.1) providing an initial defence to inhalants. These protective components include: immunoglobulin A (IgA), lysozyme, lactoferrin, α - and β -defensins and collectins (Boyton and Openshaw, 2002; Nicod, 1999).

Synthesis of pulmonary mucin occurs predominantly in goblet cells and the submucosal glands (Chilvers and O'Callaghan, 2000). Mature mucins are tightly

packed into secretory vesicles or granules and are released rapidly via exocytosis in response to secretagogues. Rapid conformational changes occur to the mucins as they are released via exocytosis; expanding and swelling by hydration (Chilvers and O'Callaghan, 2000). The resultant mucus is relatively flexible and sticky (viscoelastic properties), which aggregate in the airways forming large inter-woven networks (Rose and Voynow, 2006). This visco-elasticity makes them ideal for trapping particulate matter within the lungs, as well as absorbing gaseous aerosols (Kim *et al.*, 1997; Thompson *et al.*, 1995).

Efficient function of the muco-ciliary escalator requires cilia to be immersed in the periciliary sol, with their tip in the mucus gel phase. This allows ease of propulsion through the low viscous sol and maintenance of contact with the mucus to aid its clearance (Figure 1.5). Therefore, regulation of the periciliary sol is essential to efficient muco-ciliary clearance (Chilvers and O'Callaghan, 2000), this is maintained by a combination of Na⁺ absorption (epithelial Na⁺ channels) and Cl⁻ secretion (Cl⁻ channels, e.g. cystic fibrosis transmembrane conductance regulator) (Boucher, 2003).

The main function of ciliated cells is propulsion, and therefore clearance of, mucus along the respiratory tract, for eventual ingestion. The cilia beat in a coordinated fashion, with the frequency varying between 100-300 $\mu\text{m} \times \text{s}^{-1}$ (Nicod, 1999). Ciliated cells have the ability to modify their basal beat frequency in response to pulmonary toxicants, thereby, increasing the rate of muco-ciliary clearance (Chilvers and O'Callaghan, 2000). Numerous mitochondria located around the basal bodies, at the root of the cilia, provide the energy (ATP) required for ciliary beating (Breeze and Wheeldon, 1977).

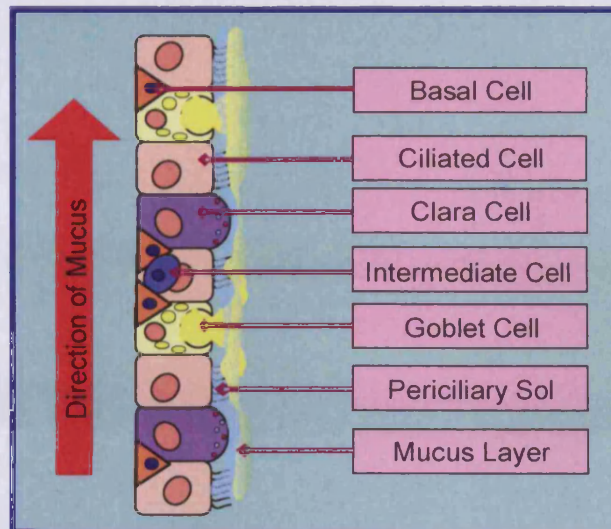


Figure 1.5 Schematic diagram of the muco-ciliary escalator. Showing the involvement of cilia in the propulsion of mucus out of the airways and into the gastrointestinal tract (Drawn by, Z. Prytherch, 2010).

1.4.2 IMMUNOLOGICAL DEFENCE MECHANISMS

The immunological defence mechanisms can be divided into the innate and adaptive responses. Innate immunity involves 'ever-present' and non-specific components of the immune system. Adaptive immunity involves the generation of an immune response to a specific antigen and generally results in the formation of immunological memory (Janeway *et al.*, 2005). Many components of the innate immune system can result in the activation of the adaptive immune system and are therefore, considered part of the adaptive response.

1.4.2.1 INNATE IMMUNE SYSTEM

Inhaled pathogens are generally detected and eliminated within minutes or hours after entry. This initial protective mechanism is performed by the innate immune system. The lungs innate immune system includes specific immune cells, the most important include, neutrophils, eosinophils, basophils, mast cells and natural killer cells (Berne *et al.*, 2004; Janeway *et al.*, 2005; Kroegel *et al.*, 1994; Nicod, 1999; Tosi, 2005; Warner and Kroegel, 1994). Protective proteins are released by these cells (such as the immunoglobulins (Ig); not covered here) and the cells of

the respiratory epithelium (major proteins listed; Table 1.3) (Berne *et al.*, 2004; Burnett, 1986; Gerritsen, 2002).

INNATE IMMUNITY PROTEINS	KEY FEATURES
Surfactant Protein	<ul style="list-style-type: none"> • Four surfactant proteins (SP), belong to the collectin family, synthesised by Type II, Clara and submucosal cells • SP-A and -D bind pathogens; enable opsonisation and phagocytosis
Lactoferrin	<ul style="list-style-type: none"> • Iron-chelating glycoprotein, produced by neutrophils, epithelial and serous cells • Agglutinates bacteria, increases Gram-negative bacteria membrane permeability, also anti-viral and anti-fungal
Secretory Leucoprotease Inhibitor	<ul style="list-style-type: none"> • Expressed by macrophages, neutrophils, goblet cells, Clara cells and serous cells • Inhibits, neutrophil elastase, mast cell chymase, cathpsin G, chymotrypsin and trypsin • Anti-bacterial, anti-viral and anti-inflammatory
β -Defensins	<ul style="list-style-type: none"> • Mainly secreted by epithelial cells • Potently antimicrobial to Gram-negative bacteria and chemotactic for leukocytes, T-cells and dendritic cells.
CCL20	<ul style="list-style-type: none"> • Bacteriocidal chemokine, produced by epithelial cells and neutrophils, upregulated by pro-inflammatory cytokines

Table 1.2 Table describing the principle proteins involved in innate immunity produced by bronchial epithelial cells. (Boyton and Openshaw, 2002; Cole and Waring, 2002; Eggleton and Reid, 1999; Gerritsen, 2000; Rogan *et al.*, 2006; Salvi and Holgate, 1999; Singh *et al.*, 1998; Thompson *et al.*, 1995; Wright, 2005).

1.4.2.2 ADAPTIVE IMMUNE SYSTEM

Failure of the innate immune system to contain and stop an attack, results in the activation of the adaptive immune response. This involves the production of specific antibodies to specific antigens, involving lymphocytes, antigen presenting cells and their associated mediators (Table 1.3) (Janeway *et al.*, 2005). The failure of these systems, or their prolonged activation of these defence mechanisms can transform the physiological defence mechanisms into a pathological response (e.g. Chronic Obstructive Pulmonary Disease; COPD) (Korpas and Honda, 1996). The adaptive immune system is the body's primary

defence mechanism in non-mucosal tissues. In mucosal tissues, such as the lung, the adaptive immune system plays a secondary role, this is essential to protect the lungs' function. Once activated the adaptive immune response is the same in the lung as in any other systemic organ (Berne *et al.*, 2004).

CELL TYPE	KEY FEATURE
T-Cells	<ul style="list-style-type: none"> • Cytotoxic T-cells (CD8⁺) detect antigens displayed by MHC class I on APCs; activates caspases (cell death) • T helper (T_H) cells (CD4⁺) activate other immune cells, are subdivided into T_H1 and T_H2 cells • <u>T_H1 cells</u>: involved in cell mediated immunity; induced by IL-12; on activation produces IL-2, IFN-γ, GM-CSF and TNF-β; causes B-cells to secrete specific IgG_{2a}, activates CD8⁺ cells and attracts neutrophils and monocytes • <u>T_H2 cells</u>: involved in humoral immunity; on activation produces IL-4, -5, -6, -10 and -13; causes B-cells to secrete specific IgG₁ and IgE and attracts basophils and eosinophils • T_H1 and T_H2 cells suppress the development of each other, via the cytokines they produce
B-Cells	<ul style="list-style-type: none"> • Activated by direct antibody-antigen contact or co-stimulation by T_H cells • Activation; initial IgM expression, can then undergo isotype switch to IgG, IgA, IgE or memory B-cells • Release of Ig's leads to agglutination, neutralisation, opsonisation or complement activation and the formation of the 'membrane attack complex'
Dendritic Cells	<ul style="list-style-type: none"> • Immature Dendritic cells located above and below the basement membrane, extend finger like projections into conducting airway lumen, constitute a highly reactive population in the lung, more prevalent in upper airways • Poor phagocytes, but most potent APCs in the airway • Express antigen-MHC complex to activate T-cells

Table 1.3 Principle cells of the adaptive immune system in the airways and their key features. MHC = major histocompatibility complex; APC = antigen presenting cell (Berne *et al.*, 2004; Boyton and Openshaw, 2002; Gordon and Read, 2002; Holtzman, 2001; Janeway *et al.*, 2005; Moore *et al.*, 2001; Nicod, 1999; Nicod, 2005; Wright, 2005).

T-cells are the most prevalent lymphocytes in normal airways and mostly express the $\alpha\beta$ T-cell receptor (TCR) (Baraldo *et al.*, 2007). These T-cells can be divided

into CD4 and CD8 T-cell populations, with the CD4⁺ population having the ability to become either T_H1 or T_H2 (T-helper) cells, their specific roles and functions are summarised (Table 1.3). Excessive activation of the T_H1 population can result in sarcoidosis, whilst in the T_H2 population can cause atopic asthma (Boyton and Openshaw, 2002). Another population of T-cells are those expressing the $\gamma\delta$ TCR, these are known as innate-like lymphocytes and have specific immunosurveillance properties and are particularly associated with epithelial surfaces, such as the bronchial epithelium. $\gamma\delta$ TCR T-cells may recognise antigens without co-stimulation from MHC molecules and have been shown to suppress the IgE response to inhaled antigens (Berne *et al.*, 2004; Janeway *et al.*, 2005).

1.5 INVESTIGATIVE MODELS OF PULMONARY TOXICITY

Methods of accurately studying inhalation toxicology, with respect to humans, have proven difficult. Testing on humans (*in vivo*) is obviously the most accurate (BéruBé *et al.*, 2009; Seagrave *et al.*, 2005); but, ethically can not be employed to study toxic compounds. Historically, animals, especially mammals, with pulmonary anatomy similar to that of humans have been utilised (Section 1.5.1). The results would then be extrapolated to predict human responses, such as toxicologic or immunologic responses. Many researchers continue to use whole animal models as a method of investigating human pulmonary responses (Section 1.5.1.1). Alternative methods of investigation do exist and involve perfused organs/tissues (Section 1.5.1.2) and cell culture (Section 1.5.2 – 1.5.3) techniques. Current models all possess advantages and disadvantages, with some degree of adaptation, to the actual human *in vivo* response, still wanting.

1.5.1 ANIMAL MODELS

1.5.1.1 WHOLE ANIMALS

Mammals commonly used by researches include, rats (Chu *et al.*, 2007), rabbits (Lin *et al.*, 2007), guinea pigs (Fiala *et al.*, 2005), dogs (Humphrey *et al.*, 1981), sheep (Jerome *et al.*, 1996) and non-human primates (Kreyling *et al.*, 1992). Test

compounds would be administered either by inhalation or intratracheal instillation, to a set number of test animals; control animals would undergo the same process minus the compound. Animals would be sacrificed and lungs removed in order to obtain bronchoalveolar lavage and tissue samples for microscopical and toxicological analysis (Housley *et al.*, 2002; Leong *et al.*, 1998; Xu *et al.*, 2004).

One of the most challenging aspects of using animals to predict human responses is to accurately extrapolate the data (Miller *et al.*, 1983). There are many discrepancies between humans and animals that will affect the reliability of these models including, particle deposition (Schlesinger, 1985); anatomical difference in the branching of the tracheobronchial tree (Brody, 1984); types and composition of cells present (Breeze and Wheeldon, 1977; Thomassen and Nettshiem, 1990); differences in biotransformation enzymes (Castell *et al.*, 2005); physiological defences such as changes in breathing pattern and reduction in metabolic rates (Mautz, 2003).

1.5.1.2 PERFUSED ORGANS

Isolated perfused organs are used to investigate the xenobiotic effects on the whole lung (Nakata and Dahms, 2000; Parker *et al.*, 1999; Rimar and Gillis, 1995; Steinhorn *et al.*, 2000; Yamane and Kawata, 1999). The lungs and the heart are removed from the animal and maintained (artificially) physiologically and anatomically as close to the *in vivo* situation as possible. The lungs undergo controlled ventilation and are perfused under constant flow rates and pressure. Many factors need to be carefully chosen and regulated to maintain close *in vivo* accuracy (e.g. perfusate, temperature and pH) (Niemeier, 1984). The perfused organ technique allows investigators to apply xenobiotics in numerous manners (e.g. inhalation, instillation and via the circulation) and also to monitor the effect on the lungs as well as diffusion across the air-blood barrier (Sakagami, 2006).

However, the technique is time-limited (2 – 3 hours), with only acute toxicant exposures possible, difficulties in determining the specific location of drug interactions, the need for a highly qualified operator (Sakagami, 2006) and they

have the problem of accurate extrapolation to human responses (Niemeier, 1984).

1.5.2 MONOLAYER CELL CULTURE MODELS

Monolayer cell culture models are much less complex than whole animals and perfused organs, with only one or a few cell types involved and the systemic effect removed. They provide an economic advantage, in so far as, replicate numbers are easier to obtain, much smaller quantities of compounds are used (due to direct application) and no animal-housing fees are paid. Additionally, the specific interactions of the xenobiotic with a particular cell type or epithelium and its response, in turn, can be elucidated with greater ease. The cells used perform many normal processes, such as proliferation. Cell cultures can be grown on solid substrates to which the cells attach or cultured in suspension (Freshney, 2005). Human cell culture models can be divided into three main groups: 1) carcinoma-derived; 2) virus-transformed; and 3) primary.

In addition to the three main cell culture models there is a rat tracheal epithelial (RTE) cell line which arose from spontaneous immortalisation of primary RTE cells. This cell line is known as SPOC1 and has upregulated mucin production compared to primary RTE cells (Doherty *et al.*, 1995; Randell *et al.*, 1996).

1.5.2.1 CARCINOMA-DERIVED CELL LINES

Carcinoma-derived cell lines have been established from normal human cells that have become carcinogenic. These cells have been immortalised and can be passaged indefinitely; a great advantage in cell culture work (Freshney, 2005). A major disadvantage is that the cell lines generally represent one cell type and therefore, do not represent the multi-cellular reactions present *in vivo*. Tight junctions do not always form and if present, are not always fully-functional. Due to their neoplastic nature, carcinoma-derived cells are likely to display untypical phenotypes, with discrepancies in the cell cycle, redox mechanisms, and metabolic functions (Forbes, 2000; Simon *et al.*, 1981). Two widely-used carcinoma-derived pulmonary cell lines are the Calu-3 and A549.

The Calu-3's are derived from a human bronchial adenocarcinoma (Forbes, 2000). They possess many features characteristically found in the human tracheobronchial region; form confluent polarised monolayers, possess TEER (with discrepancies between laboratories; BéruBé *et al.*, 2009), contain P450 enzymes (Foster *et al.*, 2000), transport systems and efflux pumps (Florea *et al.*, 2003), produce and secrete mucus glycoproteins and contain microvilli (Grainger *et al.*, 2006). Consequently, Calu-3 cells are widely used as a pulmonary drug-transport model. However, limitations of this model include, monolayer cultures, lack of some biotransforming enzymes, no cilia as well as some uncharacteristic phenotypes due to carcinogenic origin of cell type (Forbes, 2000; Grainger *et al.*, 2006).

The A549 cell line is derived from a human Type II cell adenocarcinoma. These cells are known to form confluent monolayers, demonstrate some barrier resistance (but low TEER values), contain lamellar bodies (Foster, 1998) and retain the majority of Type II metabolising enzymes (i.e. the CYP family of enzymes). Therefore, they are a relatively good model to investigate the metabolising of xenobiotics within the respiratory region of the lung (Hukkanan *et al.*, 2000). Disadvantages of the A549 include a lack of fully-functional tight junctions (Wang and Zhang, 2004) and *in vivo* Type II cells only account for approximately 5% of the total surface area of the alveoli, therefore, this model does not represent predominant alveolar cell type (by surface area), the Type I cell (Forbes, 2000).

1.5.2.2 VIRUS-TRANSFORMED CELL LINES

Viral genes or vectors have commonly been used to transform or 'immortalise' cells for use in cell culture. By immortalising the cells, the major problem of a limited Passage number with primary cells is overcome. 16HBE14o- cells are human bronchial epithelia cells transformed by SV40 (Westmoreland *et al.*, 1999) and were originally developed to study the cystic fibrosis conductance regulator (CFTR) (Gruenert, 1988). This cell culture system is known to form a polarised, multilayered culture, containing tight junctions and expresses many drug-transporters and drug-related proteins (Ehrhardt *et al.*, 2003; Forbes, 2000; Wan

et al., 2000). The major disadvantages associated with this cell line are, deficiency in producing the protective mucus covering as well as the possibility that important transcription factors of relevant genes may be altered or not expressed (Forbes, 2000).

1.5.2.3 PRIMARY CELLS

Primary cells are removed from humans or animals either during a surgical procedure or immediately after death. The cells undergo a series of enzymatic digestion and filtration treatments to separate them from contaminating cells (Elbert *et al.*, 1999). Primary cells can only undergo a definite number of Passages before they begin to lose their viable characteristics; the major drawback to primary cell cultures (Freshney, 2005).

Human alveolar (Elbert *et al.*, 1999) and tracheobronchial epithelial (Gray *et al.*, 2004; Hill *et al.*, 1998) primary cell cultures have been utilised as investigative models. Both of which have been demonstrated to form confluent cultures, providing relatively-accurate, *in vivo*-like morphological and physiological properties. In addition to this numerous researchers have cultured animal primary tracheobronchial cells in order to create *in vivo*-like models. Primary dog (Welsh, 1985), guinea pig (Adler *et al.*, 1987), bovine (Kondo *et al.*, 1993) and rat (Kaartinen *et al.*, 1993) tracheobronchial cells have all been cultured successfully *in vitro* to create morphologically and biochemically accurate models.

1.5.3 HUMAN TISSUE EQUIVALENT MODELS

Public opinion along with Government legislation has driven the need for the development of alternative *in vitro* models in order to refine, replace and reduce the number of animals used in scientific research (EU Directive 76/768/EEC, 2003; FRAME, 2010; NC3R, 2010). Tissue equivalent models are one way of answering this need, producing a reliable *in vitro* model predictive of *in vivo* toxicity. There are a number of commercially available cell models that researchers may purchase. Currently, the industry leaders are the MatTek Corporation (USA), who provide a tissue equivalent model and Lonza

(Switzerland), who provide primary human bronchial epithelial cells, from which we tissue-engineered a human bronchial epithelium model, the focal point of this research. Both systems imitate the *in vivo* characteristics of the human tracheobronchial/bronchial epithelium.

1.5.3.1 MATTEK EPIAIRWAY™ TISSUE MODEL

The EpiAirway™ model system is a primary, normal human tracheal/bronchial epithelial (NHTBE) cell system, currently available from MatTek Corporation (Ashland, MA, USA). The airway model involves growing the cells on polycarbonate membranes or 'inserts', at an 'air-liquid interface' (ALI) (Figure 1.6).

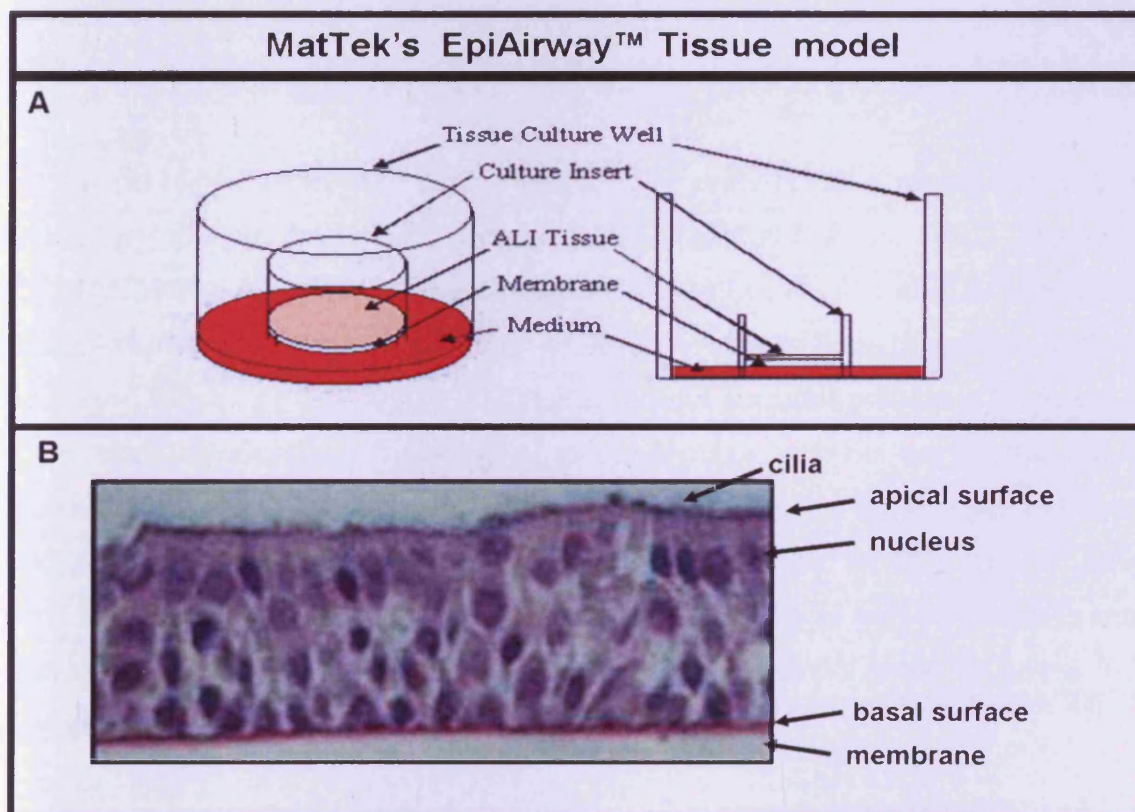


Figure 1.6 MatTek EpiAirway™ model. A: Diagrammatic representation of the insert system used to grow the NHTBE cells at an ALI and B: Light microscope image of MatTek EpiAirway™ cell cultures (MatTek, 2008).

MatTek claim that their system contains, highly-differentiated cells that are pseudo-stratified, of muco-ciliary phenotype, form tight junctions, as well as express human cytokines. However, from the images on their website the model appears more stratified than pseudo-stratified and also displays evidence of basal cell hypertrophy. Additional drawbacks of the system are its great expense and relatively small viability window, during which time the cultures can be used experimentally (e.g. 72 hours) (BéruBé *et al.*, 2009). The standard purchase price is \$1,500 USD for 24 cell culture inserts (6.5mm).

1.5.3.2 NHBE CELLS

Lonza (Basel, Switzerland) provide commercially available normal human bronchial epithelial (NHBE) cells as part of their 'Clonetics® Primary Cell and Media Systems'. These can be purchased as cryopreserved primary cells ($\geq 500,000$ cells/ampoule) or as proliferating cells (second passage; T-25 flask).

Normal bronchial epithelial cells, removed by enzymatic digestion have been cultured *in vitro* previously (Adler *et al.*, 1987; Engelhardt *et al.*, 1991; Terzaghi *et al.*, 1978; Wu *et al.*, 1986). These were all cultured at an ALI and all produced a pseudo-stratified epithelium of muco-ciliary phenotype. The downside is that it required 4 weeks of cell culture routines to obtain a working system (Figure 1.7). Advantages of this system compared to the MatTek NHTBE are its the greater exposure window (e.g. 7 days versus 72 hours) and the lower cost per insert (£600/300 inserts v \$1,500/24 inserts). The downside to this system when compared to the MatTek version is that the MatTek model comes 'ready-to-use', whereas our system needs to be cultured for ~4 weeks prior to being fully-differentiated.

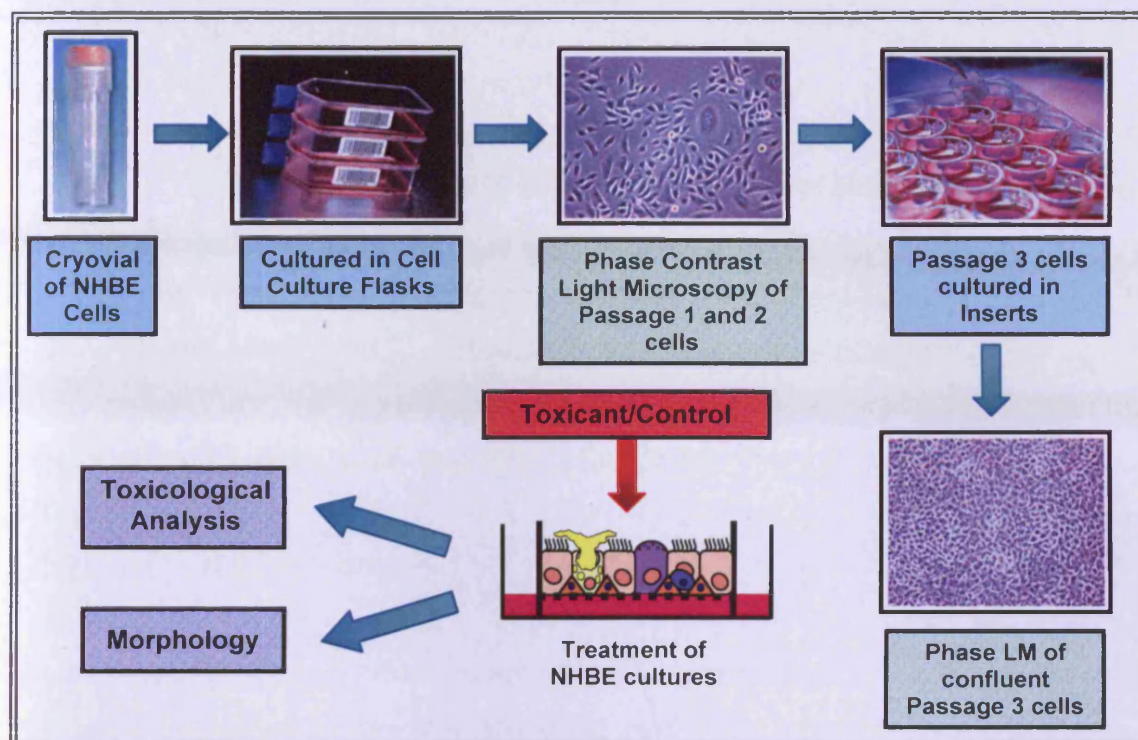


Figure 1.7 Basic outline of the operational procedures of cell culture manipulations using the NHBE model system. NHBE cells were thawed from a cryovial and third Passage NHBE cells seeded into Millipore® inserts. Once the culture was fully-differentiated, cells were treated with xenobiotic/controls followed by toxicological and morphological analysis.

1.6 VALIDATION OF A 'NEW' RESPIRATORY MODEL

Once a 'new' *in vitro* model has been developed it is important that the model undergoes full-characterisation, morphologically, biochemically and toxicologically, in order to validate it as a suitable alternative model. In order to utilise the model in toxicological testing it must be evaluated in response to known, classical pulmonary toxicants, blind-tested to unknown pulmonary toxicants and if possible compared to current *in vivo* models of respiratory toxicology.

1.6.1 BIOCHEMISTRY AND MORPHOLOGY

Extensive characterisation of an alternative, *in vitro* model for *in vivo* inhalation toxicology is essential in order to ensure that it not only morphologically resembles, but also behaves biochemically as the *in vivo* respiratory epithelium.

1.6.1.1 BIOCHEMISTRY

Important biochemical parameters (Chapter 2) to assess in an airway epithelial model are TEER (Gardener *et al.*, 1997) and analysis of the apical secretions (if present) (Rogers, 2003). TEER is used to measure junctional formation in cell cultures and considered a valid and sensitive method (Gardner *et al.*, 1997; Pasternak and Miller, 1995). A Bradford assay (detects protein) on apical washes could indicate that the model produced mucus (a proteinaceous substance) from mucus secreting cells, such as goblet cells (Balharry *et al.*, 2008).

1.6.1.2 MORPHOLOGY

Morphologically (Chapter 3), it is not only necessary to detect that region-specific cell types expected within the bronchial epithelium were present, but also to ensure that the structure resembled the epithelium. In the case of the bronchial epithelium, the model needs to be pseudo-stratified and of muco-ciliary phenotype. This can be established via microscopical analysis (light, transmission electron and scanning electron microscopy), throughout the models morphogenesis.

The identification of specific cell types within the model can be established through the basic microscopical analysis. However, it was important to confirm these observations through precise identification, for instance, using histochemistry or immunohistochemistry (Chapter 4). A cytokeratin (CK) 5/6 antibody can be used to identify these specific CK, known to be present in the basal and supra-basal cells of non-keratinising epithelia (Chu and Weiss, 2002); such as the respiratory tract epithelium (Sun *et al.*, 1979). CK 5/6 is also known to be typically expressed by hyper-proliferative cells (Neudeck *et al.*, 1997). Basal cells, which are regarded as the progenitor cells of the bronchial epithelium, can be detected through the presence of p63 (Ayers and Jeffery 1988; Baldwin, 1994; Breeze and Wheeldon, 1977; Inyama *et al.*, 1988; Yang *et al.*, 1998). Mucus secreting goblet cells can be identified by the periodic-acid Schiff stain, which is known to stain mucopolysaccharides and glycogen, the main components of mucus produced and secreted by goblet cells (Zugibe, 1970). An antibody against

the 10kDa Clara cell specific protein, CC10, can be used to detect the presence of Clara cells (Singh and Katyal, 1997; Singh and Katyal, 2000). Additionally, antibodies against tight junction proteins such as ZO-1, claudin and occludin can be used in order to detect the presence and formation of tight junctions within the epithelial model.

1.6.2 EXPOSURE TO CLASSICAL PULMONARY TOXICANTS

Once the biochemical and morphological analysis had deemed the model reflective of the *in vivo* situation, the next step should be to expose the fully-differentiated, mature, model to known pulmonary toxicants (Chapter 5). The response would then be monitored using conventional toxicological techniques. A panel of classical pulmonary compounds should be selected based on their differential biological effects, such as immunotoxic, cytotoxic, redox reactive and phospholipidotic. The panel chosen was Lipopolysaccharide (immunotoxic; Eisenbarth *et al.*, 2002), cadmium chloride (cytotoxic; Croute *et al.*, 2000), paraquat (redox reactive; Cappelletti *et al.*, 1998), Amiodarone (phospholipidotic; Camus *et al.*, 2004) and finally cigarette smoke, which initiates a plethora of effects and is the most common pulmonary toxicant leading to human exposure (IARC, 2004).

1.6.2.1 BACTERIAL DERIVED LIPOPOLYSACCHARIDE

Lipopolysaccharide (LPS) is a well classified inhalable irritant, known to cause immunotoxic effects (Becker *et al.*, 2000; Eisenbarth *et al.*, 2002; Khair *et al.*, 1996; O'Grady *et al.*, 2001). The major component of Gram-negative bacteria (i.e. *Escherichia Coli*, *Haemophilus Influenzae*, *Salmonella Entericia* and *Pseudomonas Aeruginosa*) outer membrane is LPS, accounting for approximately three-quarters of the bacterial surface. The general structure of LPS is a hydrophilic heteropolysaccharide, covalently attached to this is a lipid component, lipid A. The heteropolysaccharide segment in enterobacteriaceae can be further subdivided into the O-specific chain and the core oligosaccharide (Figure 1.8) (Rietschel *et al.*, 1994).

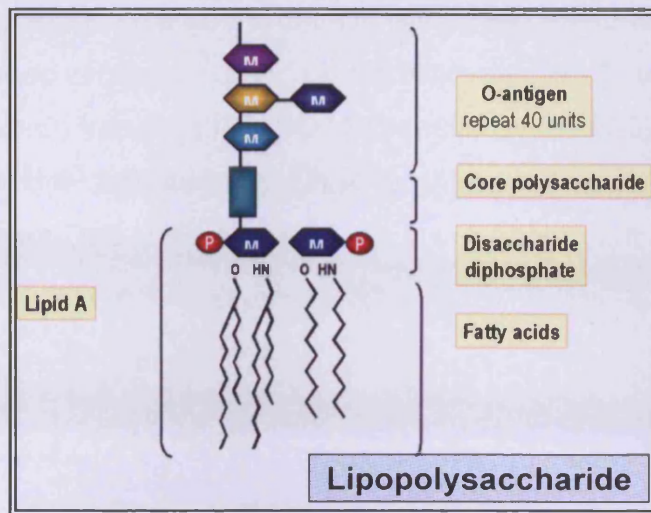


Figure 1.8 Schematic diagram of the LPS component of a bacterial cell wall. M: monosaccharide, P: phosphate, O: oxygen, H: hydrogen, N: nitrogen (Microbiology and Immunology Online, 2007).

Within the environment significantly high levels of LPS can be found in agricultural dust (e.g. grain, poultry, swine, dairy, potato), cotton mills, compost/refuse collections, woodworking, manufacturing industries (e.g. metal, paper, nylon and fibreglass), office/home dust and cigarette smoke (Reed and Milton, 2001). Inhalation of LPS can have a variety of consequences, which are dependant on many factors that include dose of LPS, allergy, hypersensitivity, pre-existing lung disease (e.g. asthma) and/or smoking. Within 'normal' individuals the initial response to low doses of LPS is the activation of the innate immune system (removes LPS without causing an unnecessary inflammatory response), prolonged/high-dose exposure, as well as, allergy/hypersensitivity results in the activation of the adaptive immune response. This results in permanent airway remodelling and potentially COPD (Liu, 2002). Systemic LPS exposure results in septic shock (collapse of the cardiovascular system) (Janeway *et al.*, 2005).

LPS triggers an increase in numerous inflammatory cells and mediators, occurring within 6 hours of exposure (in animal instillation models), basal levels are restored within 48 hours (O'Grady *et al.*, 2001). Phagocytic and epithelial cells express pattern-recognition receptors on their cell surface; these are part of the immune system and recognise well-defined, common antigens such as LPS. In the case of LPS these pattern-recognition receptors are, CD14 and TLR-4, both

are expressed on phagocytic and bronchial epithelial cell surfaces. LPS can bind un-assisted to its co-receptor CD14, or alternatively first binding with the LPS-binding protein, which transfers it to CD14 (Schalz *et al.*, 2002). Binding of LPS to CD14 results in the activation of TLR-4; this binds (intracellularly) to the accessory protein MyD88. This results in the subsequent activation of the nuclear factor (NF)- κ B pathway which up-regulates pro-inflammatory genes (Eisenbarth *et al.*, 2002).

1.6.2.2 CADMIUM

Cadmium is a toxic heavy metal (Shin *et al.*, 2003), naturally found in the environment as a mineral combined with other elements; oxygen (CdO), chlorine (CdCl₂) and sulphur (CdSO₄). The major sources of cadmium within the atmosphere arise from mining and the combustion of fossil fuels, with some entering the eco-system from certain fertilisers (ATSDR, 1999). Cadmium is cytotoxic for many organs including, liver, kidneys, lungs, bones and the reproductive organs (Crout *et al.*, 2000), it is also a known human carcinogen (IARC, 1997). Occupational exposure is highest in those involved in the manufacture of cadmium containing products such as; coatings, plastics and nickel-cadmium batteries (ATSDR, 1999). Within the general population, the major risk of cadmium exposure is from food, smoking cigarettes and industrial pollution (Shin *et al.*, 2003).

Inhalation and ingestion are main routes of entry into the body for cadmium and cadmium containing compounds (Zalups and Ahmad, 2003). The fate of inhaled cadmium is dependent on where in the respiratory tract it is deposited. Deposition within the alveoli results in as much as 90% of the cadmium being absorbed into the blood (Waalkes, 2000). However, the majority of cadmium deposited in the upper respiratory tract is cleared via the muco-ciliary escalator and subsequently ingested (ATSDR, 1999). Cadmium absorbed into the pulmonary blood stream is rapidly cleared and it becomes concentrated in various tissues; especially the kidney and liver. Absorption through ingestion is much lower with only about 5 – 10% of total cadmium ingested actually absorbed. On average Europeans absorb 1 μ g/day of cadmium via ingested food, with roughly an additional 1.4 μ g of

cadmium absorbed per pack of cigarettes (WHO, 2000). Smokers can thereby effectively double the amount of cadmium they absorb per day.

There are very few mechanisms within the body to deal with cadmium. It can not undergo direct metabolic degradation such as oxidation, reduction or alkylation to a lesser toxic compound (ATSDR, 1999; Waalkes, 2003). With the added disadvantage of having a biological half-life of over 25 years within mammals (Méplan *et al.*, 1999), long term storage and therefore damage within the body occurs. Inhalation is known to cause inflammation, chronic oedema, bronchitis (Shin *et al.*, 2003), COPD and cancer within the lung (Burge, 1994; IARC, 1997). Ingestion, either directly or indirectly and accumulation of cadmium within other areas of the body is thought to have a variety of adverse effects including kidney disease, liver damage, fragile bones, immune disorders and multiple organ carcinogenicity (Crouté *et al.*, 2000).

Through *in vitro* and *in vivo* studies certain actions of cadmium have been determined. Cadmium is thought to enter target cells by interacting and competing for binding sites on membrane proteins involved in the transportation of vital elements (e.g. calcium, zinc and iron) through ionic mimicry. Cadmium is also thought to bind to proteins involved in endocytic transport, thereby entering through homology or mimicry (Zalups and Ahmad, 2003). Cadmium has been shown to activate transcription factors which normally require zinc, with 29 cadmium-inducible genes identified. Genes known to be involved in inflammation, cell survival, apoptosis and mitogenesis are known to be induced by cadmium (Shin *et al.*, 2003; Waalkes, 2000). The mechanisms of cadmium carcinogenesis could be mediated through its ability to up-regulate cell survival, glucose metabolism (Shin *et al.*, 2003), proliferation (Waalkes, 2003) and heat shock proteins (Wagner *et al.*, 1999), along with the inhibition of; apoptosis and DNA repair (Waalkes, 2000).

1.6.2.3 PARAQUAT

Paraquat (Pq; 1,1'-dimethyl-4,4'-bipyridilium dichloride) (Figure 1.9) is a potent herbicide and therefore, an occupational hazard with large doses known to be

fatal due to lung and kidney damage (Dalvie *et al.*, 1999). Pq toxicity can either be local (skin, nails, nose and eyes) or systemic. Whether absorbed through the skin, inhaled or ingested, the outcome is relatively similar and dose-dependent. Local effects are generally contact-irritation (lesions/sores) with systemic injury resulting in selective toxicity to the lung, liver and kidney (Kuo *et al.*, 1995).

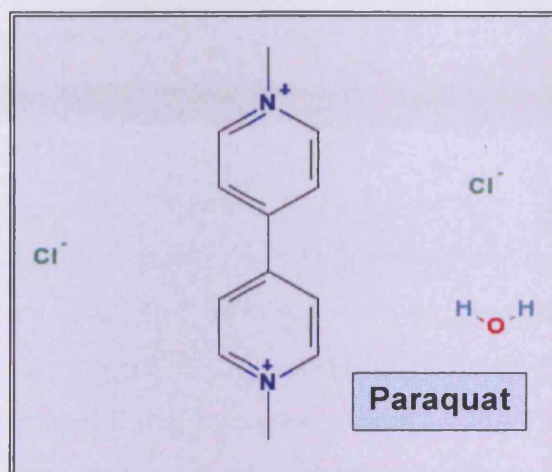


Figure 1.9 Chemical structure of paraquat; 1,1'-dimethyl-4,4'-bipyridilium dichloride (PubChem, 2007a).

Irrespective of the method Pq is administered, it is rapidly distributed to most tissues, but is specifically concentrated in the lungs and kidneys (Gram *et al.*, 1986; Suntres, 2002). Histologically, Pq toxicity within the lung typically causes oedema, a proteinaceous lining within the alveoli, alveolar thickening, collagen deposition, cellular infiltration of the alveolar airspace and pulmonary fibrosis. This essentially obliterates the alveolar and bronchilolar spaces, with the lung becoming a solid glandular-like organ incapable of gas exchange, resulting in death (Gram *et al.*, 1986; Marrs and Adjei, 2003; Takahashi *et al.*, 1994).

Pq uptake by lung is an active, energy-dependent process and is specifically accumulated in the Clara cells as well as Type I and Type II alveolar cells, explaining the specific accumulation of Pq in the lung irrespective of its route of entry (Gram *et al.*, 1986; Masek and Richards, 1990; Sauntres, 2002; Smith *et al.*, 1990). Pq toxicity within the lung occurs in two distinct phases: 1) The first phase occurs within a few days of Pq poisoning is known as the 'destructive phase', whereby the Clara and alveolar Type I and II cells are specifically damaged. If the

Pq concentration is high enough the alveolitis and infiltration of inflammatory cells is extensive enough to cause death; 2) The second phase is known as the 'proliferative phase' and is characterised by a massive infiltration and proliferation of fibroblasts, resulting in extensive collagen deposition and obliteration of the alveolar and bronchiolar spaces (Masek and Richards, 1990; Smith *et al.*, 1990).

Pq has been demonstrated, *in vitro*, to cause apoptotic cell death within human alveolar and Clara cells, which is thought to be mediated by oxidative stress and possibly via lipid peroxidation, protein inactivation or DNA damage (Cappelletti *et al.*, 1998; Kuo *et al.*, 1995; Masek and Richards, 1990). Reactive oxygen intermediates are generated from the Pq initiated redox-cycling reaction with several toxic outcomes. The first of which is the generation of the superoxide anion, which in itself can result in the generation of more toxic reactive species (such as, hydrogen peroxide and hydroxyl radical). The next is the disruption of NADPH-requiring biochemical processes via the oxidation of cellular NADPH and the third is lipid peroxidation (Kuo *et al.*, 1995; Suntres, 2002; Wang *et al.*, 1992). Other biochemical effects that enhance Pq's cytotoxicity is its ability to potentiate the generation of ROS by phagocytes (Wang *et al.*, 1992) and activation of cellular proliferation and differentiation (Kuo *et al.*, 1995). Wang and co-workers (1992) deduced that the mitochondria are the initial toxic site of Pq (*in vitro* and *in vivo*), which may explain Pq's selective cell toxicity.

1.6.2.4 AMIODARONE

Amiodarone (Am) is a benzofuron derivative (Figure 1.10) with class III antiarrhythmic activity and is used to treat cardiac arrhythmias (Bargout *et al.*, 2000). Am belongs to a group of drugs known as a cationic amphiphilic drugs, which characteristically have a hydrophilic region containing a primary or substituted nitrogen group, along with an aromatic or aliphatic ring that constitutes the hydrophobic region. Am, can interact with lipid cellular components due to its hydrophobic region and molecular polarity (Casartelli *et al.*, 2003). Am is limited in its use as a cardiac drug due to the fact that it has many adverse effects, including hepatitis and Am-induced pulmonary toxicity (AIPT), which can progress to irreversible pulmonary fibrosis (Trivier *et al.*, 1997). Patients receiving a

minimum of 400mg/day of Am have up to, a 25% chance of developing AIPT and possibly pulmonary fibrosis (Nicolesau *et al.*, 2007).

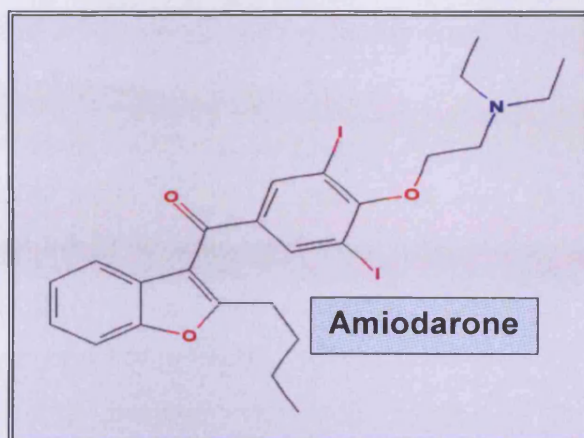


Figure 1.10 Chemical structure of amiodarone. (PubChem, 2007b)

Am and its primary metabolite *N*-desethylamiodarone (mainly hepatic biotransformation; Nicolescu *et al.*, 2007) are known to have many adverse effects and are especially toxic to the liver and lungs. The lung is the primary site of Am accumulation, especially within pulmonary macrophages (Leeder *et al.*, 1996). However, Bolt and colleagues (2001) demonstrated that both Clara cells and Type II alveolar cells were more susceptible to the toxic effects of Am and *N*-desethylamiodarone. Due to its long biological half-life and slow efflux, Am remains within the tissue up to a year after cessation of treatment. AIPT can present itself with a variety of histopathological features including, septal thickening (as a result of interstitial oedema), inflammation, interstitial fibrosis and phospholipidosis (Camus *et al.*, 2004). Other indications of Am toxicity include necrosis, apoptosis (Bargout *et al.*, 2000), cellular infiltration (including eosinophils) (Camus *et al.*, 2004), DNA fragmentation (increases in bax, caspase-3, TGF β 1) (Choi *et al.*, 2002), decreases in mitochondrial membrane potential and ATP levels (Card *et al.*, 2003). However, the exact mechanisms of Am and *N*-desethylamiodarone toxicity is unknown.

1.6.2.5 CIGARETTE SMOKE

It is estimated that around 1.3 billion people smoke tobacco worldwide (Boyle and Levin, 2008), with half of these expected to die from its effects. Tobacco is the second major cause of death in the world (WHO, 2010a). Cigarette smoke is known to cause 13 different cancers (lung, oral and nasal cavities, nasal sinuses, pharynx, larynx, oesophagus, stomach, pancreas, liver, urinary bladder, kidney, uterine cervix and myeloid leukaemia). The major diseases caused are lung cancer, bronchitis, emphysema, heart disease, COPD, microbial infections and atherosclerosis (Boyle and Levin, 2008; IARC, 2004; Sopori, 2002; WHO, 2010b). The causal relationship between tobacco smoking and lung cancer was established by the Medical Research Council in the 1950's (MRC, 1957).

Within developed countries, the most common use of tobacco is in cigarettes, which are defined as “any role of tobacco wrapped in paper or any other non-tobacco material, which when lit the burning process produces smoke that is inhaled through the unlit end” (IARC, 2004). When lit a cigarette produces three varieties of smoke: 1) mainstream – the smoke released from the mouth-end of the cigarette during puffing; 2) sidestream – the smoke released from the lit-end and through the cigarette paper; and 3) second hand (or environmental tobacco smoke) – a mixture of sidestream and exhaled mainstream smoke diluted with the air and combined with native airborne constituents (IARC, 2004).

Mainstream cigarette smoke (CS) is known to comprise around 4000 different substances, accounting for more than 95% of its mass and are mainly dispersed in the gas (or vapour) phase (Domagala-Kulawik, 2008; IARC, 2004). This gas phase primarily consists of nitrogen, oxygen and carbon dioxide (Hecht, 1999). Nicotine, tar, aromatic hydrocarbons, phenols and cresol are some of the important constituents of the particle phase of CS, with 10 – 30% of CS particles depositing in the lung (Domagala-Kulawik, 2008). Qualitatively the components of mainstream, sidestream and second hand CS are essentially identical; however, the quantitative composition may vary greatly. This is mainly due to the rapid dilution and possible interaction of sidestream and exhaled mainstream CS with the surrounding air. Inhalation of second hand CS exposes non-smoking

individuals to the same numerous carcinogens and toxic compounds as a smoker (IARC, 2004), with around 10 – 15% of lung cancer in non-smokers attributed to second hand smoke. The WHO state that there is “no safe level of exposure to tobacco smoke” (WHO, 2005).

Due to the complex nature and numerous compounds present in CS its mechanism of action on the body, lungs and more specifically the bronchial epithelium is difficult to elucidate. However, some of the effects of CS on the bronchial epithelium are: bronchial carcinoma; induction of terminal squamous differentiation; inhibition of cell growth; induction of DNA damage; particularly toxic to Clara cells, reduction in CC10 production; toxic to pulmonary cilia (due to acrolein); induction of oxidative damage; goblet cell hyperplasia, metaplasia and hypertrophy; increased mucin expression; apoptosis and/or necrosis; inhibition of mitochondrial function; genetic changes, including the induction of xenobiotic-metabolising and redox-regulating genes, downregulation of tumour suppressor and inflammatory genes; downregulation of tight junction proteins and increase in epithelial permeability (Bernard *et al.*, 1994; Hecht, 1999; Innes *et al.*, 2006; Maunders *et al.*, 2007; Takeyama *et al.*, 2001; van der Toom *et al.*, 2007; Willey *et al.*, 1987).

1.6.3 BLIND-EXPOSURE TO POSSIBLE PULMONARY TOXICANTS

Another method in the validation process would be to blind-test the model on a variety of pulmonary toxicants, non-toxic compounds and possible pulmonary toxicants, the last one focusing more the use of the model as a test system. Funding of this work by the pharmaceutical company AstraZeneca (AZ) enabled the blind-exposure of these three categories of compounds, with the additional benefit of using the model as an irritancy screen for possible pulmonary drugs (Chapter 6).

After blind-exposure and analysis of the results, the model's efficiency in distinguishing between pulmonary toxicants would be elucidated. Additionally, the results would be compared to AZ in-house *in vivo* results using the same panel of compounds and the accuracy of our model determined.

1.7 RESEARCH HYPOTHESIS, AIMS AND OBJECTIVES

1.7.1 HYPOTHESIS

The experimental hypotheses for the research project were:

1. That primary normal human bronchial epithelial (NHBE) cells can be cultured at an air-liquid interface in order to create a fully-differentiated bronchial epithelium of muco-ciliary phenotype containing basal, intermediate, Clara, serous, goblet and ciliated cells.
2. The NHBE cell model will predict drug irritancy outcomes for rat *in vivo* airway exposures.

1.7.2 SPECIFIC PROJECT AIMS AND OBJECTIVES

The first principal aim of the proposed research project was to establish and characterise the NHBE cell model as a viable alternative to *in vivo* rat airway exposure. Once the model had been established, the objective was to fully-characterise the biochemical and morphological parameters. This was undertaken during cell culture morphogenesis and was achieved by measuring TEER and apical protein content, followed by morphological evaluation using light microscopy (LM), transmission electron microscopy (TEM) and scanning electron microscopy (SEM), along with concomitant cell and epithelium specific histochemistry and immunohistochemistry (Figure 1.11; Part I).

The second principal aim of the research project involved monitoring the biochemical and morphological response of the NHBE model to pulmonary toxicants. The first part involved the exposure to classical pulmonary toxicants and the second part to unknown candidate respiratory drugs (provided by AZ). Analysis was achieved by utilising conventional toxicology tools such as, TEER, culture viability (ATP assay) and morphological changes (Figure 1.11; Part II).

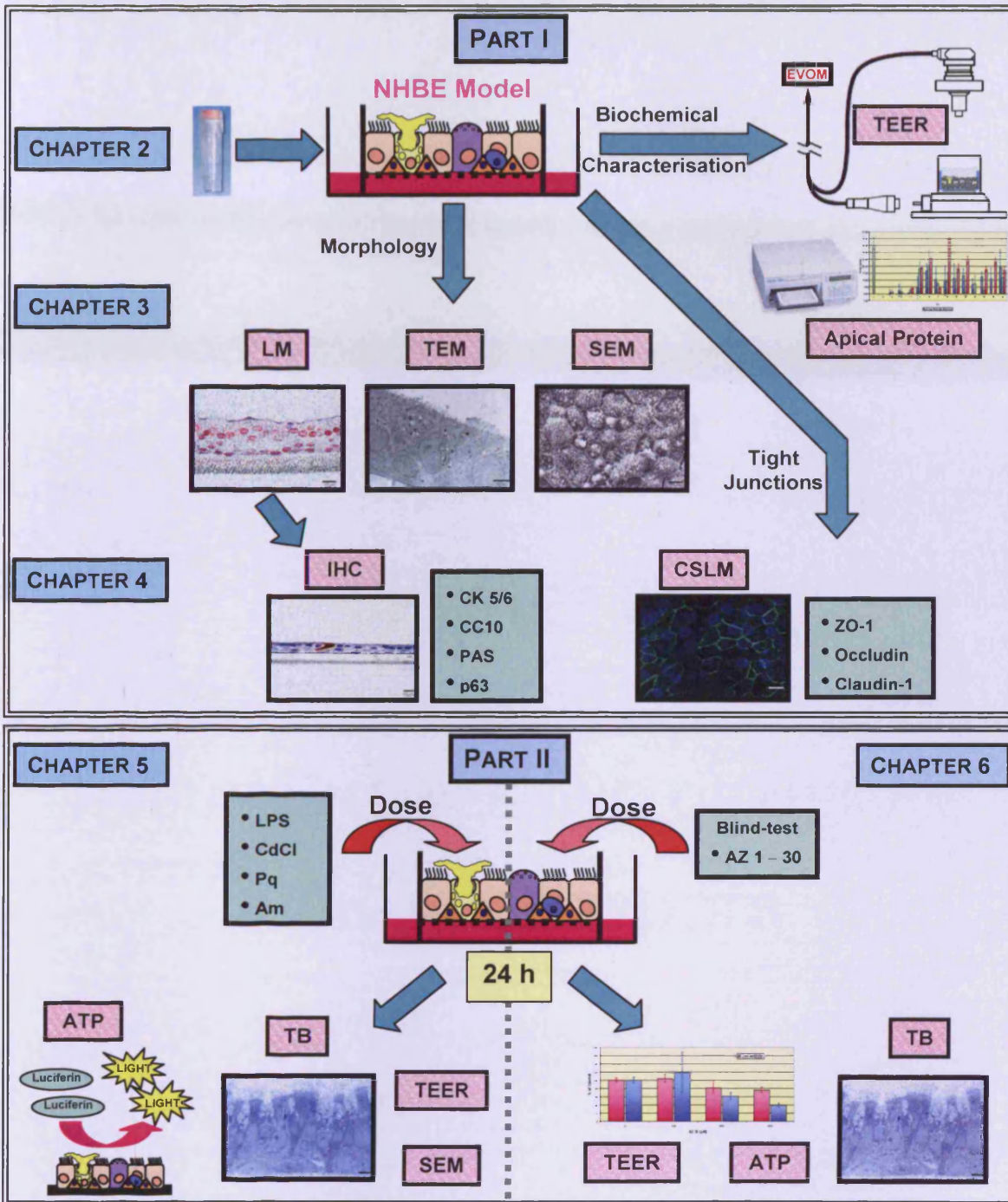


Figure 1.11 Flow chart of specific project aims and their relevant experimental research chapters.

CHAPTER 2:

TISSUE-ENGINEERING OF HUMAN LUNG CONSTRUCTS

2.1 INTRODUCTION

Scientists have explored and continue to explore *in vitro* systems in order to model/study the *in vivo* situation (Agius, 1987; BéruBé *et al.*, 2009; Lantelme *et al.*, 2008; Roguet and Schaefer, 1997). In the field of respiratory biology early *in vitro* studies involved explant cultures (Duncan and Hild, 1960; Thomas and Howard, 1974). During the 1980's major advances were made with respect to culture conditions and media, allowing differentiation of cells and formation of tissue-like constructs. The use of serum-free media supplemented with selected growth factors, hormones and antibiotics have allowed fine-tuning of this technique. The main factors added during this time were, hydrocortisone, insulin, epidermal growth factor, transferrin, cholera toxin, bovine hypothalamus extract, triiodothyronine and retinoic acid (Lechner, 1983; Wu *et al.*, 1986). Hill and colleagues (1998) demonstrated the importance of sufficient retinoic acid within the media. Retinoic acid-sufficient cultures displayed muco-ciliary differentiation; columnar cell cultures secreting substantial quantities of mucus. Retinoic acid-deficient cultures were shown to undergo metaplastic squamous differentiation (Hill *et al.*, 1998). Cell density was also deemed an important parameter, whereby insufficient densities caused cells to undergo squamous differentiation in response to foetal calf serum (FCS) or TGF- β (Ke *et al.*, 1990).

Multi-layered normal bronchial epithelial cell cultures, displaying *in vivo* differentiated characteristics, were originally achieved by using denuded tracheal grafts to culture cells (Engelhardt *et al.*, 1991; Terzaghi *et al.*, 1978). Wu and colleagues (1986) demonstrated that this phenomenon could be replicated by use of a collagen gel substrata. However, cells also required culturing at an air-liquid interface (ALI). This was achieved by the development of a 'special chamber' on which a nitrocellulose membrane was glued and cross-linked with gelatine; the collagen gel substratum was formed atop of the membrane. A spacer was placed in a tissue culture dish and the chamber rested on the spacer, allowing the culture to be fed basally (Adler *et al.*, 1987). This culture system demonstrated a polarity (i.e. apical and basal regions) in the differentiation of the cultured cells. Polarity confers development of cilia and the secretion of mucus granules on the apical

surface. Furthermore, the columnar appearance of apical cells could be demonstrated (Wu *et al.*, 1986). This allowed the development of ALI cultures originally with guinea pig tracheal epithelial cells (Adler *et al.*, 1987). ALI cultures were rapidly adopted for use with primate (Martin *et al.*, 1991), human (Gray *et al.*, 1996; Yamaya *et al.*, 1992), rat (Kaartinen *et al.*, 1993), bovine (Kondo *et al.*, 1993) and canine tracheal epithelial cells (Mochizuki *et al.*, 1994).

A combination of all of the parameters mentioned must be used in order to produce a well-differentiated culture of normal human bronchial epithelia that accurately reflect their *in vivo* counterparts. Development of primary normal human bronchial epithelial (NHBE) cell cultures for toxicological applications requires the following culturing considerations: 1) media and hormone supplementation through basal means; 2) cell density and passage number; 3) ALI culturing; 4) ciliogenesis; and 5) secreted proteins. Each of these factors must be fulfilled in order to develop a fully functional (i.e. active cilia, mucus secretion, cytokine expression, polarity) primary NHBE cell culture for use in assessing the toxicity of xenobiotics.

The focus of this chapter was to establish a differentiated culture, as determined by morphological characteristics (e.g. cobblestone appearance) (Lee *et al.*, 1986), trans-epithelial electrical resistance (TEER) (Gardener *et al.*, 1997) and apical protein secretions (Rogers, 2003) as validation of a functional NHBE lung-construct; accepted features of a viable construct (BéruBé *et al.*, 2009).

2.2 MATERIALS AND STOCK SOLUTIONS

2.2.1 MATERIALS

MATERIALS	SUPPLIER
NHBE Cells, Cryopreserved in Bronchial Epithelial Growth Medium® (BEGM®), with Retinoic Acid	Lonza Group Ltd., Switzerland

Table 2.1 Table of materials used and their suppliers.

MATERIALS	SUPPLIER
T75 and T175 Cell Culture Flasks	Fisher Scientific, Manchester, UK
CellBind® T75 and T175 Cell Culture Flasks Costar® Transwell® Cell Culture Inserts; 6.5mm, 0.4 µm pore size	Corning Life Sciences, Schipol-Rijk, The Netherlands
Millicell Hanging Cell Culture Insert, Polyethylene Terephthalate; 6.5mm diameter, 0.4µm pore size	Millipore Ltd., Watford, UK
24-Well Cell Culture Plate 96-Well Plate	Grenier Bio-one Ltd., UK

Table 2.1 Continued table of materials used and their suppliers.

2.2.2 STOCK SOLUTIONS

STOCK SOLUTIONS	SUPPLIER
PureCol™	Biomaterials, Fremont, USA
Bronchial Epithelial Basal Medium (BEBM) BEGM® SingleQuots® AccuGENE® Molecular Biology Water Dulbecco's Modified Eagle's Medium (DMEM), with 4.5g/L Glucose, L-Glutamine, without Pyruvate Penicillin-Steptomycin-Amphotericin B	Lonza Group Ltd., Switzerland (Formerly Cambrex Bioscience, Workingham, Berkshire, UK)
Hank's Balanced Salt Solution (HBSS) Trypsin-EDTA RPMI-1640 Phosphate Buffered Saline (PBS), pH 7.4, without CaCl ₂ or MgCl ₂	Invitrogen Ltd., Paisley, Scotland
Foetal Calf Serum (FCS)	JRH BioScience, Kansas, USA
Retinoic Acid Bradford Reagent Bovine Serum Albumin	Sigma, Dorset, UK

Table 2.2 Table of stock solutions used and their suppliers.

2.2.3 EQUIPMENT

EQUIPMENT	SUPPLIER
Rotanta 460R Centrifuge	Hettich Zentrifuga, Tuttlingen, Germany
Phase Contrast Light Microscope (DM2500) Leica Image Analysis Software	Leica Ltd., Milton Keynes, UK
ENDOHM-6 Endohm Chamber EVOM Epithelial Voltohmmeter	World Percision Instruments, Stevenage, UK
Opsys MR-Dynex Microplate Reader	Dynex Technologies, Worthing, UK

Table 2.3 Table of equipment used and their suppliers.

2.3 METHODS

2.3.1 CELL CULTURE

2.3.1.1 INITIAL SEEDING AND CULTURE TO CONFLUENCE OF NHBE CELLS

An initial experiment involved the seeding of thawed NHBE cells in either a collagen coated T75 cell culture flask (1:100; v/v) PureCol™/Sterilised water solution was poured into T75 flasks and left to set (2 hours), excess water was removed from the flasks prior to addition of cells) or a T75 CellBind® (pre-coated with collagen) flask. Later experiments involved seeding thawed NHBE cells in non-treated T75 cell culture flasks. Bronchial Epithelial Growth Medium® (BEGM®) was prepared with commercially purchased Bronchial Epithelium Basal Medium (BEBM) and BEGM® SingleQuots® (10ml BEGM: 10ml BEBM, 40µl Bovine Pituitary Extract and 10µl of insulin, hydrocortisone, transferrin, triiodothyronine, epinephrine, epidermal growth factor, Gentamicin/Amphotericin and retinoic acid). A cryovial of NHBE cells (~500,000 cells) was rapidly (2 – 3 minutes) thawed (37°C) and suspended in 30ml of BEGM® (37°C). NHBE–BEGM® mixture (15ml) was transferred into each T75 flask. During an overnight incubation (~18

hours), the NHBE cells attached to the base of the flask. The BEGM[®] (15ml) was replaced with 15ml fresh BEGM[®] medium and was then replaced (20ml) every third day until the cells reach 70% confluency (~2 – 3 days).

2.3.1.2 SECOND PASSAGE

Confluent cell cultures were rinsed twice with 5ml HBSS (37°C). Trypsinisation of cells was achieved by addition of 3ml Trypsin-EDTA solution for 3 – 5 minutes at room temperature (RT), until 90% of the cells were detached. FCS (10%) in RPMI (30ml) was added to neutralise the trypsinisation and the cell suspension was removed into a 50ml universal centrifuge tube. Cell suspensions were centrifuged (72 x g for 4 minutes) and the supernatant removed. Cell pellets were re-suspended in a total of 2ml BEGM[®] (37°C) and added to the remaining 178ml BEGM[®] (37°C). BEGM[®]-cell suspension (30ml) was placed into each of six T175 cell culture flasks (The initial experiment involved 3x PureCol[™] coated T175 flasks and 3x CellBind[®] flasks). During an overnight incubation (~18 hours) the NHBE cells attached to the base of the T175 flasks. The BEGM[®] (30ml) was replaced with 30ml fresh BEGM[®] medium. BEGM[®] (30ml) was replaced every third day until the cells reached 70% confluency (~ 2 – 3 days).

2.3.1.3 SEEDING INTO CELL CULTURE INSERTS

Confluent cell cultures were rinsed twice with 5ml HBSS (37°C). Trypsinisation of cells from the collagen layer was achieved by addition of 4ml Trypsin-EDTA solution for 3 – 5 minutes (RT), until 90% of the cells were detached. FCS (10%) in RPMI (30ml) was added to neutralise the trypsinisation and the cell suspension was removed into a 50ml universal centrifuge tube. Cell suspensions were centrifuged (72 x g for 4 minutes) and the supernatant removed. Cell pellets were re-suspended and combined in a total of 4ml BEGM[®] (37°C). The cell concentration of the BEGM[®]-cell suspension was determined by using a 5x5 grid on a haemocytometer. The required seeding density for imputing into inserts was 0.5 million cells/ml. BEGM[®]-cell suspension was added to the required volume of BEGM[®] for seeding and 150µl BEGM[®]-cell suspension was placed into each insert, with 500µl of BEGM[®] placed in each well beneath the insert (24-well cell

culture plate). During the overnight incubation (~18 hours) the NHBE cells attached to the insert membrane. NHBE cells were seeded into Millipore® inserts, as well as into 6x Transwell® inserts, as Transwell® inserts allow visualisation of the cells using phase contrast microscopy (Section 2.3.2).

2.3.1.4 CONFLUENT INSERT CULTURES

Following seeding into inserts, apical media was removed to create an ALI culture (Day 1; Figure 2.1). The basal media (BEGM®) was replaced with 300µl of ALI media (20ml ALI media: 10ml BEBM, 10 ml DMEM, 80µl Bovine Pituitary Extract and 20µl of insulin, hydrocortisone, transferrin, triiodothyronine, epinephrine, epidermal growth factor, Gentamicin/Amphotericin and retinoic acid). Basal ALI media was changed daily, adding 300µl of fresh ALI media into each well for the first week, then 6 days a week. Once the cells began to show mucin secretion (a layer of clear viscous liquid on the apical surface of the cultures), it was carefully removed by aspiration every second day to prevent mucin accumulation (as there was no muco-ciliary escalator to remove the mucin).

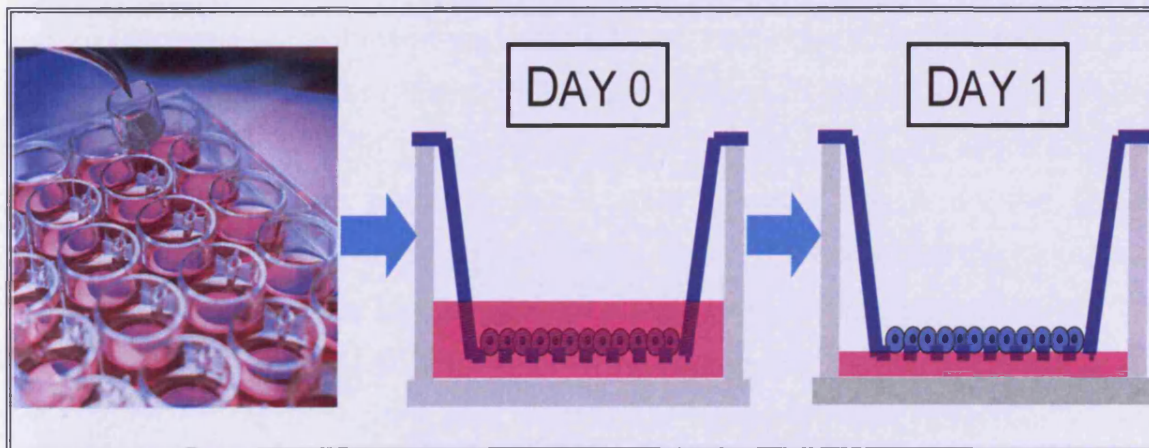


Figure 2.1 Schematic diagram depicting the inserts within a 24-well plate, the cultures at Day 0 (seeding of cells) and Day 1 (removal of apical media) (Drawn by Z. Prytherch, 2010).

2.3.2 PHASE CONTRAST LIGHT MICROSCOPY

Cell cultures were visually monitored and images taken using a phase contrast light microscope (Leica Ltd., UK), to evaluate the stages of growth and

development in cell culture flasks (T75 and T175), as well as in cell culture inserts. This was done daily and allowed monitoring of the health (adherence and shape of cells) and confluency (percentage area occupied by cells). These were important observations in the determination of when to split Passage 1 and 2 cultures. In the Passage 3 cells, or cell insert cultures, the microscope was used to capture images of the cultures every 3 days (including Day 1).

2.3.3 TRANS-EPITHELIAL ELECTRICAL RESISTANCE

Membrane channels, pumps and junctions enable cells to concentrate ions either intracellularly or extracellularly, this creates a difference in voltage between the interior and exterior of the cell and is known as a membrane potential. This membrane potential allows a cell to function as a battery. This battery property enables the use of Ohm's law ($I = V/R$; where I = current, V = voltage and R = resistance) to determine the electrical resistance of a cell or culture.

The TEER values of cell cultures were evaluated using the Endohm chamber (Figure 2.2). The chamber was filled with 1ml of PBS solution immersing the bottom electrode. A cell insert was then placed inside the Endohm chamber and PBS solution (150 μ l) was placed on the apical region of the cultures (i.e. into the insert). The top electrode (lid) was placed on top of the insert and the TEER reading was taken by pressing the 'current release' button on the EVOM (epithelial voltohmmeter), releasing the current. The EVOM detected the strength of the current reaching the bottom electrode, converting it into the resistance (Ω) created by the insert (Figure 2.3). Prior to measuring the resistance values for the cell cultures, a 'blank' reading was recorded by using an insert without cells (with PBS as above) and was later subtracted from that of the cell culture inserts prior to conversion of values from Ω to $\Omega.cm^2$.

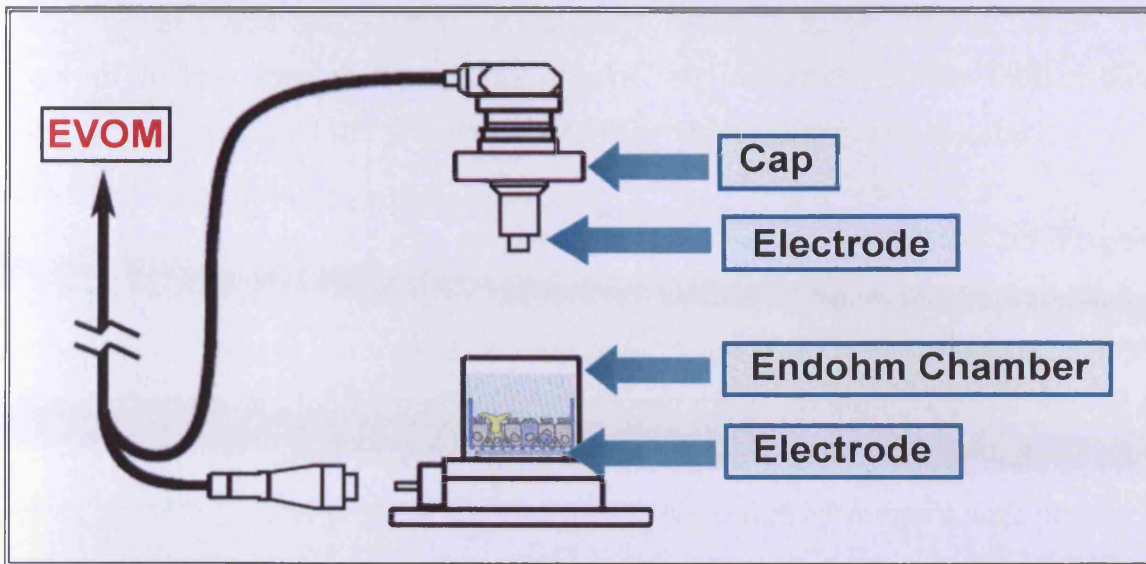


Figure 2.2 Schematic diagram of the EVOM and Endohm chamber used to record TEER (Drawn by Z. Prytherch, 2010).

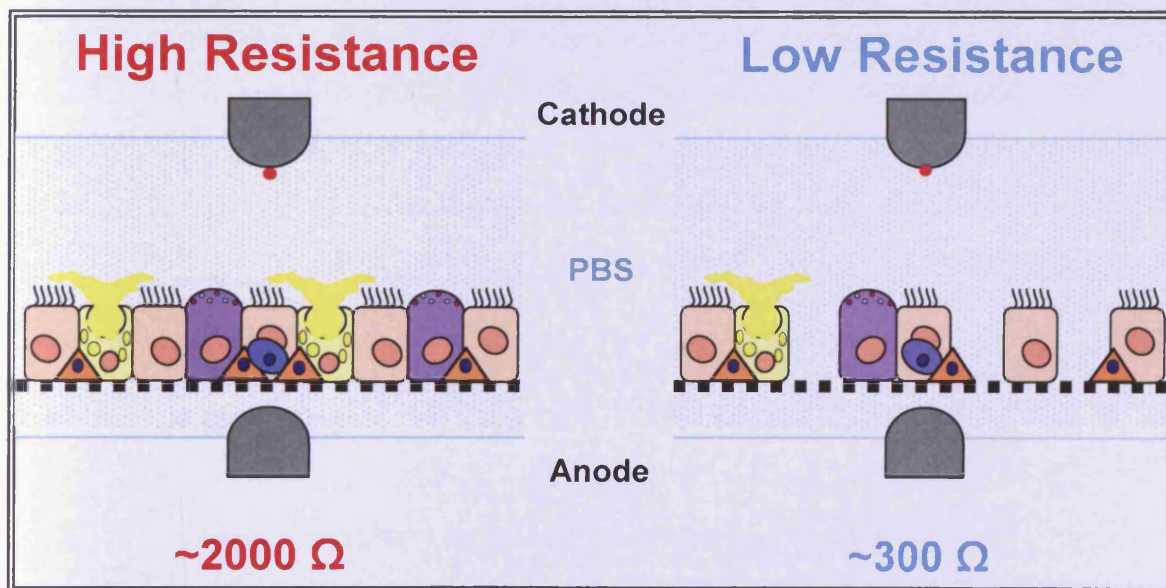


Figure 2.3 Schematic diagram depicting the differences in TEER readings between a healthy (~2000Ω) confluent epithelial culture and a culture with disrupted tight junctions (~300Ω) (Drawn by Z. Prytherch, 2010).

2.3.4 BRADFORD ASSAY

Apical washes were collected from the cell inserts at defined time-points in order to collect any secretions which may be present on the apical cell surface. An apical wash was achieved by removing the apically added PBS (150µl) from the

TEER reading, and storing in an eppendorf tube (4°C) to be analysed later. The Bradford assay was performed to provide an indication of the total protein produced by cells over the time-course of the model (Pingoud *et al.*, 2002).

In order to accurately measure protein concentration using the Bradford reagent, (colorimetric chemical agent), a number of standards were run to establish a concentration curve. This was accomplished using a bovine serum albumin protein standard of 2mg/ml that was diluted into the following concentrations: 2, 4, 6, 8, 10, 12, 14 and 16µg/ml. Bradford reagent (50µl) was added to each standard (150µl). The protein standard with the Bradford reagent was placed in the plate reader and read at 590nm wavelength. A standard curve was established from which unknown sample protein concentrations could be determined.

In order to determine the unknown sample protein concentrations, apical wash: PBS 1:10 (v/v) solution (200µl) was placed in a well of a 96-well plate; Bradford reagent (50µl) was added and mixed into each sample. These were read in a plate reader at 590nm. Assuming all readings returned below 1, the protein concentration was determined by extrapolation from the earlier prepared standards.

2.4 RESULTS

2.4.1 CELL CULTURE AND PHASE CONTRAST LIGHT MICROSCOPY

Previous uses of NHBE cells to create an accurate lung construct involved three passages: Passage 1; re-hydrating one cryovial into one T75 flask, Passage 2; transferring into one T175 flask, Passage 3; seeding into inserts (Richter, 2005). In order to make this system more financially viable by increasing the number of inserts gained from each cryovial, the three Passages are now: Passage 1; seeding one cryovial into two T75 flasks, Passage 2; seeding each T75 into three T175 flasks, Passage 3; seeding into inserts. This greatly increased the insert yield for all experiments (60:300 inserts Richter:Prytherch).

The first cryovial of cells was seeded into one PureCol™ coated T75 and one CellBind® T75. The PureCol™ coated flask was then Passaged into 3x PureCol™ coated T175 flasks and likewise the CellBind® T75 was Passaged into 3x CellBind® T175 flasks. NHBE cells grown in PureCol™ coated flasks reached 70% confluence when the CellBind® flasks were only approximately 60% confluent. However, both flasks were Passaged at the same time. During Passage 2, the PureCol™ coated flasks reached 70% confluence two days before the CellBind® flasks achieved the same level of confluency. The three PureCol™ flasks were seeded into Transwell® inserts, once the CellBind® flasks obtained 70% confluency they were also seeded into Transwell® inserts. Once seeded into inserts the 2 sets behaved similarly (Figure 2.4).

A second set of cells were cultured in non-coated flasks (the rest of the method remained the same). NHBE cells cultured in non-coated flasks reached 70% confluency 24 hours after NHBE cells cultured in both the PureCol™ and CellBind® flasks. After seeding into the T175 flasks (Passage 2), the NHBE cells in the non-coated flasks obtained 70% confluency at the same time frame as the PureCol™ coated flasks (96 hours post-seeding into T175 flasks). The NHBE cells from the non-coated flasks were mainly seeded into Millipore® inserts, with 6x Transwell® inserts also seeded. Once seeded into inserts NHBE cells from all three different culture methods behaved similarly (Figure 2.4).

All NHBE cells 24 hours post-seeding into inserts, began to take on a regular pavement or 'cobblestone' style appearance, remaining viable until the end of the experiment (Day 42; Figure 2.5). Real-time observations using the phase contrast light microscope revealed ciliary action at Day 15, which manifested as tiny 'flickers'. Once the cobblestone organisation and ciliary flicks appeared, the culture sustained these features until its demise (Day 42).

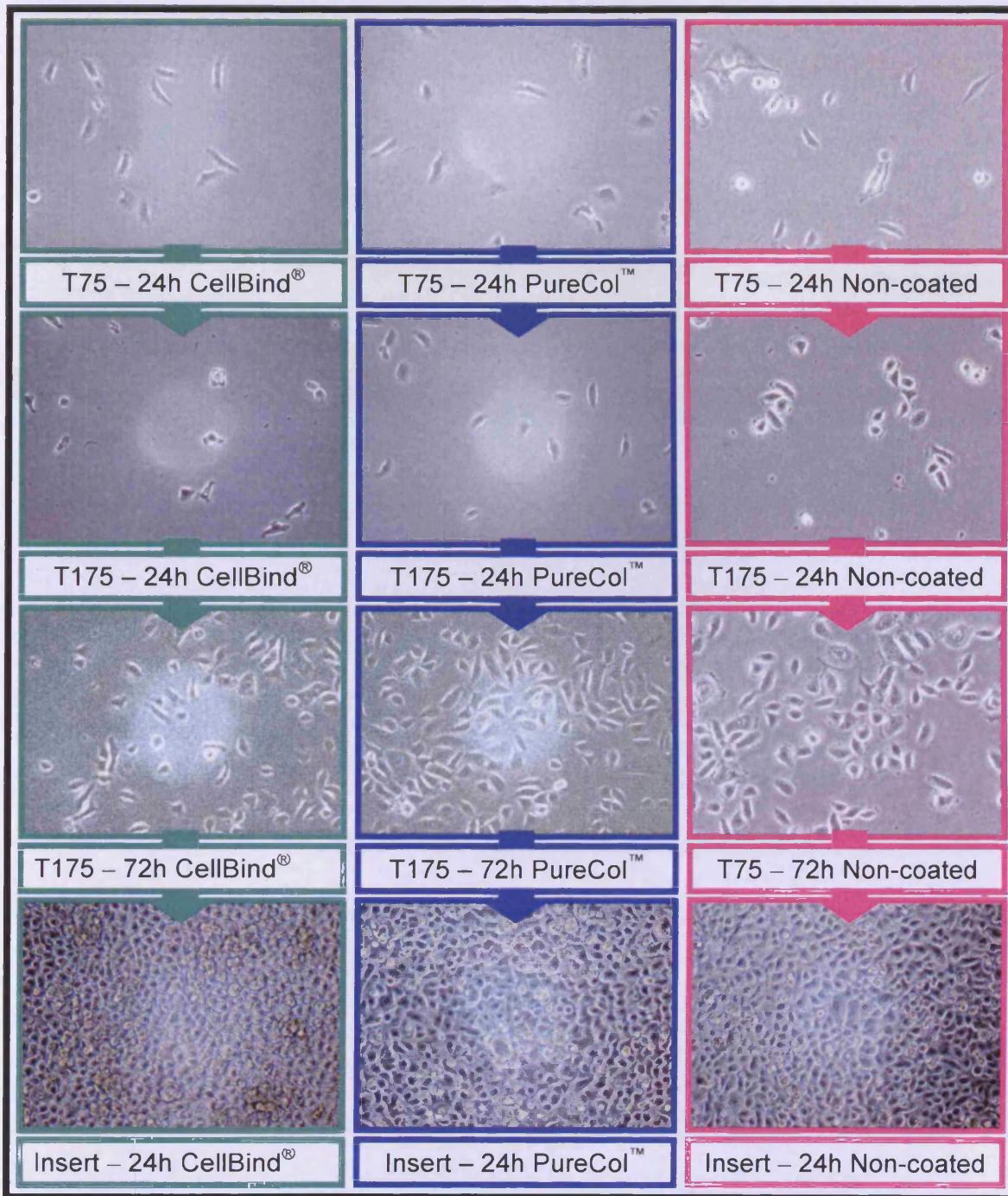


Figure 2.4 Phase contrast light microscopy images of NHBE cells grown in either CellBind® (Green), PureCol™ coated (Blue), or non-coated (Pink) flasks until seeding into Transwell® inserts. Time under each image refers to hours post-seeding. Cells in PureCol™ coated and non-coated flasks appear of similar confluence throughout, CellBind® slightly less confluent. By Day 1 (24 hours post-seeding) in cell culture insert all developed the characteristic cobblestone appearance.

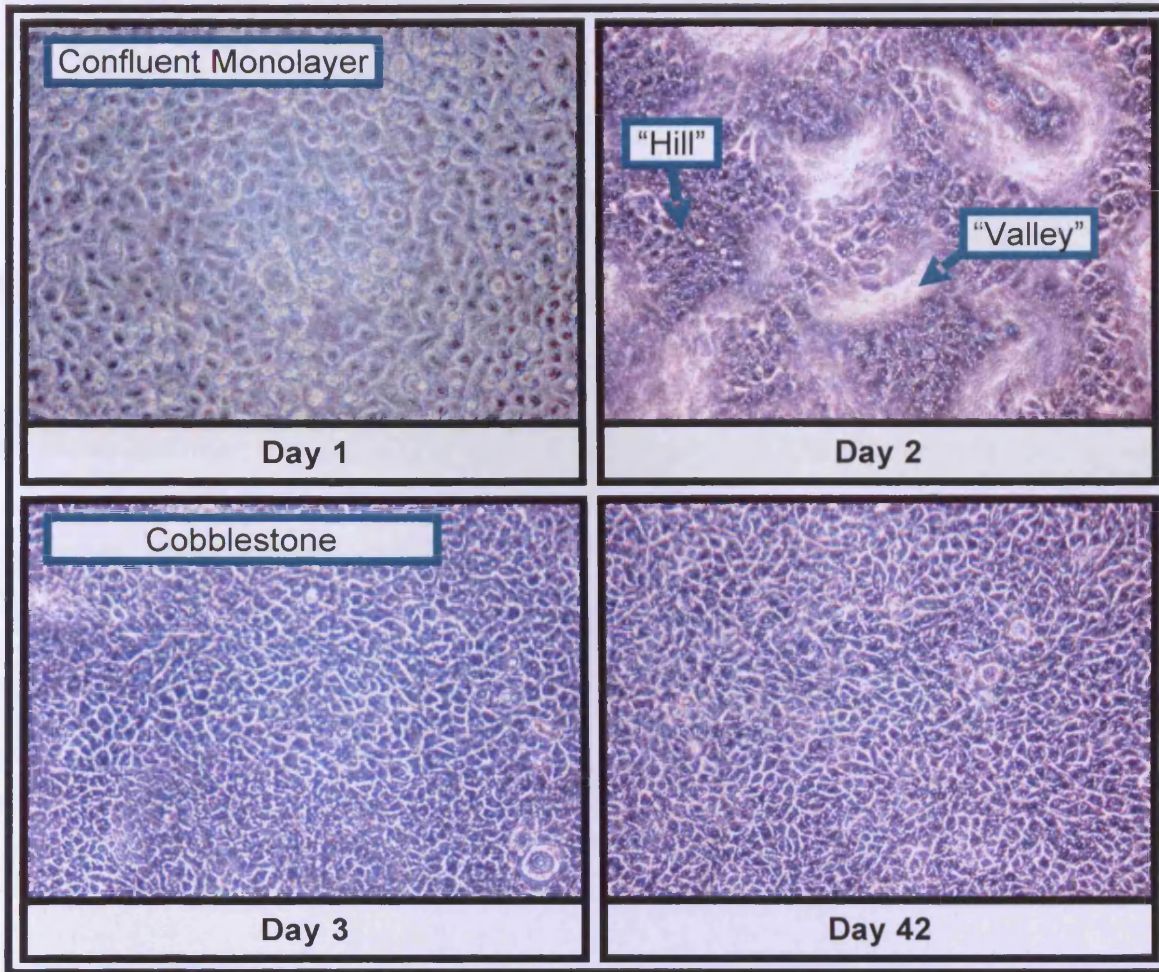


Figure 2.5 Phase contrast light microscopy images of NHBE cells grown in Transwell[®] inserts. Days are post-seeding into inserts.

2.4.2 TRANS-EPITHELIAL ELECTRICAL RESISTANCE

TEERs were measured on cultures in inserts ($n = 3$) every three days on donors 5F, 8F and 9F over a 42 day period (Figure 2.6); In respect to donors, 5, 8 and 9 refer to the year in 2000 in which they were isolated, all were non-smoking donors. The data revealed that all donors provided similar TEER trends throughout the development of the model.

The 5F donor's TEER increased gradually from Day 1 ($\sim 20 \Omega \cdot \text{cm}^2$) to Day 9 ($\sim 1200 \Omega \cdot \text{cm}^2$). There was a large increase in TEER values at Day 12 ($\sim 5950 \Omega \cdot \text{cm}^2$), which continued until Day 15 ($\sim 8,800 \Omega \cdot \text{cm}^2$). A plateau was reached between Days 21 – 39, with average TEER values remaining within the range

6,900 – 8,000 $\Omega\cdot\text{cm}^2$. Although the average TEER value for Day 42 had only decreased slightly from the plateau range ($\sim 6,000 \Omega\cdot\text{cm}^2$), the actual TEER readings ranged greatly between inserts ($\sim 6 - 12,950 \Omega\cdot\text{cm}^2$; Figure 2.6).

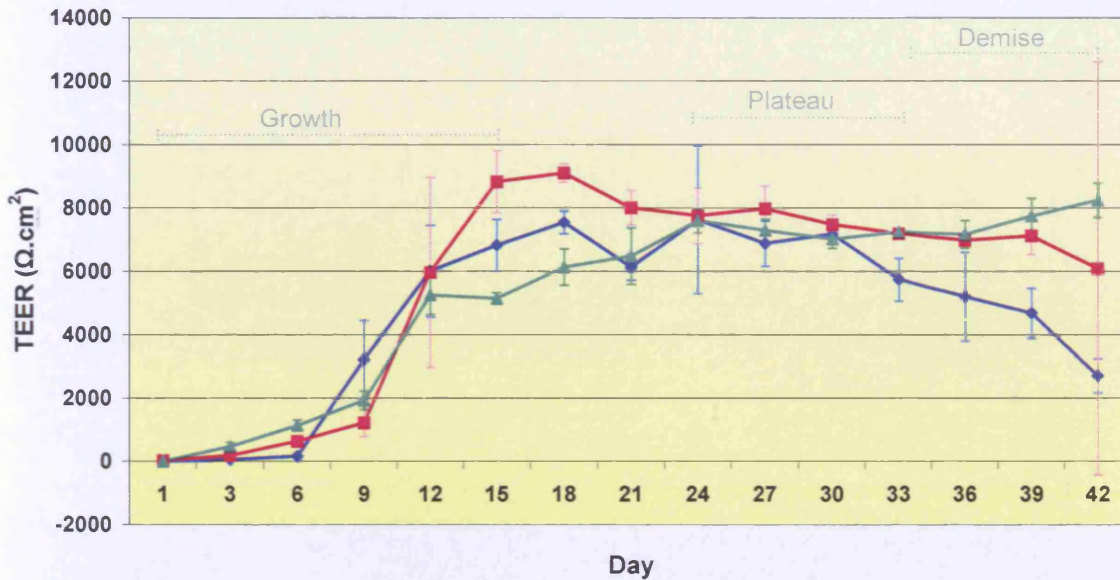


Figure 2.6 Graph displaying average TEER values for three sets of cells over the culture period (Days 1 - 42). 5F Donor (■), 8F Donor (◆), 9F Donor (▲); $n = 3$. Error bars display standard deviation. The growth, plateau and demise periods have been identified for each key TEER period.

The 8F donor's TEER increased gradually from Day 1 ($\sim 15 \Omega\cdot\text{cm}^2$) to Day 6 ($\sim 180 \Omega\cdot\text{cm}^2$). A steeper increase in TEER values occurred to Day 9 ($\sim 3,230 \Omega\cdot\text{cm}^2$) followed by a relatively steady rise to Day 18 ($\sim 7,550 \Omega\cdot\text{cm}^2$). There was a drop in average TEER values at Day 21 ($\sim 6,150 \Omega\cdot\text{cm}^2$), with the TEERs reaching a plateau between Days 24 – 30; average values remaining within the range $6,880 - 7,630 \Omega\cdot\text{cm}^2$. After Day 30, there was a gradual decline in TEER values, reaching $\sim 2,720 \Omega\cdot\text{cm}^2$ by Day 42 (Figure 2.6).

The 9F donor's TEER increased gradually from Day 1 ($\sim 20 \Omega\cdot\text{cm}^2$) to Day 9 ($\sim 1,950 \Omega\cdot\text{cm}^2$), followed by a sharper increase to Day 12 ($\sim 5,250 \Omega\cdot\text{cm}^2$). TEERs gradually increased from Day 15 ($\sim 5,150 \Omega\cdot\text{cm}^2$) until Day 24 ($\sim 7,600 \Omega\cdot\text{cm}^2$), where they plateaued until Day 39 ($\sim 7,000 - 7,800 \Omega\cdot\text{cm}^2$). There was then a slight rise in TEER values at Day 42 ($\sim 8,250 \Omega\cdot\text{cm}^2$; Figure 2.6).

2.4.3 BRADFORD ASSAY

The protein content of apical washes was determined on culture inserts ($n = 3$), via the Bradford assay. This was undertaken on 3 donors, 5F_a, 5F_b and 8F over the 42 day culture period (Figure 2.7).

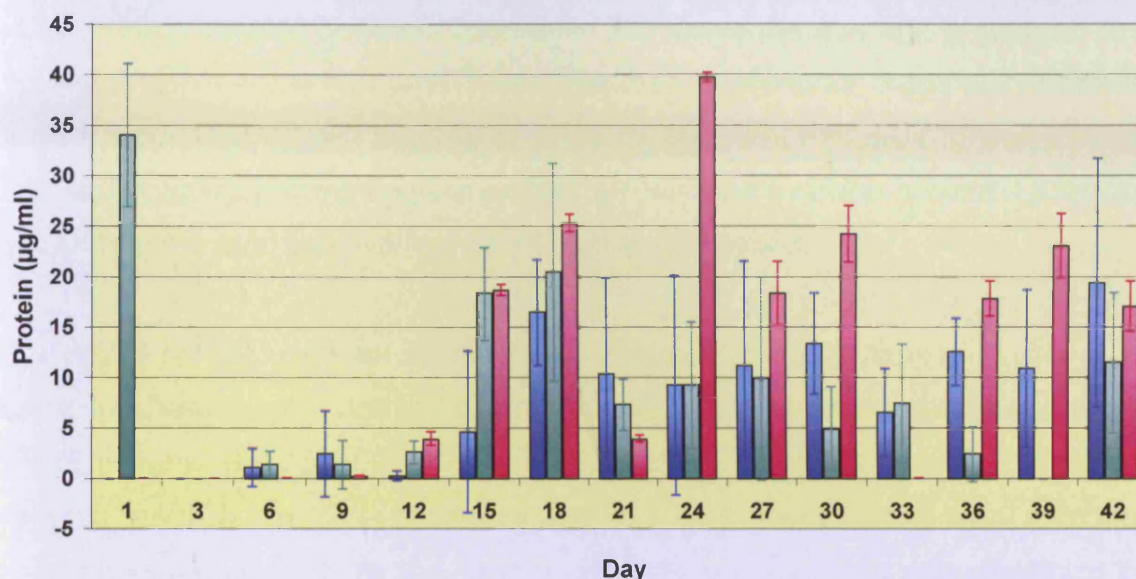


Figure 2.7 Average protein concentrations for three sets of cells over the culture period (Days 1 - 42). 5F_a Donor (■), 5F_b Donor (■), 8F Donor (■); $n = 3$. Error bars display standard deviation.

The apical media used for seeding was removed on Day 1 prior to taking an apical wash for the 5F_a donor. No protein was detected on the apical surface of NHBE cultures until Day 6 (~1.1µg/ml), the protein content remained relatively low until Days 15 and 18 (~4.6µg/ml and 16.5µg/ml, respectively) where a definite increase was observed. At this time a clear visco-elastic fluid was observed on the apical surface and was removed every 2 – 3 days to prevent excess mucin build-up. There was a plateau period in the apical protein content between Days 21 – 39, where the average protein content remained within 6.5 – 13.4µg/ml. There was then an increase in the apical protein content on Day 42, with the average at 19.4µg/ml.

The apical media used for seeding was not removed on Day 1 prior to taking the apical wash for the 5F_b donor. Therefore, the protein concentration at Day 1 was high (~34.1µg/ml). No protein was then detected on the apical surface of NHBE

cultures until Day 6 (~1.4µg/ml), the protein content remained relatively low until Days 15 and 18 (~18.4µg/ml and 20.5µg/ml, respectively) where there was a definite increase. At this time a clear visco-elastic fluid was observed on the apical surface and was removed 24 hours prior to removal of the apical wash. This was done to prevent excess mucin build-up and keep protein readings reflective of mucin production over 24 hours. There was a plateau period in the apical protein content between Days 21 – 33, where the average protein content remained within 4.9 – 10µg/ml. There was then a decrease in the apical protein content from Day 36 (~2.5µg/ml) to none by Day 39. This was followed by an increase in apical protein content on Day 42, with the average around 11.5µg/ml, higher than the average reading within the plateau period.

The apical media used for seeding was removed on Day 1 prior to taking an apical wash for the 8F donor. No protein was detected on the apical surface of NHBE cultures until Day 9 (~0.2µg/ml), the protein content remained relatively low until Days 15 and 18 (~18.7µg/ml and 25.3µg/ml, respectively) where a definite increase was observed. At this time a clear visco-elastic fluid was observed on the apical surface and was removed every 2 – 4 days to prevent excess mucin build-up. Between Days 21 and 42 the range in the apical protein concentration was large (0µg/ml – 39.7µg/ml), this was probably an artefact of the mucin removal schedule.

2.5 DISCUSSION

The principal challenge of working with an *in vitro* human lung model for inhalation toxicology was the correlation of *in vitro* data to the *in vivo* situation. The cellular model will only provide an insight into a very small piece of the overall toxicological puzzle of the human response; “by working with a very simplified cellular model, one removes many confounding factors and biodynamic interactions, which would be taking place in the human” (Adler and Li, 2001). Despite these obstacles, cellular models provide an important insight into the human physiological response to inhaled toxicants.

The airway epithelium is thought to provide the first line of defence to inhaled toxicants (Janeway *et al.*, 2005). The response of the cells lining the human respiratory tract to inhaled particles could conceivably provide an accurate insight into physiological changes that occur *in vivo*. Monitoring the early responses of these cells to various inhaled toxicants would enable increasingly accurate evaluation of drug toxicity, the identification of possible biomarkers to early pulmonary injury and the identification of new therapeutic molecular targets. The use of conventional toxicological measurements such as TEER and protein secretion was employed to evaluate the integrity of the NHBE model, when not being challenged with a toxicant, which could then be used as parameters for assessing injury to the model.

2.5.1 CELL CULTURE

Visual monitoring of cellular confluence in both T75 and T175 flasks was achieved by phase contrast light microscopy. The difference in growth rates between the PureCol™ and CellBind® flasks could also be visualised in this way. Monitoring the physical and chemical changes in cultures throughout the timeline, including culturing within inserts, forming confluent cultures with multiple-layers ('hills and valleys'; Figure 2.5), production of mucin and the presence of cilia was an effective approach. These biochemical and morphological features parallel the human lung epithelia *in vivo* (Breeze and Wheeldon, 1977).

Flasks coated in PureCol™ increased cellular growth of NHBE cells when compared to the commercially available CellBind® flasks. This increased time (48 hours) that the cells remained in Cellbind® flasks, prior to seeding into inserts, had no adverse effect on the establishment of the tissue model (plateau period; Days 21 – 36). Maintenance of NHBE cell cultures at the ALI in Transwell® inserts and the use of BEGM®/ALI media, proved to be a successful combination for establishing viable, differentiated cultures, as demonstrated by the multi-layered, mucus secreting and functional cilia.

However, when NHBE cells were cultured without collagen in the flasks, no adverse effect was observed. Despite the fact that the NHBE cells required an

additional 24 hours in T75 flasks compared to the PureCol™ and CellBind® flasks, once seeded into T175 flasks they reached confluency the same time as the PureCol™ coated flasks (96 hours post-seeding). Therefore, as no collagen coating was necessary for the culturing of the NHBE cells, this was removed from the protocol. Moreover, non-coated flasks are less expensive and remove a potential source of contamination. Prior to the culturing of NHBE cells in non-coated flasks a colleague determined that: the culturing of NHBE cells in Millipore® inserts produced better cultures than those in Transwell® inserts (culture viability and TEER; Hughes, 2009). Based on these observations it was decided to culture NHBE cells in Millipore® inserts. However, Millipore® inserts do not allow visualisation of cultures via phase contrast light microscopy, and as such Transwell® inserts ($n = 6$) were also seeded from every batch to allow this.

2.5.2 TRANS-EPITHELIAL ELECTRICAL RESISTANCE

TEER values are considered to be a valid measurement of junctional formation in cell cultures (Gardner *et al.*, 1997). It was apparent from the TEER values over the development of the model that junctions form in the NHBE lung construct (Figure 2.6). Different sets of NHBE cells produced similar TEER profiles throughout the development of the model. The rapid increase in TEER values before the plateau stage (Days 6 – 18) implied that cellular junctions were forming during this period. Tissue integrity, with respect to junction formation, was maintained during the plateau phase (Days 24 – 33). Variation in TEER values was observed after this period (Days 36 – 42), with some values exceeding and others below the plateau range. An increase in the TEER at this stage could indicate a defence mechanism, whereby cultures are attempting to ‘rescue’ themselves from culture deterioration. Those cultures that produced a low or non-existent TEER reading are thought to have undergone culture demise.

2.5.3 BRADFORD ASSAY

The Bradford assay confirmed that NHBE cells secreted a proteinaceous substance onto their apical surface. As a general rule there was no significant amounts of protein present on the apical surface until around Day 15/18, this

suggested that goblet cells may now be present within the cultures. More significance should be taken on the apical protein concentrations of the 5F_b donor, as the apical mucin from this donor was the most consistently removed. However, the others must not be discarded, but interpreted with caution. As a general rule, from all three donors, the protein concentration increased gradually before reaching a plateau level between Days 21 – 33. During the tail-end of the culture life the protein concentration decreased (Days 36 – 39) before increasing at Day 42. This general pattern correlated relatively well with the TEER pattern, with both parameters following similar profiles. The changes in protein content near the end of the culture period could also indicate problems with the cultures and the beginning of their demise. Prior to Day 36, mucin was thought to be the source of the protein secreted apically, as upon close inspection the clear substance appeared highly viscous (Widdicombe, 2002). However, further confirmation, via a PAS stain (Chapter 4), was required to prove this assumption. From Day 36 onwards, this viscous substance was produced by some, but not all cultures, indicating an alternative reason for the protein content obtained in apical washes. Combining this information with the TEER data, it was deduced that increases in protein at Day 42 may be due to cellular debris, in co-ordination with the deterioration of the culture.

2.6 CONCLUSIONS

Data from the cell culture optimisation and physiochemical characterisation experiments suggested that the NHBE cell culture system may represent a viable *in vitro* model for further exploration as an alternative for *in vivo* inhalation toxicology studies. The collective findings over a 42 day characterisation period suggested that experimentation might be performed within a relatively large time frame; the consistent plateau in data occurring between Day 21 and Day 33. This wider experimental window presents an advantage to working with this system versus commercial models (e.g. MatTek[®] system), allowing both acute and chronic injury/repair mechanisms to be investigated. Additionally, the close correlation observed between the 3 donors indicated that there was little donor variation and as long as definite parameters are set-out during experimentation this does not need to be considered further. During the latter part of the culture

period, the NHBE culture appeared to undergo culture demise. This was not wholly unexpected, since primary cells only possess a finite number of cellular divisions (Freshney, 2005).

Changes in growth parameters such as, TEER, cell viability and protein secretion provide a better understanding of the response of human bronchial epithelial cells to possible toxins. Other characterisation parameters need to be explored to further validate this model as a viable *in vitro* alternative of the human tracheobronchial epithelia. These will include detailed morphological analysis of the mixed muco-ciliary phenotype (Chapter 3 and 4), formation of tight junctions (Chapter 4) and the confirmation of mucin producing goblet cells (Chapter 4).

CHAPTER 3:

CHARACTERISATION OF

MORPHOGENESIS IN THE NHBE

MODEL

3.1 INTRODUCTION

Previous work (Chapter 2), determined the key biophysical properties of the NHBE construct. In order to compliment these parameters, parallel, morphological analysis was undertaken. Characterisation of the cell culture morphogenesis involved light and electron microscopic evaluation of the key cellular events (e.g. cell-cell contacts, confluency, tight junction formation, ciliogenesis, differentiation, etc) as denoted by the biophysical data. Morphogenesis was characterised every 3 days for 42 days of culture growth. The culture development was also compared to the *in vivo* regeneration of the respiratory epithelium from biopsy samples removed from a chronic obstructive pulmonary disease (COPD) patient.

Light microscopy (LM) provided a general picture of the cell viability and tissue morphology of the culture system, allowing cell numbers, layers and shape to be visualised. Cultures were fixed, sectioned, mounted on glass slides and stained for histological evaluation. LM histological assessment provided cross-sectional views of the cultures at the microscopic level. Comparison of NHBE sections against human lung biopsy samples enabled a direct comparison with the *in vivo* situation.

Transmission electron microscopy (TEM) allowed cross-sectional observation of the cellular ultrastructure at the sub-micron level. This permitted identification of the fine structural details of the cells/tissue not visible at the LM level. Intra-cellular components found in eukaryotic animal cells, as well as the determination of inter-cellular junctions, could be elucidated. Apical structures such as microvilli and cilia were also observed. Scanning electron microscopy (SEM) enabled the 3-dimensional observation of the surface topography of the NHBE constructs at the sub-micron level, thus, enabling a more complete picture of the culture morphology at the interior and exterior levels.

The specific research aim of the following chapter of work was to obtain a working knowledge of the physio-chemical growth parameters of the cell culture model. This was done firstly to validate the NHBE model as an *in vivo* alternative and

secondly in order to evaluate any changes, in response to toxicological challenges (Chapters 5 and 6).

3.2 MATERIALS AND STOCK SOLUTIONS

3.2.1 MATERIALS

MATERIALS	SUPPLIER
Copper Grids, 200-mesh, 3.05mm Whatman N° 1 Filter Paper, 90mm LEIT Adhesive Carbon Tabs, 12mm Aluminium Stubs, 12.5mm diameter, 8mm pin length	Agar Scientific, UK

Table 3.1 Table of materials used and their suppliers.

3.2.2 STOCK SOLUTIONS

SOLUTIONS	SUPPLIER
1% Gluteraldehyde	EM Services, Heath Campus, Cardiff University, UK
2% Osmium Tetroxide 2% Uranyl Acetate (UA) Propylene Oxide Araldite CY212 Dodyceny Succinic Anhydride Benzyl Dimethylamine Reynold's Lead Citrate	Agar Scientific, UK
Sodium Acetate Maleic Acid	Fisher Scientific, Manchester, UK
0.5% Toluidine Blue DPX Mountant	VWR International Ltd., Poole, UK

Table 3.2 Table of stock solutions used and their suppliers.

SOLUTIONS	SUPPLIER
1% Borax 10% Neutral Buffered Formalin Xylene (Mixture of Isomers)	Sigma, Dorset, UK
Micromount	Surgipath Europe Ltd., Peterborough, UK

Table 3.2 Continued table of stock solutions used and their suppliers.

3.2.3 EQUIPMENT

EQUIPMENT	SUPPLIER
Diamond Knife, 2.5mm edge, 45° blade angle	Agar Scientific, UK
Leica RM2135 Microtome Phase Contrast LM (DM2500) Digital Camera (Leica DFC 320)	Leica Ltd., Milton Keynes, UK
TEM 208	Phillips, UK
Critical Point Drier (CPD 030)	Balzers, Liechtenstein
EMScope (Sputter Coater)	EMScope Laboratories, Ashford, UK
FE-SEM Philips XL-30	Philips Electron Optics, Eindhoven, Netherlands

Table 3.3 Table of equipment used and their suppliers.

3.3 METHODS

3.3.1 LIGHT MICROSCOPY: TOLUIDINE BLUE

Optimisation of the methods in this section was aided by Dr. A. Hann (Biosciences Electron Microscopy Unit) and Mr. C. von Ruhland (Heath Campus Electron Microscopy Unit, Cardiff University, UK), along with technical help and support.

3.3.1.1 TISSUE PROCESSING

Cell culture inserts were immersed in 1% glutaraldehyde (RT) for 2 hours. This method of fixation preserved the cellular structure of the tissue by cross-linking proteins via their amine groups. The sample was then removed from the glutaraldehyde and placed in a fresh 25ml Universal tube with 2ml phosphate buffered saline (PBS) and stored at 4°C.

Culture inserts were placed in a 24 well plate and immersed in fresh PBS (10 minutes). Post-fixation was carried out by osmication (1% osmium tetroxide in PBS) for 2 hours (RT). This was removed and cultures washed with 0.05M sodium acetate (pH 5.9) for 15 minutes (x4).

3.3.1.2 STAINING

Culture inserts were stained with 0.5% uranyl acetate (UA), pH 6.2. UA (0.5%) was made with 2% UA 1:4 v/v with maleic acid. The final sodium acetate (0.5M) wash was removed and replaced with 0.5% UA (45 minutes, RT).

3.3.1.3 DEHYDRATION

UA (0.5%) was removed and discarded in a radioactive waste container and replaced with 0.05M sodium acetate (pH 5.9). Inserts containing cultures were passed through a series of graded alcohols; 30% → 50% → 70% → 90% → 100% (x2), 10 minutes in each. Once dehydrated, culture inserts were pinned upside-down with tweezers in a beaker of 100% ethanol; a scalpel was used to cut the membrane out from the insert.

3.3.1.4 RESIN INFILTRATION

Membranes were placed in 100% ethanol, which was pipetted off and replaced with propylene oxide for 10 minutes (x2). Membranes were then left overnight in a 1:1 (v/v) resin:propylene oxide mixture. The resin contained, araldite CY212 (10g), dodyceny succinic anhydride (10g), benzyl dimethylamine (0.3g). During

the overnight incubation (~12 – 18 hours), in fume cupboard (RT), the propylene oxide slowly evaporated leaving only the resin.

3.3.1.5 RESIN EMBEDDING

The resin used for embedding the cultures was prepared (5g araldite CY212, 5g dodyceny succinic anhydride, 0.15g benzyl dimethylamine) and mixed with a wooden spatula, causing bubbles to form in the resin mixture. The resin was placed in an oven (60°C) until the bubbles disappeared. A section of the culture (~2.5 x 8mm) was cut to ensure it fitted in the resin mould (12 x 5 x 3mm). The resin mould was half filled with resin prior to placing the membrane slice into it. Once the membrane slice was placed into the mould, it was filled with resin, ensuring no bubbles formed. The resin embedded cultures were placed in an oven (60°C) for 48 hours.

3.3.1.6 SEMI-THIN SECTIONING

Following resin polymerisation, the resin block containing the culture section was removed from the mould. Excess resin was trimmed from the blocks until the tissue was exposed. Resin blocks were sectioned into 2µm sections using a diamond knife. Toluidine blue staining was performed by drying the sections on to the slide by placing them on a 60°C hotplate. Once the slides had dried, several drops of 0.5% toluidine blue (in 1% borax) was placed onto the sections for 1 – 2 minutes depending on depth of colour required (slides remained on the hotplate throughout this process). The excess stain was removed by gentle, but thorough rinsing with distilled water, the slides were then air-dried and cover-slips mounted with Micromount (20µl).

3.3.2 TRANSMISSION ELECTRON MICROSCOPY

Methods in this section and technical support were provided by Dr. A. Hann (Biosciences Electron Microscopy Unit, Cardiff University, UK).

3.3.2.1 TISSUE PROCESSING

NHBE cultures to be processed for TEM were initially prepared in the same way as those for light microscopy: toluidine blue, up until the end of the resin embedding step (Sections 3.3.1.1 – 3.3.1.5). The culture membranes were then sectioned (Section 3.3.2.2).

3.3.2.2 ULTRA-THIN SECTIONING

Resin blocks were sectioned to 60 – 90nm on a Leica RM2135 microtome using a diamond knife. Sections were floated on a water trough and collected onto clean 200-mesh, 3.05mm copper grids.

3.3.2.3 COUNTER-STAINING

Prior to visualisation of the tissue sections via TEM, heavy metal staining or “counter-staining” was required to help resolve the ultrastructure of the cells. Counter staining was achieved by using Reynold’s lead citrate and 2% aqueous UA. These heavy metal stains are general purpose and not very specific.

Droplets of each stain were placed in rows on the sterile side of parafilm and the grids were floated section side down on a given drop. Sections were stained for 10 minutes with UA, followed by staining with Reynolds Lead Citrate for 5 minutes. Finally, the grids were washed by transferring over 3 drops of filtered de-ionised water. The grids were allowed to air dry at room temperature in filter paper-lined Petri dishes prior to viewing in the TEM. The sections were imaged using a Phillips TEM 208 at an acceleration voltage of 80 KeV.

3.3.3 SCANNING ELECTRON MICROSCOPY

3.3.3.1 TISSUE PROCESSING

NHBE cultures to be processed for SEM were initially prepared in the same manner as those for light microscopy: toluidine blue, up until the end of the

dehydration step (Sections 3.3.1.1 – 3.3.1.3). The culture membranes were then immersed in 100% ethanol in preparation for critical point drying (CPD).

3.3.3.2 CRITICAL POINT DRYING

Still immersed in 100% ethanol, the membranes were transferred into individual wells in a 6-well metal specimen holder. The specimen holder containing the membranes was placed into the specimen chamber of the critical point drier, which was filled with 100% ethanol. The critical point dryer (CPD 030) was programmed to cool the chamber to 4°C. The 'medium in' button was pressed, which added liquid carbon dioxide (CO₂) to the specimen chamber, until the air bubbles disappeared. The 'medium in' button, followed by the 'medium out' button was pressed in order to purge the ethanol out of the specimen chamber. Filter paper was used to detect the presence of ethanol exiting the specimen chamber at the outlet tube (wetness = ethanol). Once all the ethanol had been flushed out, the chamber was re-filled with liquid CO₂. The CPD was programmed to gradually raise both the temperature (to 37°C) and the pressure (to 80 bar). Once these conditions were met, the CPD gradually (over 2 hours) lowered both the temperature and pressure back to normal (21°C and 0 bar). The dried (CPD) membranes were removed from the specimen holder ready for mounting.

3.3.3.3 MOUNTING

A double-sided adhesive carbon 'sticker' was secured onto a labelled, SEM specimen stub (aluminium; 12mm diameter). Dried membranes were examined under a stereoscope in order to locate the cell-side of the membrane (dull side). Tweezers were then used to transfer the membrane and stick it cell-side-up onto the adhesive carbon tab. Taking care to only ever touch the outer-edge of the membrane, the edges were pressed down gently to ensure adequate attachment to the carbon sticker.

3.3.3.4 SPUTTER COATING

The metal SEM sample stubs, with attached membranes, were placed into the sample chamber (maximum 6 stubs) of the sputter coater machine (EMScope). The sample chamber lid was closed and the 'start cycle' button pressed. The argon gas replaced the air within the sample chamber; once replaced by argon, a current generated the release of gold particles onto the top of the specimen, coating them in a 0.5µm layer of gold. The vacuum inside the specimen chamber was then released, causing the lid to open. Samples were coated twice with gold before being removed from the sputter coater specimen chamber. The samples were now deemed ready for viewing and images were taken with the Field Emission-SEM (Phillips XL-30) with an accelerating voltage of 20kV, spot size of 4.0 and a working distance between 5 and 10.1mm.

3.3.4 LIGHT MICROSCOPY: *IN VIVO-IN VITRO* CORRELATIONS

Images of archival, human, lung biopsy samples from a COPD patient were provided by AstraZeneca (Dr. Martyn Foster, AstraZeneca R&D, Loughborough, UK). Samples had previously been sectioned and stained for standard LM histological examination (by AstraZeneca) using Haematoxylin and Eosin (H&E); a routine stain chosen for its ability to stain various cellular components of tissue. Haematoxylin is a basic dye that stains nuclear heterochromatin and cytoplasm rich in ribonucleoprotein blue. Eosin is an acid dye that stains cytoplasm, muscle and connective tissue various shades of pink. Photomicroscopy was undertaken by Dr. Martyn Foster, chief pathologist (AstraZeneca R&D, Loughborough, UK). The COPD H&E stained sections were compared with NHBE H&E sections (Section 3.3.4.1 – 3.3.4.6) over the models development (Days 1 – 42).

3.3.4.1 TISSUE PROCESSING

Cell culture inserts were immersed in 10% neutral buffered formalin (4°C) for 24 hours, in preparation for paraffin embedding and sectioning. Tissue processing, i.e. paraffin embedding, sectioning and staining, was carried out by a histotechnologist, Mr Derek Scarborough (School of Biosciences, Cardiff

University, UK). A brief overview of these procedures has been outlined below in Sections 3.3.3.1 – 3.3.4.6.

Once the tissue was fixed (Section 3.3.4.1), it had to be processed into a form in which it could be made into thin microscope sections. This was achieved by embedding tissues in paraffin, that was similar in density to tissue and could be sectioned at anywhere from 3 – 10µm. The main steps in the processes dealing with wet-fixed tissue were 'dehydration', 'clearing' and 'paraffin infiltration'.

Wet-fixed tissues, such as the NHBE cell cultures from this study, could not be directly infiltrated with paraffin. The water from the tissues had to be removed by 'dehydration' via a series of alcohols (e.g. 70% to 95% to 100%). Following dehydration, the next step was 'clearing' and consisted of replacement of the dehydrant (i.e. alcohol), with a substance that would be miscible with the paraffin. The common clearing agent was xylene and the tissues were processed through several changes of this. The final step in processing was to infiltrate the tissue with molten paraffin wax at 60°C; several changes of wax were used. All the above processes were undertaken by placing the NHBE cultures in plastic processing cassettes and placed in an automated, fully-enclosed, Vacuum Tissue Processor (Leica TP1050, Leica UK).

3.3.4.2 PARAFFIN EMBEDDING

It was essential for the tissue to be fully supported by paraffin wax to prevent tissue shredding during sectioning. This was achieved by placing the "cleared" tissue into a vacuum to remove all air pockets. The NHBE cell culture membrane was then placed into a plastic 'embedding mould' and embedded in warm paraffin wax (Leica EG1140 Embedding Centre, Leica, UK). After allowing the wax to set (30 minutes on a cold plate), the tissue was removed from the embedding mould and the sample was ready for sectioning.

3.3.4.3 SECTIONING

Following tissue processing and paraffin embedding, the NHBE cell culture had to be cut into sections that could be placed on a glass slide for the purpose of LM. Sectioning was achieved using a Leica RM2135 microtome. The embedded lung tissue samples were placed on ice to ensure uniform sections were obtained. The ice hardened the wax and softened the tissue, so the entire sample was of the same consistency for sectioning. The tissue was then cut into 5µm sections using the microtome.

Once sections were cut, they were floated on a warm water bath (40 – 50°C) that facilitated the removal of any wrinkles and air bubbles produced during sectioning. Paraffin embedded sections were then collected on to a pre-coated, poly-L-lysine, glass microscope slides; for improved adhesion of sections. Samples were then left to bind to the slides on a hot plate for 15 – 30 minutes, then in an oven (37 – 45°C) for a minimum of 24 hours.

3.3.4.4 DE-WAXING

The embedding process must be reversed (de-waxing) in order to remove paraffin wax from the tissue allowing water soluble dyes to penetrate the sections. Therefore, before any staining could be accomplished, the slides were “deparaffinized” by running them through xylene (x2) followed by series of graded alcohol; 100% (x2) → 95% → 70%. The slides were immersed in each of these solutions for 2 minutes, followed by being placed under running tap water for 2 minutes.

3.3.4.5 HAEMATOXYLIN AND EOSIN STAINING

Once de-waxed, tissue sections were immersed with Mayer’s haematoxylin for 1.5 minutes. Excess dye was removed by placing the slides in running tap water for 5 minutes.

3.3.4.6 DEHYDRATION

The H&E stained slides were dehydrated by immersing (2 minutes) in an increasing series of alcohol; 70% → 95% → 100% (x2) and xylene (x2).

Slides remained in xylene until ready for cover-slips to be fixed onto them. A small drop (20µl) of DPX mountant was placed on a cover-slip and the slide carefully lowered onto the cover-slip and DPX. The sections were viewed using a Leica Phase Contrast LM (DM2500) attached to a digital camera (Leica DFC 320) and images saved as TIF files.

3.4 RESULTS

3.4.1 LIGHT MICROSCOPY: TOLUIDINE BLUE

3.4.1.1 DAYS 1 – 6

NHBE cells prepared from Day 1 (24 hours post-seeding) inserts demonstrated a monolayer of cells with a patchy adherence (i.e. gaps between cells). Cellular integrity was verified by intact cellular membranes and nuclear components. Free surfaces of the cells (i.e. not in contact with the insert membrane) appeared to have many cellular projections, with some of these beginning to form cell-cell contacts and inter-cellular gaps separated other cells (Figure 3.1[A]).

By Day 3, a confluent culture had formed, with two distinct layers visible. Small inter-cellular gaps were still observed between cells (Figure 3.1[B]). Cells at Day 6 remained squamous in shape, with the two distinct cell layers more compact and inter-cellular gaps receding into the basal regions. However, intermediate cells could be observed in between the two distinct cell layers. Additionally, microvilli could be defined on the apical surface (Figure 3.1[C]).

3.4.1.2 DAYS 15 – 30

No major changes were noted between Days 6 and 18, at the microscopic level, apart from culture compaction and cell de-squamation (evident at Day 15; Figure 3.2[A]). By Day 18 cells appeared more columnar and cultures displayed evidence of differential cell types within. Basal cells were evident in the basolateral region of the cultures and were more rounded in comparison to the cells forming the apical barrier (Figure 3.2[B]). Further development into a fully-differentiated, pseudo-stratified, bronchial epithelium occurred after Day 18 and was clearly evident in cultures at Day 30 (Figure 3.2[C]). This differential morphology remained until Day 36.

3.4.1.3 DAYS 36 – 42

The tissue became slightly distorted at Day 36, with the two nuclear layers becoming less distinct. Inter-cellular gaps began to appear around the basal cells (Figure 3.3[A]).

Day 39 cultures displayed further deterioration, with vacuoles developing inside the cells at the apical region and between the basal and surrounding cells. The basal cells became squamated and the previously columnar-shaped cells at the apex, also developed a squamous phenotype (Figure 3.3[B]).

By Day 42, cultures deteriorated significantly, as denoted by an undifferentiated monolayer culture. Demise in culture viability was apparent given that the nuclei were barely detectable and the toluidine blue staining was very faint (Figure 3.3[C]).

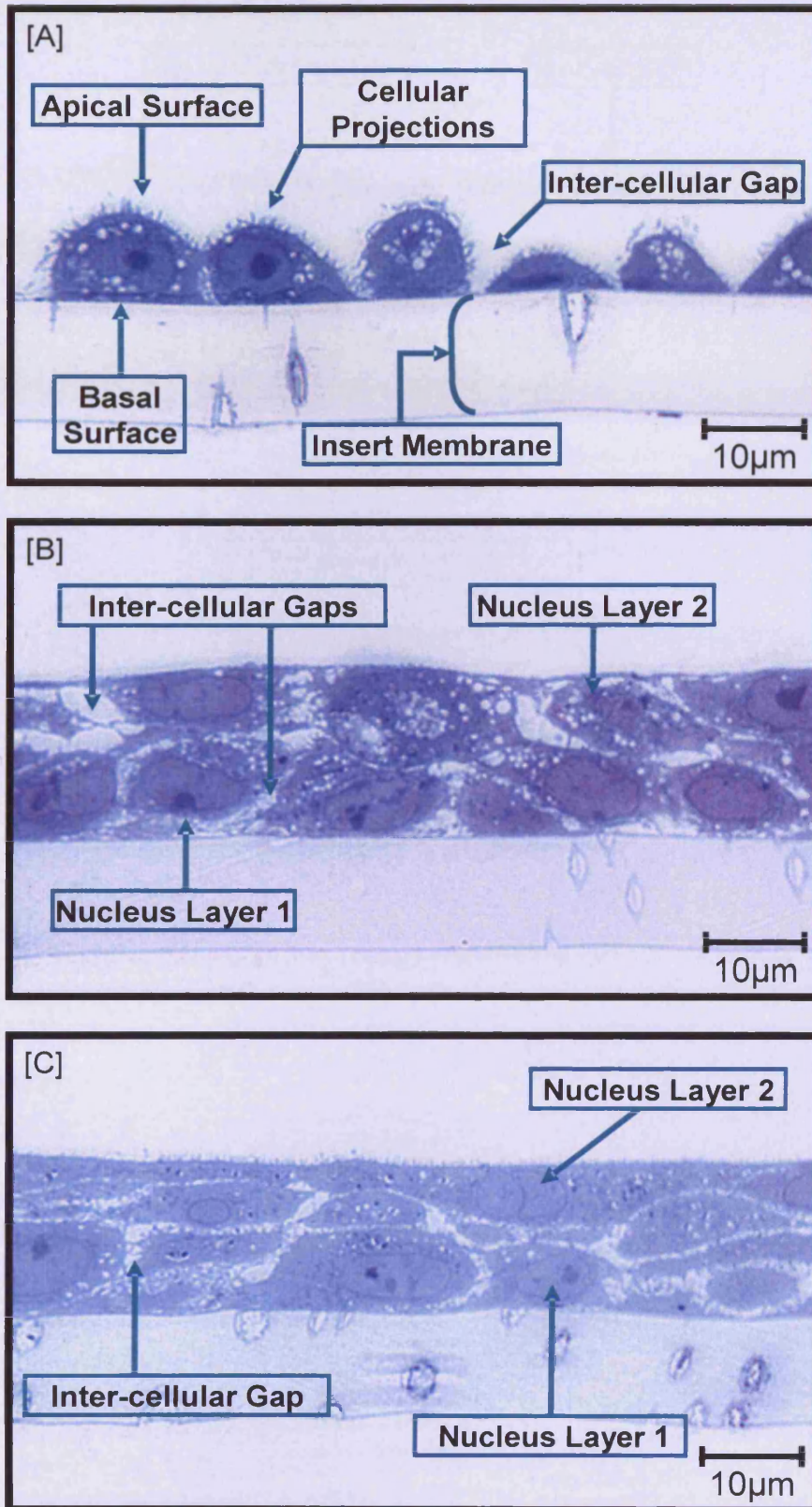


Figure 3.1 LM images of NHBE cultures stained with toluidine blue. [A] Day 1; cells attached to the membrane, covered with cellular projections forming cell-cell contacts. [B] Day 3; smaller intra-cellular gaps and two distinct cell layers formed. [C] Day 6; cellular attachments compact the culture further, inter-cellular gaps more basal and microvilli visible on the apical surface.

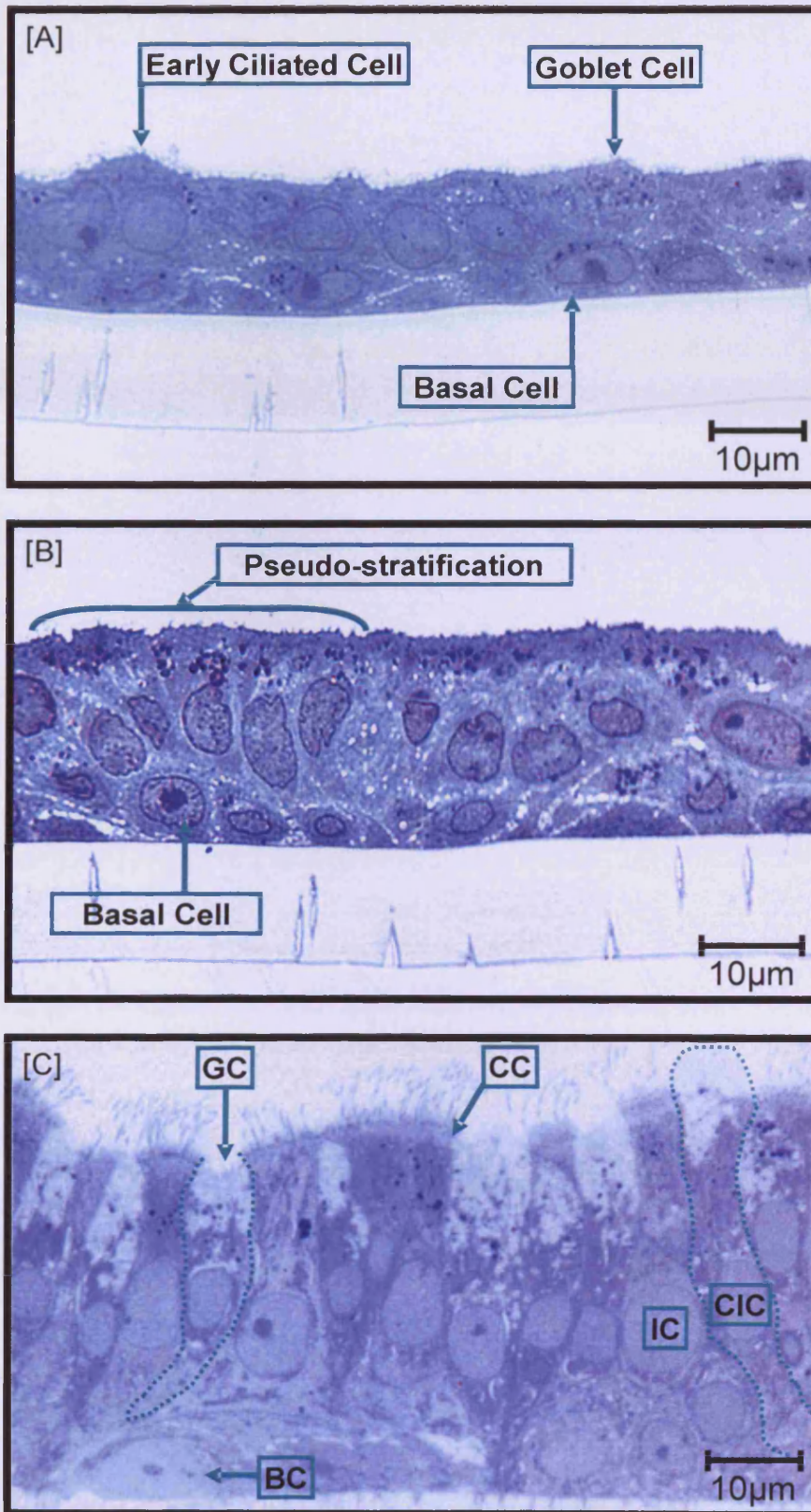


Figure 3.2 LM images of NHBE cultures stained with toluidine blue. [A] Day 15; cell-cell junctions tighter. [B] Day 18; columnar and basal cells distinguishable, mucin granules on apical surface of some cells. [C] Day 30; fully-differentiated, pseudo-stratified epithelium, containing goblet cells (GC), ciliated cells (CC), Clara cells (CIC), intermediate cell (IC) and basal cells (BC).

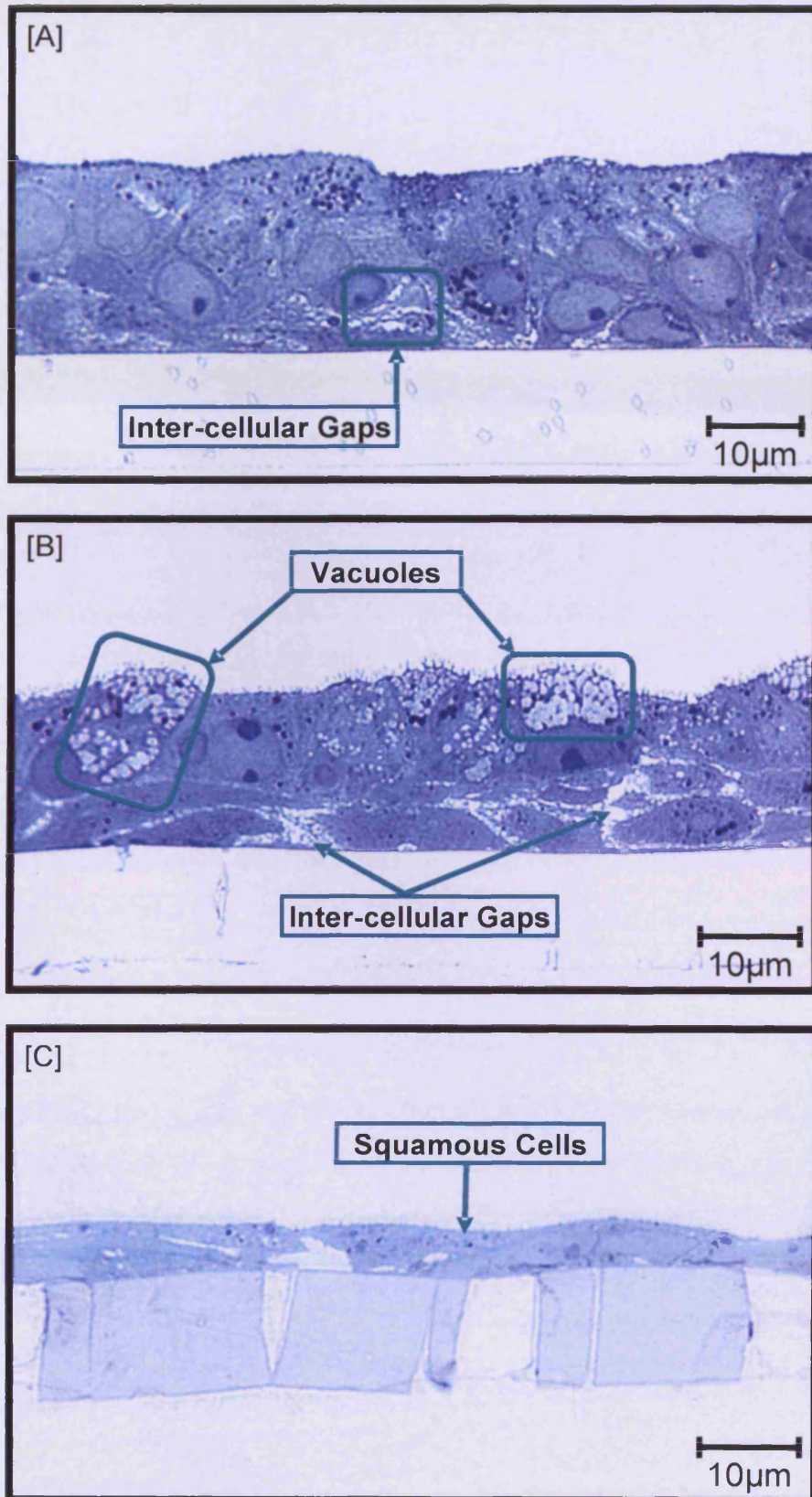


Figure 3.3 LM images of NHBE cultures stained with toluidine blue. [A] Day 36; cultures begun to deteriorate, formation of inter-cellular gaps. [B] Day 39; cells were relatively squamous containing vacuoles and inter-cellular gaps throughout cultures. [C] Day 42; cultures were undifferentiated and squamous. Multi-layered regions deteriorated to squamous monolayered regions.

3.4.2 TRANSMISSION ELECTRON MICROSCOPY

3.4.2.1 DAYS 1 – 9

Day 1 revealed a single cell layer adhered to the insert membrane. Inter-cellular gaps were present between neighbouring cells, with numerous cellular projections protruding from the cell surface (Figure 3.4[A]).

Culture structure changed drastically by Day 3, with the loss of inter-cellular gaps and an increase in cellular organelles (Figure 3.4[B]). Microvilli were clearly observed along the apical surface of the cells (Figure 3.4[C]).

Further development was apparent at Day 6, as revealed by two nuclear layers and evidence of cellular differentiation. Basal cells appeared more rounded and were present at the basolateral surface (Figure 3.5[A]). Clara cells were identified by their numerous electron-lucent and -dense membrane bound inclusions (confirmed experimentally, Chapter 4, Section 4.4.2). By Day 9, initial tight junction formation, as well as other cell-cell attachments in the form of adherens junctions and desmosomes, were apparent (Figure 3.5[B] – [C]).

3.4.2.2 DAYS 12 – 21

The models complexity increased greatly by Day 12, with immature goblet cells identified (Figure 3.6[A]). Mature tight and adherens junctions were observed at the most apical co-joining of cells. Desmosomes, inter-cellular junctions and interdigitations were present at cell-cell attachments throughout (Figure 3.6). A serous cell, with apically located electron-dense, secretary granules was identified, with high magnification revealing the glycocalyx around microvilli (Figure 3.6[D]).

Cilia were clearly visible at Day 18, enabling concise identification of ciliated cells. Cilia were anchored by basal bodies, with numerous mitochondria located in the apical region of ciliated cells (Figure 3.7[A]). Intermediate cells were also easily

identified due to their location between the basal and apical regions, as well as their loose cell-cell contacts (to allow migration and expansion) (Figure 3.7[B]).

Cultures were well-differentiated at Day 21, containing basal cells (image not shown), cilia covered ciliated cells, goblet cells (image not shown) and Clara cells. The Clara cell depicted was identifiable by its cytoplasmic content, domed-shaped apex with finger-like projections that protruded above the ciliated cell and the interdigitations with the bordering ciliated cell (Figure 3.7[C]).

3.4.2.3 DAYS 30 – 33

Cultures at Day 30 displayed a well-defined, pseudo-stratified epithelium, containing: basal, goblet, Clara and ciliated cells, with all cells appearing to attach to the membrane and non-basal cells being columnar in shape (Figure 3.8[A]). Mucin release was evident (Figure 3.8[B]) along with mature cilia, surrounded by mucin and/or glycocalyx (Figure 3.8[C]).

Day 33 cultures displayed the differentiated phenotype, with tight junctions and interdigitations clearly observed (Figure 3.9[A]). High magnification cross-sections of cilia revealed the characteristic “9+2” structure of the axonemes (Figure 3.9[B]).

3.4.2.4 DAYS 36 – 42

Morphological observations at Day 36, revealed the onset of cell/epithelial deterioration. Cells appeared squamous, with less distinction between basal and non-basal cells, vacuoles appeared within the cytoplasmic compartments of cells, as well as the formation of inter-cellular gaps (Figure 3.9[C]).

At Day 39 the dedifferentiation process was in full force, as denoted by; widespread deterioration and squamation, development of large vacuoles, indistinct cellular organelles and structures and an increase in goblet cells (Figure 3.10[A]). However, interdigitations could still be observed between cells (Figure 3.10[B]). Cultures at Day 42 revealed continued deterioration (Figure 3.10[C]).

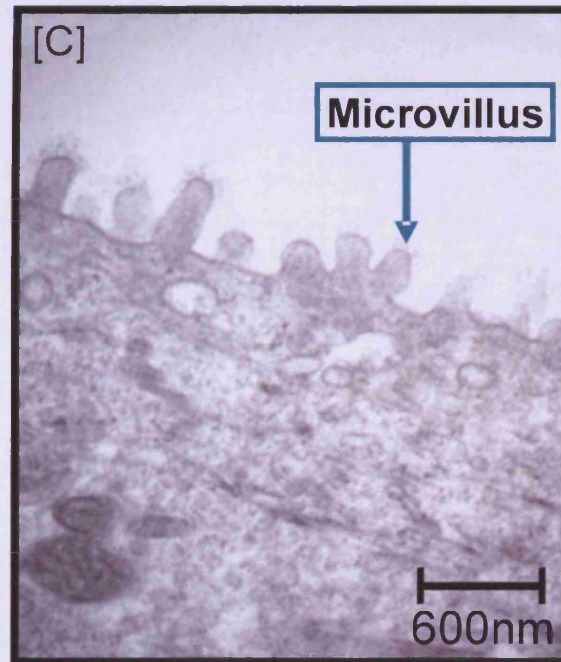
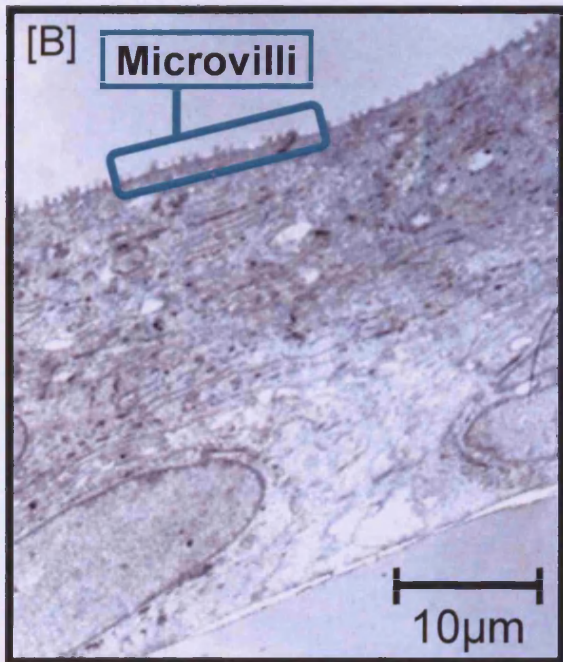
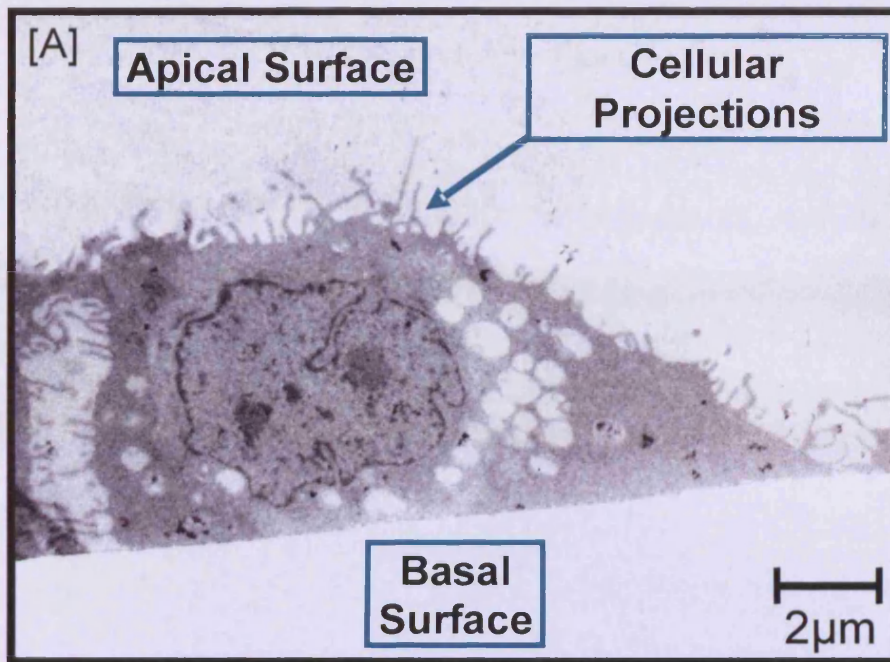


Figure 3.4 TEM images of NHBE cultures on Day 1 and 3. [A] Day 1; inter-cellular gaps appear between cells, numerous cell surface projections beginning to form cell-cell contacts. [B] Day 3; overview of cultures, cell-cell contacts formed, microvilli visible on the apical surface. [C] Day 3; high magnification of the apical surface, clearly showing microvilli and evidence of organelle development.

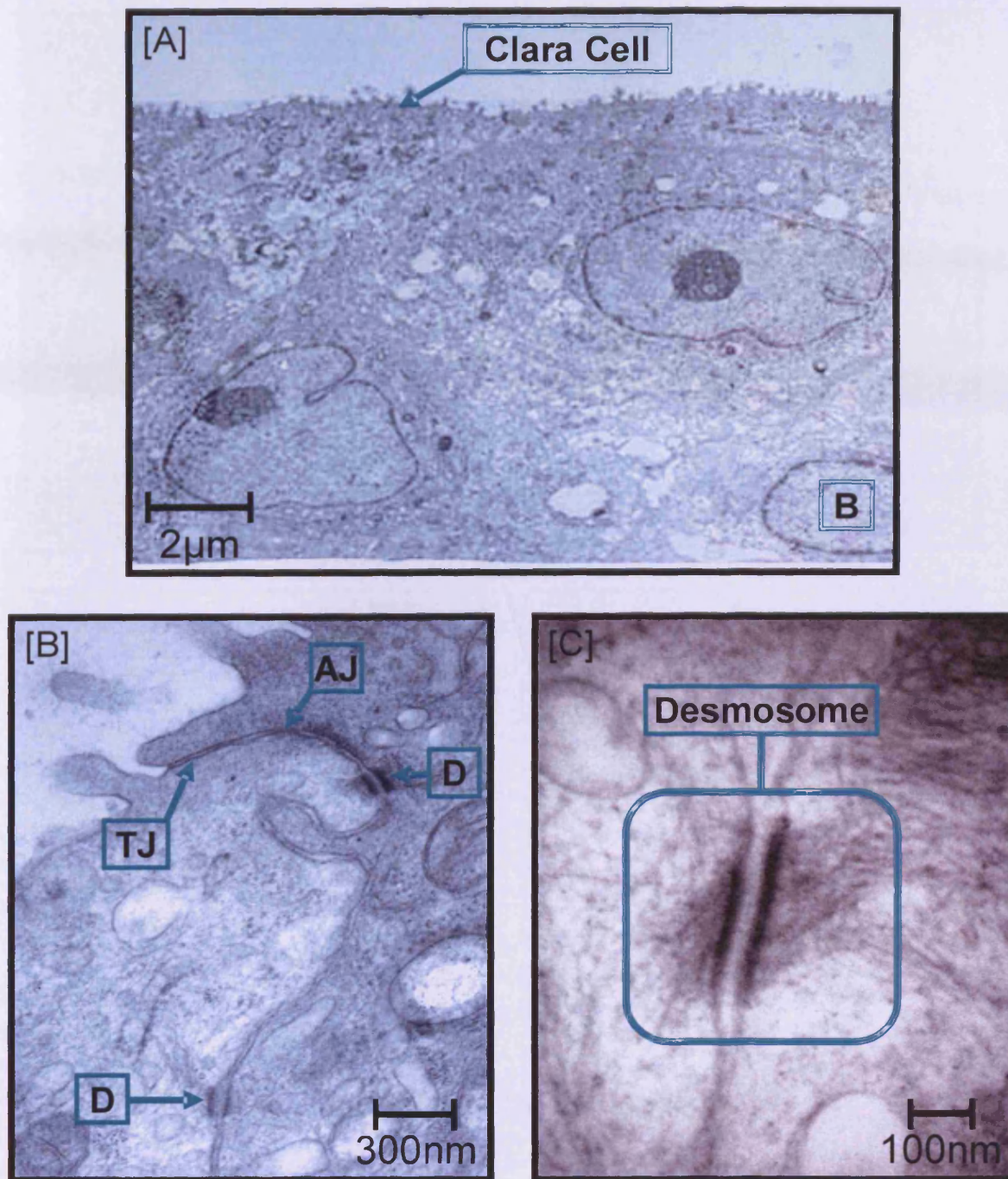


Figure 3.5 TEM images of NHBE cultures on Day 6 and 9. [A] Day 6; overview of the culture, basal cells (B) and a Clara cell can be observed. [B] Day 9; high magnification of the cell-cell contacts between two adjacent cells displaying a tight junction (TJ), adherens junction (AJ) and desmosomes (D). [C] Day 9; high magnification of a desmosome observed between two adjacent cells.

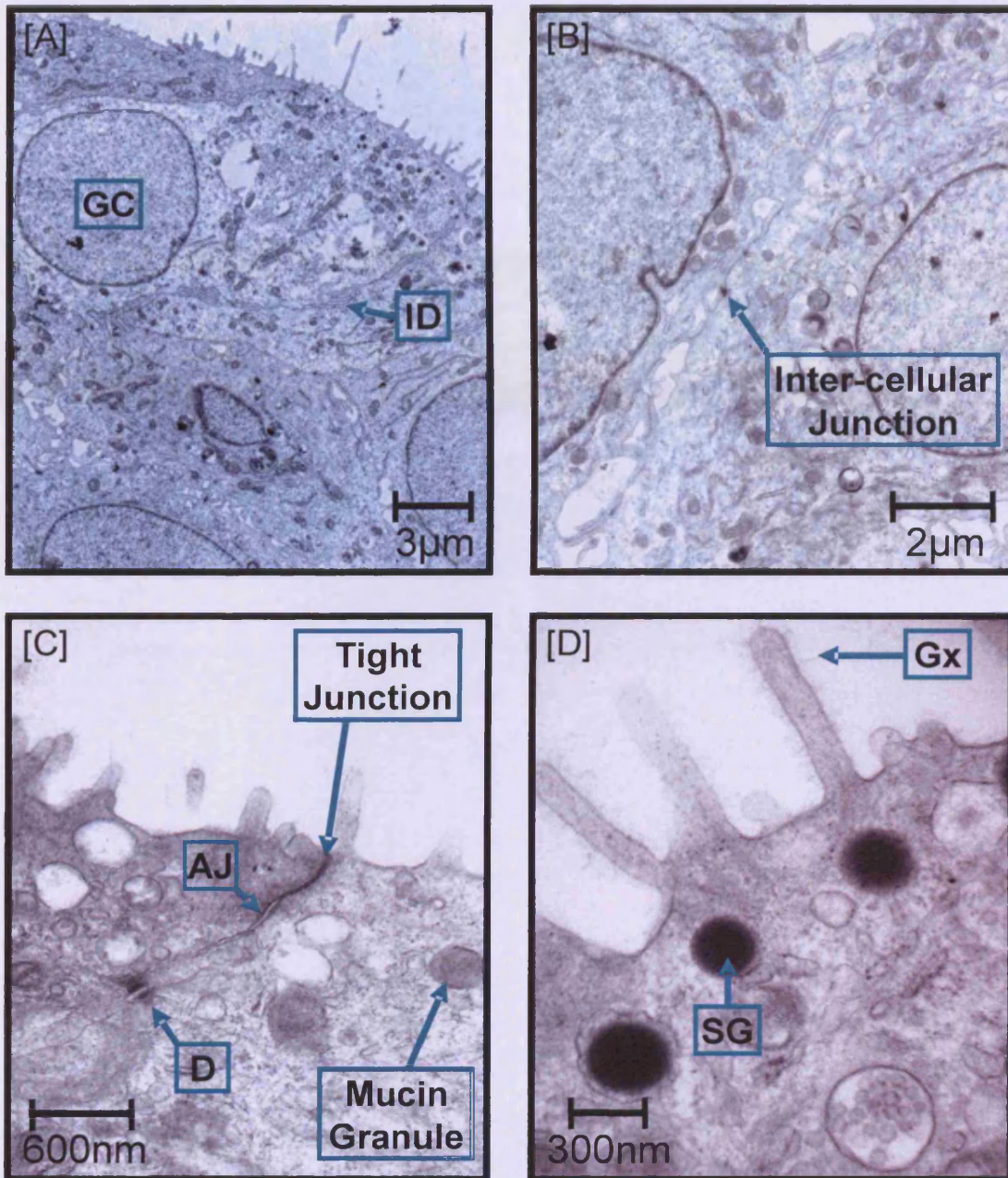


Figure 3.6 TEM images of NHBE cultures on Day 12. [A] An immature goblet cell is observed as well as interdigitations (ID) between it and the neighbouring cell. [B] Higher magnification displaying an inter-cellular junction. [C] High magnification depicting a classic tight junction, adherens junction (AJ), desmosome (D) and mucin granules. [D] High magnification of a serous cell with electron-dense secretory granules (SG) potentially containing lysozyme at the apical surface. Glycocalyx (Gx) can be observed on the apical surface.

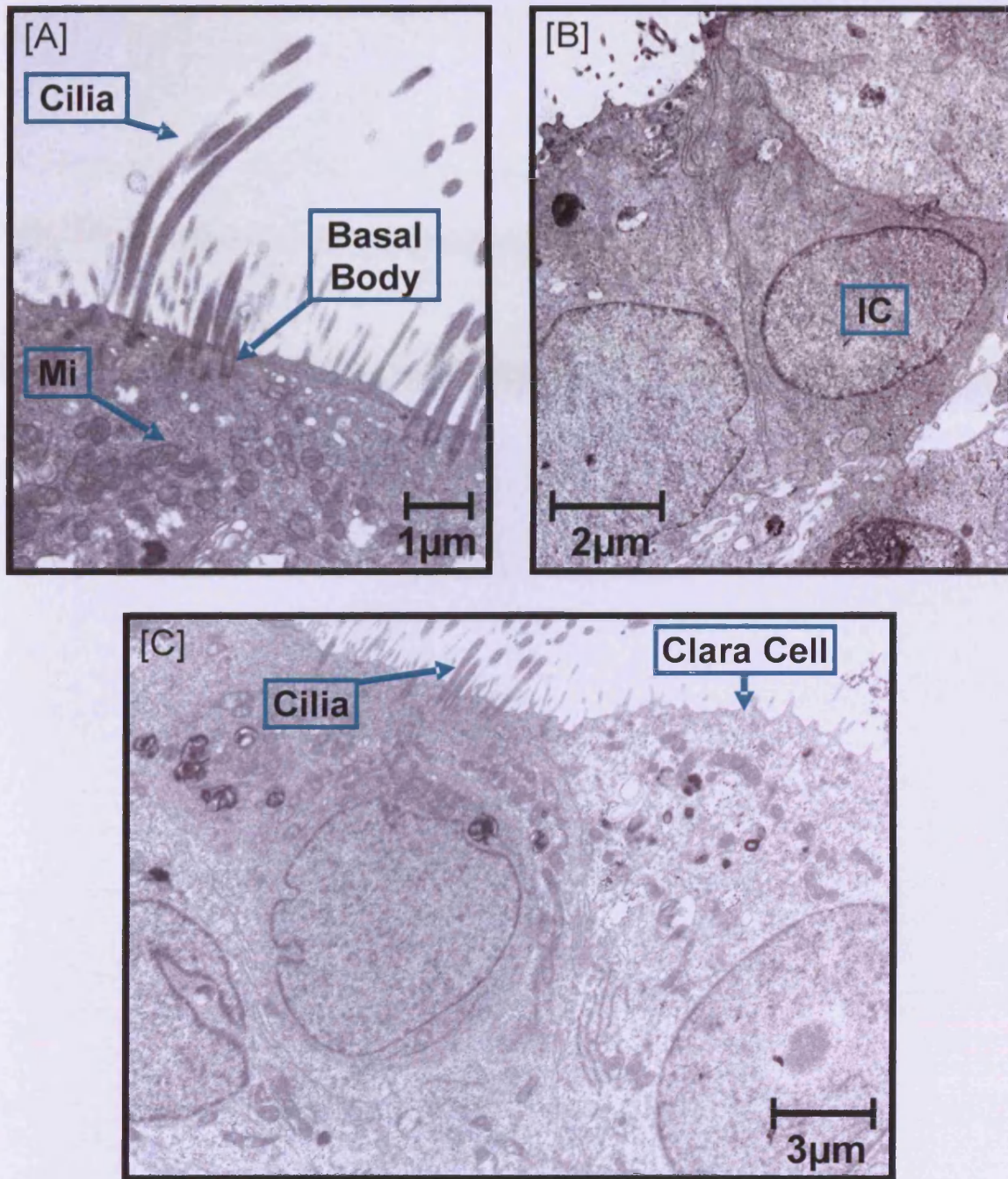


Figure 3.7 TEM images of NHBE cultures on Day 18 and Day 21. [A] Day 18; higher magnification of the apical region of a ciliated cell. Cilia are clearly observed, stemming from basal bodies, numerous mitochondria (Mi) are located in the apical region of the cell. [B] Day 18; displaying an intermediate cell (IC). [C] Day 21; NHBE culture displaying a ciliated cell next to a Clara cell.

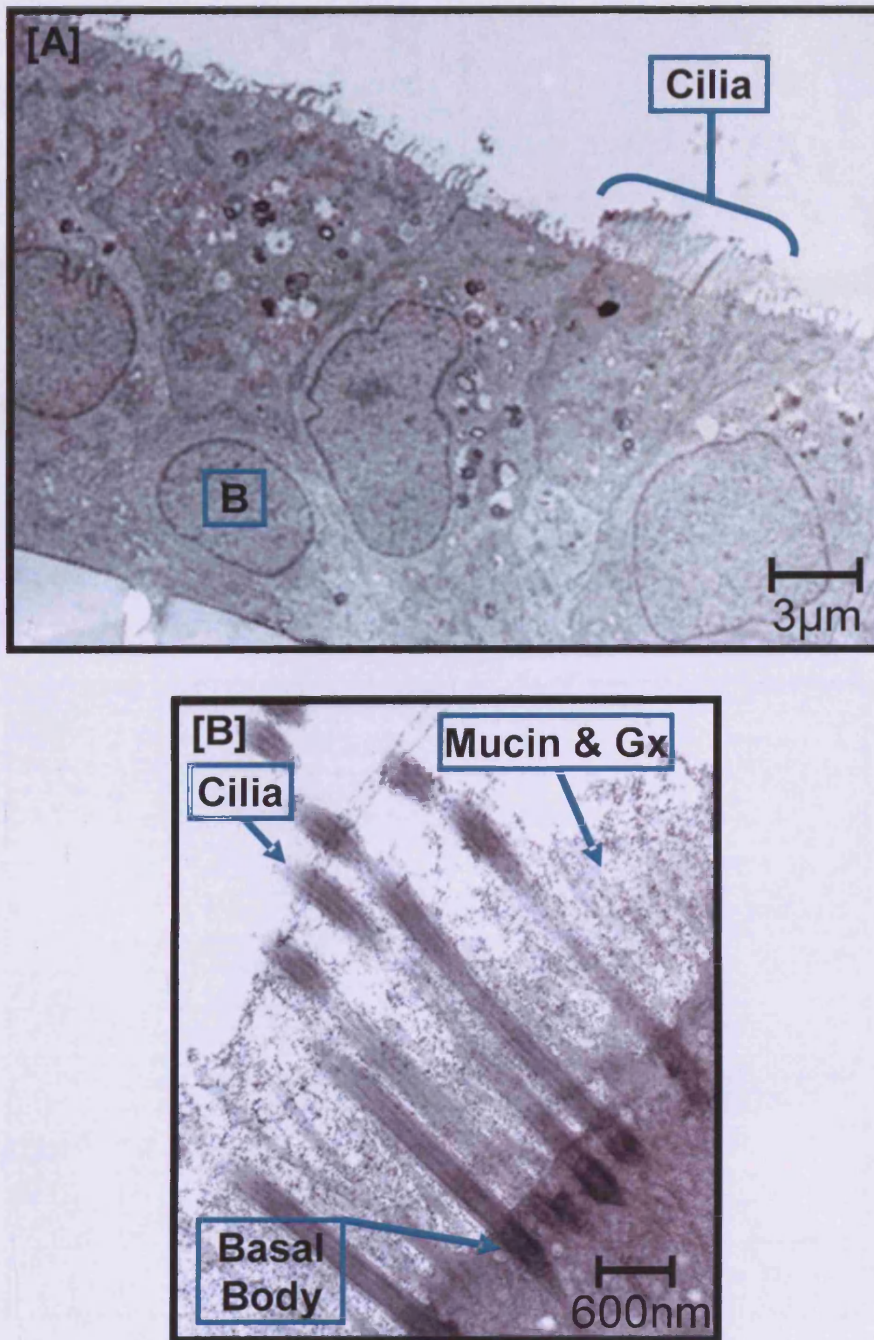


Figure 3.8 TEM images of NHBE cultures on Day 30. [A] Overview of the culture clearly displaying basal (B) and ciliated cells. [B] High magnification of cilia with anchoring basal bodies, located at the apical surface of a ciliated cell. Mucin and glycocalyx (Gx) can be observed between the cilia.

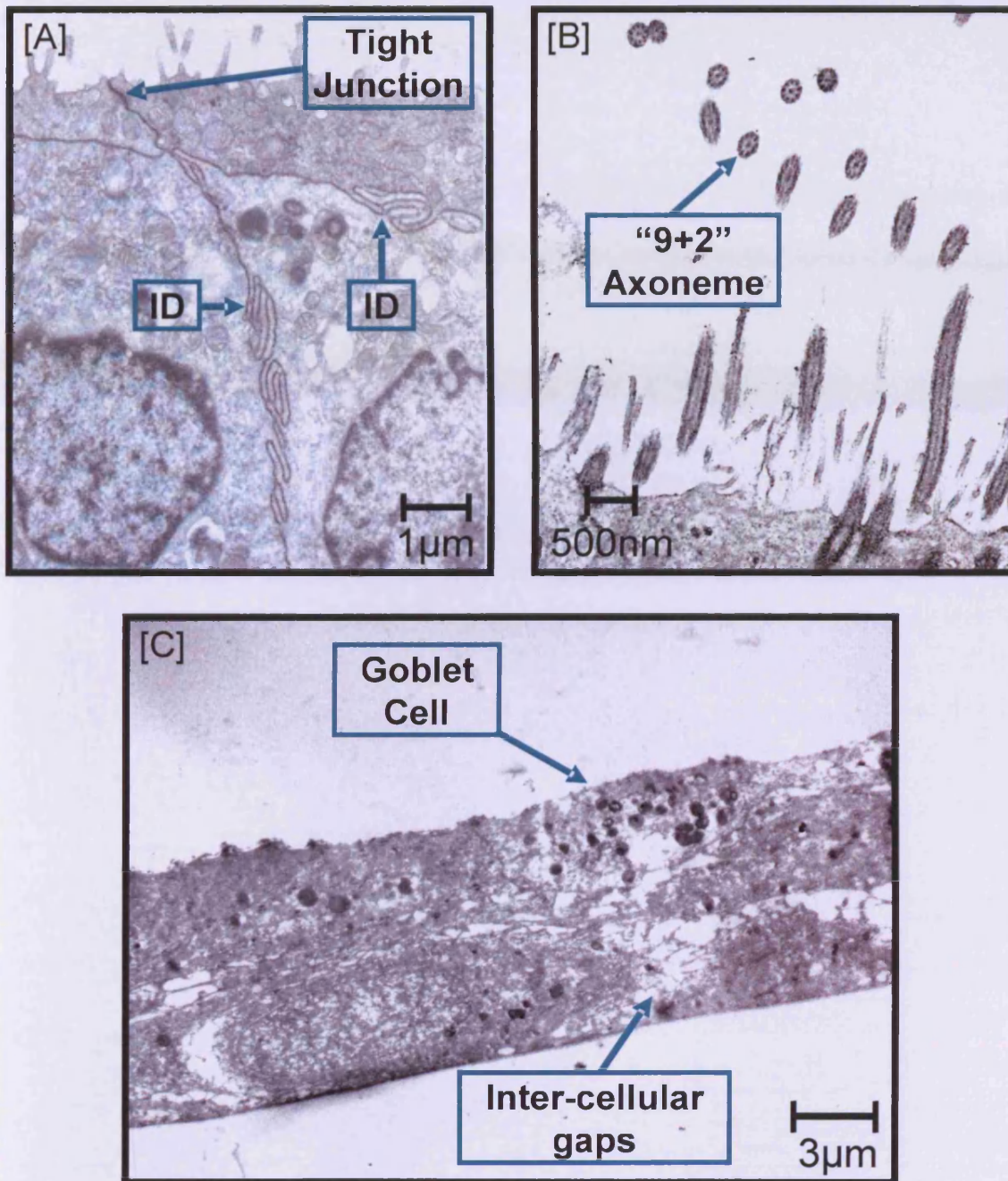


Figure 3.9 TEM images of NHBE cultures on Day 33 and 36. [A] Day 33; high magnification clearly displaying interdigitations (ID) and a tight junction between cells. [B] Day 33; high magnification of the cilia, where a transverse section of the cilia reveals the classic "9+2" axoneme configuration. [C] Day 36; overview of the model with a goblet cell as it begins to deteriorate. Cells are more squamous and inter-cellular gaps have appeared between cells.

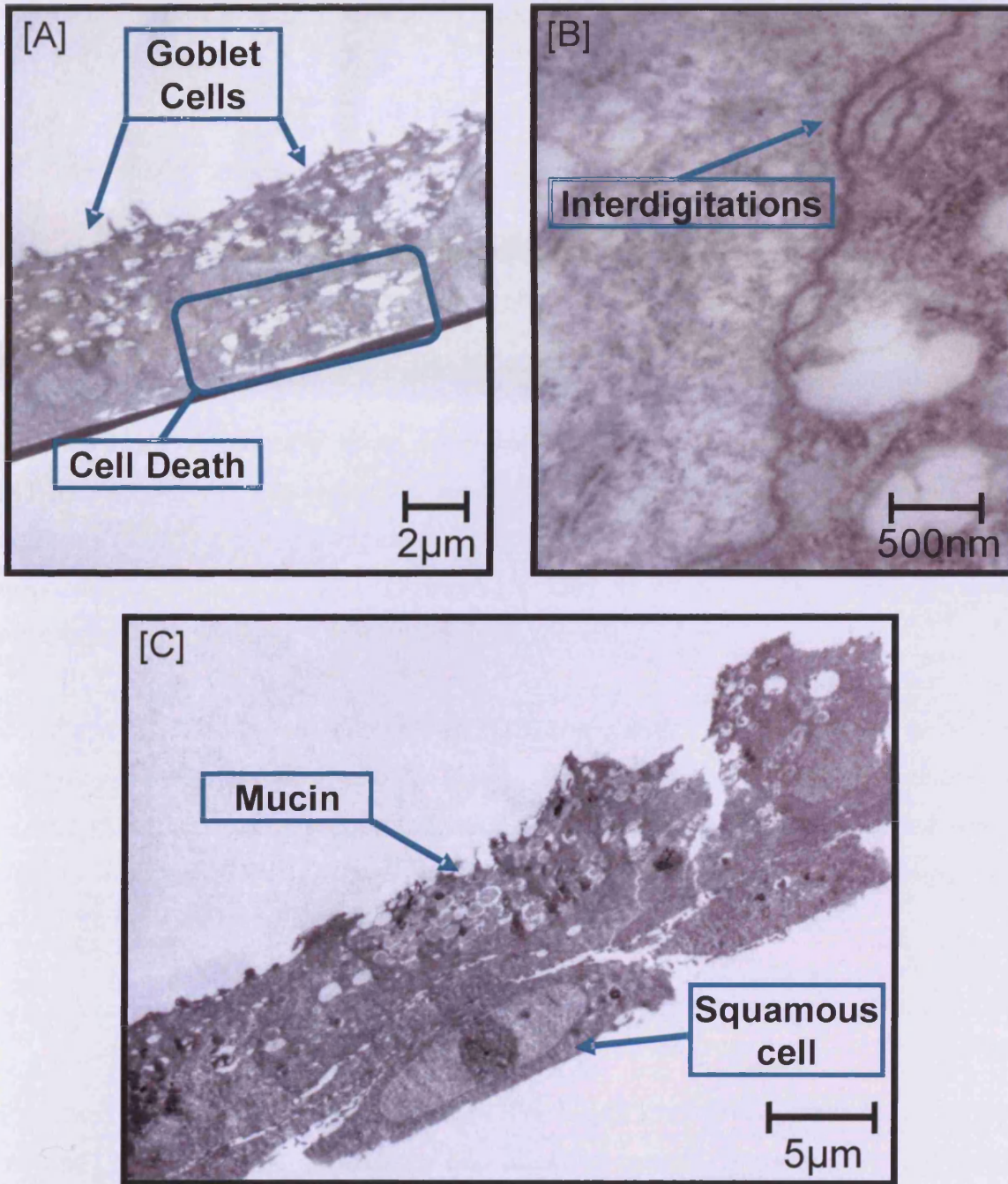


Figure 3.10 TEM images of NHBE cultures on Day 39 and Day 42. [A] Day 39; overview of the culture containing, goblet cells, basal cells were squamous and large vacuoles located throughout. [B] Day 39; high magnification displays that interdigitations were present. [C] Day 42; overview of the culture displaying the deterioration and dedifferentiation of the culture.

3.4.3 SCANNING ELECTRON MICROSCOPY

3.4.3.1 DAYS 1 – 12

The presence of a monolayer of rounded cells was observed at Day 1. The cells did not form cell-cell contacts and inter-cellular gaps could be seen clearly. Closer inspection of the cells revealed that their surface was highly-ruffled, containing many cellular projections (Figure 3.11).

By Day 3, individual cells could not be distinguished and cells exhibited cell-cell attachments. The cells were no longer rounded and appeared flattened. Cell surfaces did not display a highly-convoluted topography; however, microvilli were now visible (Figure 3.12). Cultures at Day 6 were denoted by the same morphological characteristics (images not shown).

On Days 9 (images not shown) and 12, the surface of the culture appeared continuous, with no inter-cellular gaps. Microvilli were abundantly dispersed across the apical surface, with individual cells delineated by a dense and raised area of microvilli. The surface of some cells were more densely covered with microvilli than others (Figure 3.13).

3.4.3.2 DAYS 15 – 33

By Day 15, the apical surface of the culture had changed, where the enclosed surfaces of the cells became either depressed or raised. Cilia were present on the surface of the more differentiated ciliated cells. The surfaces of these ciliated cells were raised and microvilli populations inter-mingled between the cilia (Figure 3.14).

Cultures at Day 24 were topographically similar to those at Day 15. Observationally the number of ciliated cells, the density of cilia-per-cell and the length of the cilia all increased (Figure 3.15). At higher magnifications, mucin globules were observed on the surface of the culture (Figure 3.15[C]), as well as at the tips of the cilia (Figure 3.15[D]).

The cell surface became increasingly variable by Day 27. Ciliated cells were fully-differentiated (Figure 3.16).

By Day 33, the culture surface took on its most complex appearance, with every apical surface either being densely covered in some form of cellular projection or actively secreting mucus. A 'new' cell type appeared from Day 30 that was also present on Day 33. This cell had many rounded projections that were each covered in what appeared to be short, closely packed microvilli-like structures (Figure 3.17).

3.4.3.3 DAYS 36 – 42

The culture underwent a level of dedifferentiation at Day 36. Apart from the presence of a few ciliated cells, the surface of the other cells were only covered in microvilli. For the first time since Day 9, the cells lost their microvillus delineation (Figure 3.18). Cultures at Day 39 exhibited the same morphology (images not shown).

The cellular delineation re-appeared or became more prominent by Day 42. A few, yet very sparse ciliated cells could still be observed, but microvilli remained the common feature on the culture surface. Numerous pore-like ruptures were visible throughout the apical surface (Figure 3.19).

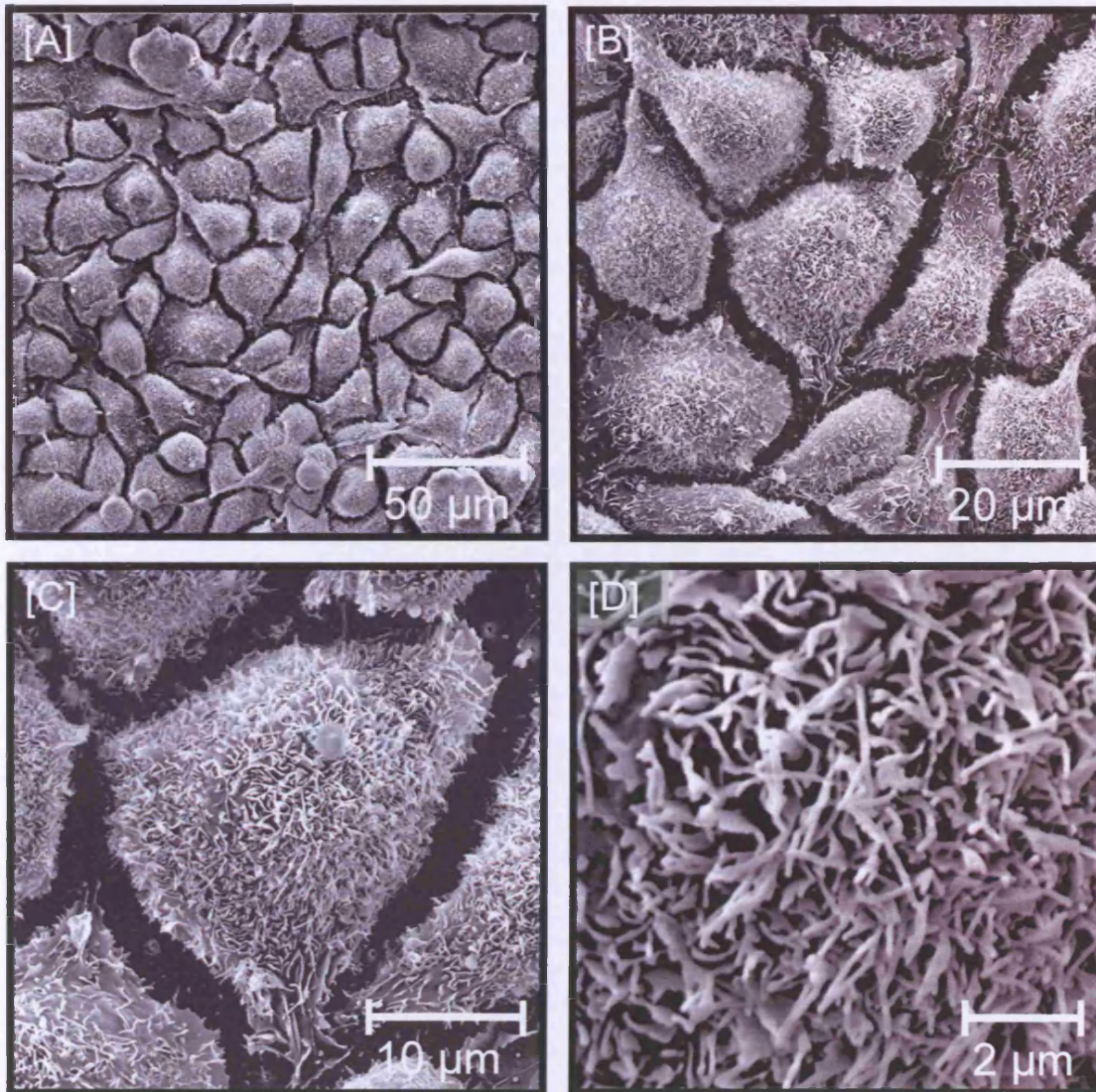


Figure 3.11 SEM images of the apical region of NHBE cultures at Day 1. [A] A monolayer of rounded cells can be seen with inter-cellular gaps between them. [B] A closer image of the rounded cells. [C] Higher magnification displaying a single cell and the inter-cellular gap around it. [D] High magnification of the surface of the cells revealed many cellular projections.

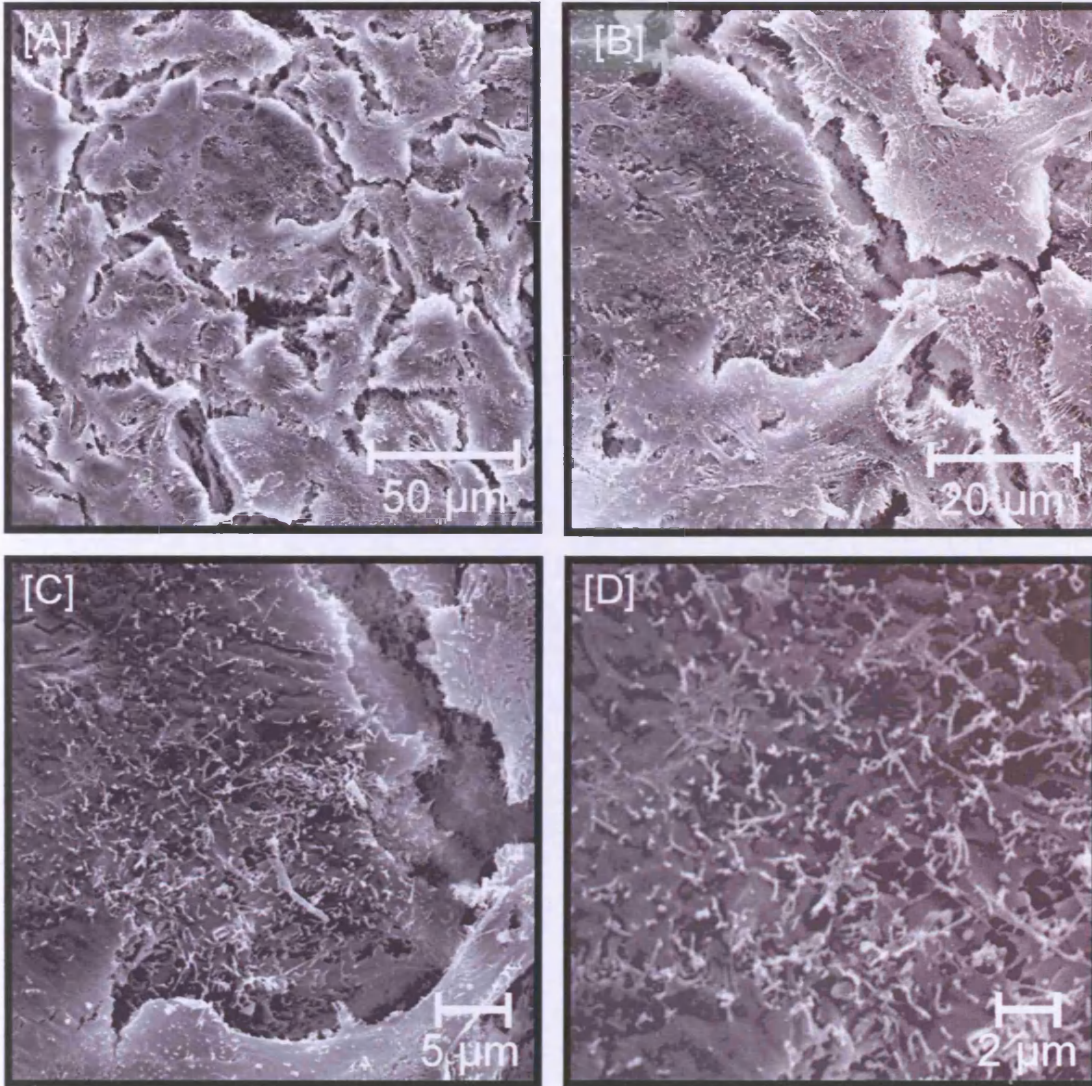


Figure 3.12 SEM images of the apical region of NHBE cultures at Day 3. [A] Overview of cultures; individual cells could no longer be identified. Cells appeared flattened with large cellular projections forming cell-cell contacts. [B] The cellular projections could be observed 'stretching' between cells. [C] High magnification revealed cellular projections on the surface of the cell. [D] High magnification observations suggested the presence of microvilli on the surface of the cells.

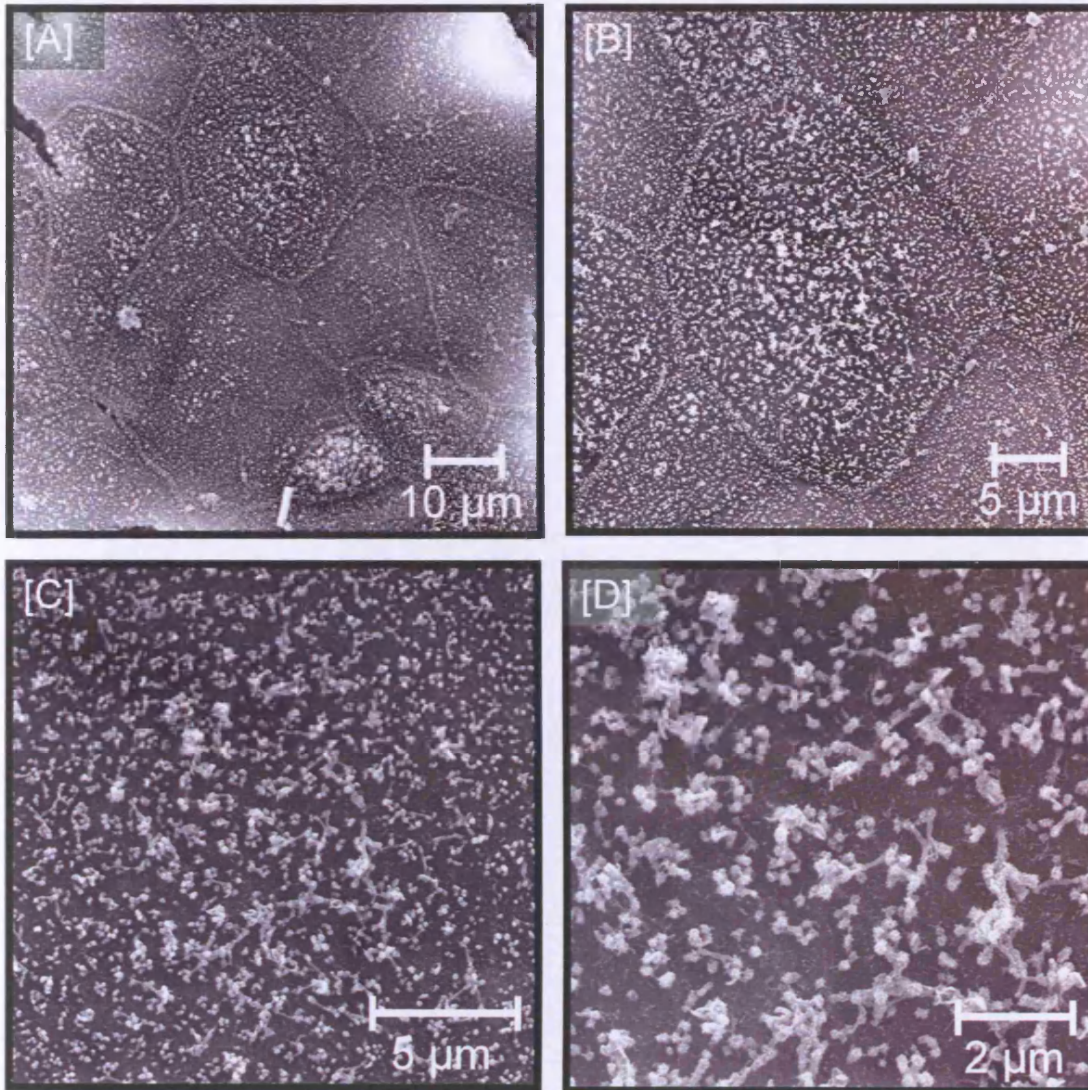


Figure 3.13 SEM images of the apical region of NHBE cultures at Day 12. [A] Overview of culture; cell-cell contacts formed and cells appeared delineated by a dense-raised area of microvilli. Microvilli were uniformly dispersed across the surface of the culture. [B] Cells were delineated by a border of dense-raised microvilli. [C] and [D] Higher magnification images of microvilli on the surface of the cells.

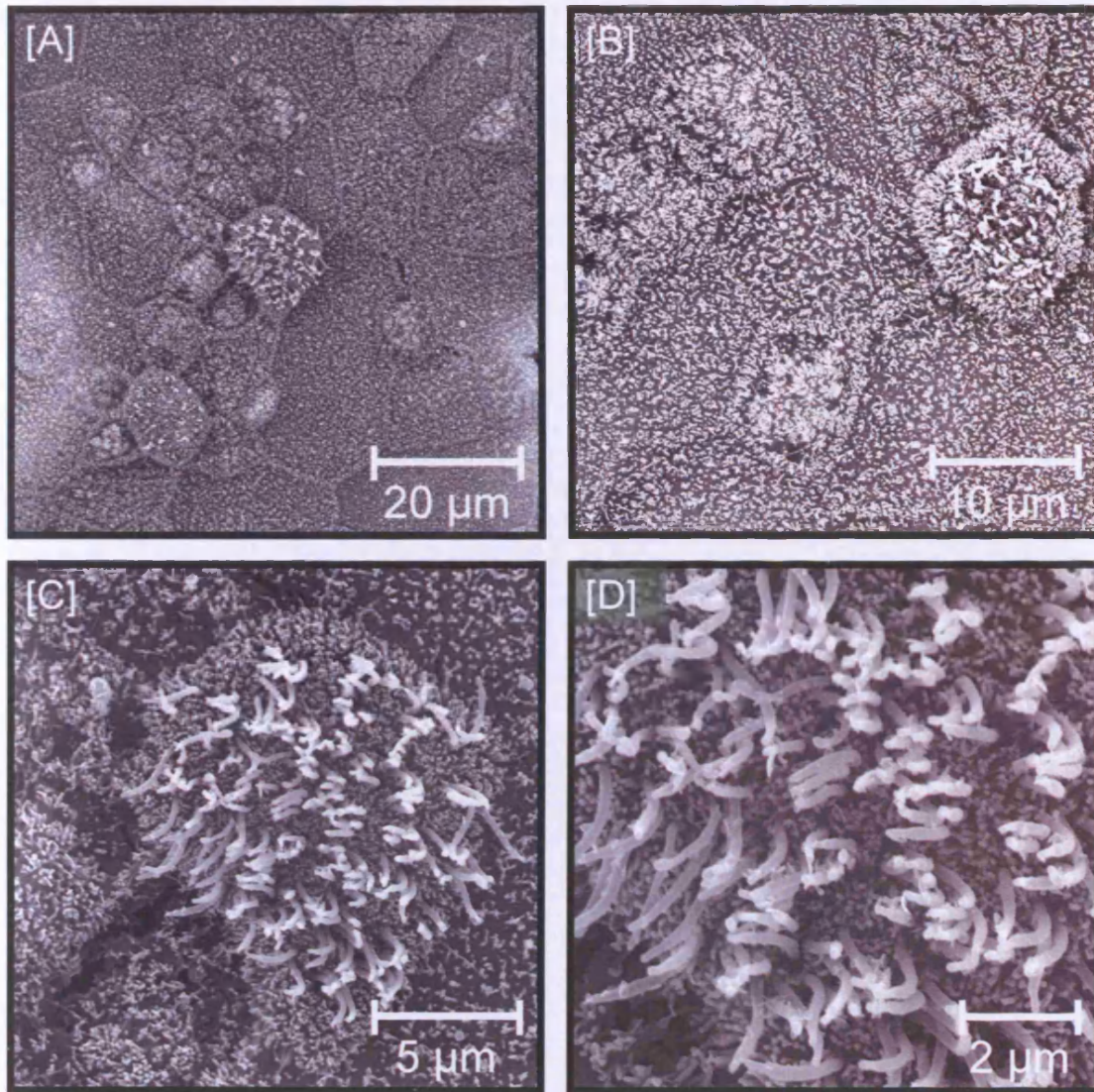


Figure 3.14 SEM images of the apical region of NHBE cultures at Day 15. [A] and [B] Overview of cultures; cells remained delineated by dense-raised areas of microvilli. The surface of cells within these delineated regions became either depressed or raised and were all covered by microvilli. A ciliated cell could be distinguished by the presence of cilia. [C] and [D] Higher magnification of ciliated cell denoted the presence of cilia on the raised surface of cell. Note that the microvilli appeared to surround the cilia.

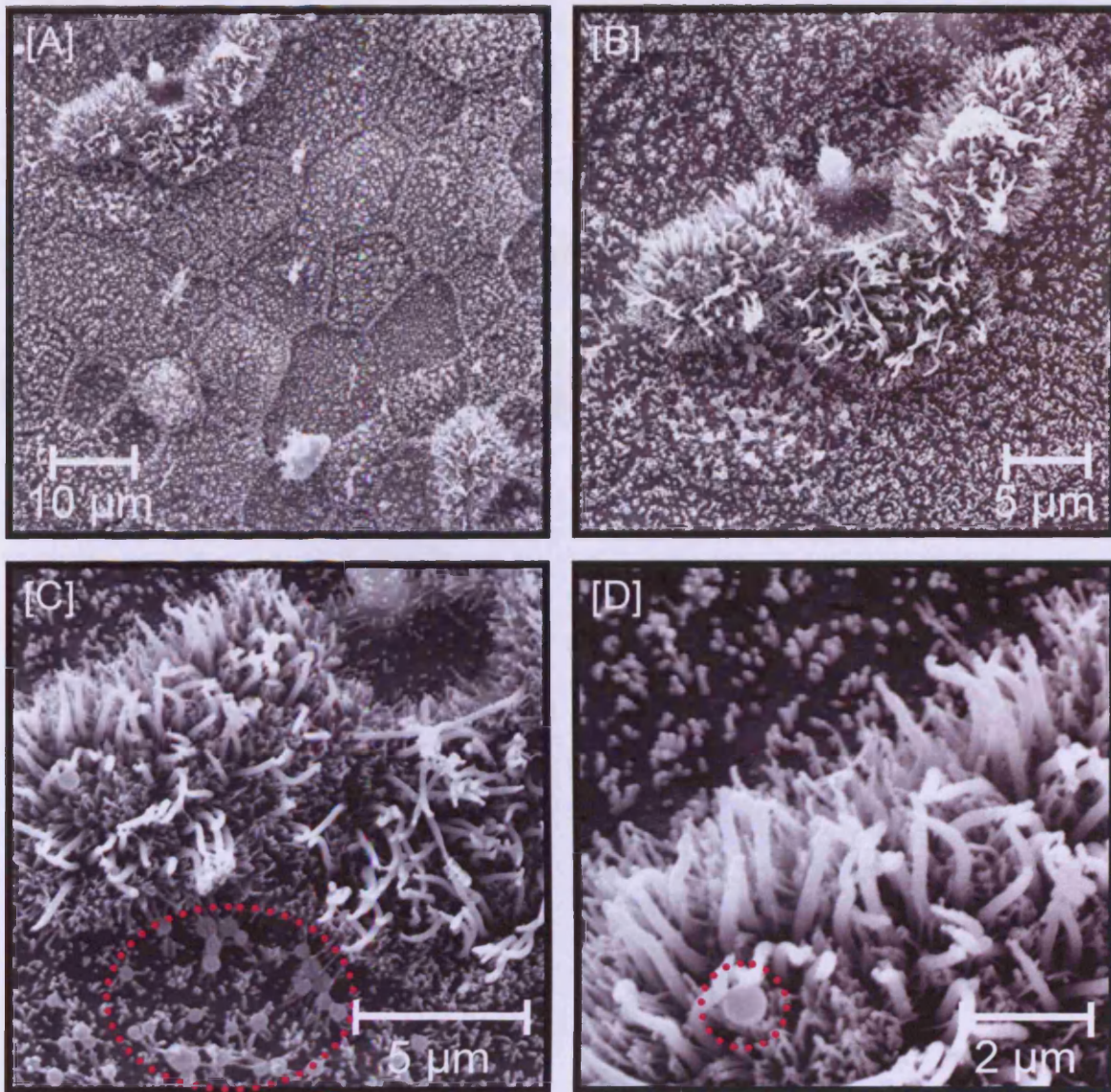


Figure 3.15 SEM images of the apical region of NHBE cultures at Day 24. [A] and [B] Overview of cultures; the morphology was similar to cells at Day 15 (Figure 3.14), apart from the increase in a number of ciliated cells and the number of cilia on these cells. [C] and [D] High magnification demonstrating potential cell secreted products on the surface next to the ciliated cells (highlighted) and also on top of the cilia themselves (circled).

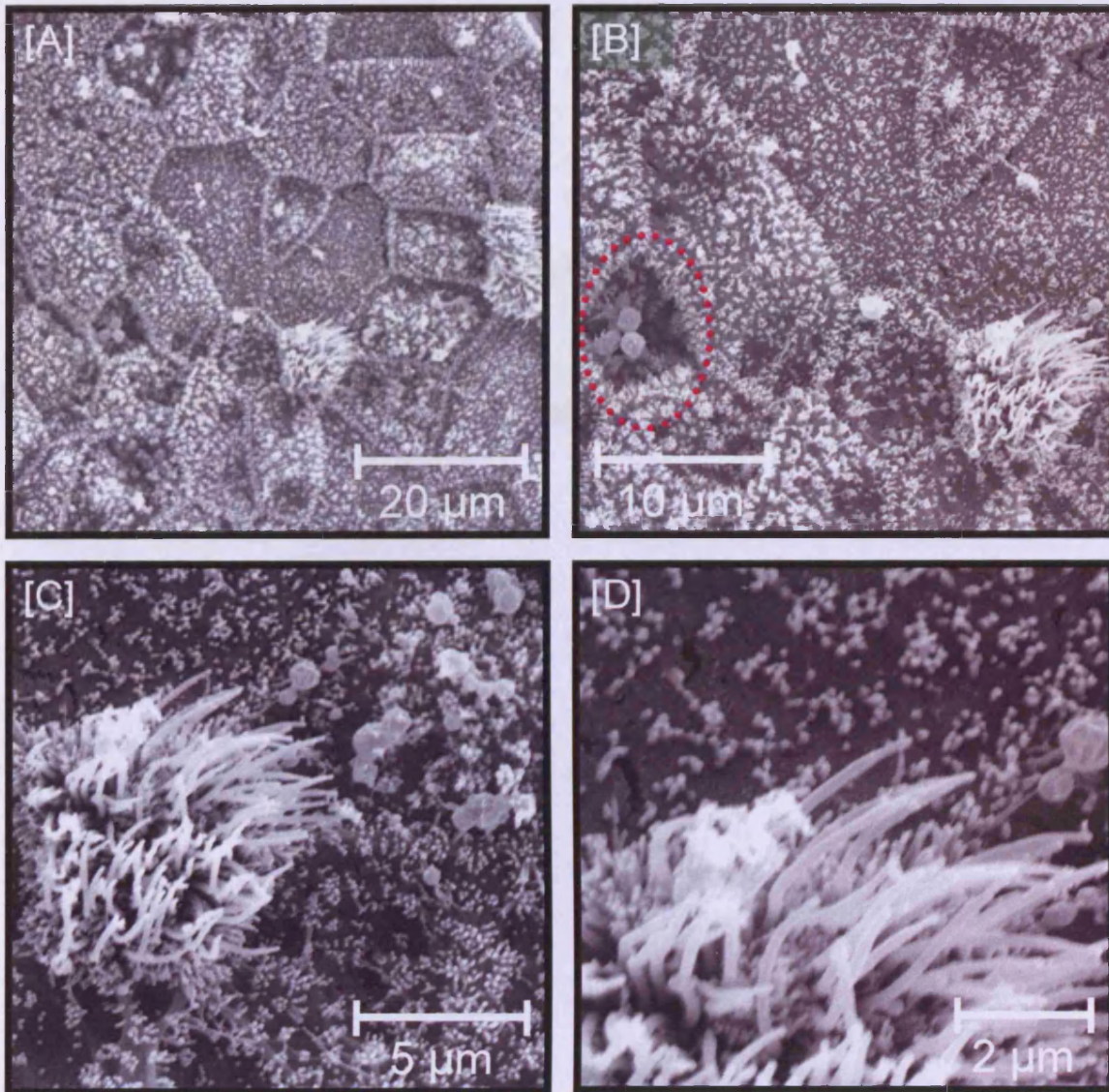


Figure 3.16 SEM images of the apical region of NHBE cultures at Day 27. [A] Overview of the culture; there was a vast surface variability between cells; raised/depressed, cilia and/or microvilli and mucus secreting cells. [B] Overview of the culture; goblet cell secreting mucin globules (circled). [C] and [D] High magnification of a ciliated cell and mucin globules on the apical surface. Note the difference in size between cilia (foreground) and microvilli (background).

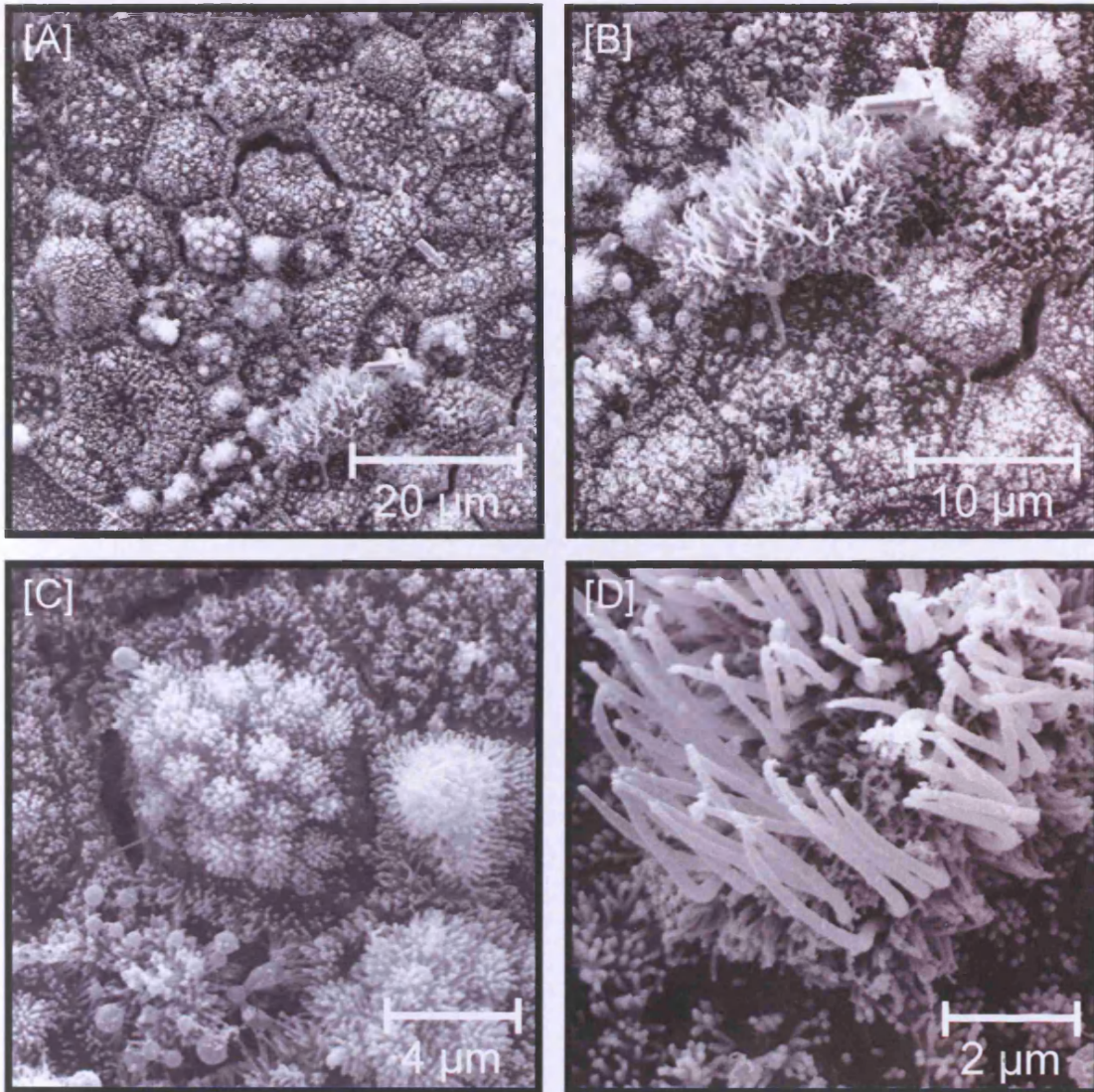


Figure 3.17 SEM images of the apical region of NHBE cultures at Day 33. [A] and [B] Overview of the culture; representing the most complex and diverse surface organisation of the culture during the viable time-line. Every cell was either covered in some form of cellular projection (microvilli, cilia) or secreting mucin. [C] High magnification; an unknown cell type with numerous large round projections for which each was covered in small microvilli-like projections and a mucus secreting goblet cell could also be observed. [D] High magnification image of a ciliated cell.

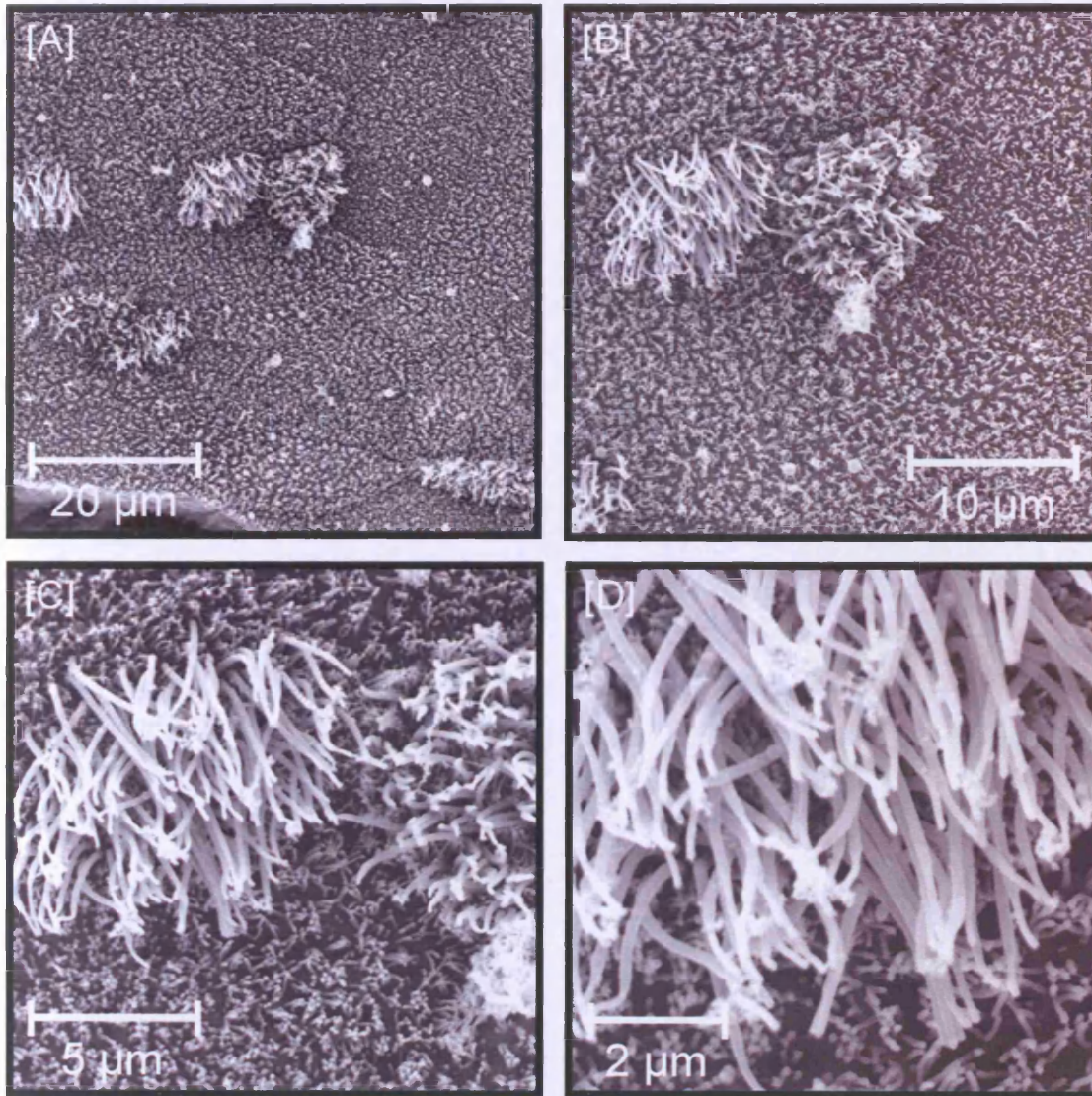


Figure 3.18 SEM images of the apical region of NHBE cultures at Day 36. [A] and [B] Overview of culture; a decrease in the prevalence of ciliated cells and an increase in de-differentiated cells along with a loss of microvillus delineation, at cell borders. [C] and [D] High magnification of ciliated cell; cilia appeared fully-formed, but the cell was no longer raised.

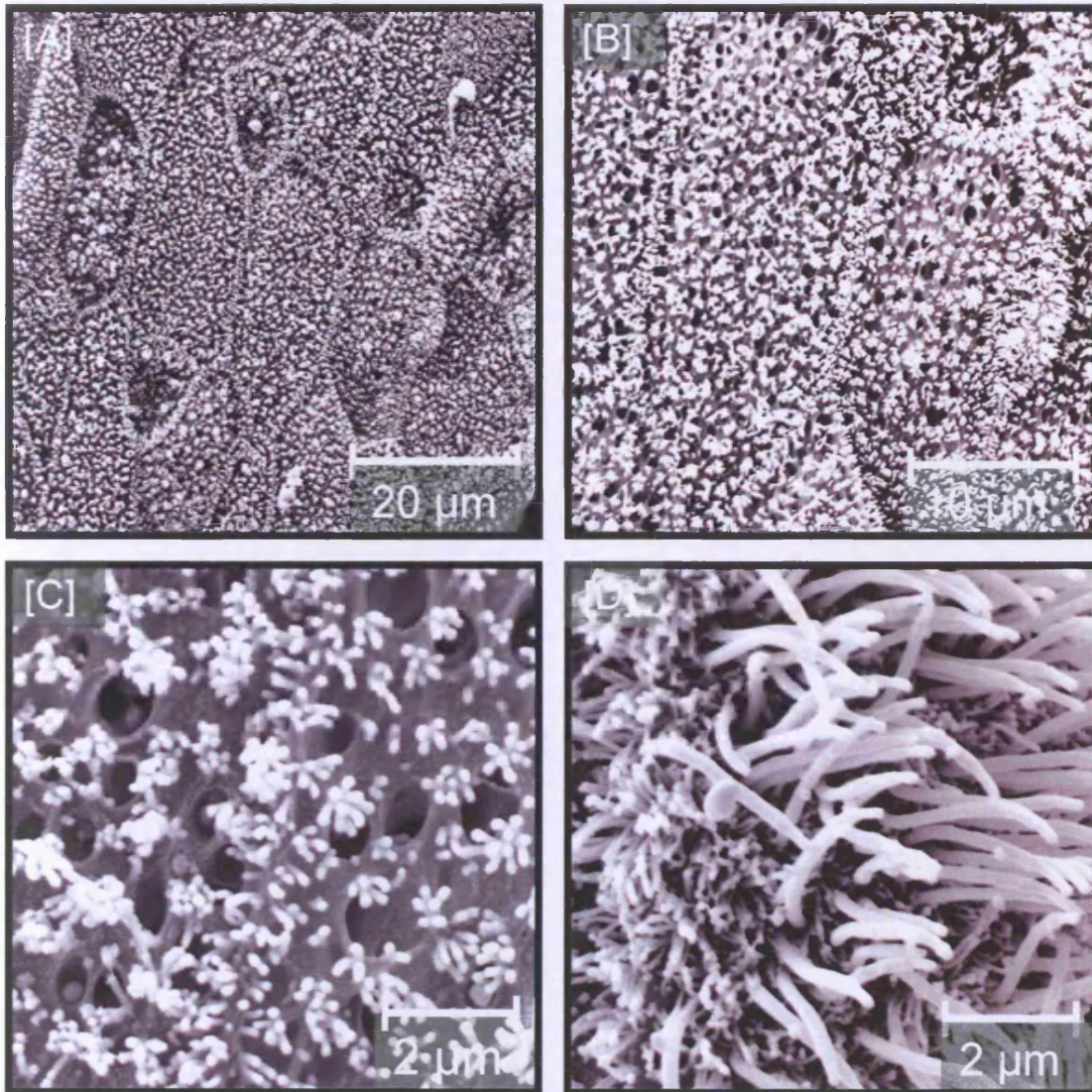


Figure 3.19 SEM images of the apical region of NHBE cultures at Day 42. [A] Overview of culture; the surface was covered in microvilli, faint delineation of cells was visible. [B] Ruptures in the apical surface could be observed. [C] High magnification of these pore-like openings and microvilli interspersed on the surface. [D] Ciliated cells were few and far between, their morphology was intact.

3.4.4 LIGHT MICROSCOPY: *IN VIVO*-*IN VITRO* CORRELATIONS

The development of NHBE cultures (*in vitro*) were compared to the re-epithelialisation in the bronchi of a COPD patient (*in vivo*).

NHBE cultures at Day 1 displayed a monolayer of cells with a large nuclear-to-cytoplasm ratio (Figure 3.20[E]). Corresponding *in vivo* sections of re-epithelialisation of the airway also displayed a monolayer of cells with a large nuclear-to-cytoplasm ratio (Figure 3.20[A]).

By Day 6 *in vitro* cultures had formed two squamous cell layers with cells, characterised by a large nuclear-to-cytoplasm ratio (Figure 3.20[F]). *In vivo* sections displayed similar morphological features (Figure 3.20[B]).

Day 12 NHBE cultures and corresponding *in vivo* (COPD biopsy) samples developed an epithelium with two distinct nuclear layers. The cells with more apically located nuclei were becoming increasingly columnar (Figure 3.20[C] and [G]).

The NHBE culture exhibited a fully-differentiated, pseudo-stratified, muco-ciliary culture at Day 27. Basal, ciliated and goblet cells could all be identified (Figure 3.20[H]). The fully-differentiated epithelium *in vivo* exhibited the same mixed-cell phenotypes (Figure 3.20[D]).



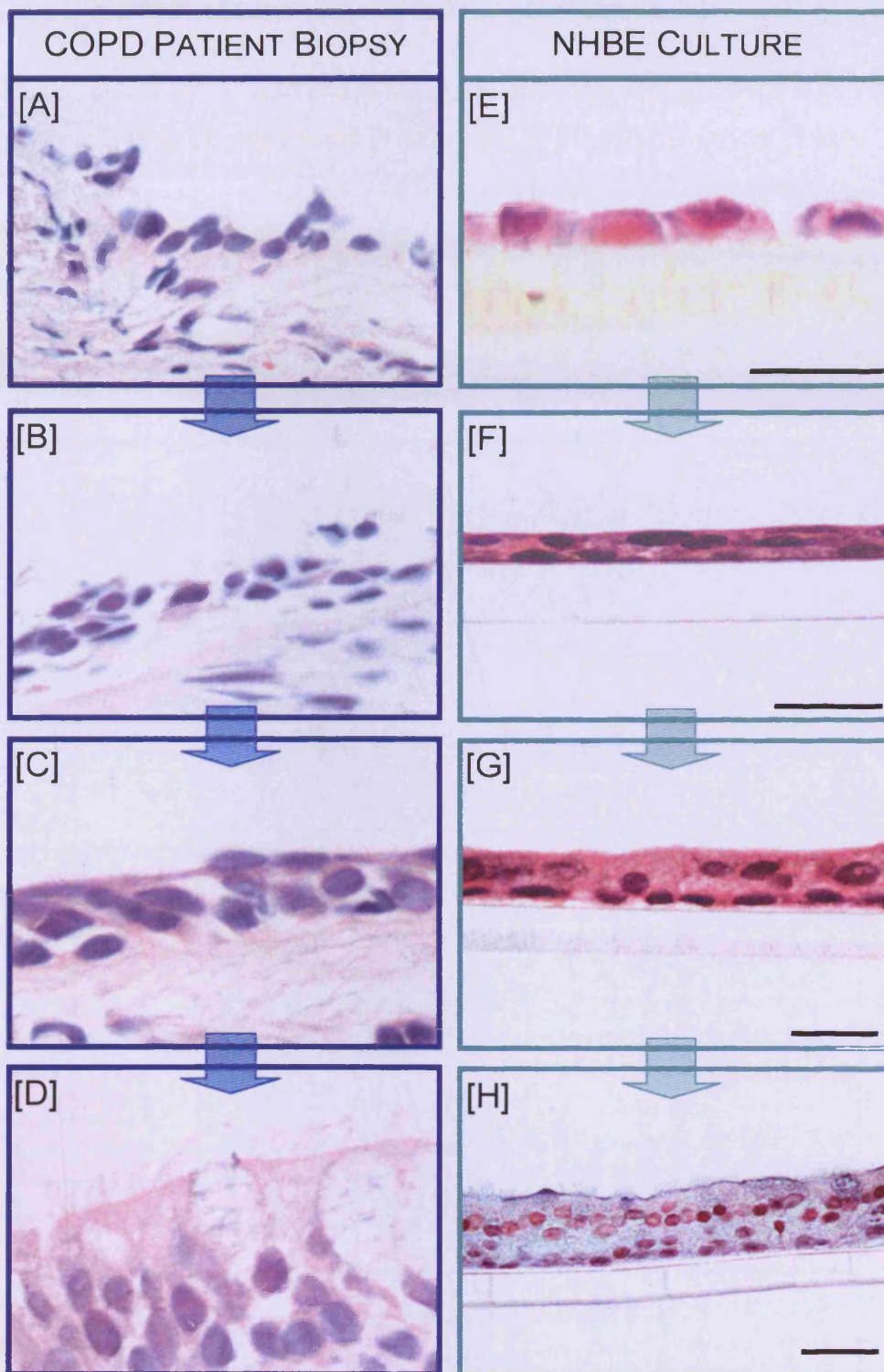


Figure 3.20 LM images of human biopsy sections ([A-D]) and NHBE cultures ([E-H]) stained with H&E. [A] Initial re-epithelialisation. [E] Day 1; monolayer of cells with inter-cellular gaps. [B] Two cell layers. [F] Day 6; two cell layers. [C] Two cell layers. [G] Day 12; squamous basal cells, apical cells becoming columnar. [D] Fully-differentiated epithelium, cilia present on apical surface and goblet cells observed. [H] Day 27; Pseudo-stratified epithelia, cilia present on apical surface, goblet and basal cells were observed. Scale bar = 20 μ m.

3.4.5

CORRELATION OF BIOCHEMICAL AND MORPHOLOGICAL DATA

Biochemical (Chapter 2) and morphological characterisation data was compared to provide a concise physicochemical overview of the NHBE model (Table 3.4).

	Day 1 [†]	Days 3 – 6	Days 6 – 12	Days 12 – 21	Days 21 – 33	Days 36 – 42
Epithelial Integrity*	23	251–657	657 – 5741	5741 – 7593	6728 – 7661	5684 – 6512 (Min 6 [#])
Apical Protein Concentration*	11	0 – 1	1 – 2	2 – 21	5 – 19	11 – 16
Ultrastructural and Topographical Changes (LM, TEM, SEM)	<ul style="list-style-type: none"> • Monolayer of cells • Adherence to insert membrane • Inter-cellular gaps • No discernable organelles (apart from nucleus) • Numerous surface projections 	<ul style="list-style-type: none"> • 2 nuclear layers • Formation of cell-cell contacts • Microvilli on apical surface • Clara cells present • A variety of intra-cellular organelles observed 	<ul style="list-style-type: none"> • Tight junctions observed • Desmosomes present • Interdigitations observed • Goblet cell differentiation • Mucin granules and vacuoles present 	<ul style="list-style-type: none"> • Formation of cilia • Presence of basal bodies anchoring cilia • Mucin globules observed on apical surface • Glycocalyx around cilia and microvilli 	<ul style="list-style-type: none"> • Pseudo-stratified morphology • Increase in length and number of cilia • Maturation of ciliated cell; becoming columnar • Formation of unknown cell type 	<ul style="list-style-type: none"> • Dedifferentiation of culture • Appearance of vacuoles • Squamation of cells • Appearance of pore-like ruptures in apical cell membranes • Deterioration to monolayer culture

Table 3.4 Correlation of key biochemical and morphological changes in NHBE cultures from Day 1 to 42. * Minimum and maximum average TEER ($\Omega \cdot \text{cm}^2$) and apical protein concentration ($\mu\text{g}/\text{ml}$), from 3 donors. [†]Average of 3 donors. [#] Minimum recorded value. Values displayed to N.W.N.

3.5 DISCUSSION

Morphological characterisation of the NHBE human lung construct complimented the biochemical characterisation already undertaken (Chapter 2). This further characterisation was essential in providing a more complete and accurate picture of the NHBE construct, with the aim to validate the model as a suitable *in vitro* alternative to other *in vivo* (animal) models. This extensive characterisation could enable the mechanisms of injury and repair in response to inhaled xenobiotics to be elucidated.

3.5.1 LIGHT MICROSCOPY: TOLUIDINE BLUE

Analysis by LM enabled an initial insight into the structure and morphology of the construct at the microscopic level. This analysis was conducted throughout the models' development and subsequent demise. Initially, the culture began as a monolayer of adherent cells with inter-cellular gaps (Day 1), which quickly formed a confluent, multilayered culture without inter-cellular gaps. Morphologically, the next prominent change was the basal cells becoming rounded and the non-basal cells taking on a more columnar shape. Mucus secreting cells could be distinguished due to the presence of mucin granules and intermediate cells were observed in between the basal and apical layers (Breeze and Wheeldon, 1977). Deterioration of the culture could be observed from Day 36 onward. This included the formation of vacuoles throughout the culture, dedifferentiation of the mucociliary phenotype, squamation of cells and a reversal to a monolayer phenotype.

3.5.2 TRANSMISSION ELECTRON MICROSCOPY

TEM analysis has been used to visualise the ultrastructure of the respiratory epithelia by many scientists (Breeze and Wheeldon 1977; Rhodin, 1966; Rogers, 2003). TEM analysis of the NHBE constructs enabled a detailed observation of fine cellular structures and components. The general morphology of the construct correlated with that determined by LM, but at a more robust and detailed level. TEM demonstrated the formation of microvilli and confirmation of cilia. Individual microtubules could be identified, along with the characteristic "9+2" axoneme and

anchoring basal bodies. The presence of cellular junctions and relative cytoskeletal filaments as well as cellular organelles (e.g. mitochondria, Golgi, endoplasmic reticulum, etc) were also observed. Mucin granules were also observed within goblet cells (Rogers, 2003).

The deterioration of the cultures as defined by LM observations was supported by TEM, from Day 36 onwards. The formation of vacuoles throughout the culture, dedifferentiation of the muco-ciliary phenotype, squamation of the cells and the loss of intra-cellular organelles and structures, were clearly defined events at the TEM level.

Comparison with the biochemical observations (Chapter 2) revealed some correlation with the morphological data (Table 3.1). Morphologically, the appearance of the tripartite junctional complex occurred between Day 9 and 12 (Figure 3.5 – 6). The tripartite junctional complex consists of the tight junction, adherens junction and desmosome (Farquahr and Palade, 1963). The tight junctions are the most apically located component and were characterised by the fusion of the two adjacent cell membranes and elimination of the inter-cellular space (Farquahr and Palade, 1963). Desmosomes are the most basally located of the three junctions. They appear as two electron dense plaques on adjacent cell membranes with a more translucent inter-cellular gap, intermediate filaments can be observed spanning out from the plaques into the cytoplasm (Garrod and Chidgey, 2008). Adherens junctions are located between the tight junction and the desmosomes and were identified at the TEM level in this location, where the adjacent membranes were completely parallel for $\sim 0.2 - 0.5\mu\text{m}$ (Niessen and Gottardi, 2008). The appearance and maturation of these cellular junctions from Day 9 (Figure 3.5) corresponded with the large increase in average TEER values determined between Days 9 to 18 (Figure 2.6), indicating that tight junctions had formed during this period. However, the initiation of these cell-cell contacts, later to become cell junctions, is thought to begin as early as Day 1. TEM images of Day 1 cultures revealed that numerous cellular projections appear on the outer-surface of the cells, these were thought to be due to actin filament accumulation that create these filopodia projections during nascent adhesion and subsequent junction formation (Miyoshi and Takai, 2008).

Clara cells are non-ciliated, non-mucus, secretory epithelial cells and appear from Day 6 (Figure 3.5), mature Clara cells were observed from Day 21 in cultures. Their apical surfaces contained few microvilli and were characteristically dome-shaped. Electron-dense proteinaceous granules were found within the Clara cells apical cytoplasm and being very metabolically active, contained numerous mitochondria (Boers *et al.*, 1999). The appearance of Clara cells (confirmed experimentally Chapter 4, Section 4.4.2) at Day 6 also corresponded to the slight increase observed in apical protein content (Figure 2.7). Goblet cells developed later and were identified by TEM around Day 12 /15 (Figure 3.6). Morphologically, goblet cells were identified by their typical 'drinking cup' (i.e. goblet) shape, that results from the accumulation of secretory mucous granules in the apical portion of the cell, with the basal portion tapering around intermediate and basal cells (Rhodin, 1966). However, immature or discharged goblet cells were generally more columnar in comparison (Breeze and Wheeldon, 1977). Goblet cells contained numerous electron-lucent mucin granules (Rogers, 1994). The appearance of goblet cells in the NHBE culture was associated with a larger increase in the apical protein content (Figure 2.7). Their continued maturation and increased incidence, up until Day 18, also paralleled the gradual increase in apical protein. Networks of polysaccharides were observed around the cilia and microvilli (Figure 3.6 and 3.8) and are known as 'glycocalyx' and they occur normally in the human airway lumen in this manner (Martins and Abairos, 2002).

Ciliated cells were more readily confirmed by TEM than via LM. Cilia were identified at the electron microscope level not only by their increased length compared to microvilli, but due to their distinct morphology. Electron-dense striations were observed along the length of cilia (Figure 3.7 – 3.9), due to the microtubules that formed their axoneme (Hasleton and Curry, 1996). Transverse TEM sections revealed the classical "9+2" axoneme formation (Figure 3.9). Cilia were also anchored into the ciliated cell via basal bodies and surrounded by numerous mitochondria (Figure 3.9) (Hasleton and Curry, 1996; Sorokin, 1968). The NHBE model matured and entered a period of relative stability, according to biochemical and morphological characterisation, between Days 27 and 33. Beyond Day 33, the cultures deteriorated and underwent dedifferentiation (Figure 3.9 – 3.10), most likely due to the limited amount of doublings primary cells

undergo (Chepko and Smith, 1999). There was a slight increase in apical protein observed between Days 36 to 42, which correlated with culture demise; confirmed morphologically at both the LM and TEM levels. These observations suggested that the increase in protein was likely due to an increase in cellular debris.

Consequently, any toxicological experimentation should be undertaken between Days 27 and 33, when the model was fully-differentiated and of muco-ciliary phenotype.

3.5.3 SCANNING ELECTRON MICROSCOPY

SEM was utilised to examine the surface topography of the NHBE human lung construct. The information gathered by SEM analysis provided a new dimension to the morphological characterisation not provided by LM and TEM.

SEM images of Day 1 cultures demonstrated the existence of numerous cellular projections/ruffles which encompassed the free surfaces of every cell; this may represent the initial attempts to create cell-cell contacts, through the formation of actin filaments (Miyoshi and Takai, 2008). TEM images of Days 3 and 6 gave the impression that cell-cell contacts had been established and that the apical surface was smooth. SEM images revealed that the formation of these cell-cell contacts were still on-going and continued to be so until Day 9. The surface topography of cultures at Day 9 displayed the delineation of individual cells by a dense-raised border of microvilli, which had not been perceptible from LM or TEM images. This delineated border may be characteristic of immature ciliated or basal cells (Breeze and Wheeldon, 1977) or an even artefact of tight junction formation (Farquahr and Palade, 1963).

Cilia were clearly observed from Day 15 onwards by all three microscopical methods. Contrary to TEM observations, SEM images allowed the visualisation of mucin globules resident on the apical surface, clearly seen from Day 24. At Day 30, a 'new' or previously unobserved, cell type became apparent. Surface topography of this cell was unlike the ciliated or goblet cell; it appeared raised,

covered in many large rounded projections, each enveloped in small microvilli-like structures. This cell may be a 'brush cell' or an 'exhausted goblet cell', as described by Breeze and Wheeldon (1977). Which stated, that exhausted goblet cells had a "dense population of microvilli on the luminal surface", also that "brush cell microvilli are taller, wider and more uniform and contain more prominent intracellular axial filaments than the microvilli of goblet cells or potential ciliated cells" (Breeze and Wheeldon, 1977).

The topographical complexity of the constructs was discernable by SEM, especially at Days 30 to 33. Visualisation of this complexity created a vast contrast with cultures at Day 36, where the dedifferentiation of the cultures could be clearly observed, with only cilia and microvilli remaining on the surface. Observation of cultures at Day 42 revealed numerous 'pores' or 'holes' across the surface of many cells. The presence of which, correlated to both, the low TEER values (Section 2.4.2) and the high apical protein concentration (Section 2.4.3), observed at Day 42. Based on SEM characterisation, any toxicological experimentation should be undertaken between Days 27 and 33, where the model appeared to have a fully-differentiated, muco-ciliary phenotype. SEM images of the mature NHBE surface topography displayed similar features to the human bronchial epithelium *in vivo* (Jeffery and Li, 1997).

3.5.4 IN VITRO-IN VIVO CORRELATION

Analysis of overall NHBE tissue morphology revealed several similarities to excised (biopsy) human tracheobronchial epithelium. The NHBE construct displayed a polarised, pseudo-stratified culture of muco-ciliary phenotype, similar to the *in vivo* situation. Architecturally, the only difference to *in-situ* human tissue was that the NHBE construct appeared less columnar and Clara cells were not identified. However, this could be due to LM processing artefacts, as semi-thin sections revealed an accurate morphological picture as well as identification of Clara cells (Figure 3.2[C]).

Comparison of individual cell types present within LM semi-thin sections of NHBE cultures, revealed the presence of ciliated, goblet, basal and intermediate cells;

all of which are located in the human bronchial epithelium. These cells exhibited similar characteristics and structures to their counterparts found *in vivo* (Breeze and Wheeldon, 1977). Non-basal cells appeared more columnar, ciliated cells displayed cilia (Rhodin, 1959), goblet cells were also identified due to their paler appearance; possibly due to the presence of mucin granules (Rogers, 2003). Basal cells were located at the basal end of the culture and appeared round in comparison to non-basal cells (Baldwin, 1994).

3.6 CONCLUSIONS

Morphological characterisation demonstrated that the 'in-house' NHBE model was able to develop into a stable, well-differentiated, muco-ciliary phenotype epithelium, suggesting that it is a viable *in vitro* alternative of the human bronchial epithelium. Characterisation at all levels (i.e. biochemical and morphological) was undertaken in order to elucidate the response of the construct to a given xenobiotic (Chapter 5 and 6). This would enable a clearer understanding of the morphological modifications that may occur during any injury and repair processes. Further characterisation of the NHBE culture was undertaken over the time course in order to more specifically identify and further confirm the different cell types present (Chapter 4).

The main advantages to this NHBE model were: 1) accurate reflection of the bronchial epithelium *in vivo*; 2) a relatively long exposure window (Day 27 – 33); and 3) high number of inserts (~300) produced, from a single cryovial (~500,000 cells). The main disadvantages to this model were its long morphogenesis cycle leading to maturity, and therefore, its subsequent demise from Day 36.

CHAPTER 4:

**DEVELOPMENTAL HISTOLOGY OF
THE NHBE MODEL**

4.1 INTRODUCTION

In previous experimental work, the biochemical and physiological properties (Chapter 2), along with the morphological development (Chapter 3) of the NHBE model, was assessed over the 42 days of ALI culture. This revealed that the NHBE model was fully-differentiated and of muco-ciliary phenotype. Additional characterisation work would now include complimentary histochemical and immunohistochemical procedures in order to: 1) detect integral cytoskeletal components; 2) establish the presence of Clara cells; 3) confirm mucin producing goblet cells; 4) identify the models progenitor cells; and 5) verify the existence of integral tight junction proteins.

An anti-cytokeratin (CK) 5/6 antibody was used to identify these specific cytokeratins which are known to be present in the basal and supra-basal cells of non-keratinising epithelia (Chu and Weiss, 2002), such as the respiratory tract epithelium (Sun *et al.*, 1979). CK 5/6 is also known to be typically expressed by hyper-proliferative cells (Neudeck *et al.*, 1997).

The 10kDa Clara cell specific protein, CC10, was utilised in order to detect their presence within the NHBE model (Singh and Katyal, 1997; Singh and Katyal, 2000). As one descends down the respiratory tract goblet cells become less frequent and are replaced by Clara cells. Clara cells are predominantly located in the terminal and respiratory bronchioles (Boers *et al.*, 1999; Widdicombe, 2002).

The identification of inter- and intra-cellular mucin and therefore, presence and development of goblet cells, was achieved by a positive Periodic-Acid Schiff (PAS) stain. PAS is known to stain mucopolysaccharides and glycogen, which are the main components of the mucus produced and secreted by goblet cells (Zugibe, 1970).

In order to determine the role of basal cells during the development of the fully-differentiated, NHBE model, a basal cell specific marker, p63 (Yang *et al.*, 1998; Yang *et al.*, 1999; Wang *et al.*, 2002), was monitored. Yang and co-workers (1999) deduced that p63 preserved the self-renewal capacity (i.e. progenitor

activity) of cells as p63 was highly expressed in basal cells, yet rapidly degraded upon differentiation.

One of the major functions of the respiratory epithelium is its ability to 'maintain a barrier' between the airway lumen and the internal milieu. The tight junctions are the most apically located of all epithelial junctions and were first discovered by Farquar and Palade in 1963. Despite this, the specific proteins involved in tight junctions were not discovered until much later; ZO-1 (Stevenson *et al.*, 1986), occludin (Furuse *et al.*, 1993) and claudin (Furuse *et al.*, 1998). These are the three integral tight junction proteins that will be the focus in this Chapter. ZO-1 is a tight junction associated protein present on the cytoplasmic side (Anderson *et al.*, 1988) and occludin and claudin are both 4-pass transmembrane proteins present at the point of tight junction membrane contacts (Furuse *et al.*, 1993; Furuse *et al.*, 1998).

4.2 MATERIALS AND STOCK SOLUTIONS

4.2.1 STOCK SOLUTIONS

SOLUTIONS	SUPPLIER
EDTA	Fisher Scientific, Manchester, UK
Tween ²⁰ PBS with 1% BSA Mayer's Hematoxylin Gill's Hematoxylin Paraformaldehyde Triton X-100	Sigma, Dorset, UK
Normal Goat Serum Mouse Anti-Human Cytokeratin 5/6 Mouse IgG ₁ (Negative Control) Streptavidin:Biotynylated Enzyme Complex Liquid DAB Chromagen	Dako, Ely, UK

Table 4.1 Table of stock solutions used and their suppliers.

SOLUTIONS	SUPPLIER
Biotinylated Goat Anti-Mouse IgG Rabbit IgG (Negative Control) Vectorshield Mounting Medium with DAPI	Vector Laboratories, Peterborough, UK
Clara Cell Protein (CC10)	BioVendor, Heidelberg, Germany
Histostain® Plus Rabbit Primary Kit Rabbit Anti-Human ZO-1 (Mid) Rabbit Anti-Human Claudin-1 Mouse Anti-Human Occludin AlexaFluor® 594, Goat Anti-Rabbit IgG AlexaFluor® 488, Goat Anti-Mouse IgG ₁	Invitrogen, Paisley, UK
1% Periodic-Acid Schiff's Reagent	Pioneer Research Chemicals Ltd., Essex, UK
Mouse Anti-Human p63 (Clone 4A4)	BD Pharmingen™, Oxford, UK
Mouse IgG _{2a} (Negative Control)	Bio-Stat, Stockport, UK
DPX Mountant	VWR International Ltd., Poole, UK

Table 4.1 Continued table of stock solutions used and their suppliers.

4.2.2 EQUIPMENT

EQUIPMENT	SUPPLIER
Humidity Chamber	Mechanical Workshop, Cardiff University, UK
Phase Contrast LM (DM2500) Digital Camera (DFC 320) Q550 IW Workstation QWin Image Analysis Software (v.3) Confocal Microscope (DM6000) Confocal System (TCS SP2 A0BS) LCS Lite Confocal Software (v.2.6.1)	Leica Ltd., Milton Keynes, UK

Table 4.2 Table of equipment used and their suppliers.

4.3 METHODS

4.3.1 TISSUE PROCESSING FOR LIGHT MICROSCOPY

Cell culture inserts were immersed in 10% neutral buffered formalin (4°C) for 24 hours in preparation for paraffin embedding and sectioning, outlined previously (Sections 3.3.4.1 – 3.3.4.4). Following this, culture sections can then undergo immunohistochemical or histochemical detection (Sections 4.3.2 – 4.3.5). All washes were done with sections in a slide rack within a glass jar and all incubations were performed in a LM humidity chamber.

4.3.2 IMMUNOHISTOCHEMISTRY: CYTOKERATIN 5/6

EDTA (1mmol/L, pH 9.0) was heated to boiling before immersing NHBE specimen (5µm sections; $n = 3$) slides in the solution (2 minutes). Slides were rinsed twice with buffer wash (PBS pH 7.4 with 0.05% Tween), followed by immersion in 0.5% H₂O₂ in methanol for 10 minutes (to block endogenous peroxidase activity), and then washed in wash buffer 2 minutes (x3). Non-specific binding of the 2° antibody was blocked by incubating in 20% normal goat serum (200µl) for 20 minutes.

Excess serum was removed and sections incubated with either 100µl of 2.2µg/ml cytokeratin 5/6 1° antibody (diluted using antibody dilutant: 1% BSA in PBS [pH 7.4] with 0.05% Tween), or mouse IgG₁ negative control for 1 hour. Sections were washed with buffer wash for 2 minutes (x3). Slides were incubated with 100µl of 15µg/ml biotinylated goat anti-mouse IgG 2° antibody (diluted with antibody dilutant) for 20 minutes, followed by washing in buffer wash for 2 minutes (x3).

Tissue sections were covered with 100µl of the streptavidin: biotinylated enzyme complex for 20 minutes (complex allowed to form for 30 minutes prior to incubation). Slides were washed with buffer wash for 2 minutes (x3). Sections were incubated with liquid DAB chromagen (100µl) for 3 minutes and then

washed in distilled water. Counterstaining was done with Mayer's hematoxylin for 45 seconds, followed by rinsing in running tap water (20 seconds).

Tissue sections underwent dehydration and cover-slips were mounted before images were captured (Section 4.3.6). LM images were captured using the Q550 IW Workstation at x40 magnification and saved as TIFF images. A specific length of each membrane (15cm on screen) was selected for analysis within the QWin3 program. The 'colour detect' feature was used to detect the quantity (area, μm^2) of CK 5/6 staining in each image. The total surface area (μm^2) of culture was also detected and the quantity of CK 5/6 staining calculated as a percentage of this.

4.3.3 IMMUNOHISTOCHEMISTRY: CC10

NHBE specimen slides (5 μm sections; $n = 3$) were immersed in 0.5% H_2O_2 in methanol for 10 minutes (to block endogenous peroxidase activity), and then washed in buffer wash (PBS pH 7.4 with 0.05% Tween) 2 minutes (x3). Non-specific binding of the 2° antibody was blocked by incubating in 20% normal goat serum (200 μl) for 20 minutes.

Excess serum was removed and sections incubated with either 100 μl of 10 $\mu\text{g/ml}$ CC10 1° antibody (diluted using antibody dilutant: 1% BSA in PBS [pH 7.4] with 0.05% Tween), or rabbit IgG negative control for 30 minutes. Sections were washed with buffer wash for 2 minutes (x3). Sections were incubated with 100 μl of 10 $\mu\text{g/ml}$ biotinylated goat anti-rabbit IgG 2° antibody (Histostain® Plus Rabbit Primary kit) for 20 minutes, followed by washing in buffer wash for 2 minutes (x3).

Tissue sections were covered with 100 μl of the streptavidin peroxidase-HRP for 20 minutes (Histostain® Plus Rabbit Primary kit). Slides were washed with buffer wash for 2 minutes (x3). Sections were incubated with liquid DAB chromagen (100 μl) for 3 minutes then washed in distilled water. Counterstaining was done with Mayer's hematoxylin for 45 seconds, followed by rinsing in running tap water (20 seconds).

Tissue sections underwent dehydration and cover-slips were mounted before images were captured (Section 4.3.6). LM images were captured using the Q550 IW Workstation at x40 magnification and saved as TIFF images. A specific length (15cm on screen) of each membrane was selected for analysis within the QWin3 program; the number of CC10⁺ stained cells within this area were counted. The total number of cells was determined and the number CC10⁺ stained cells calculated as a percentage of this.

4.3.4 PERIODIC-ACID SCHIFF STAINING

NHBE culture sections (5µm) were prepared for PAS staining and $n = 1$ section was stained for each insert. PAS staining was performed by histotechnologist Ms. Hilary Marshall (AstraZeneca, R&D Loughborough, UK), as outlined below.

Sections were treated with 1% periodic-acid for 5 minutes, followed by several washes in dH₂O. Then sections were treated with Schiff's reagent for 8 minutes, followed by washing in running tap water for 10 minutes. Counterstaining was undertaken with Gill's hematoxylin for 2 minutes, followed by washing in running tap water for 10 minutes.

Sections underwent dehydration and cover-slips were mounted before images were captured. LM images were captured using the Q550 IW Workstation at x40 magnification and saved as TIFF images.

4.3.5 IMMUNOHISTOCHEMISTRY: P63

NHBE specimen slides (5µm sections; $n = 3$) were immersed in 6% H₂O₂ in methanol for 10 minutes (block endogenous peroxidase activity), followed by washing in buffer wash (PBS [pH 7.4] with 0.05% Tween) for 2 minutes (x3). Non-specific binding of the 2° antibody was blocked by incubating in 20% normal goat serum (200µl) for 20 minutes.

Excess serum was removed and sections were incubated with either, 100µl of 5µg/ml p63 1° antibody (diluted using antibody dilutant: 1% BSA in PBS [pH 7.4])

with 0.05% Tween), or mouse IgG₂a negative control overnight (4°C). Slides were then washed with buffer wash for 2 minutes (x3). Sections were incubated with 100µl of 15µg/ml biotinylated goat anti-mouse 2° antibody (diluted using antibody dilutant) for 20 minutes, followed by washing slides in buffer wash for 2 minutes (x3).

Tissue sections were covered with 100µl of the streptavidin: biotinylated enzyme complex for 20 minutes (complex allowed to form for 30 minutes prior to incubation). Slides were washed with buffer wash for 2 minutes (x3). Sections were incubated with liquid DAB chromagen (100µl) for 2 minutes then washed in distilled water (2 minutes). Counterstaining was done with Mayer's hematoxylin for 45 seconds, followed by rinsing in running tap water (20 seconds).

Tissue sections underwent dehydration and cover-slips were mounted before images were captured (Section 4.3.6). LM images were captured using the Q550 IW Workstation at x40 magnification and saved as TIFF images. A specific length (15cm on screen) of each membrane was selected for analysis within the QWin3 program; the number of p63⁺ stained nuclei within this area were counted. The total number of nuclei was determined and the number of p63⁺ cells calculated as a percentage of this.

4.3.6 DEHYDRATION AND ADDITION OF COVER-SLIPS

Treated sections must be covered with a glass cover-slip to, protect the tissue, provide better optical quality for viewing under the LM and to preserve the tissue section for archival purposes. The treated slides were dehydrated by immersing (2 minutes) in an increasing series of alcohol; 70% → 95% → 100% (x2) and xylene (x2).

Slides remained in xylene until ready for cover-slips to be attached. A small amount (20µl) of DPX mountant was placed on a cover-slip and the slide carefully lowered onto the cover-slip and DPX. The slide is left cover-slip side up overnight (RT). Sections were viewed using a Leica Phase Contrast LM (DM2500) attached to a digital camera (Leica DFC 320) and images saved as TIF files.

4.3.7 STATISTICAL ANALYSIS

Data was assessed for normality with the Anderson-Darling test for homogeneity in Minitab 15 (Microsoft Inc., WA, USA); none of the data tested was normally distributed. Therefore, the non-parametric Mann-Whitney test (SPSS 15.0, SPSS Inc. IL, USA) was performed in order to assess if there was any significant differences between the NHBE cultures at different days. Significance was accepted at $p \leq 0.05$, whilst $p \leq 0.01$ indicated high statistical significance (Dytham, 2003). Standard deviation was used to represent experimental variation.

4.3.8 CONFOCAL MICROSCOPY: TIGHT JUNCTIONS

NHBE culture inserts were fixed and tested for the presence of the tight junction proteins; ZO-1, claudin-1 or occludin ($n = 2$), over the development of the model (Day 1 – 42). The cultures were either used for the detection of one tight junction protein; ZO-1 or claudin-1 (Section 4.3.8.1 – 4.3.8.2) or two tight junction proteins; ZO-1 and occludin or claudin-1 and occludin (Section 4.3.8.1 – 4.3.8.3). Detection was the same for both methods (Section 4.3.8.4).

4.3.8.1 INITIAL CULTURE PROCESSING FOR CONFOCAL MICROSCOPY

Cell culture inserts were immersed in 4% paraformaldehyde (RT) for 10 minutes and stored in PBS (pH 7.4) at 4°C until used (stored for no longer than 72 hours). After storing, inserts were washed in PBS (pH 7.4) for 2 minutes (x3). Cultures were permeabilised with 200µl Triton X 0.1% in antibody dilutant (1% BSA in PBS [pH 7.4] with 0.05% Tween) for 20 minutes (RT) and then removed. Non-specific binding of the 2° antibody was blocked by incubating in 20% normal goat serum (200µl) for 20 minutes.

4.3.8.2 INCUBATION WITH FIRST PRIMARY AND SECONDARY ANTIBODIES

Excess serum was removed and inserts ($n = 2$ for each 1° antibody) were incubated with either 150µl of 2.5µg/ml ZO-1 1° antibody (diluted using antibody dilutant), 2.5µg/ml claudin-1 1° antibody (diluted using antibody dilutant), or

2.5µg/ml rabbit IgG₁ negative control for 1 hour. Cultures were washed with PBS (pH 7.4) for 2 minutes (x3). Followed by, incubation with 150µl of 1:200 Alexa Fluor[®] 594 2° antibody (diluted using antibody dilutant) for 1 hour (dark), followed by washing in PBS (pH 7.4) for 2 minutes in the dark (x3). If an NHBE inserts was being used for the detection of a second 1° antibody, the protocol followed on to Section 4.3.8.3. If only one 1° antibody was being detected, the protocol skipped onto Section 4.3.8.4.

4.3.8.3 INCUBATION WITH SECOND PRIMARY AND SECONDARY ANTIBODIES

Inserts were incubated with either 150µl of 5µg/ml occludin 1° antibody (diluted using antibody dilutant), or 5µg/ml rabbit IgG₁ negative control for 1 hour (dark). Cultures were washed with PBS (pH 7.4) for 2 minutes in the dark (x3). Followed by, incubation with 150µl of 1:200 Alexa Fluor[®] 488 2° antibody (diluted using antibody dilutant) for 1 hour (dark), followed by washing inserts in PBS (pH 7.4) for 2 minutes in the dark (x3).

4.3.8.4 COUNTERSTAINING, MOUNTING AND DETECTION

Inserts were incubated with 300nM DAPI nuclear stain (200µl) for 2 minutes (dark). The membrane was then cut from the insert using a scalpel and mounted using Vectorshield with DAPI, cell side up. Slides were stored in the dark (4°C) until images were taken. NHBE cultures were viewed and images taken as TIFF files using the Leica DM6000 Microscope, Leica TCS SP2 A0BS Confocal System and Leica Confocal Software v.2.6.1.

4.4 RESULTS

NHBE cultures ($n = 7$) were collected every 3 days over a 42 day period; $n = 2$ inserts were prepared for LM using standard techniques (Chapter 3) and the other 5 inserts were prepared for confocal microscopy (Section 4.3.6). Histological and immunological analysis was undertaken on every time point over the 42 day culture period. Ck 5/6 detection enabled identification of basal and intermediate cells of epithelial origin; CC10 antibody revealed the presence of

Clara cells; PAS staining highlighted mucin secreting goblet cells; p63 antibody highlighted the basal/progenitor cells within the cultures and ZO-1, occludin and claudin-1 were used to verify the formation of tight junctions. All negative controls resulted in a negative response (images not shown). However, some Day 42 control inserts from the tight junction work displayed some autofluorescence that was associated with dead/dying cells.

4.4.1 CYTOKERATIN 5/6: EPITHELIAL CELLS

The almost confluent monolayer of NHBE cells at Day 1 (24 hours post-seeding) displayed CK 5/6⁺ staining throughout the cytoplasm of all cells present. The nuclei of cells remained unstained, resulting in ~70% of the total culture area being positively stained (Figure 4.1[A]). The percentage total of CK 5/6⁺ staining gradually decreased to ~50% by Day 9, with the staining receding to the basal and supra-basal layers (Figure 4.1[B]). The accumulation of staining within the basal and supra-basal layers continued until about Day 18, where the total stain amounted to 45% (Figure 4.1[C]). CK 5/6⁺ staining within cultures stabilised, both in location and percentage coverage between Days 12 – 24 at approximately 45% (Figure 4.3).

From Day 24 CK 5/6⁺ staining gradually decreased from 44% (Day 24) to ~28% by Day 36 (Figure 4.3). Visually, staining remained of the same quantity and location, however, as the apical cells underwent pseudo-stratification, the total area of the culture increased, with the total percentage area of CK 5/6⁺ staining decreasing. Day 36 revealed culture deterioration, with CK 5/6⁺ staining becoming less intense within the supra-basal layer, but remaining within the basal layer (Figure 4.2[A]). Further deterioration and squamation of cultures occurred by Day 39, with CK 5/6⁺ staining focally accumulated in the basal layer (Figure 4.2[B]). NHBE cultures at Day 42 appeared squamous, however, CK 5/6⁺ staining within the culture displayed a highly significant increase ($p < 0.001$) from Day 39, from ~22% to ~40%, with defined staining observed within the basal and supra-basal layers (Figure 4.2[C]).

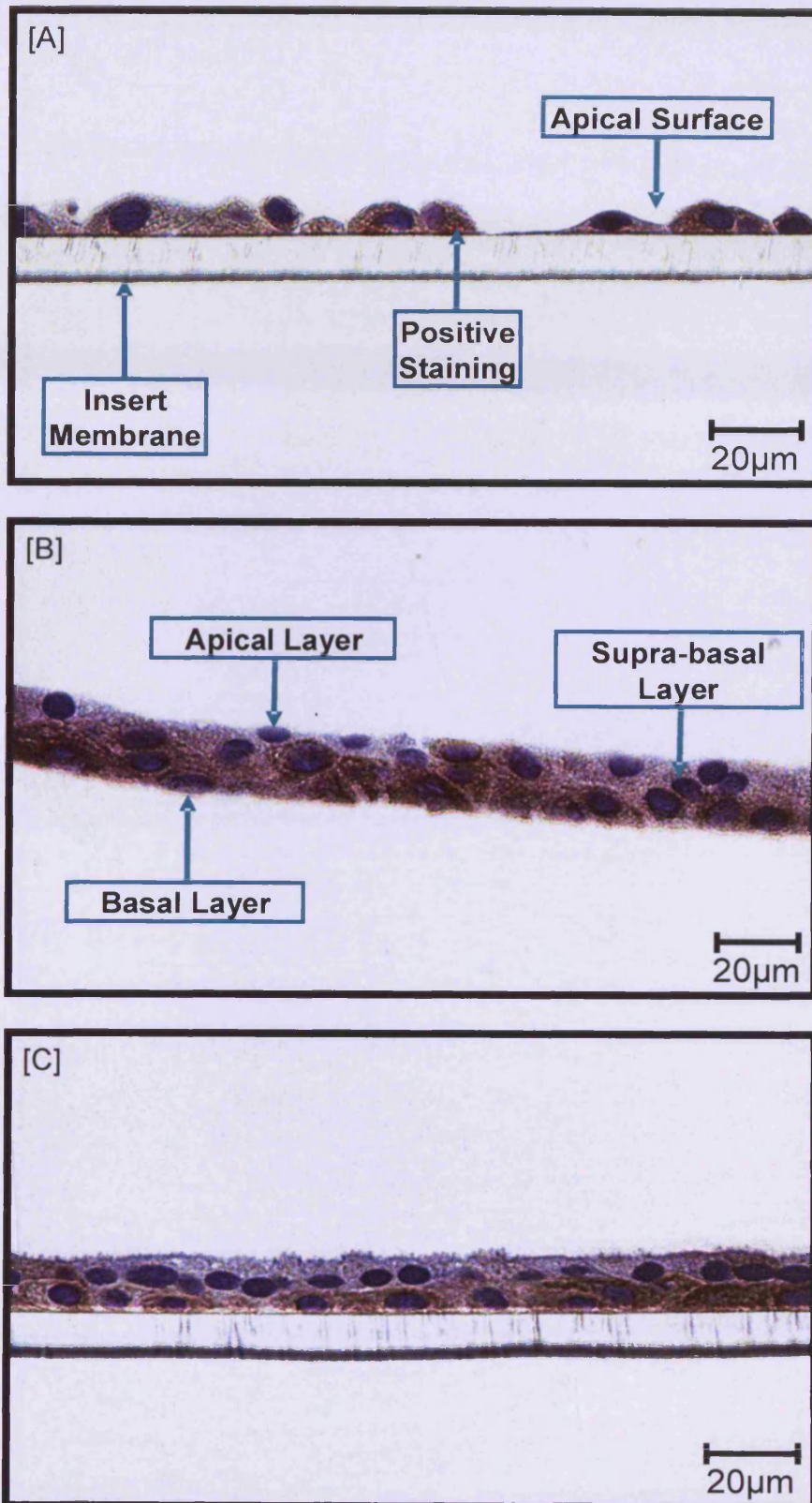


Figure 4.1 LM images of NHBE cultures stained for CK 5/6 (red/brown colour). [A] Day 1; staining in cytoplasm of all cells. [B] Day 9; staining observed in the cytoplasm in the majority of cells, less so in the apical layer. [C] Day 18; staining predominantly in the cytoplasm of basal and supra-basal cells.

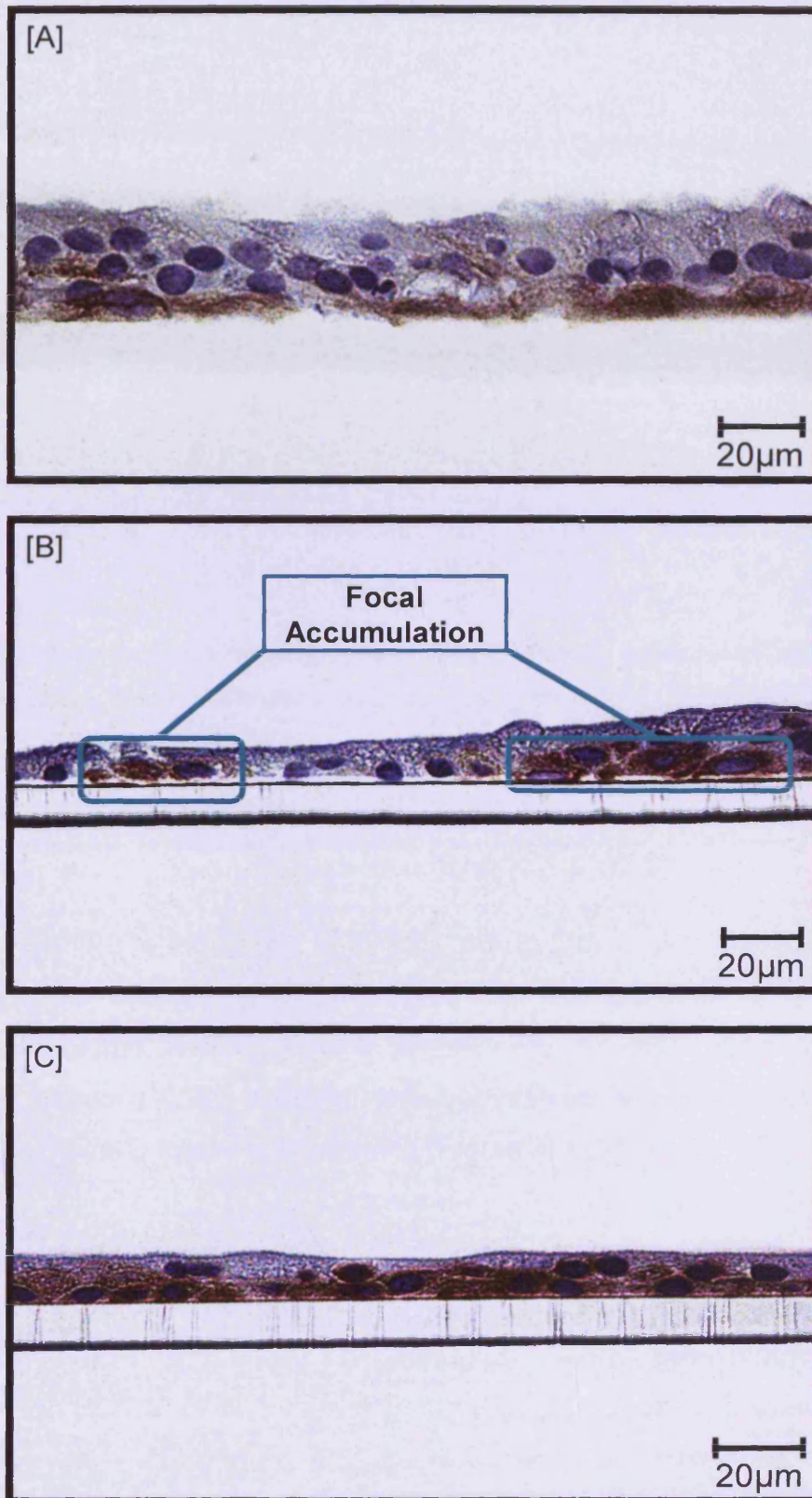


Figure 4.2 LM images of NHBE cultures stained for CK 5/6 (red/brown colour). [A] Day 36; staining in cytoplasm of basal and some supra-basal cells. [B] Day 39; focal accumulation of stain observed in some basal cells. [C] Day 42; intense staining observed in the cytoplasm of basal and supra-basal cells.

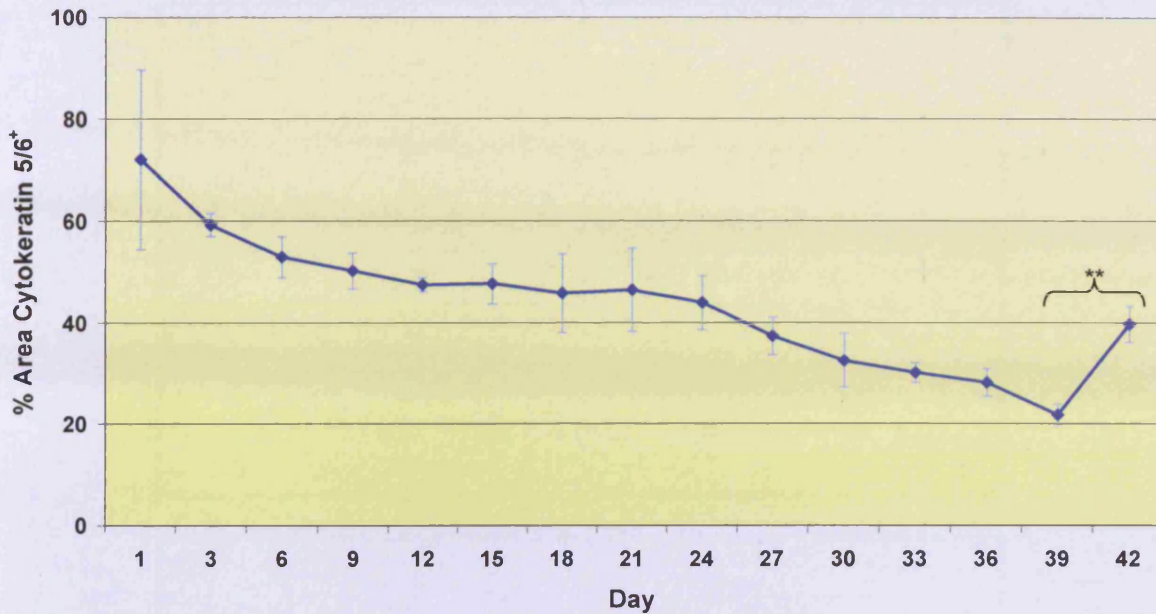


Figure 4.3 Graph displaying percentage area of CK 5/6⁺ staining within NHBE cultures over the culture period (Days 1 – 42). Standard deviation was displayed (I), ** denotes high significant difference ($p < 0.001$), $n = 3$.

4.4.2 CC10: CLARA CELLS

The almost confluent monolayer of NHBE cells at Day 1 (24 hours post-seeding) displayed no CC10⁺ staining (Figure 4.4[A]). No positive staining was observed until Day 9 (Figure 4.4[B]), where around 7% of cells were stained. The percentage total of CC10⁺ staining remained at this level until Day 21 (Figure 4.6), with the staining intensity increasing (Figure 4.4[C]).

Cultures at Day 24 revealed an increase in the number of CC10⁺ cells (Figure 4.5[A]), with the percentage of these cells remaining at ~17% until Day 36 (image not shown) (Figure 4.6). Day 39 revealed culture deterioration, with the percentage of CC10⁺ cells increasing significantly ($p < 0.001$) from the stable period; Days 24 – 36 (Figure 4.5[B]). However, the number of CC10⁺ cells remained the same as Days 24 – 36, but due to the culture deterioration and squamation, the percentage of CC10⁺ cells appeared to increase. Cultures at Day 42 were very squamated and the number and percentage of CC10⁺ cells displayed a highly significant ($p < 0.001$) decrease compared to Days 24 - 39 (Figure 4.5[C] and 4.6).

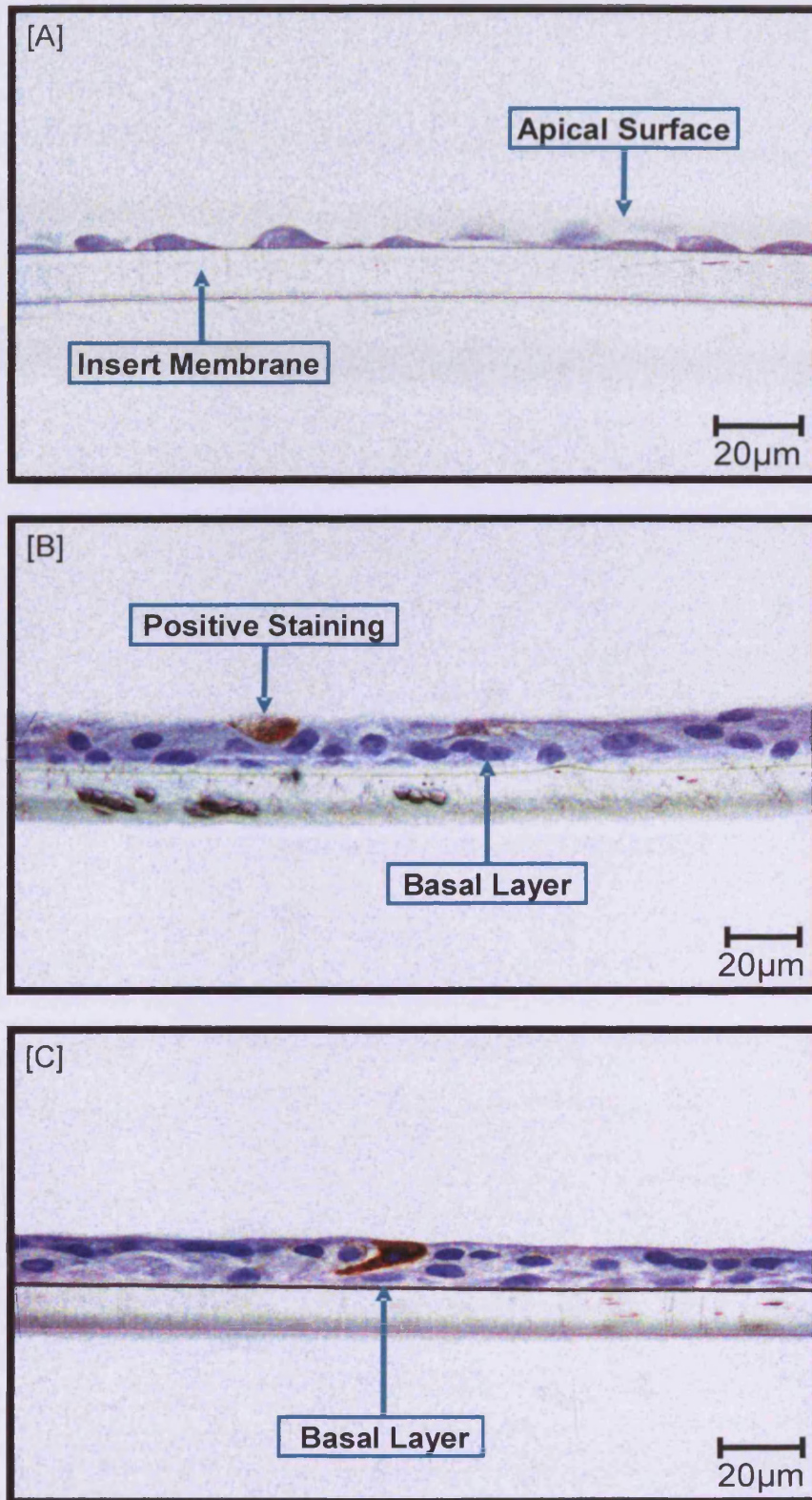


Figure 4.4 LM images of NHBE cultures stained for CC10 (red/brown colour). [A] Day 1; no staining observed. [B] Day 9; staining observed in the cytoplasm of an apically located cell. [C] Day 21; staining observed in an apically located cell, with the cytoplasm stained all the way throughout the cell, until it reached the membrane.

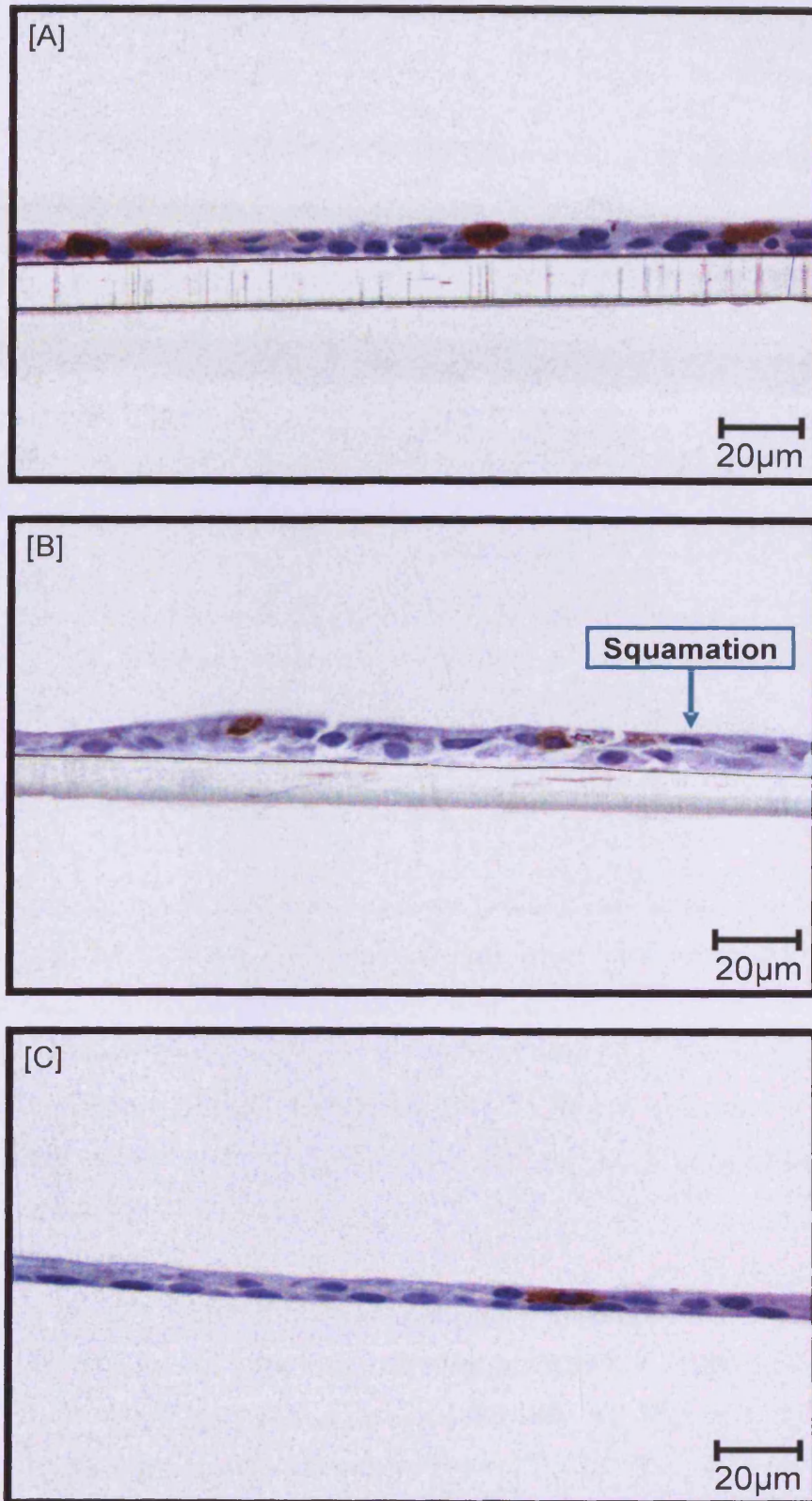


Figure 4.5 LM images of NHBE cultures stained for CC10 (red/brown colour). [A] Day 24; staining observed in the cytoplasm of some apically located cells. [B] Day 39; staining observed in the cytoplasm of some cells and others becoming squamous. [C] Day 42; staining observed in fewer cells, culture appeared squamous.

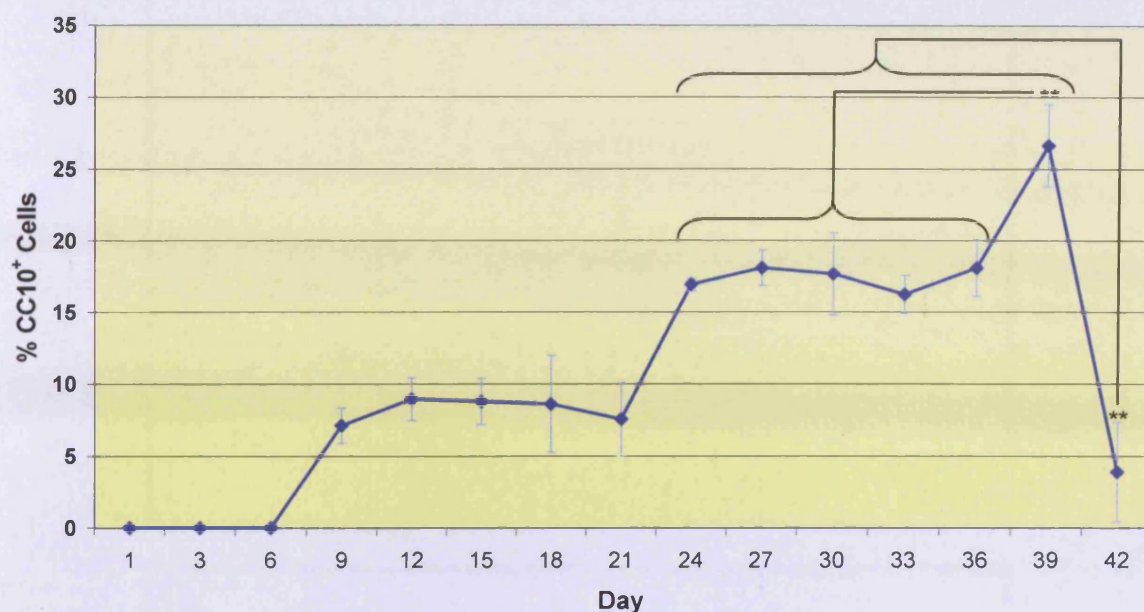


Figure 4.6 Graph displaying percentage of CC10⁺ cells within NHBE cultures over the culture period (Days 1 – 42). Standard deviation was displayed (I), ** denotes high significant difference ($p < 0.001$), $n = 3$.

4.4.3 PERIODIC-ACID SCHIFF: GOBLET CELLS

NHBE cultures, 24 hours post-seeding (Day 1) displayed no positive PAS staining (Figure 4.7[A]). No positive PAS staining was observed within the culture until Day 12. At Day 12 positive staining could be observed within a few cells, however staining did not fill the entire cell and no staining could be observed on the apical surface of the culture (Figure 4.7[B]). By Day 15, entire cells in the apical layer were positively stained, with an almost consistent thin layer of positive staining on the apical surface (Figure 4.7[C]).

PAS staining within cultures remained relatively consistent until Day 42. The only difference was a slight increase in the number of positively stained cells up to Day 21, where it remained relatively constant until Day 42 (Figure 4.8[A]). Cultures began to deteriorate structurally from Day 36. On Day 42, cultures either displayed a large increase in positively stained cells or cultures deteriorated to a squamous monolayer, with a low level of staining (Figure 4.8[B] and [C]).

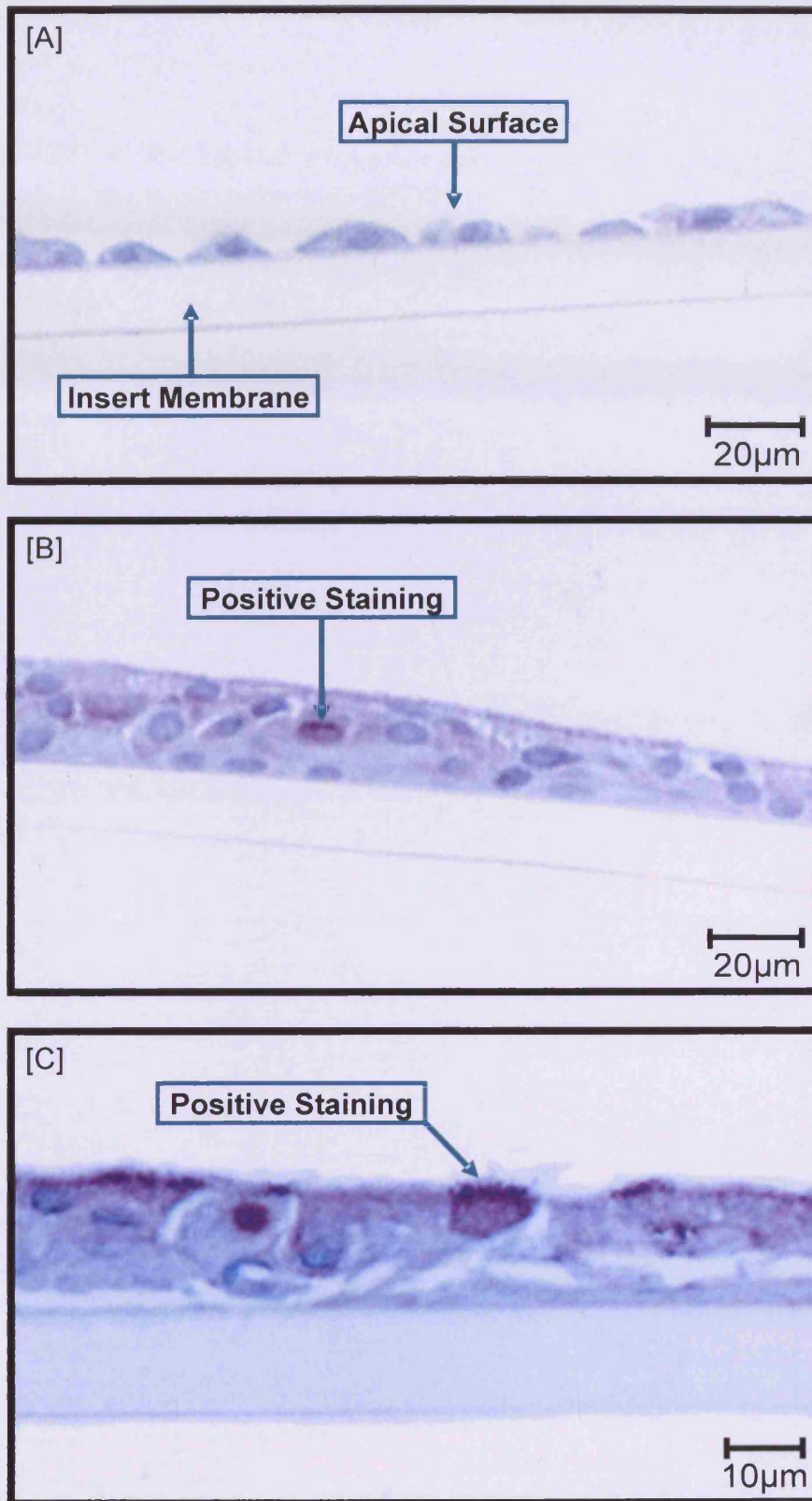


Figure 4.7 LM images of NHBE cultures stained with PAS (dark purple colour). [A] Day 1; no positive staining observed. [B] Day 12; some staining observed within the culture, but not definite goblet cells. [C] Day 15; numerous cells intensely stained throughout the culture.

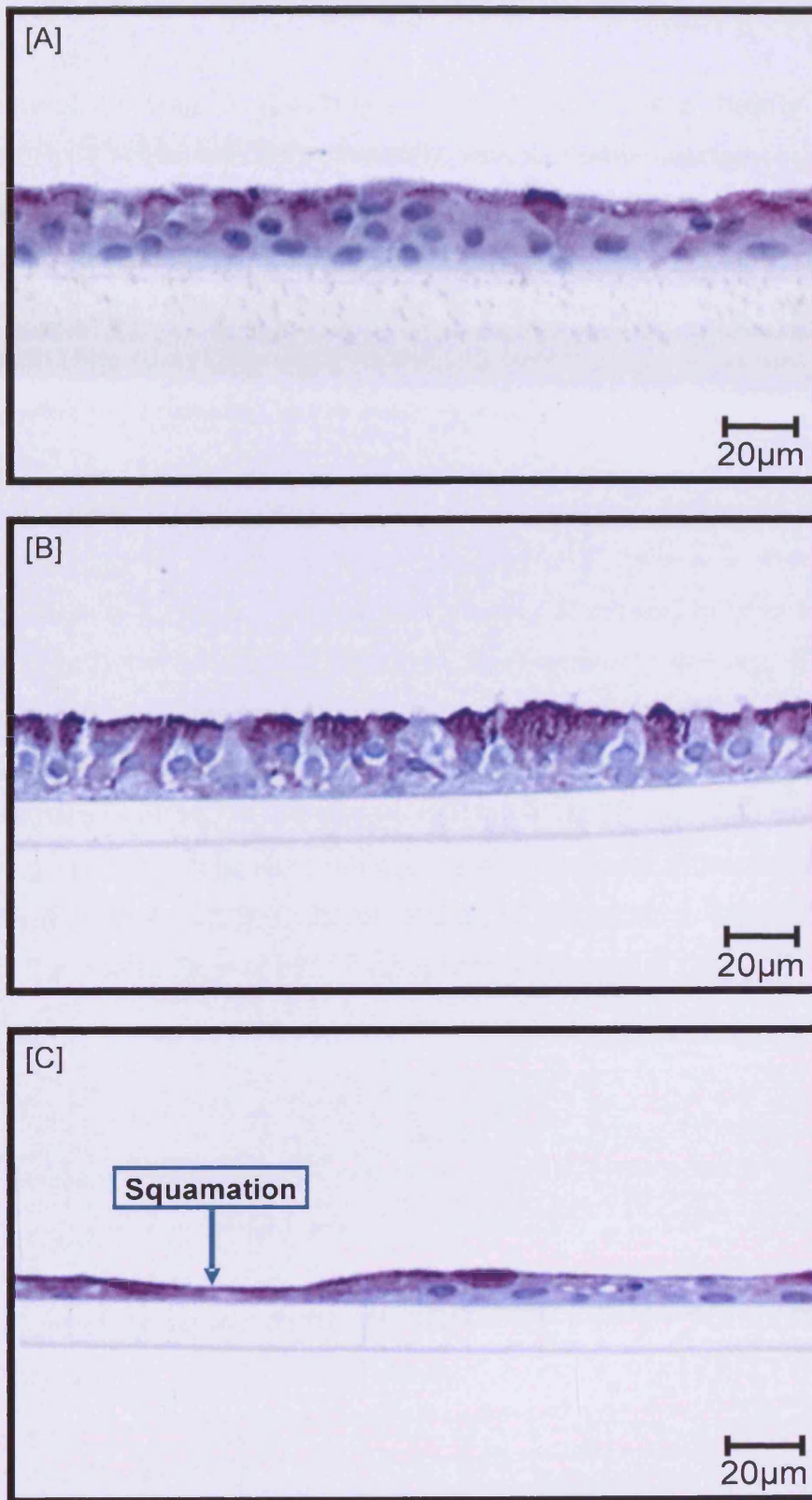


Figure 4.8 LM images of NHBE cultures stained with PAS (dark purple colour). [A] Day 27; several cells intensely stained throughout the culture. [B] Day 42; numerous cells heavily stained throughout the culture. [C] Day 42; culture deterioration, less cells positively stained.

4.4.4 P63: BASAL/PROGENITOR CELLS

NHBE cultures at Day 1 (24 hours post-seeding) were nearly completely comprised of p63⁺ cells with approximately 98% of nuclei stained (Figure 4.9[A]). As the model developed with an increase in the number of cells, the percentage of p63⁺ cells in the construct gradually decreased. Positive p63 staining at Day 6 was detected in the nuclei of basal and supra-basal cells, with ~60% of total nuclei stained (Figure 4.9[B]). Positive staining continued to decrease to ~50% by Day 9, with staining retreating to the basal layer (Figure 4.9[C]).

A gradual decrease in p63⁺ cells occurred after Day 1 and continued until Day 15, where it accounted for around 38% of cells, the p63⁺ cells are observed in the basal layer (Figure 4.10[A]). Positive p63 staining stabilised both in location and number of cells between Day 15 and Day 39 (Figure 4.10[A] and [B]). Positive staining was mainly contained to the basal cells, with some supra-basal cells positively stained; the quantity of staining remained between 25 – 38% (Figure 4.11). Deterioration of the NHBE culture by Day 42 coincided with an increase in p63⁺ staining; all basal cells were stained as well as some supra-basal cells (now apical cells) (Figure 4.10[C]). Cultures at Day 42 exhibited a significant ($p < 0.05$) increase in the percentage of p63⁺ cells when compared to Days 15 - 39 (Figure 4.11).

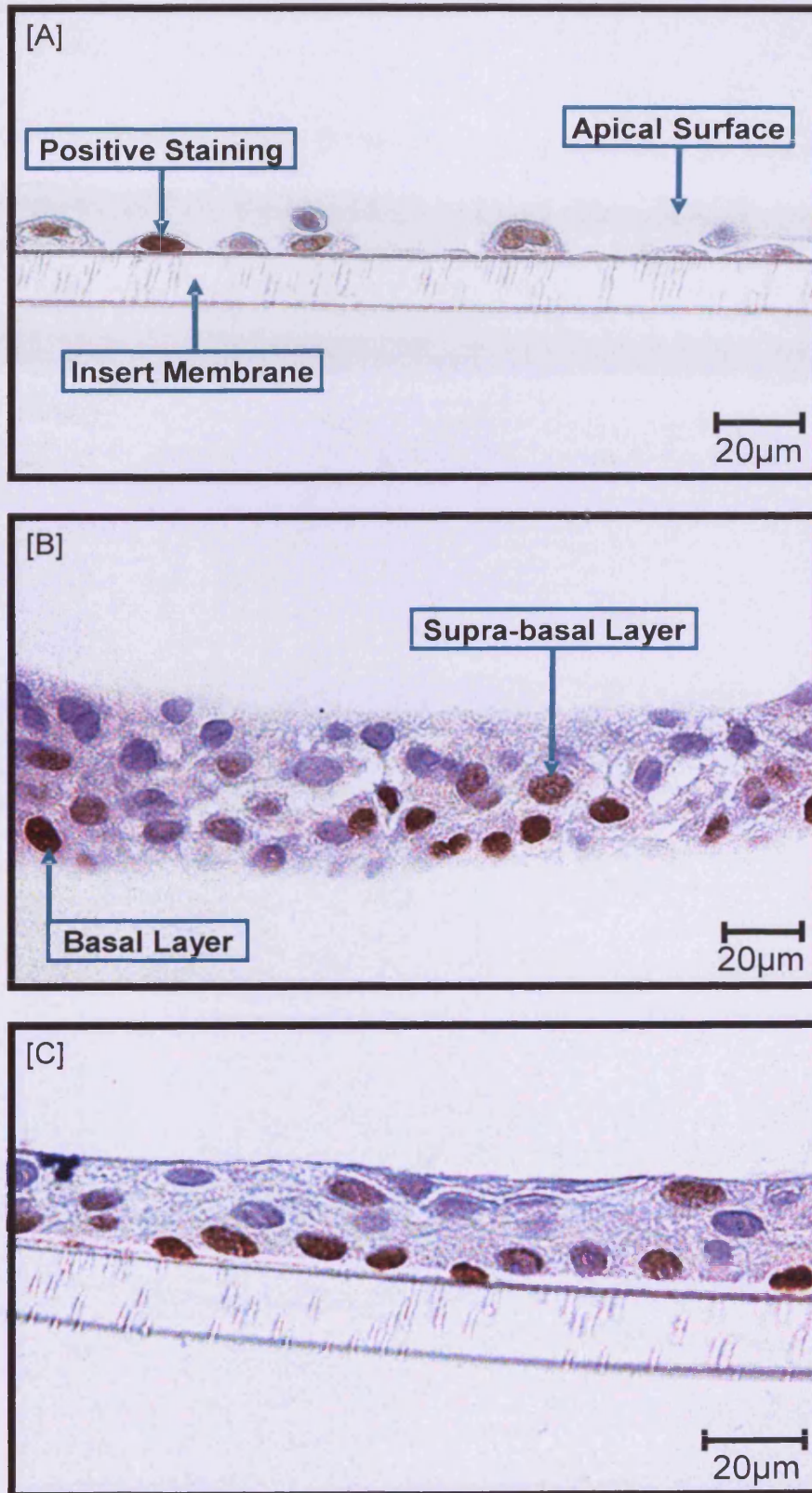


Figure 4.6 LM images of NHBE cultures stained with p63 (red/brown colour). [A] Day 1; staining seen in nuclei of all cells present. [B] Day 6; nuclear staining observed in basal cells and some supra-basal cells. [C] Day 9; nuclear staining observed mainly in basal cells, with some staining of supra-basal cells.

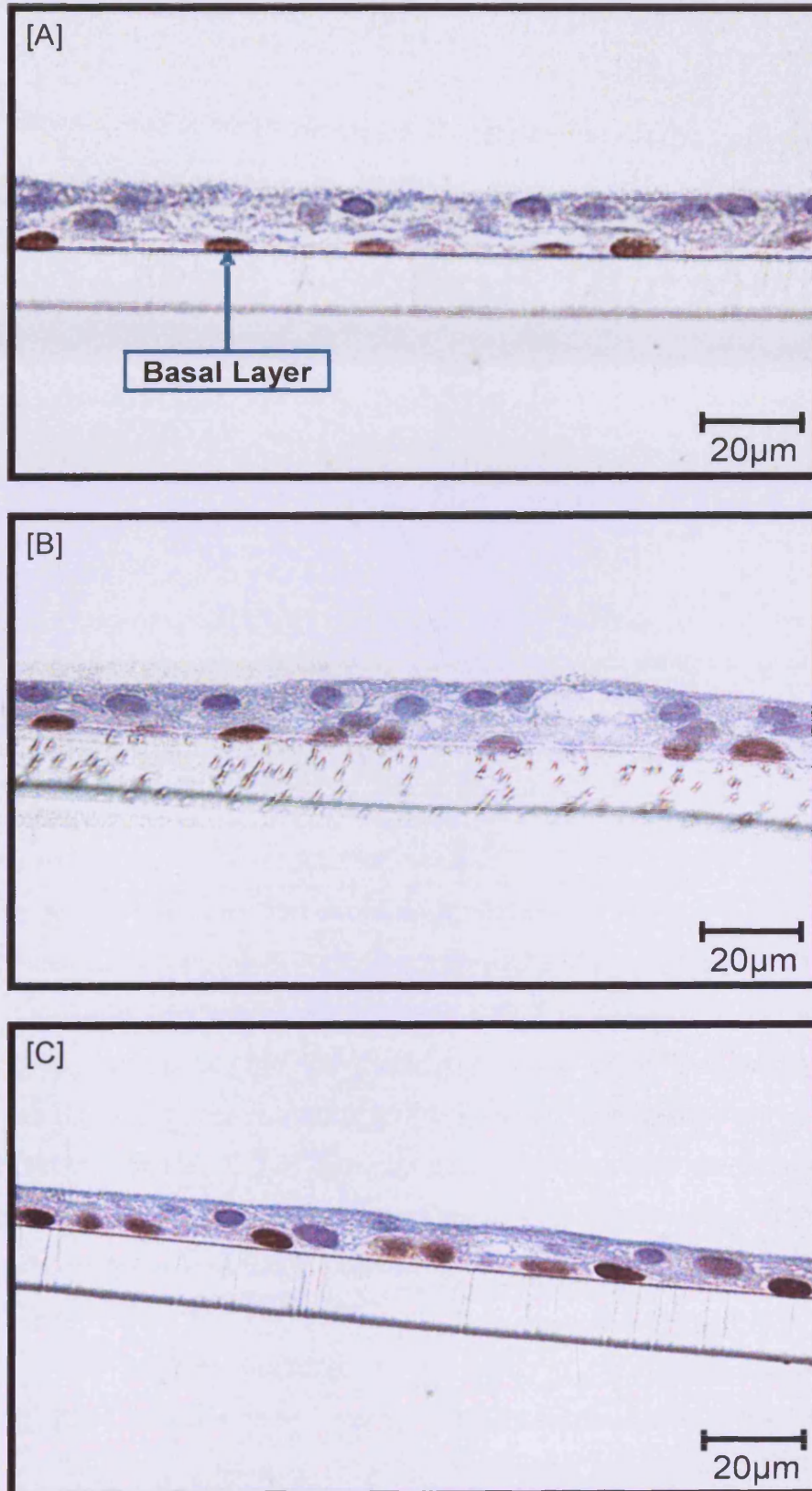


Figure 4.7 LM images of NHBE cultures stained with p63 (red/brown colour). [A] Day 15; staining located in nuclei of basal cells. [B] Day 39; nuclear staining detected in basal cells and some supra-basal cells. [C] Day 42; nuclear staining observed in basal cells, with light staining of supra-basal cells (i.e. apical cells).

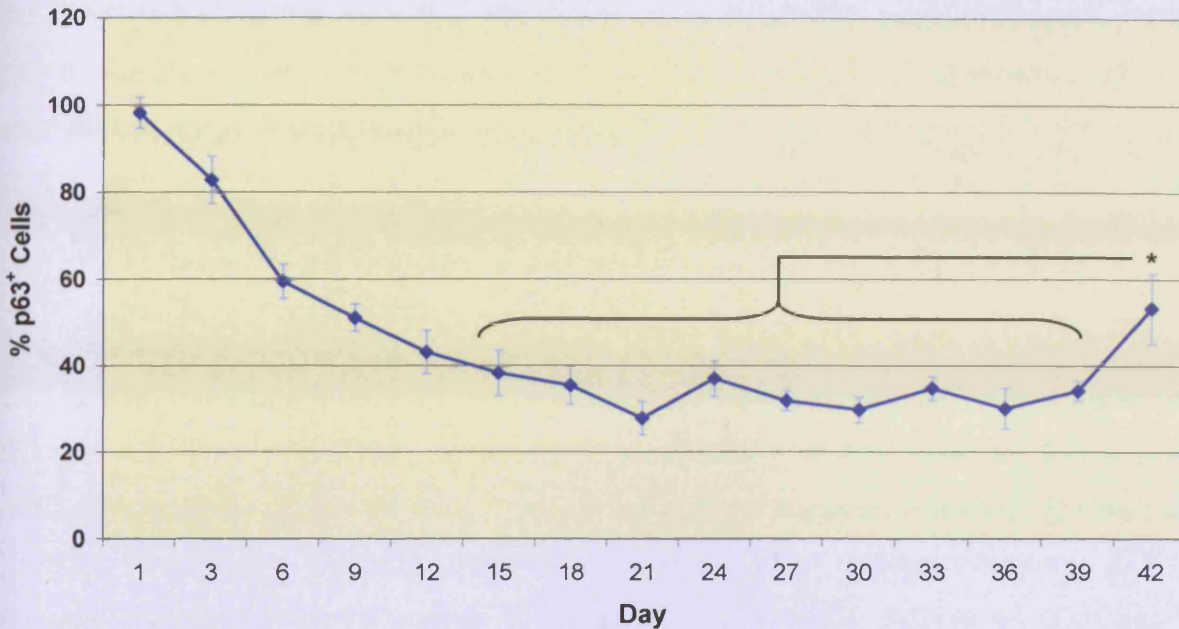


Figure 4.8 Graph displaying percentage of p63⁺ cells within NHBE cultures over the culture period (Days 1 – 42). Standard deviation displayed (I), * denotes significant difference ($p < 0.05$), $n = 3$.

4.4.5 TIGHT JUNCTION PROTEINS

NHBE cultures at Day 1 (24 hours post-seeding) displayed some positive staining for all three of the tight junction proteins investigated (Figure 4.9; Day 1). 'Hot-spots' of positive ZO-1 could be observed throughout the cytoplasm of most cells on Day 1. Occludin was positively detected in the cytoplasm of some cells, with the staining intensified around the periphery of the cells, the majority staining. However, the level of occludin staining throughout the cultures was less than that of either ZO-1 or claudin-1. Positive claudin-1 staining was detected throughout the cytoplasm of the majority of cells on Day 1, with the staining more dispersed and hot-spots more intense when compared to ZO-1.

After Day 1, the positive staining for the tight junction proteins appeared to accumulate at the cell periphery, rather than throughout the cytoplasm; as was observed on Day 6 (Figure 4.9; Day 6). ZO-1 was still present throughout the cytoplasm, with a few intense areas appearing on the periphery of some cells. The presence of occludin within NHBE cultures was still lower than the other tight junction proteins, however, a few very intense areas of staining were evident at the borders of some cells. Occludin appeared to co-localise in the same regions

as ZO-1, but were not always in the exact same spot, with occludin appearing in more places at the cell periphery without ZO-1, than ZO-1 appeared without occludin (overlay image not shown). Claudin-1 staining had migrated to the edge of the cells, yet staining did not form the clear lines that ZO-1 and occludin did; with staining remaining as numerous individual spots.

The migration of the tight junction proteins to the edge of the cells continued after Day 6, with clear delineation of cells by Day 15, especially with ZO-1 and occludin (Figure 4.9; Day 15). This characteristic delineation of the cells by ZO-1 and occludin could be observed over most of the culture surface, however, it was not present throughout. Occludin staining was again more widespread than ZO-1. Claudin-1 staining did not appear to follow the exact same pattern as both ZO-1 and occludin, with staining remaining within the cytoplasm and any delineation persisted as a 'dotted' rather than a 'solid' line.

The stable period for the NHBE cultures, in so far as these tight junction proteins were concerned, was Days 24 – 33 (Figure 4.9; Days 24 – 33). Both ZO-1 and occludin proteins formed a network of positive staining along the borders of the cells. Claudin-1 staining was more intense at the cell borders, forming 'dotted' as apposed to 'solid' lines, although considerable staining was observed within the cytoplasm of the cells.

The deterioration of the tight junction proteins ZO-1 and occludin was not observed until Day 42, claudin-1 staining revealed the beginning of deterioration earlier, by Day 36. In the more 'healthy' cultures, the characteristic staining network of ZO-1 and occludin could still be observed on Day 42, however, there were gaps in the network (Figure 4.9; Day 42). In the 'not-so healthy' cultures this staining pattern had practically disappeared, with most of the fluorescence appearing as autofluorescence; associated with dead/dying cells (image not shown). The deterioration of the claudin-1 staining was observed from Day 36 (image not shown) until Day 42 (Figure 4.9; Day 42). The positive staining receded from the cell periphery, with most of the other staining attributed to the autofluorescence associated with dead/dying cells.

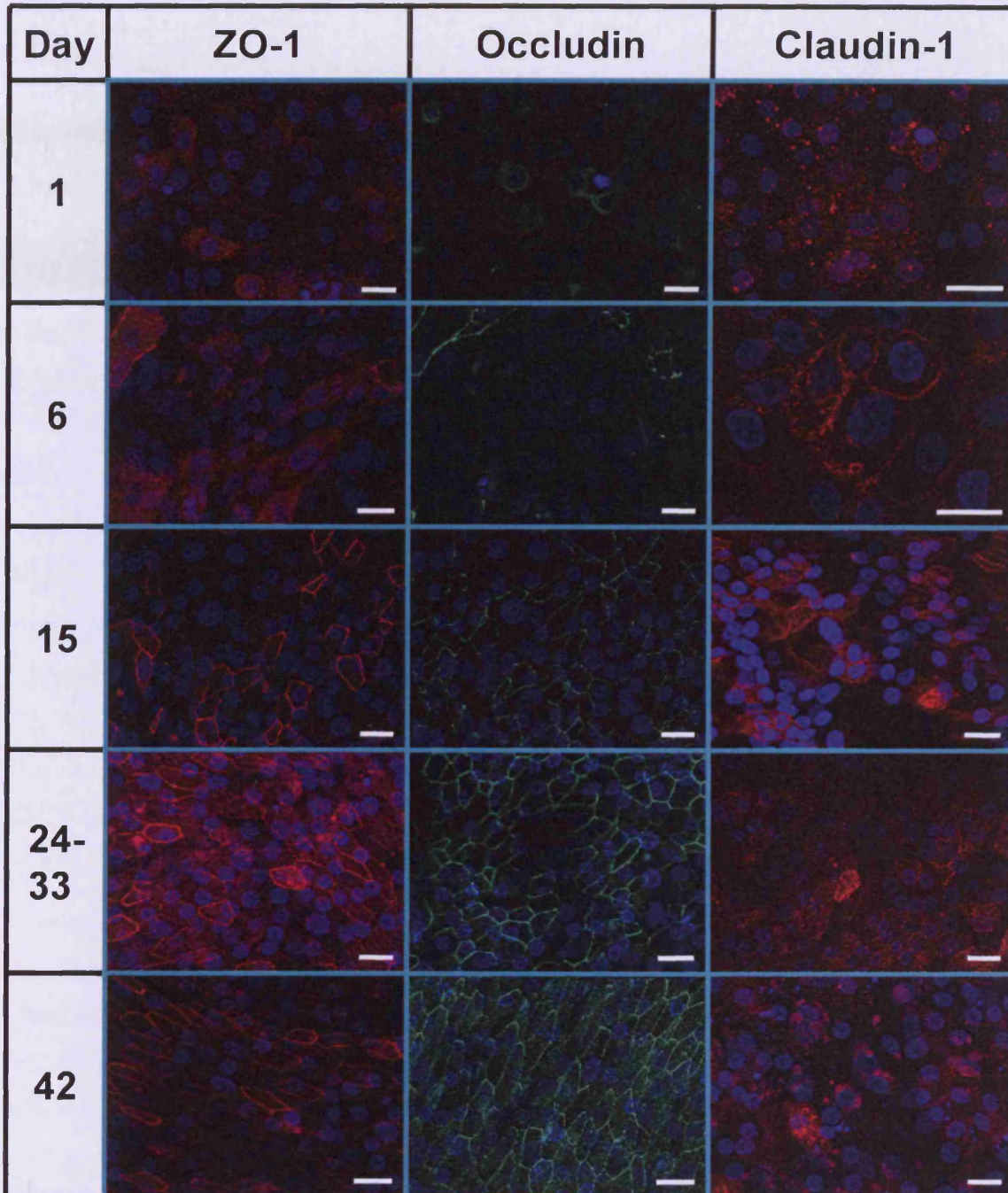


Figure 4.9 Confocal LM images of NHBE cultures stained with DAPI and the tight junction proteins. NHBE cultures on Days 1, 6, 15, 24 – 33 and 42 displayed stained with the nuclear stain DAPI (blue fluorescence) and either of the tight junction (TJ) proteins; ZO-1, claudin-1 (both red fluorescence) or occludin (green fluorescence). Day 1; positive staining observed for all TJ proteins. Day 6 and 15; migration and accumulation of staining at the cell periphery. Day 24 – 33; maturation of characteristic staining pattern. Day 42; deterioration of TJ staining. Scale bar = 20 μ m.

4.5 DISCUSSION

Previous work on the NHBE model concentrated on the morphogenic and biochemical characteristics of the human tissue equivalent of the respiratory epithelia (Chapters 2 and 3). This chapter's component of characterisation, during the model development, involved the confirmation of crucial functional characteristics and further affirmation of specific cell types. These included epithelial cytoskeletal components, presence of Clara, mucin secreting and progenitor cells (basal cells), as well as tight junction formation.

4.5.1 CYTOKERATIN 5/6: EPITHELIAL CELLS

Observations were made on the presence of CK 5/6 within the NHBE model over the 42 days of ALI culture. This was conducted both in terms of total distribution and locality. CK 5/6 was present throughout the cytoplasm of all cells present in cultures 24 hour post-seeding (Day 1), with only 70% total culture staining, due to the lack of staining within the nuclei. The total staining within the cytoplasm of all cells present at this stage coincided with CK 5/6 being a marker of hyper-proliferative epithelial cells (Neudeck *et al.*, 1997). Nelson and Sun (1983) demonstrated that certain embryonic epithelial cells expressed the CK 5/14 pair prior to stratification and that its expression appeared to be co-ordinated with the potential to stratify, with Stosiek and co-workers (1992) demonstrating that CK5/6 were present in the basal cells of the pseudo-stratified respiratory epithelium. Cells isolated from a fully-differentiated epithelium and cultured *in vitro* showed a tendency to cease expression of their differentiation-specific cytokeratins. However, these cells continued to express at least the baseline level of the CK 5/14 pair along with a significant increase in the hyper-proliferation keratin pair of CK 6/16, 17 (Goldman and Steinert, 1990).

Development of a monolayered NHBE culture to a pseudo-stratified epithelium resulted in the gradual decrease of total CK 5/6 staining, with a noticeable depletion and even eradication of staining within cells on the apical surface by Day 18. Day 18 demonstrated the typical staining pattern observed within this mature culture from this day until Day 36. CK 5/6 staining was now intense and

present mainly in the basal and occasionally, within the supra-basal cell layers. Staining was presumed to be due to the presence of the CK 5/14 pair rather than the CK 6/16, 17 pair. This would be consistent with many observations that CK 5/14 is found in basal cells as a marker of stratified or pseudo-stratified epithelium (Goldman and Steinert, 1990; Moll *et al.*, 1982; Presland and Dale, 2000; Presland and Jurevic, 2002; Voynow *et al.*, 2005). As previously stated, total CK 5/6 staining from Day 18 until 24 remained relatively constant (~44%). However, the total percentage of CK 5/6 staining within the cultures did decrease from Days 24 – 36. This was not thought to be due to a decrease in the quantity of CK 5/6 staining, but more due to the pseudo-stratification of the apical layer of cells, resulting in an increase in the total and non-staining area of the cultures.

Culture deterioration from Days 36 to 39, revealed that CK 5/6 staining was less intense within the supra-basal layer, but did however, remain within the basal layer. Day 39, exhibited cells on the basal surface (resting on the insert membrane) that had no CK 5/6 staining. This could simply be due to loss of basal cells resulting in the apical layer 'falling down' in its place. Day 42 revealed a highly significant increase ($p < 0.001$) in the CK 5/6 staining compared to Days 27 – 39; this may have been due to the culture's attempt to 'rescue' itself and that as CK 5/6 were known to be involved in the mitotic process, the increased expression could be due to this (Franke *et al.*, 1983). However, it may be due to squamation of the culture resulting in a decrease in total and therefore, non-stained area of the culture.

4.5.2 CC10: CLARA CELLS

An antibody to the 10kDa Clara cell specific protein, CC10, was used to identify the presence and prevalence of Clara cells during the development of the NHBE cell culture model (Singh and Katyal, 1998).

No positive response was obtained from the CC10 antibody until Day 9, where staining appeared in the cytoplasm of some apically exposed cells. The number and percentage of CC10⁺ cells on Day 9 was approximately 1.5% and 7%, respectively. This increased slightly by Day 12 (2% and ~8%, respectively),

although the values remained relatively constant until Day 21. Many of the CC10⁺ cells demonstrated staining throughout the cell, highlighting the fact that these cells reached the insert membrane and proving the culture was pseudo-stratified.

The number and percentage of CC10⁺ cells increased after Day 21 and plateaued between Days 24 – 36 (~3.5 and 17%, respectively). This again further confirmed this period to be the stable phase for the NHBE model. Additionally, Boers and colleagues (1999) established that roughly 11% of the cells in the terminal bronchioles and 22% in the respiratory bronchioles were Clara cells, indicating that the patient donor samples used were derived from the lower respiratory tract, even in the vicinity of the terminal bronchioles. Although the percentage of CC10⁺ cells increased on Day 39 from the plateau phase, the average number of CC10⁺ cells remained the same. This was due to the fact that the cultures began to deteriorate and undergo squamation, meaning that there were less non-CC10⁺ cells within the region measured. However, by Day 42 a highly significant ($p < 0.001$) change occurred in the Clara cell profile, with the cell number and percentage being severely decreased when compared to the plateau period. This again further re-enforced the conclusion that the NHBE culture was undergoing demise and dedifferentiation. Additionally, the decrease in Clara cells (as apposed to an increase) would suggest that although Clara cells were thought to contribute to renewal in the bronchial epithelium (Boers *et al.*, 1999; Brody *et al.*, 1987), they were not attempting to contribute to the repair in the NHBE epithelium, at this time.

Although the exact physiological role that Clara cells play has not entirely been identified, they contain the P450-dependent, mixed-function oxidase enzyme; known to oxidatively metabolise xenobiotics within the lungs (Boyd, 1977; Devereux, 1984; Peão *et al.*, 1993). This is an important function to have within the NHBE system, as some xenobiotics are specifically metabolised to harmful metabolites (e.g. 4-ipomeanol) within the lung (Boyd, 1977).

4.5.3 PERIODIC-ACID SCHIFF: GOBLET CELLS

The appearance of goblet cells within the NHBE culture was studied over the 42 day culture period by using PAS to stain the mucopolysaccharides and glycogen components located within them (Zugibe, 1970).

No positive PAS staining was observed within the NHBE culture until Day 12. The relatively late appearance of mucopolysaccharides was anticipated because the culture needed to first undergo proliferation and squamous metaplasia prior to re-differentiation into ciliated and goblet cells. Puchelle and co-workers (2006) seeded disassociated adult human airway epithelial cells into a denuded rat trachea. These cells initially proliferated into a confluent squamous epithelium prior to pseudo-stratification and then re-differentiation into an epithelium of muco-ciliary phenotype (Puchelle, 2006).

Positive staining within cells observed at Day 12, may have suggested the presence of goblet cells beginning to synthesise mucopolysaccharides; as staining only accounted for a small region within the cell. Clearly identifiable goblet cells were detected at Day 15, by positive PAS staining, with goblet cells remaining within the cultures until Day 42. A thin layer of staining was observed on the apical surface of the cultures, indicating that the goblet cells themselves were releasing mucins into the 'lumen' (apical region).

Deterioration of cultures, from Day 36 onwards, demonstrated cultures were reverting back to squamous monolayers, with a low level of PAS staining. Controversially, some cultures displayed goblet cell hyperplasia. This could be a defence mechanism, to produce more mucin as a protective mechanism during culture demise (Ward *et al.*, 2002; West, 2003).

4.5.4 P63: BASAL/PROGENITOR CELLS

Basal cells were identified, through p63 positive staining, as the progenitor cells of the NHBE model and therefore, in the bronchial epithelium (Yang *et al.*, 1998; Yang *et al.*, 1999; Wang *et al.*, 2002).

Almost all cells seeded onto inserts were p63⁺ 24 hours post-seeding (Day 1), inferring that the vast majority (98% average) of cells were basal cells. Proliferation and subsequent development of the NHBE model resulted in a gradual decrease in the percentage of p63⁺ cells as the progeny began the process of differentiation and therefore, rapid degradation of p63 (Yang *et al.*, 1998). By Day 6, positive staining was restricted to the basal and supra-basal layers, with nucleic staining retreating to the basal layer by Day 9, with 50% of nuclei stained. This gradual decrease in p63 staining continued until Day 15, where the percentage of p63 positive cells remained constant (25 – 38%).

This stability in percentage p63⁺ cells (25 – 38%), along with staining locality (mainly the basal layer and occasionally the supra-basal layer) occurred from Days 15 to 39. This was consistent with the findings of Boers and colleagues (1998) who reported that, in airways of diameters $\geq 4\text{mm}$, the mean basal cell population was 31% in the steady-state lung and that these were the progenitor cells (i.e. capable of renewal and repair in the bronchial epithelium). Deterioration of the NHBE culture by Day 42 coincided with an increase in the intensity of p63 expression and also the migration of positively stained cells to the apical layer. This may be either a 'rescue' attempt of the cells to reform an intact epithelial barrier, through proliferation and/or differentiation, or that p63 may be involved in the initiation of cell cycle arrest and/or apoptosis. Accumulation of p63 isoforms within cells have been shown to cause the induction of differentiation, cell cycle arrest and apoptosis (Petitjean *et al.*, 2008).

4.5.5 TIGHT JUNCTION PROTEINS

The presence of three of the major tight junction proteins, ZO-1 (Stevenson *et al.*, 1986), occludin (Furuse *et al.*, 1993) and claudin-1 (Furuse *et al.*, 1998), were monitored in order to ascertain the temporal and spatial development and formation of epithelial tight junctions within the NHBE model.

4.5.5.1 ZO-1

ZO-1 was the first tight junction specific protein to be discovered (Stevenson *et al.*, 1986). Anderson and colleagues (1988) confirmed that ZO-1 was a peripheral membrane, tight junction-associated protein. Madara (1987) suggested that there may also be an association between actin microfilaments and intestinal tight junctions, possibly via tight junction-associated proteins such as ZO-1.

ZO-1 was observed throughout the cytoplasm of cells on Day 1, which was in agreement with the fact that, during early development of E-cadherin-based adherens junctions (Miyoshi and Takai, 2008), the ZO-1-catenin complex (associated with E-cadherin), mobilised ZO-1 to the plasma membrane (Rajasekharan *et al.*, 1996). Moreover, ZO-1 contains an actin binding region, which is not only important in the regulation of established tight junctions, but also in the translocation of ZO-1 to the free edges of cells, prior to junction formation (Paris *et al.*, 2008). As the NHBE model matures, ZO-1 staining began to accumulate at the cell-cell contacts (Days 6 – 15).

After Day 15, ZO-1 staining continued to delineate cells throughout the cultures until Day 42, indicating that tight junctions were fully formed. The N-terminal region of ZO-1 is known to associate with domain E of occludin (Fanning *et al.*, 1998; Furuse *et al.*, 1994; McCarthy *et al.*, 1996). Therefore, since an individual culture from each time point was stained for both ZO-1 and occludin, it was possible to observe the co-localisation of these tight junction proteins during NHBE culture tight junction formation. However, ZO-1 also appeared in regions not associated with occludin, especially before Day 15. This was probably due to the fact that, as well as binding occludin, the PDZ1 domain of ZO-1 binds directly to the COOH-terminal of claudins (Itoh *et al.*, 1999), as well as the C-terminal end of some of the transmembrane JAM proteins; through the PDZ2 domain of ZO-1 (Chiba *et al.*, 2008). Cultures on Day 42 revealed significant staining at the cell-cell contacts, however, some areas were devoid of this specific staining pattern, implying that there were problems with, or deterioration of, cell junctions.

4.5.5.2 OCCLUDIN

Occludin, a four transmembrane protein was the next of the three tight junction proteins detected to be discovered (Furuse *et al.*, 1993). Some faint, mainly cytoplasmic, staining was observed in the NHBE cultures on Day 1, with the staining quantity and intensity much less than either ZO-1 or claudin-1, at the same time point. This may be indicative of occludin being incorporated into the tight junctions at a slightly later time point than the other two.

Occludin staining on Day 6 exhibited intense staining at the borders of some cell-cell contacts, suggesting that, at this point, occludin was being incorporated into the tight junctions. Furthermore, these more intense regions of staining corresponded to the same areas of intense staining of ZO-1; inferring that occludin may be associated with ZO-1, at this time (Furuse *et al.*, 1994). From Days 6 to Day 15, occludin continued to accumulate at the cell-cell contacts as it was integrated into the tight junctional complexes.

NHBE cultures from Days 24 to 39 appeared relatively stable in their expression of occludin, with a strong network of staining delineating cells. On Day 42, this delineation was still observed, however, there were areas where this pattern no longer existed and an increase in cytoplasmic staining was more prominent. The effect this may have on the TEER of the cultures may be minimal. Balda and colleagues (1996) deduced that even though a COOH-terminally truncated occludin resulted in a discontinuous occludin staining pattern, the tight junction formation on freeze-fracture electron microscopy appeared normal. However, McCarthy and co-workers (1996) demonstrated that the incorporation of chick occludin into canine cells resulted in a 30 – 40% increase in TEER. Both of these researchers may be right, with occludin being important, but not necessary for the formation of tight junctions, but as a contributing factor to the 'tightness' (i.e. higher TEER) of the tight junction itself.

4.5.5.3 CLAUDIN-1

Claudin-1 is a member of the claudin family of transmembrane proteins, of which there are currently 24 identified in humans; with different members displaying varying tissue distribution (Furuse *et al.*, 1998; Morita *et al.*, 1999; Turksen and Troy, 2004). On Day 1, claudin-1 expression was dispersed throughout the cytoplasm of most cells, with occasional focal 'hot-spots' of intense staining. This would suggest that claudin-1 was being trafficked towards the cell membrane. ZO-1, which is known to target occludin to the correct region for tight junction formation via actin microfilaments (Fanning *et al.*, 1998; Furuse *et al.*, 1994; McCarthy *et al.*, 1996), has also been shown to bind claudin-1 at its COOH-terminal via its (ZO-1) PDZ1 domain (Itoh *et al.*, 1999). Due to the fact that detection of both claudin-1 and ZO-1 used the same 2° antibody it was not possible to detect any co-localisation between the two. However, some co-localisation between occludin and claudin-1 and ZO-1 and occludin was observed, suggesting that some degree of co-localisation between ZO-1 and claudin-1 was probable.

After Day 1, claudin-1 staining appeared to migrate towards the cell borders, once there (Days 6 – 33), claudin-1 staining did not produce the characteristic 'unbroken' delineation of the cells, as ZO-1 and occludin did, but instead produced a 'dotted' line appearance. Furuse and colleagues (1998) demonstrated in lung tissue with well developed tight junctions, the level of claudin-1 and -2 expression was relatively low compared to occludin, indicating that claudin-1 was not abundantly expressed in the lung. Claudin-1, -3, -4, -5, -7 and -8 were all known to be expressed in the airway epithelium *in vivo*, with claudin-4, -7 and -8 expressed at especially high levels (Coyne *et al.*, 2003; Morita *et al.*, 1999). Therefore, the fact that the NHBE cells exhibited a non-characteristic (i.e. dotted delineation) expression of claudin at the cell borders (ZO-1 and occludin gave unbroken delineation), could be due to the fact that only claudin-1 and no other isoform was tested. Coyne and co-workers (2003), noted that 1° cell cultures derived from human airways only expressed claudin-1 and -4 and consequently, it would be interesting to delve further and discover if this was the case with the NHBE cell model.

NHBE cultures from Days 36 – 42 displayed a change in claudin-1 staining. Staining had receded from the cell-cell contacts, appearing more prevalent in the cytoplasm. There was also excess autofluorescence, associated with dead/dying cells. This may imply that changes in claudin expression were associated with initiation of tight junction deterioration. It would also be interesting to determine if the expression of claudin-3, -5, -7 and -8 were present in the NHBE model and if not, would they prevent this.

4.6 CONCLUSIONS

Histological analysis of the NHBE model development allowed an insight into individual cellular differentiation and culture formation. Positive CK 5/6 staining provided confirmation of the pseudo-stratified epithelial origins of the tissue, with its change in expression over the 42 days confirming model development and maturity. Earlier morphological analysis (Chapter 3) suggested the presence of Clara cells, immunohistochemistry work verified this. The fact that the NHBE model contained Clara cells signified that this was a representative model of the bronchial epithelium and potentially, contained important metabolic enzymes, such as the P450-dependent mixed-function oxidase (not detected in this project).

Although the apical secretions of the cultures were assumed to contain mucins (visually [visco-elastic fluid] and the positive Bradford assay – Chapter 2), positive PAS staining reinforced this assumption by identification of mucin secreting goblet cells. Positive p63 staining identified the progenitor cells of the NHBE model, which were the basal cells. The ability to form tight junctions is essential in any model of the human respiratory epithelium. Without tight junctions, the specific barrier properties this epithelium has *in vivo*, would be lost, as would the models application for toxicity testing. Three of the major tight junction proteins were identified in the 'in-house' NHBE model.

Base-line expression and cell numbers of CK 5/6⁺ cells, Clara cells, goblet cells, p63⁺ (basal/progenitor) cells and tight junction proteins of the mature NHBE model could be utilised to monitor the specific effects of any mechanical or toxicological induced injury and subsequent repair within the airway.

CHAPTER 5:

RESPONSE OF THE NHBE MODEL TO CLASSICAL PULMONARY TOXINS

5.1 INTRODUCTION

The natural history of the epithelium/cell morphogenesis within the NHBE model was characterised in Chapters 2, 3 and 4. This full characterisation enabled the identification of the toxicological experimental window (Days 27 – 33). In this Chapter, the model's response to a panel of classical pulmonary toxicants (CPT) was evaluated.

The purpose of challenging this *in vitro* system was to monitor the biochemical responses (culture viability and TEER) and morphological changes (LM and SEM) of the NHBE epithelium to well-defined pulmonary toxicants. The panel of CPT chosen were Lipopolysaccharide (LPS; immunotoxic; Eisenbarth *et al.*, 2002), cadmium chloride (CdCl₂; cytotoxic; Croute *et al.*, 2000), paraquat (Pq; redox reagent; Cappettetti *et al.*, 1998), Amiodarone (Am; phospholipidotic; Camus *et al.*, 2004) and cigarette smoke (CS; most common inhaled human toxicant; IARC, 2004). The final experimental work involved evaluation of the cytokine response of the model to LPS.

The hypothesis for this chapter of work was:

- That when challenged with classical pulmonary toxins the NHBE model would respond with general and toxicant specific responses.

5.2 MATERIALS AND STOCK SOLUTIONS

5.2.1 MATERIALS

MATERIALS	SUPPLIER
Kentucky Research Cigarettes, 3R4F	Tobacco-Health Research, University of Kentucky, USA
Matrix 96-Well Polystyrene Plates, White, Flat Bottom	Fisher Scientific, Manchester, UK

Table 5.1 Table of materials used and their suppliers.

5.2.2 STOCK SOLUTIONS

SOLUTIONS	SUPPLIER
Lipopolysaccharide (from <i>E. coli</i> 0127: B8) Cadmium Chloride Dulbecco's Phosphate Buffered Saline (PBS), with MgCl ₂ and CaCl ₂ , sterile-filtered Methyl Viologen Dichloride Hydrate 98% (Paraquat) Amiodarone Hydrochloride	Sigma, Dorset, UK
Hanks' Balanced Salt Solution (HBSS)	Invitrogen Ltd, Paisley, UK
ViaLight [®] Plus Cell Proliferation and Cytotoxicity BioAssay Kit (ATP Assay)	Lonza Group Ltd., Switzerland
RayBio [®] Human Cytokine Array 3.1	Tebu-Bio, Peterborough, UK

Table 5.2 Table of stock solutions used and their suppliers.

5.2.3 EQUIPMENT

EQUIPMENT	SUPPLIER
Smoking Robot RM20S (Smoking Machine)	Borgwaldt-kc Technik, Hamburg, Germany
FLUOstar OPTIMA OMPTIMA Control Program	BMG LABTECH, Aylesbury, UK
BioSpectrum [®] AC Imaging System	UVP Ltd, Cambridge, UK
GeneTools	SYNGENE, Cambridge, UK
RayBio [®] Antibody Array Analysis Tool	Tebu-Bio, Peterborough, UK

Table 5.3 Table of equipment used and their suppliers.

5.3 METHODS

5.3.1 DOSING

Third Passage NHBE cells grown at an ALI (Section 2.3.1) were dosed when cells were between Day 27 and Day 33. TEERs were checked prior to dosing to ensure that they were above 1,500 Ω (~4,550 Ω .cm²) for Lipopolysaccharide (LPS), cadmium chloride (CdCl₂), paraquat (Pq) and Amiodarone (Am) dosing (Section 5.3.1.1 – 5.3.1.4) and above 1,000 Ω (~3,030 Ω .cm²) for cigarette smoke exposure (Section 5.3.3.5).

Each CPT dose (50 μ l) was applied apically to NHBE cultures ($n = 3$). After incubation with CPT or carrier solution (24 hours), the TEER was recorded on each NHBE culture insert (Section 5.3.2), that same insert was then used to assess culture viability (Section 5.3.3). Both the TEER and cellular viability (ATP Assay) were expressed as a percentage of the controls. The doses that were determined to cause a 5% or 20% decrease in culture viability compared to controls (i.e. TD₅ [toxic dose 5%] and TD₂₀), were then assessed for morphological changes (Section 5.3.4 – 5.3.5).

5.3.1.1 LIPOPOLYSACCHARIDE

LPS (1mg) was dissolved in HBSS, to produce a 1mg/ml stock solution (w/v). This stock was further diluted in HBSS to produce the dose range: 0.1, 0.2, 0.3, 0.4, 0.5, 0.6, 0.7, 0.8, 0.9 and 1.0mg/ml. HBSS was used as the control solution. In addition, TD₅ and TD₂₀ doses were used to monitor the cytokine response of the NHBE model to LPS (Section 5.3.6).

5.3.1.2 CADMIUM

CdCl₂ (100mM) was dissolved in PBS, to produce a 1mM stock solution (v/v). This stock was further diluted in PBS to produce the dose range: 0.05, 0.1, 0.15, 0.2, 0.25, 0.3, 0.35, 0.4, 0.45 and 0.5mM. PBS was used as the control solution.

5.3.1.3 **PARAQUAT**

Pq was dissolved in PBS (100µl) overnight, to produce a 100mM stock solution (w/v). This stock was further diluted in PBS to produce the dose range: 150, 300, 450, 600, 750, 900, 1050, 1200, 1350 and 1500µM. PBS was used as the control solution.

5.3.1.4 **AMIODARONE**

Am was dissolved in dH₂O (500µl) overnight, to produce a 5mg/ml stock solution (w/v). This stock was further diluted in dH₂O to produce the dose range: 100, 200, 300, 400, 500, 600, 700, 800, 900 and 1000µg/ml. The control solution was dH₂O.

5.3.1.5 **CIGARETTE SMOKE EXPOSURE**

The smoke exposure of the NHBE cells was undertaken at AstraZeneca R&D (Loughborough, UK), using their smoking machine (Smoking Robot RM20S; Figure 5.1). Experiments were performed with the expert help of Senior Scientist Ms. Wendy Merrison.

The smoking machine was set up to smoke the NHBE cultures ($n = 3$) at one of the three different constant smoke dilutions; 1:20, 1:30 or 1:50. Smoke was drawn from Kentucky Research Cigarettes 3R4F using the International Organisation for Standardisation standard conditions (35ml puff drawn over 2 seconds, exhaled over 20 seconds, every minute). The cells were smoked continually for 30 minutes (~4 – 5 cigarettes to each smoking chamber). NHBE cell cultures were placed in the smoking chambers (Figure 5.2) containing 38ml ALI media (therefore, cells had media on the basal side and exposed to the air/smoke on the apical side). NHBE cells in the smoking chambers were kept in a cell culture laminar flow hood for the smoke exposure (RT). Control cells were left in a cell culture laminar flow hood with ALI media for the duration of the experiment so that equivalent temperatures were maintained. Following treatment the NHBE cultures were placed back into 24-well plates, containing fresh ALI media (300µl;

37°C) in each well, and re-placed back into the cell culture incubator for a defined 'recovery-time'. NHBE cultures ($n = 3$) exposed to 1:20 and 1:50 smoke dilutions were allowed to recover for 4 hours (1:20-4h and 1:50-4h). With additional NHBE cultures ($n = 3$) exposed to 1:20, 1:30 and 1:50 smoke dilutions, that were allowed to recover for 24 hours (1:20-24h, 1:30-24h and 1:50-24h).

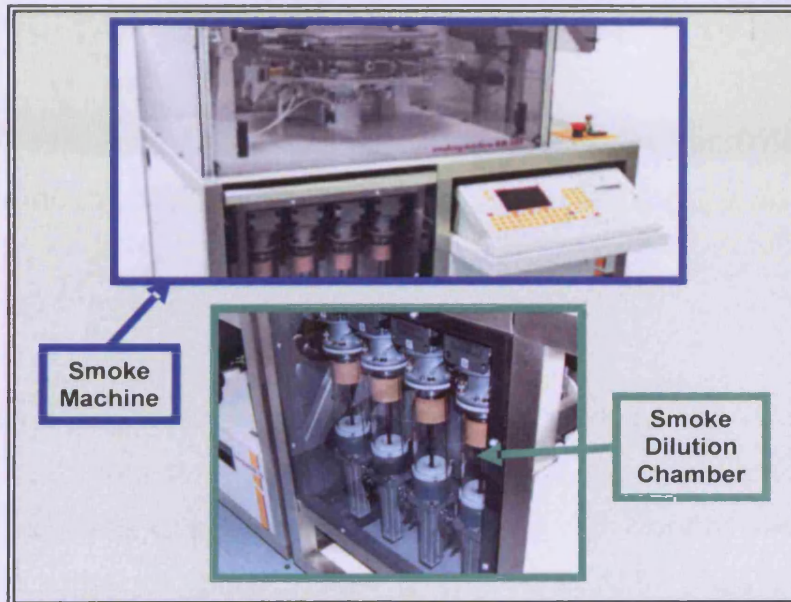


Figure 5.1 Image of the Smoking Robot RM20S and a closer view of the smoke dilution chambers used to dilute the cigarette smoke to the required concentrations.

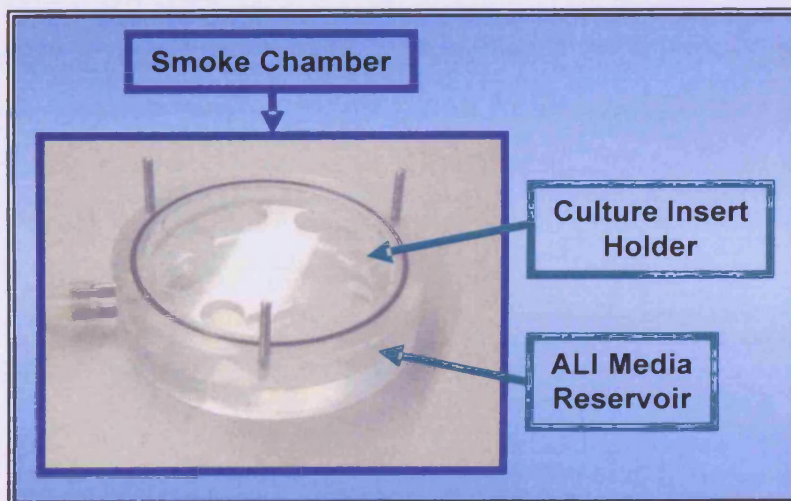


Figure 5.2 Image of the base of the smoking chamber used to hold and 'smoke' the NHBE cell cultures. The ALI media resides in the large well at the base, the NHBE culture inserts are placed into the appropriate holder. The lid is placed on top and the pipes to the smoke machine are attached (Image not shown).

After recovery (4 or 24 hours) the TEER was recorded on each NHBE culture insert (Section 5.3.2), that same insert was then used to assess culture viability (Section 5.3.3). Both the TEER and cellular viability (ATP Assay) were expressed as a percentage of the controls. Each smoke dilution, for each recovery period, were assessed for morphological changes (Section 5.3.4 – 5.3.5).

5.3.2 TRANS-EPITHELIAL ELECTRICAL RESISTANCE

The TEER of NHBE cultures, immediately prior to- and 24 hours post-dosing, was established using the method previously described (Section 2.3.3).

5.3.3 ATP ASSAY

The ViaLight® Plus Cell Proliferation and Cytotoxicity BioAssay Kit (Lonza, Switzerland) was used to assess cellular ATP activity. ATP Monitoring Reagent Plus (AMR Plus) was prepared by reconstituting the lyophilised AMR Plus (1 vial) with the supplied Assay Buffer (50ml). The AMR Plus was allowed to equilibrate for 15 minutes at RT. Cell lysate solution was brought up to RT before use and stored in workable aliquots after (-20°C).

NHBE inserts that had been dosed and had their TEER read were then placed in an empty well in preparation for the ATP assay. Cell lysis reagent (100µl) was applied apically to each insert and incubated for at least 10 but no more than 20 minutes. The cell lysate (100µl) was then placed into a well of a white, flat-bottomed 96-well plate. AMR Plus reagent (100µl) was added to the cell lysate in each well and incubated for 2 minutes (dark). The luminescence was read using the FLUOstar OPTIMA and analyzed using the OPTIMA Control System software (BMG LABTECH, Aylesbury, UK).

5.3.4 LIGHT MICROSCOPY: TOLUIDINE BLUE

Inserts dosed with controls, TD₅, TD₂₀ and all CS doses for 4 and/or 24 hours, were then prepared for semi-thin sectioning and staining with toluidine blue and images taken (Section 3.3.1).

5.3.5 SCANNING ELECTRON MICROSCOPY

Inserts dosed with controls, TD₅, TD₂₀ and all CS doses for 4 and/or 24 hours, were then prepared for scanning electron microscopy and images taken (Section 3.3.3).

5.3.6 CYTOKINE ARRAY

The RayBio[®] Human Cytokine Array 3.1 (Tebu-Bio, Peterborough, UK) which detects 42 cytokines, chemokines and growth factors, was used to monitor the changes in the cytokine profile of the NHBE cultures in response to LPS.

5.3.6.1 PREPARATION OF SAMPLES

The 2x Cell Lysis Buffer diluted with dH₂O to produce a 1x Cell Lysis Buffer. The 1x Cell Lysis Buffer (1ml) was added apically to each NHBE culture insert and cells lysed for 10 minutes. Cell lysate was spun-down and stored in -80°C for future use. The lysates were thawed thoroughly before continuation of cytokine analysis.

5.3.6.2 BLOCKING AND INCUBATION

Each array membrane was placed in a separate well in the plate provided, taking care only to touch the corner of the membrane with the tweezers. Membranes were incubated with 2ml of 1x Blocking Buffer (dilute 2x Blocking Buffer with dH₂O) for 30 minutes. The 1x Blocking Buffer was removed and the membranes were incubated with 1ml of sample (cell lysate) for 1 hour. The sample was removed and membranes were washed in 2ml of 1x Wash Buffer I (dilute 20x Wash Buffer I with dH₂O) for 5 minutes on a shaker table and then removed (x3). Membranes were washed in 2ml of 1x Wash Buffer II (dilute 20x Wash Buffer II with dH₂O) for 5 minutes on a shaker table and removed (x2).

The 1x Blocking Buffer (100µl) was added to each Biotin-Conjugated Anti-Cytokines tubes, mixed by gentle inversion, then transferred to a tube containing

2ml of 1x Blocking Buffer. Membranes were incubated in 1ml of the diluted Biotin-Conjugated Anti-Cytokines for 1 hour (RT). This was removed and membranes were washed in 2ml of 1x Wash Buffer I for 5 minutes (x3), then in 2ml of 1x Wash Buffer II for 5 minutes (x2). Membranes were incubated for 2 hours in 2ml of 1,000 fold diluted HRP-conjugated streptavidin. This was removed and membranes were washed in 2ml of 1x Wash Buffer I for 5 minutes (x3), followed by washing in 2ml of 1x Wash Buffer II for 5 minutes (x2).

5.3.6.3 DETECTION

Detection Buffer A (500µl) and Detection Buffer B (500µl) were mixed for every array membrane. Excess wash buffer was drained from the membranes by holding membranes vertically with the tweezers. Membranes were incubated in Detection Buffer AB for 1 minute. Detection buffer was removed and membranes placed protein side up on a plastic sheet. Another piece of plastic sheet was placed over the membranes, and air bubbles removed carefully. Signals were detected using the BioSpectrum[®]AC Imaging System (UVP, Cambridge).

5.3.6.4 ANALYSIS OF RESULTS

Images of the array signal were converted to JPEGs and opened using the GeneTools software (SYNGENE, Cambridge, UK). Spot blot analysis was undertaken and raw values exported to Excel (Microsoft Office 2003). Values were imported into the RayBio[®] Antibody Array Analysis Tool (Tebu-Bio, Peterborough, UK) which normalized the data and subtracted background signal. This data was used to calculate the signal of each cytokine as a percentage of the control signals. Signals changed by ≥ 1.5 fold were considered significant.

5.4 RESULTS

NHBE cultures grown in cell culture inserts at an ALI (Days 27 – 33) were used in evaluating CPTs. Many different dose ranges of the pulmonary toxins were used on cultures, with TEER and cellular viability acquired, in order to obtain a dose range that included the TD₅ and TD₂₀ doses. Once established, NHBE cultures (*n*

= 3) were dosed with each CPT over that dose range (for 24 hours), then assessed for TEER (Section 5.3.2) and ATP content (Section 5.3.3). NHBE cultures were then dosed with TD₅ and TD₂₀ doses (24 hours) and underwent morphological analysis (Section 5.3.4 – 5.3.5). This provided an insight into the biochemical and corresponding structural reactions of the NHBE model to each CPT.

5.4.1 NHBE RESPONSE TO LIPOPOLYSACCHARIDE

5.4.1.1 CULTURE VIABILITY AND TRANS-EPITHELIAL ELECTRICAL RESISTANCE

A dose range (0mg/ml – 1mg/ml) of LPS contained the desired TD₅ and TD₂₀ responses. The ATP assay for viability over this dose range displayed a biphasic response, where an initial drop in culture viability was followed by an increase and subsequent drop in culture viability (compared to control cultures) (Figure 5.3). The lower doses of LPS (0.1 – 0.2mg/ml) exhibited a reduction in culture viability, compared to controls; the TD₅ dose was obtained from this initial drop in culture viability (0.1mg/ml). Subsequently, as the concentrations increased there was an increase in culture viability, to approximately 120% (0.3mg/ml), followed by a slight drop to 115% (0.4mg/ml). However, when the concentration of LPS was increased to 0.5mg/ml, a significant drop in culture viability was observed (80%); yielding the TD₂₀ dose. Increasing the LPS dose up to 0.8mg/ml had a limited effect on culture viability (remaining ~80%). A slight decrease in viability at 0.9mg/ml and 1.0mg/ml (~50%) was observed.

TEER values over the dose range (0 – 1.0mg/ml) did not give the biphasic response observed with the ATP assay. TEER values decreased gradually between 0.1 – 0.5mg/ml of LPS, to approximately 4% of the control. Higher doses of LPS had no further effect on TEER values, which remained extremely low (0.5 – 5%) (Figure 5.3).

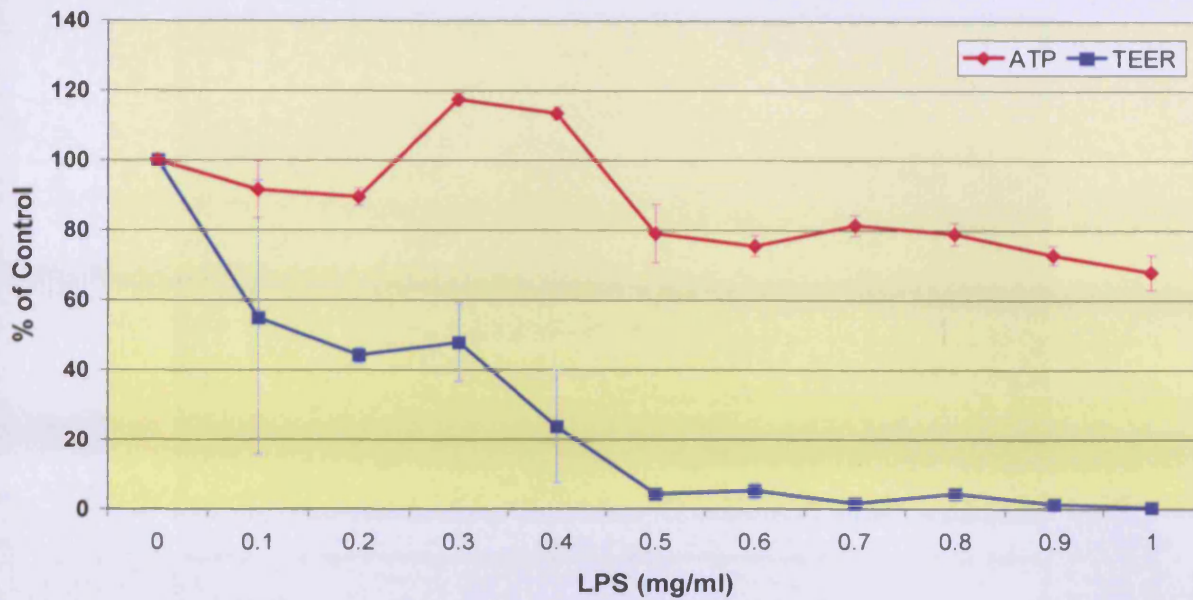


Figure 5.3 Graph displaying NHBE culture TEER and ATP assay after 24 hours treatment with Lipopolysaccharide. ATP (◆) and TEER (■) values displayed as percentage of control values. Standard Deviation was shown for both ATP (I) and TEER (I), $n = 3$.

5.4.1.2 LIGHT MICROSCOPY: TOLUIDINE BLUE

Control cultures (treated with HBSS) appeared pseudo-stratified and well-differentiated. However, prominent gaps around the cell-cell contacts between the basal and supra-basal cells were apparent (Figure 5.4[A]). The TD₅ dosed cultures revealed morphological changes, with evidence of hypotrophy, focal loss of cells and an increase in mucin producing cells, with possible increased mucin secretion (Figure 5.4[B]). Basal cells appeared to be the most structurally effected, with cell shrinkage and apparent loss of cell-cell attachments (Figure 5.4[B]).

The TD₂₀ dosed cultures exhibited significant morphological changes, with multi-focal cell loss and degeneration apparent (Figure 5.4[C]). Numerous inter-cellular gaps and intra-cellular vacuoles were present and clear disruption of cellular junctions were apparent. Cell shrinkage was evident throughout and especially noticeable in the columnar cells, which appeared to have detached from the membrane (Figure 5.4[C]).

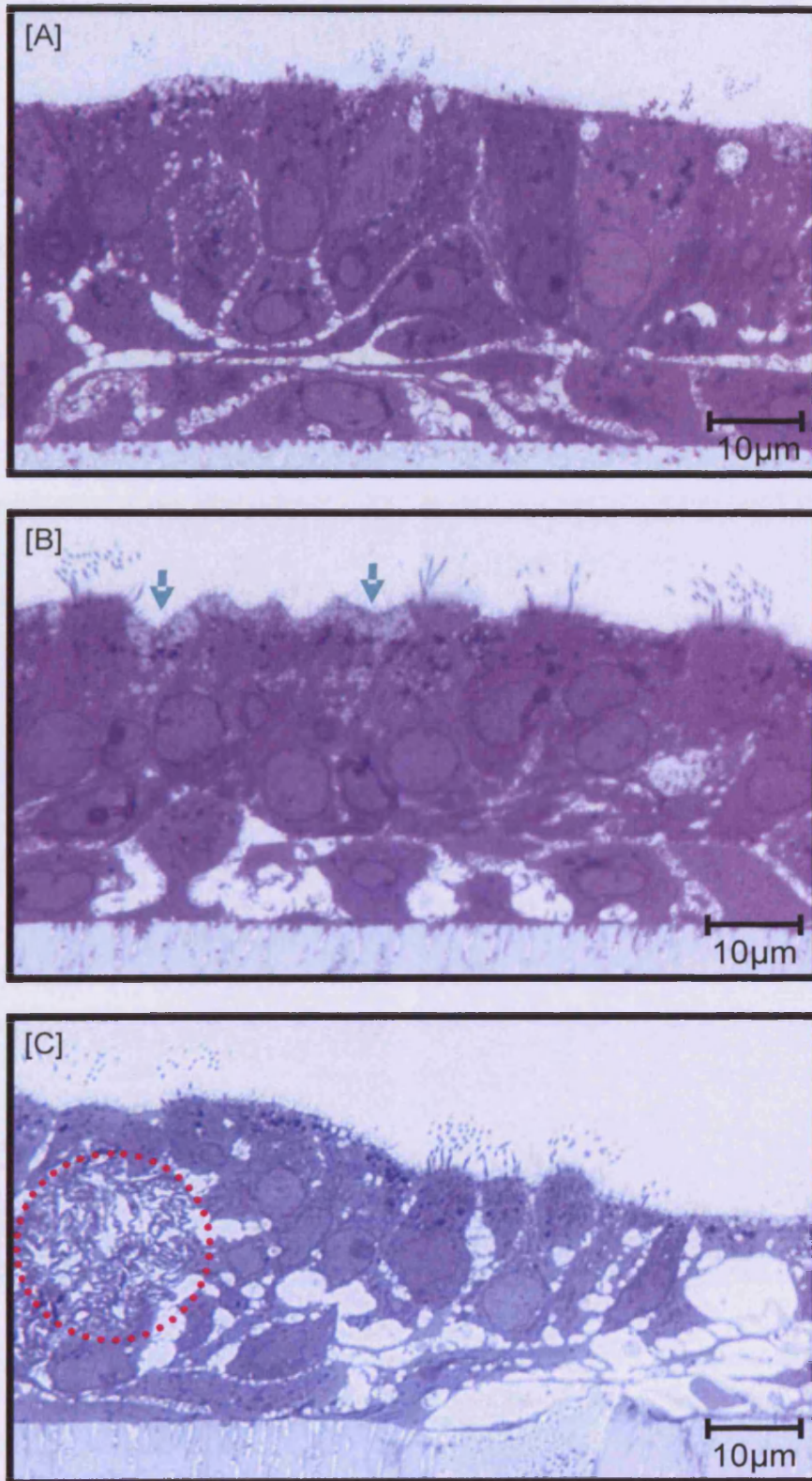


Figure 5.4 LM images of NHBE cultures treated with LPS, stained with toluidine blue. [A] Control cultures treated with HBSS (carrier solution). [B] NHBE cultures treated with TD₅ (0.1mg/ml) LPS; basal cell shrinkage and damage was evident, arrows indicate increased mucin production. [C] NHBE cultures treated with the TD₂₀ (0.5mg/ml) LPS; clear disruption of cell contacts, columnar cell shrinkage; dotted area displays degenerative material, such as reticular fibre or ECM debris.

5.4.1.3 SCANNING ELECTRON MICROSCOPY

Topographically, both control and TD₅ cultures exhibited a structurally intact apical surface, denoted by the presence of numerous populations of cilia and microvilli (Figure 5.5[A] and [B]). Cultures treated with the TD₂₀ dose of LPS displayed focal regions of damage to the apical surface, characterised by detached, shrunken, rounded cells, with many protruding cilia (Figure 5.5[C]). Other areas of the cultures consisted entirely of multiple layers of spherical cells with protruding cilia (Figure 5.5[D]).

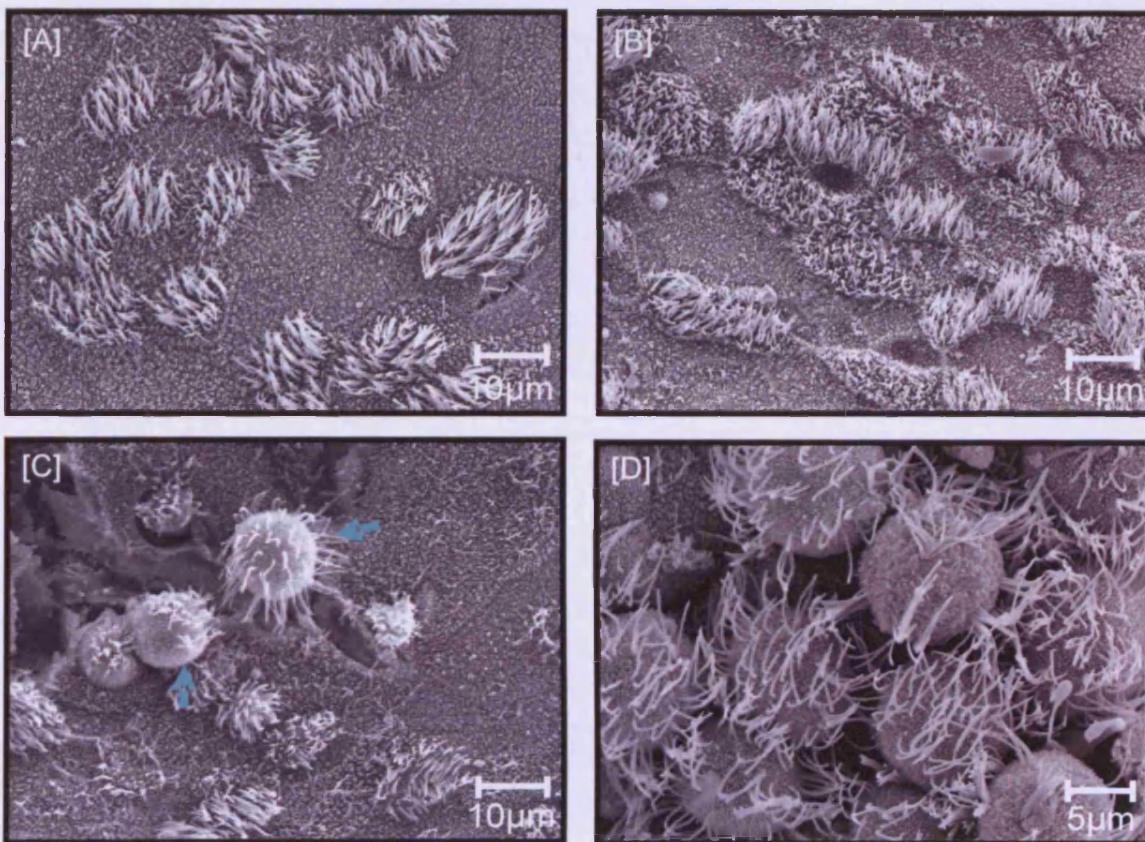


Figure 5.5 SEM images of NHBE cultures treated with LPS. [A] Control cultures treated with HBSS (carrier solution). [B] NHBE cultures treated with TD₅ (0.1mg/ml) LPS. [C] NHBE cultures treated with TD₂₀ (0.5mg/ml) dose of LPS; arrows indicate detached (balled-up) cells. [D] NHBE cultures treated with TD₂₀ dose of LPS; higher magnification of an area of increase focal damage, displaying multiple layers of detached cells, with many protruding cilia.

5.4.2 NHBE RESPONSE TO CADMIUM

5.4.2.1 CULTURE VIABILITY AND TRANS-EPITHELIAL ELECTRICAL RESISTANCE

A dose range of 0 – 0.5mM of CdCl was determined to encompass both target TD₅ and TD₂₀ doses. The ATP assay for viability over the dose range displayed a biphasic response (Figure 5.6). At 0.05mM CdCl, there was a reduction in culture viability when compared to the control values, this was deemed to be the TD₅ dose. At 0.1mM CdCl, there was a rise in culture viability (~110%), this was a transient increase in viability, but the ATP activity remained above control levels until 0.3mM (102%). When the concentration of CdCl was increased to 0.35mM, there was a significant decrease in culture viability (75%). The TD₂₀ dose was then calculated from this graph as 0.34mM. In response to higher doses, a steady-rate of decreased culture viability (35% at 0.5mM) was observed.

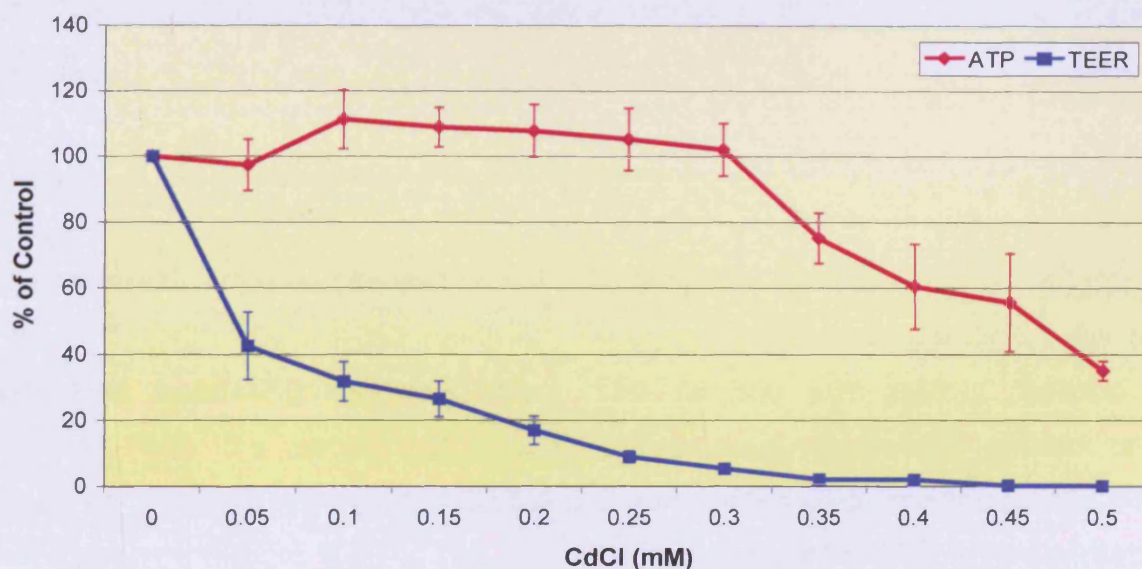


Figure 5.6 Graph displaying NHBE culture TEER and ATP assay after 24 hours treatment with cadmium chloride. ATP (◆) and TEER (■) values displayed as percentage of control values. Standard Deviation was shown for both ATP (|) and TEER (|), $n = 3$.

TEER values over the dose range (0 – 0.5mM) did not elicit the biphasic response observed with the ATP assay. TEER values gradually decreased between 0.05 – 0.35mM CdCl to approximately 2% of the control. Higher doses of

CdCl did not affect the TEER, which remained extremely low (0 – 2%) and deemed negligible (Figure 5.6).

5.4.2.2 LIGHT MICROSCOPY: TOLUIDINE BLUE

Control cultures (treated with PBS) exhibited the characteristic pseudo-stratified and muco-ciliary culture (Figure 5.7[A]). Morphologically, the TD₅ dosed cultures were degenerated; undergoing basal squamation and hypertrophy, columnar cuboidalisation and dedifferentiation of goblet and Clara cells (Figure 5.7[B]). Basal cells appeared hypertrophic, remained attached to the membrane, with an increase in cytoplasmic vacuoles. Vacuoles were also observed in the apical layer of cells. Some ciliated cells appeared to 'bulge' into the apical region, as if detaching from the epithelium (Figure 5.7[B]). The NHBE epithelium was severely compromised in the area observed after treatment with the TD₂₀ concentration; cultures had deteriorated to a squamous monolayer, with a few cells detached from the membrane altogether and many displaying signs of cell death (Figure 5.7[C]).

5.4.2.3 SCANNING ELECTRON MICROSCOPY

Control NHBE cultures (treated with PBS), exhibited normal surface topography (Figure 5.8[A]). TD₅ treated cultures, displayed only minor damage, with the epithelium appearing relatively intact. The surface was mainly covered in microvilli, with the occasional ciliated cell present. Numerous ciliated cells appeared to have detached and 'balled-up', surrounded by protruding cilia or cilia-like structures (Figure 5.8[B]). The surface topography of NHBE cultures treated with the TD₂₀ dose was significantly changed. In areas where the epithelium was relatively intact, it appeared dedifferentiated; in addition, there were numerous regions of spherical, detached cells and/or highly protruding undifferentiated cells (Figure 5.8[C]). Other areas of the NHBE cultures appeared more severely damaged, with numerous layers of undifferentiated, balled-up cells, devoid of cilia possibly undergoing cell death, with an unusual stringy covering observed, possibly cell debris or ECM material (Figure 5.8[D]).

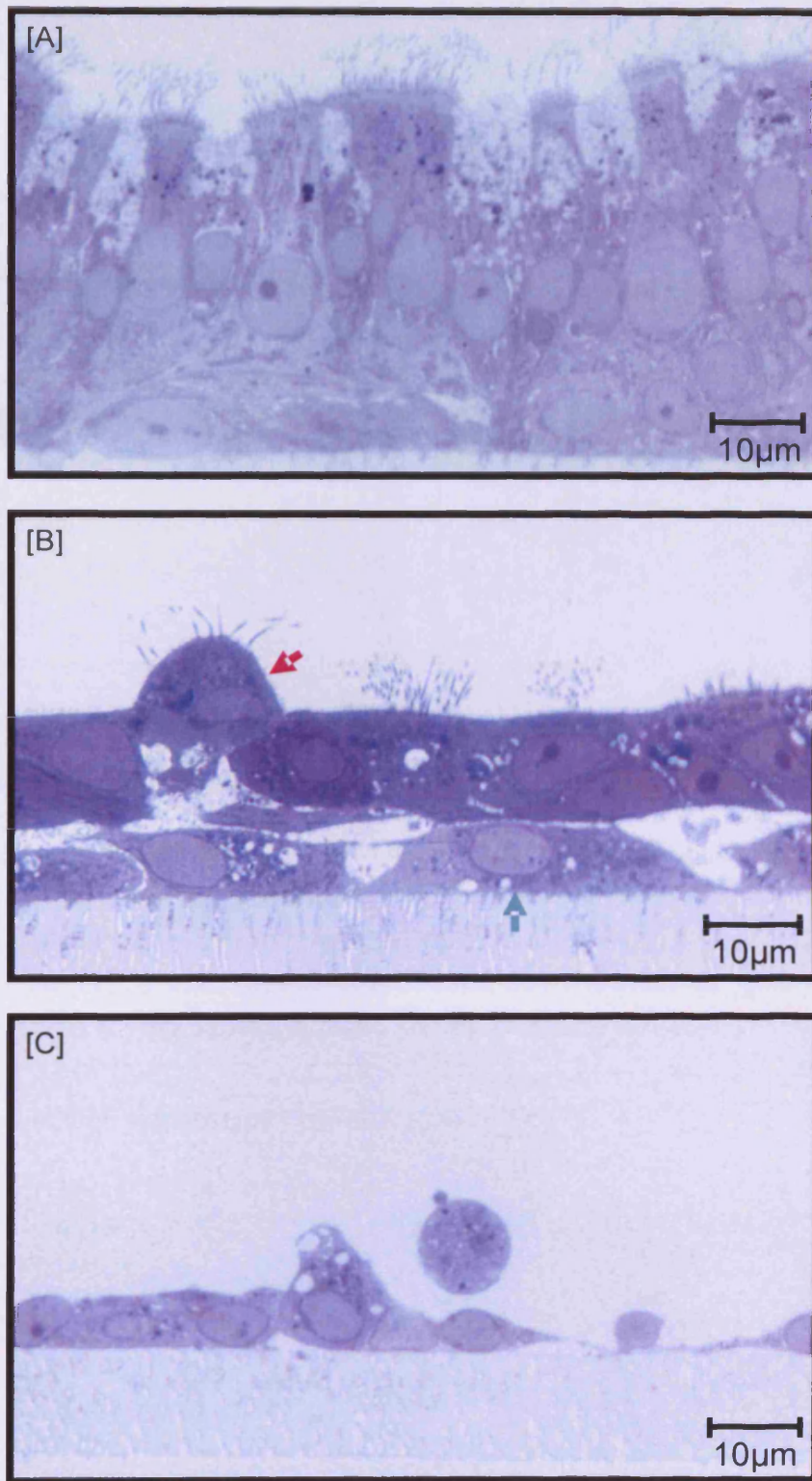


Figure 5.7 LM images of NHBE cultures treated with CdCl₂ stained with toluidine blue. [A] Control cultures treated with PBS (carrier solution). [B] NHBE cultures treated with TD₅ (0.05mM) CdCl₂; aqua arrow demonstrates basal cell hypertrophy and squamation, pink arrow indicates a ciliated cell detaching from the epithelium. [C] NHBE cultures treated with TD₂₀ (0.34mM) CdCl₂; squamous epithelium, displaying increased cellular damage.

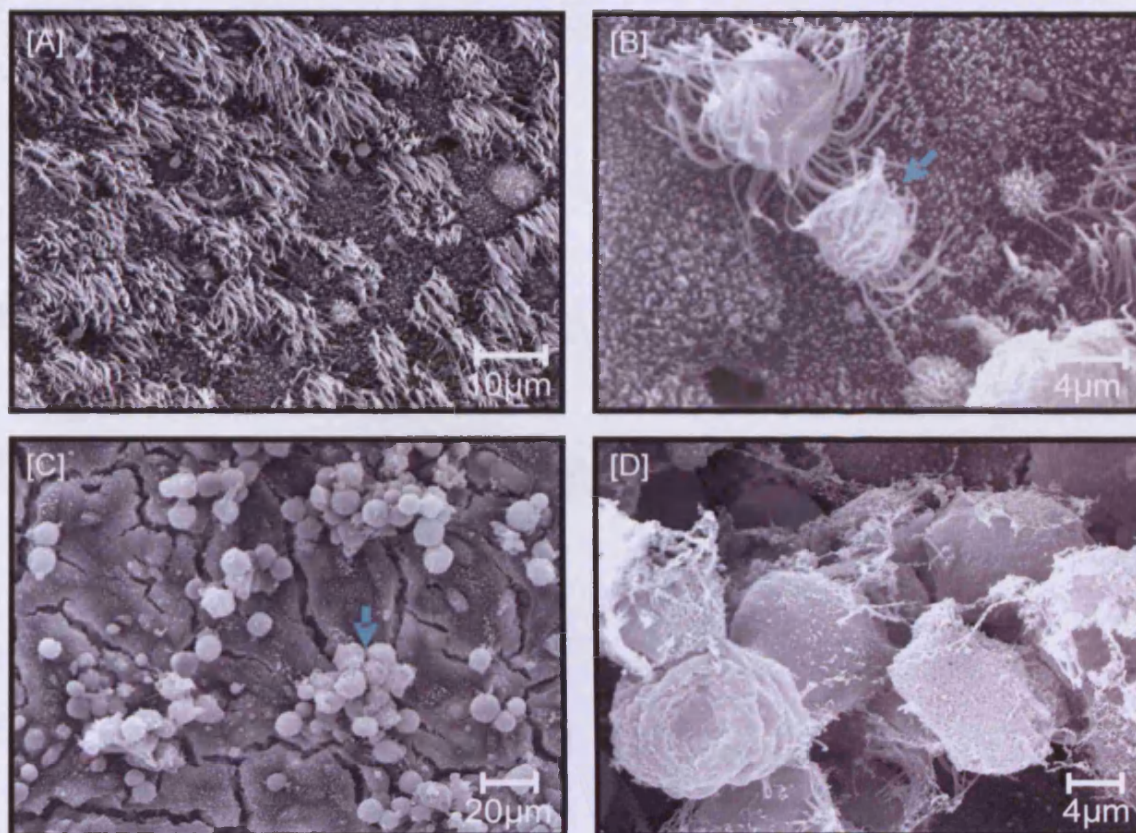


Figure 5.8 SEM images of NHBE cultures treated with CdCl. [A] Control cultures treated with PBS (carrier solution). [B] NHBE cultures treated with TD₅ (0.05mM) dose of CdCl; a few detached 'balled-up' ciliated cells observed (arrows). [C] NHBE cultures treated with TD₂₀ dose of CdCl; arrows indicate bulging cells. [D] NHBE cultures treated with TD₂₀ (0.34mM) dose of CdCl; higher magnification of area of severe damage, detached cells covered in stringy covering.

5.4.3 NHBE RESPONSE TO PARAQUAT

5.4.3.1 CULTURE VIABILITY AND TRANS-EPITHELIAL ELECTRICAL RESISTANCE

A dose range of 0 – 1500µM of Pq was determined to encompass both target TD₅ and TD₂₀ doses. The ATP assay displayed a slow, steady decline in culture viability with increasing doses of Pq (Figure 5.9). The TD₅ dose was determined as 75µM Pq, with the culture viability gradually decreasing, 750µM Pq was deemed to be the TD₂₀ dose. In response to higher doses the culture viability continued to decline at a slow-rate, to ~65% at 1500µM Pq.

TEER values elicited a biphasic response, with an initial increase of NHBE cultures exposed to 150 μ M (~135%) and 300 μ M (~145%) Pq. TEER values decreased dramatically in response to 450 μ M Pq (~13%). TEER values showed little change above 600 μ M Pq, with TEER values between 1.5 and 9% of the control (Figure 5.9).

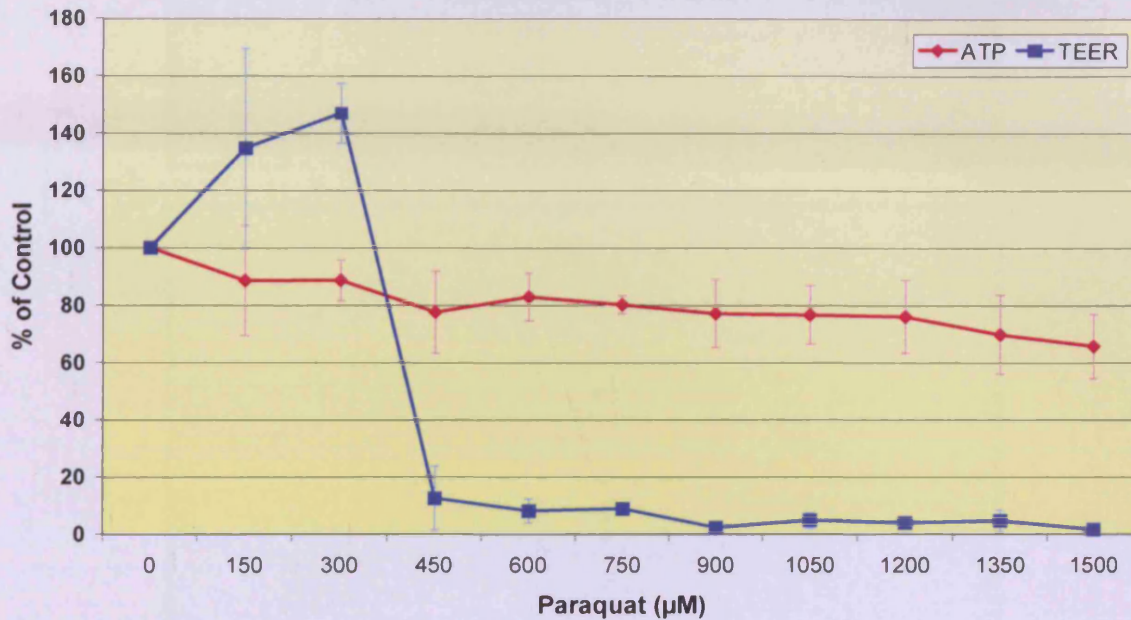


Figure 5.9 Graph displaying NHBE culture TEER and ATP assay after 24 hours treatment with paraquat. ATP (\blacklozenge) and TEER (\blacksquare) values displayed as percentage of control values. Standard Deviation was shown for both ATP (I) and TEER (I), $n = 3$.

5.4.3.2 LIGHT MICROSCOPY: TOLUIDINE BLUE

Control cultures (treated with PBS) exhibited the characteristic multi-layered, pseudo-stratified and fully-differentiated culture (Figure 5.10[A]). The NHBE epithelium underwent major changes in response to the TD₅ dose of Pq (Figure 5.10[B]). The epithelium became a cuboidal stratified epithelium (Figure 5.10[B]), with basal cell hypertrophy and squamation. There was a loss of ciliated cells, along with an increase in secreting cells. Apart from these phenotypic changes, there was little evidence of damage to the epithelial integrity; however, a large vacuole was observed (Figure 5.10[B]). After treatment with the TD₂₀ dose, cultures appeared as an undifferentiated squamous/cuboidal monolayer (Figure 5.10[C]).

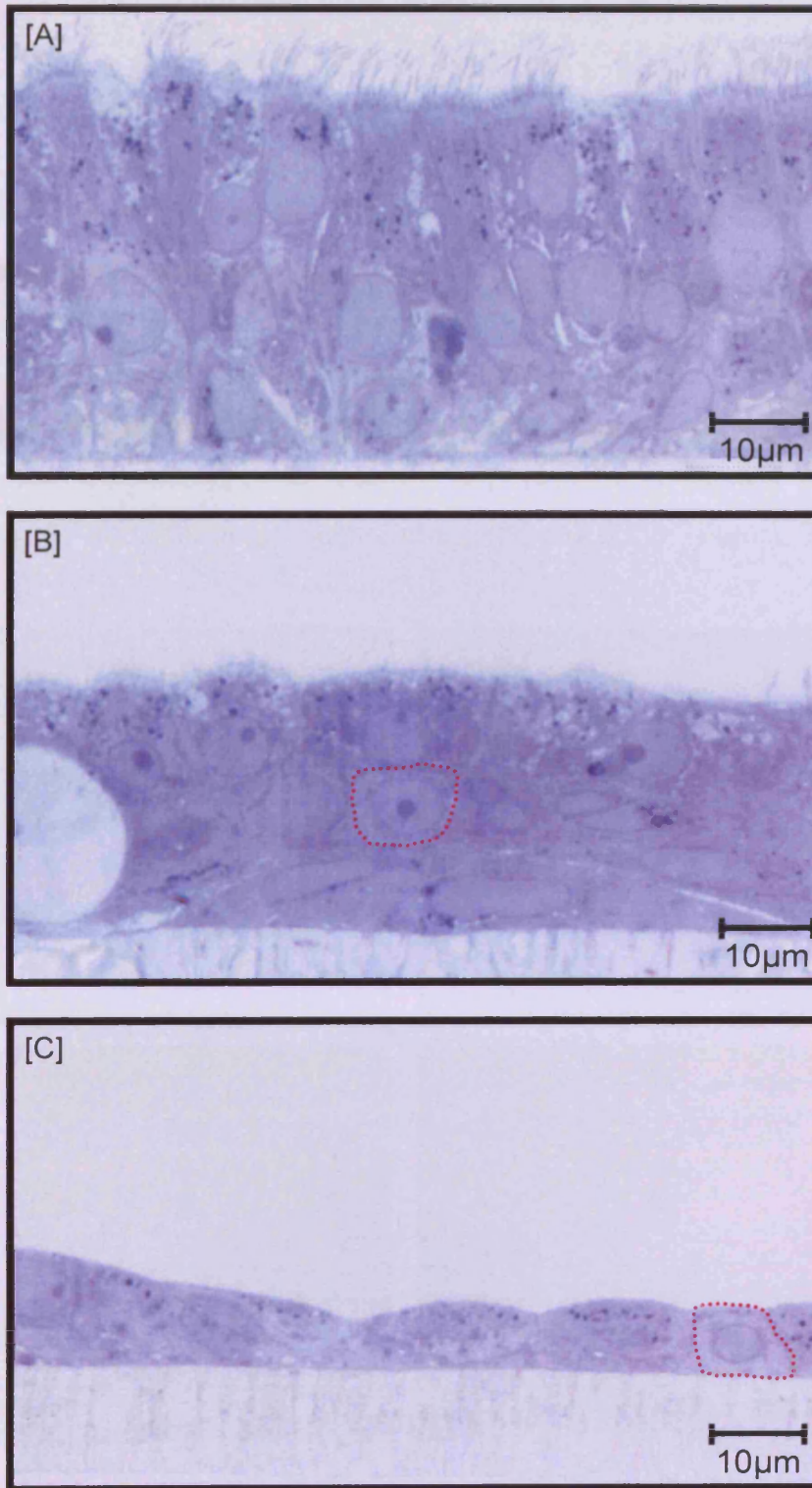


Figure 5.10 LM images of NHBE cultures treated with Pq stained with toluidine blue. [A] Control cultures treated with PBS (carrier solution). [B] NHBE cultures treated with TD₅ (75μM) dose of Pq; cuboidal stratified epithelium, one cuboidal cell highlighted, increased cellular secretion observed at the apical surface. [C] NHBE cultures treated with TD₂₀ (750μM) dose of Pq; undifferentiated, squamous/cuboidal epithelium, dotted area highlighting cuboidal cell.

5.4.3.3 SCANNING ELECTRON MICROSCOPY

Control NHBE cultures (treated with PBS), exhibited normal surface topography (Figure 5.11[A]). NHBE cultures treated with TD₅ Pq displaying minor damage to the epithelial integrity. However, there was evidence of dedifferentiation, with microvilli covering the vast majority of the surface (Figure 5.11[B]). The surface topography of NHBE cultures treated with the TD₂₀ dose of Pq was dramatically transformed. There was loss of epithelial integrity and microvilli, occasional detached cells and cellular blebbing as a probable result of apoptosis (Figure 5.11[C]). Higher magnification revealed a few remaining ciliated cells, loss of epithelial integrity and numerous cells undergoing cell death (Figure 5.11[D]).

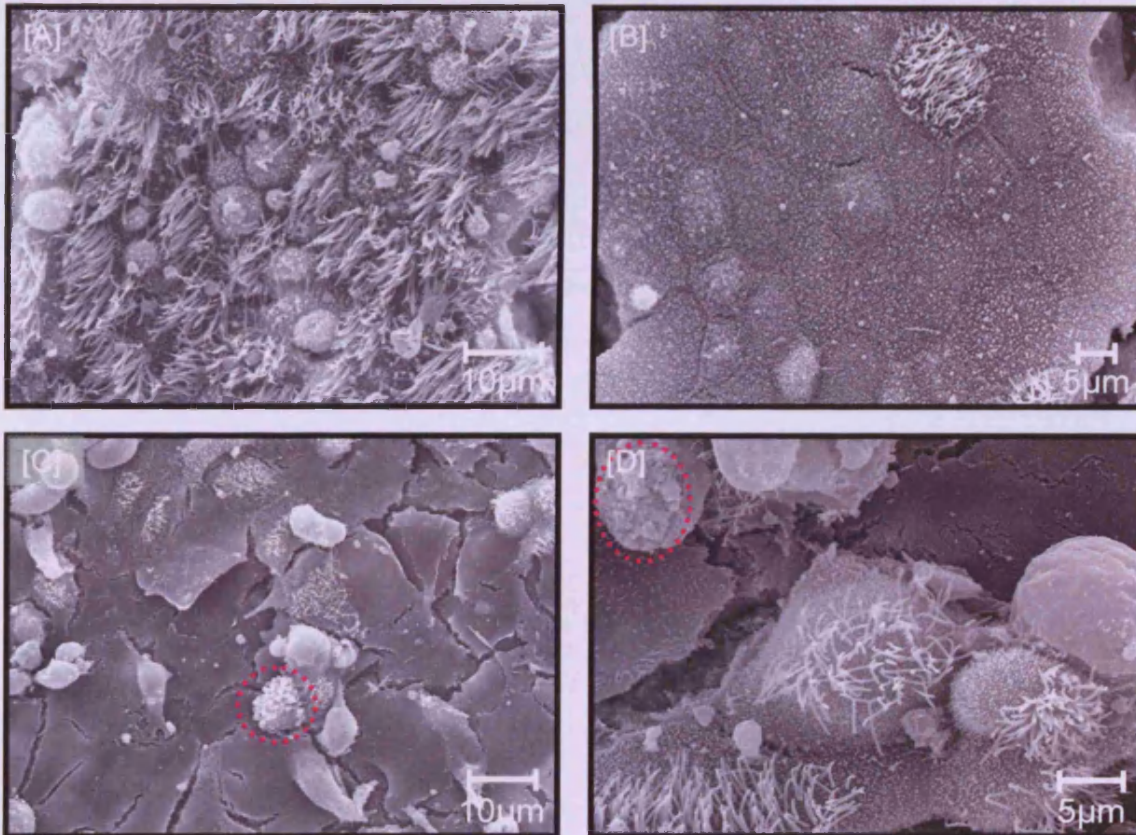


Figure 5.11 SEM images of NHBE cultures treated with Pq. [A] Control cultures treated with PBS (carrier solution). [B] NHBE cultures treated with TD₅ (75µM) dose of Pq; dedifferentiation of cultures, few ciliated cells remain, microvilli cover the surface. [C] NHBE cultures treated with TD₂₀ (750µM) dose of Pq; loss of epithelial integrity and microvilli, dotted region highlighting blebbing cell. [D] NHBE cultures treated with TD₂₀ dose of Pq; higher magnification of damaged area, loss of epithelial integrity and microvilli, dotted region highlighting blebbing cell.

5.4.4 NHBE RESPONSE TO AMIODARONE

5.4.4.1 CULTURE VIABILITY AND TRANS-EPITHELIAL ELECTRICAL RESISTANCE

A dose range of 0 – 1000 μ g/ml of Am was determined to encompass both target TD₅ and TD₂₀ doses. The ATP assay for viability over the dose range displayed a very gradual decrease in culture viability (Figure 5.12). At 300 μ g/ml Am, there was a 5% reduction in culture viability (TD₅ dose), the culture viability continued to gradually decrease, with the TD₂₀ dose calculated as 850 μ g/ml Am. In response to higher doses a slight decrease in culture viability was observed (~75% at 1000 μ g/ml).

TEER values over the dose range (0 – 1000 μ g/ml) elicited a biphasic response, however, average TEER values did not increase above control values. TEER values gradually decreased between 100 – 200 μ g/ml Am, to approximately 75% of the control, this was followed with a return to normal TEER values by 300 μ g/ml. Higher doses of Am resulted in a gradual decrease in TEER readings, down to 87% by 700 μ g/ml, followed by a steeper decrease in TEER; 67% at 800 μ g/ml and 53% at 1000 μ g/ml (Figure 5.12).

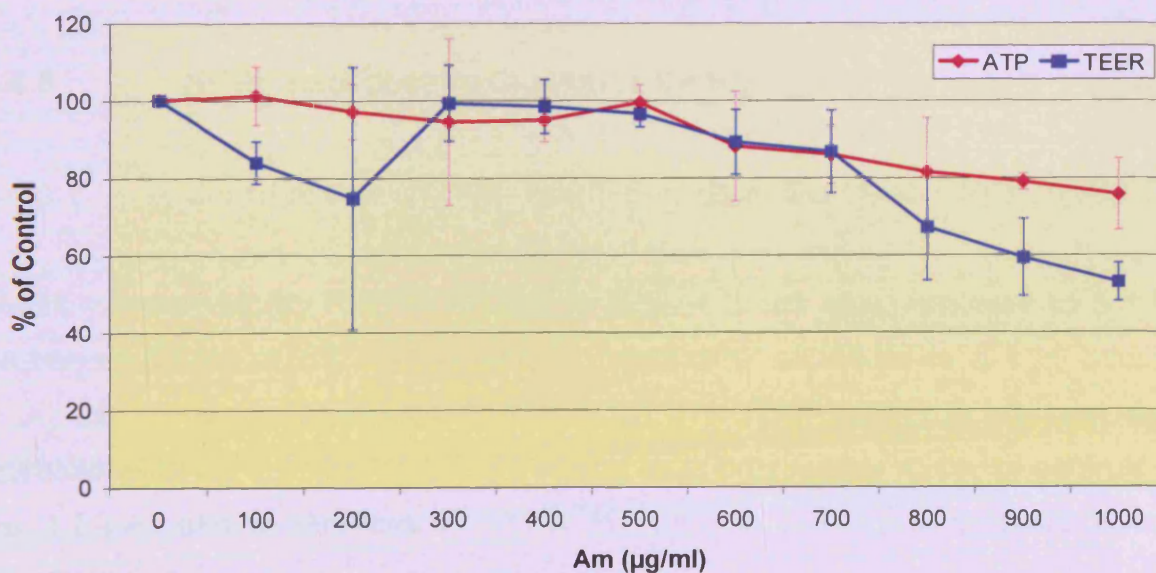


Figure 5.12 Graph displaying NHBE culture TEER and ATP assay after 24 hours treatment with Amiodarone. ATP (\blacklozenge) and TEER (\blacksquare) values displayed as percentage of control values. Standard Deviation was shown for both ATP (I) and TEER (I), $n = 3$.

5.4.4.2 LIGHT MICROSCOPY: TOLUIDINE BLUE

Control cultures (treated with dH₂O) exhibited the characteristic pseudo-stratified, muco-ciliary culture (Figure 5.13[A]). The TD₅ dosed cultures underwent a certain amount of dedifferentiation, appeared squamous and lost cilia. There was also evidence of cellular loss and deterioration of cellular junctions (Figure 5.13[B]). The major changes observed after treatment with the TD₂₀ dose was further squamation of cultures. The epithelial integrity on the surface appeared relatively intact, with little to no disruption of cell contacts in this area, with occasional cilia present on the apical surfaces (Figure 5.13[C]).

5.4.4.3 SCANNING ELECTRON MICROSCOPY

Control NHBE cultures (treated with dH₂O), exhibited normal surface topography (Figure 5.14[A]). NHBE cultures treated with a TD₅ dose of Am displayed minimal damage to the surface topography, with cultures appearing as controls (Figure 5.14[B]). Even in response to the higher, TD₂₀ dose of Am, there was little visible damage to the surface topography of NHBE cultures. There were some gaps probably due to the loss of cells (Figure 5.14[C]) and evidence of cilia loss and possible regeneration (presence of cilia/microvilli pediments) (Figure 5.14[D]).

5.4.5 NHBE RESPONSE TO CIGARETTE SMOKE

5.4.5.1 CULTURE VIABILITY AND TRANS-EPITHELIAL ELECTRICAL RESISTANCE

NHBE culture viability had decreased to 82%, 4 hours after exposure to a 1:50 dilution (1:50-4h) of CS and to 54%, 4 hours after exposure to a 1:20 dilution (1:20-4h), compared to controls (Figure 5.15). The TEER response however, was biphasic, with an increase in TEER reading to approximately 125% of controls at the 1:50-4h and a decrease in TEER to ~65% to the higher 1:20-4h dilution (Figure 5.15).

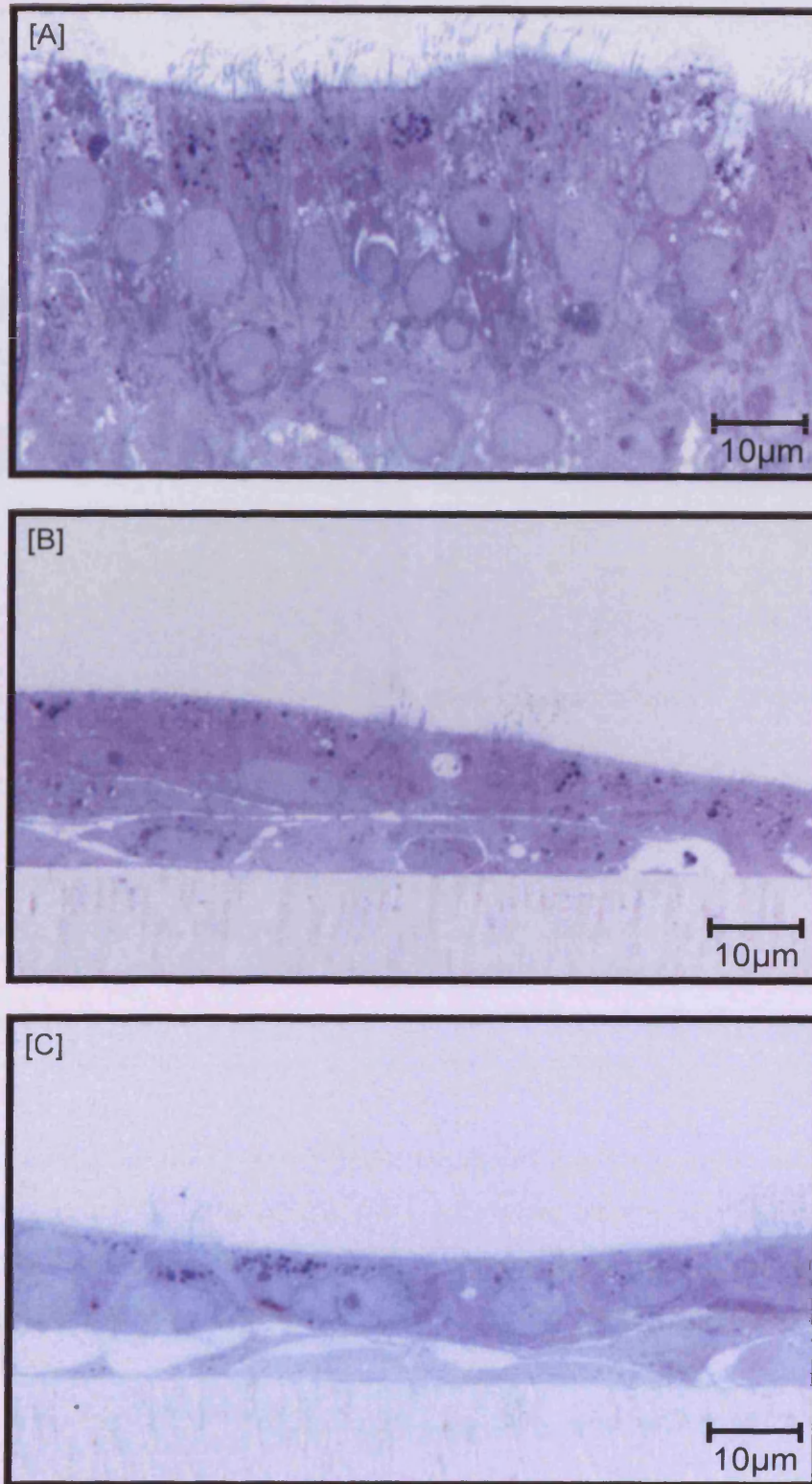


Figure 5.13 LM images of NHBE cultures treated with Am and stained with toluidine blue. [A] Control cultures treated with dH₂O (carrier solution). [B] NHBE cultures treated with TD₅ (300 µg/ml) dose of Am; squamating epithelium, dedifferentiation and loss of cilia. [C] NHBE cultures treated with TD₂₀ (850 µg/ml) dose of Am; deterioration of epithelium.

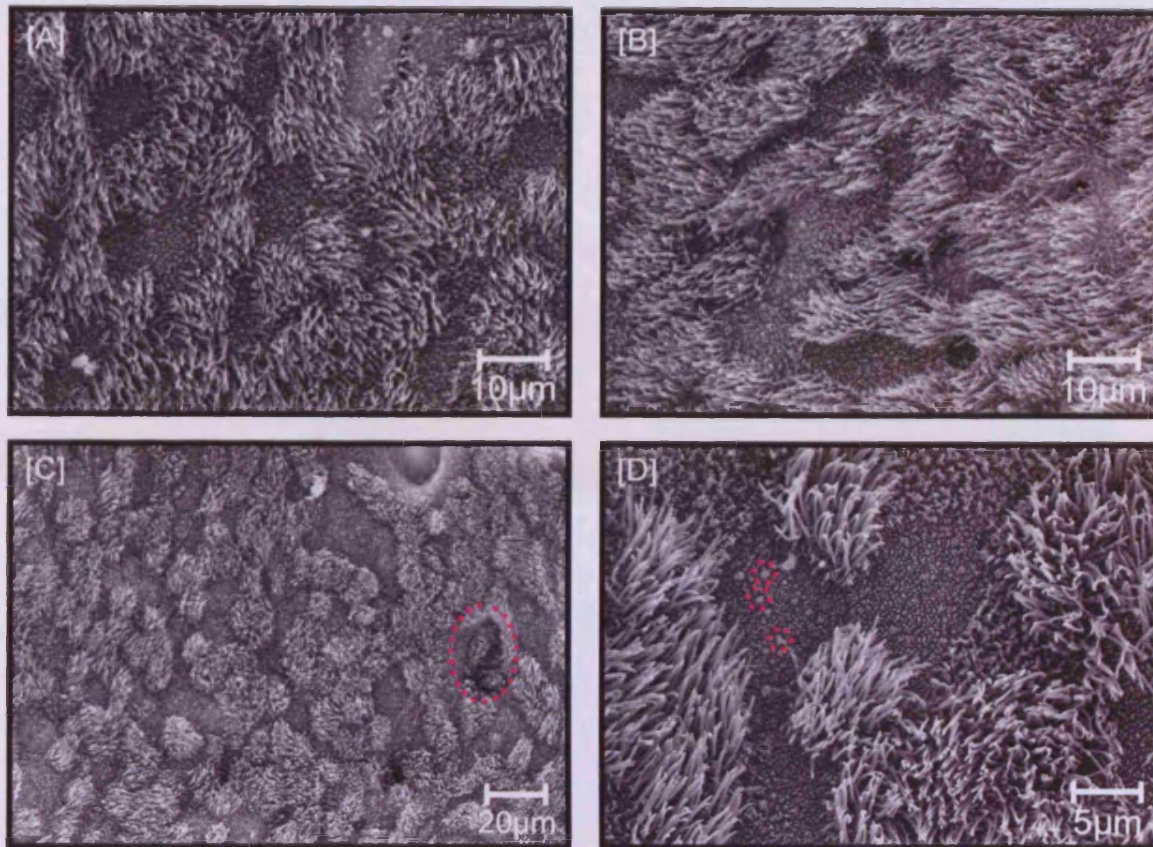


Figure 5.14 SEM images of NHBE cultures treated with Am. [A] Control cultures treated with dH₂O (carrier solution). [B] NHBE cultures treated with TD₅ (300µg/ml) dose of Am; no real damage observed. [C] NHBE cultures treated with TD₂₀ (850µg/ml) dose of Am; highlighted region displaying some minor surface damage. [D] NHBE cultures treated with TD₂₀ dose of Am; higher magnification, highlighted areas displaying cilia/microvilli pediments.

Both NHBE culture viability and TEER displayed a steady decrease in response to increasing concentrations of CS, 24 hours after treatment (Figure 5.16). After exposure to a 1:50-24h dilution of CS, the culture viability had decreased to 60% and the TEER to ~25%. A 1:30-24h dilution of CS caused a reduction in culture viability to 32% and TEER to ~5%. The higher concentration of CS, 1:20-24h, resulted in a further drop in both culture viability and TEER, 10% and ~4.5%, respectively (Figure 5.15).

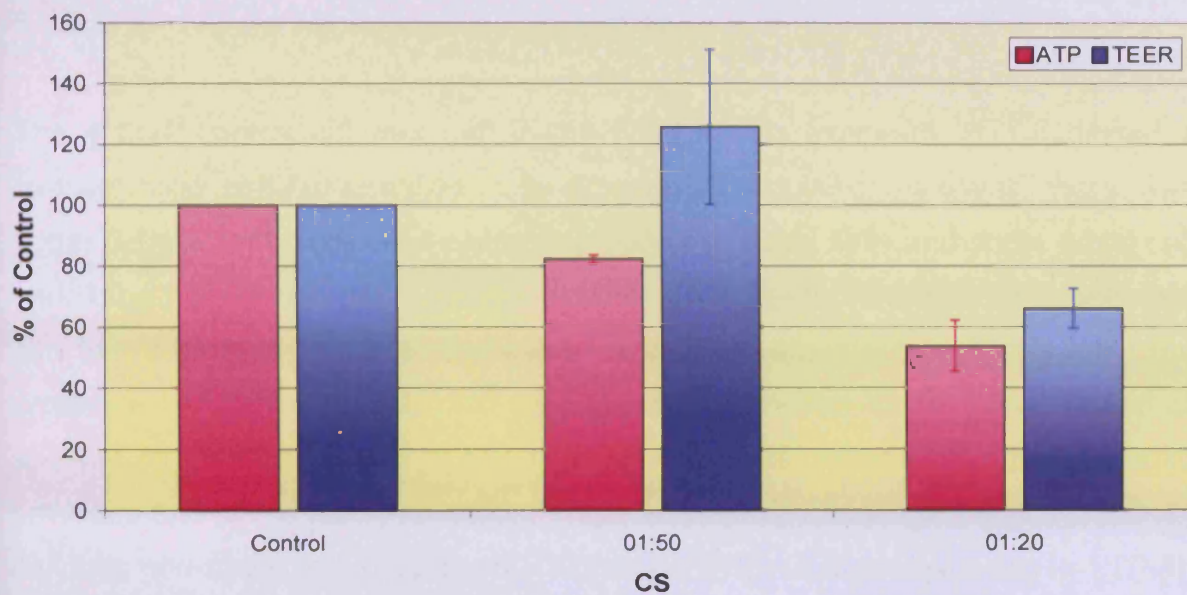


Figure 5.15 Graph displaying NHBE culture TEER and ATP assay after 30 minutes exposure to CS and 4 hours recovery. ATP (■) and TEER (■) values displayed as percentage of control values. Standard Deviation was shown for both ATP (I) and TEER (I), $n = 3$.

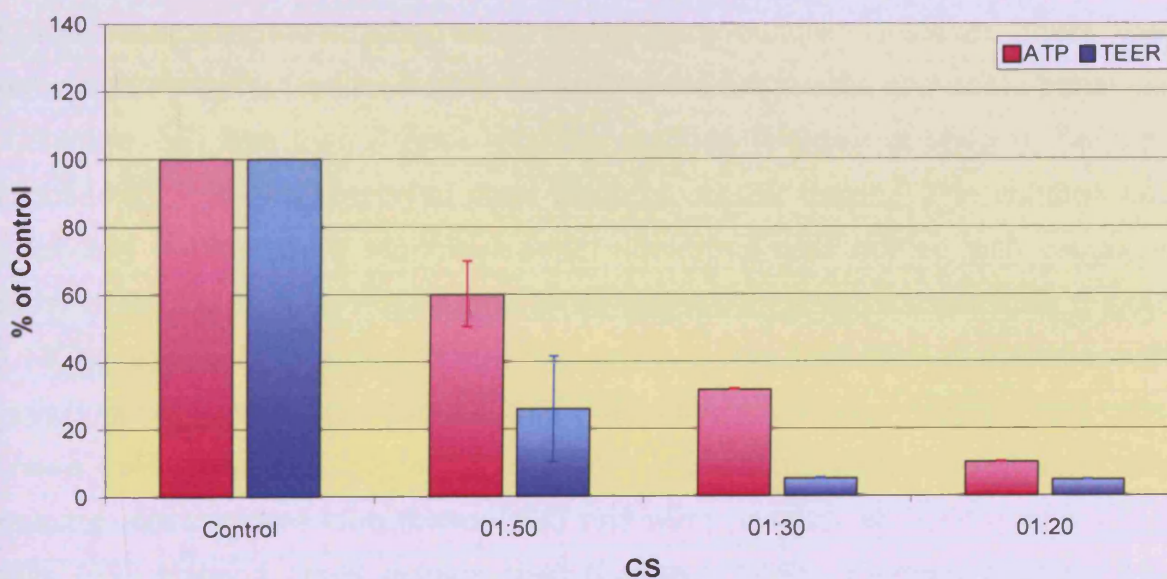


Figure 5.16 Graph displaying NHBE culture TEER and ATP assay after 30 minutes exposure to CS and 24 hours recovery. ATP (■) and TEER (■) values displayed as percentage of control values. Standard Deviation was shown for both ATP (I) and TEER (I), $n = 3$.

5.4.5.2 LIGHT MICROSCOPY: TOLUIDINE BLUE

The 4 hour control cultures (left in the hood during exposure, RT) exhibited a characteristic pseudo-stratified, fully-differentiated culture; however, there was some detachment of cell-cell contacts around the basal cells and some basal cell shrinkage (Figure 5.17[A]). Cultures exposed to 1:50-4h CS appeared to separate into two distinct layers, with the apical layer relatively intact, with cilia loss, but presence of microvilli. The most damage was observed at the basal region of apically located cells and in the cells of the basal layer, with disruptions to junctions and presence of vacuoles. There was also evidence of dedifferentiation, cell loss and basal cell hypertrophy (Figure 5.17[B]). Cultures exposed to 1:20-4h CS appeared as a monolayer, where numerous cells displayed signs of damage denoted by both intra-cellular vacuoles and inter-cellular gaps (Figure 5.17[C]).

The 24 hour control cultures (left in the hood during exposure, RT) exhibited the characteristic pseudo-stratified and muco-ciliary culture. However, there was some detachment of cell-cell contacts around the basal cells and some basal cell shrinkage, but less than 4 hour recovery cultures (image not shown). Cultures exposed to 1:50-24h displayed clear signs of cellular toxicity. The cultures had practically reverted to a monolayer, with numerous cells riddled with vacuoles. Many of the cells present appeared to be large, hypertrophic basal cells (Figure 5.18[A]). Exposure to 1:30-24h, CS resulted in a very high level of damage, with individual cells almost unattached from the membrane and/or neighbouring cells. These cells contained numerous vacuoles, no distinct nucleus and very pale staining with toluidine blue (basophilia) and were possibly all hypertrophic basal cells (p63 staining could confirm this) (Figure 5.18[B]). Extreme damage was observed with cultures exposed to 1:20-24h CS, as denoted by the absence of cells on all areas sectioned and stained for toluidine blue (Figure 5.18[C]).

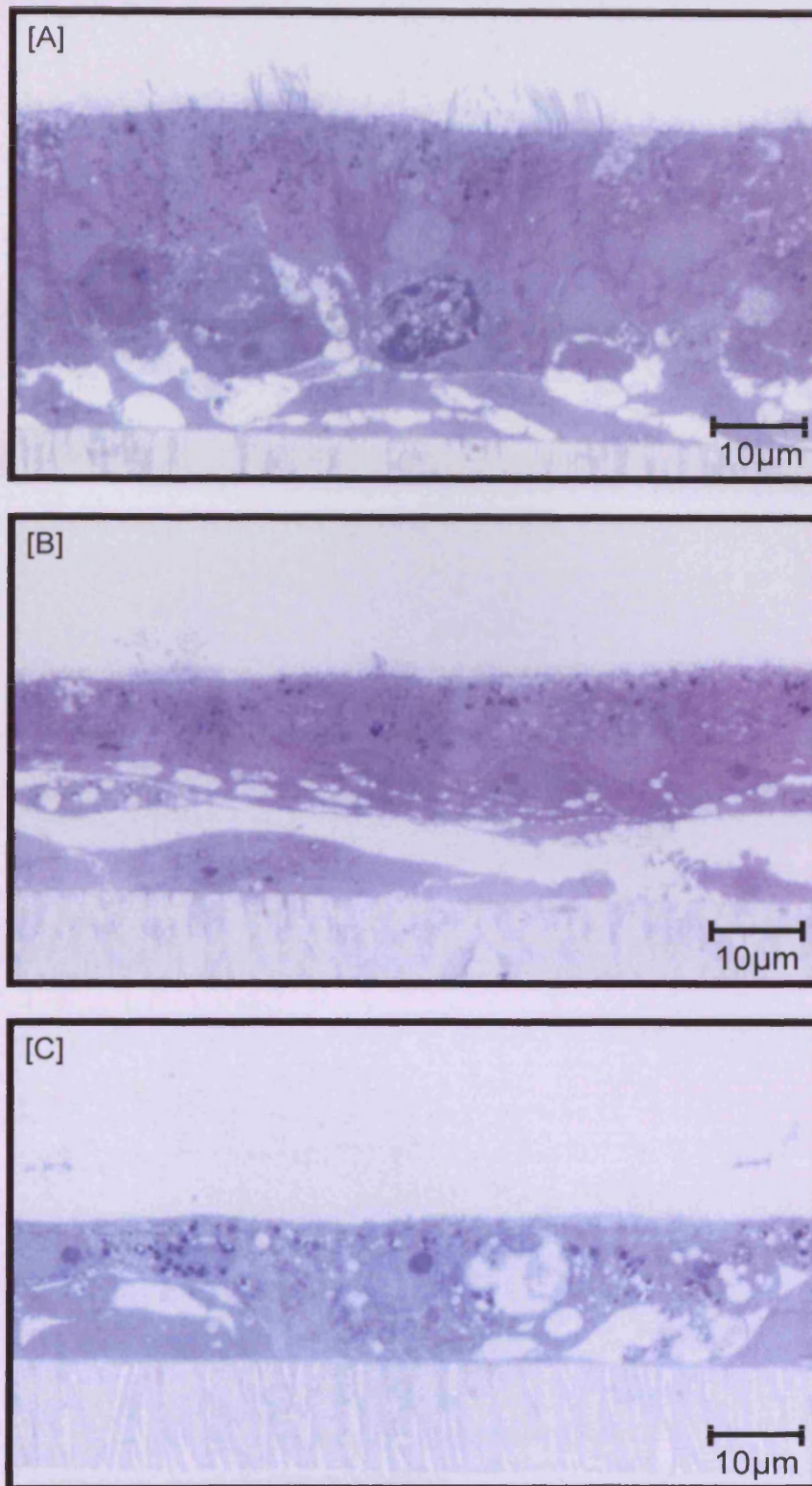


Figure 5.17 LM images of NHBE cultures 4 hours after 30 minutes exposure to CS and stained with toluidine blue. [A] Control cultures; air exposed. [B] NHBE cultures treated with a 1:50 dilution of CS; cultures split into two cell layers, evidence of dedifferentiation, cilia loss and cell death. [C] NHBE cultures treated with 1:20 dilution of CS; loss of normal epithelial structure, dedifferentiation and numerous dead cells.

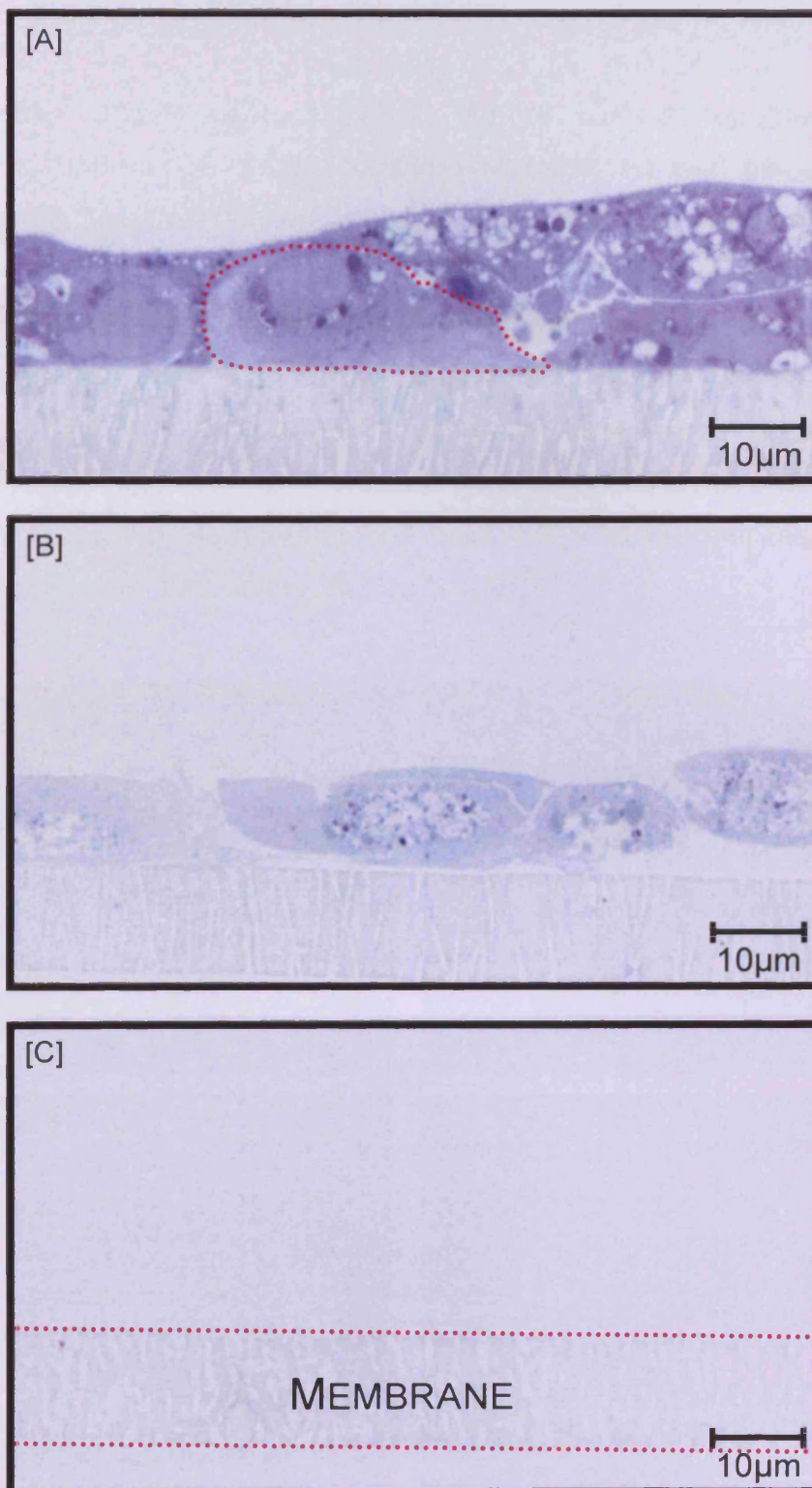


Figure 5.18 LM images of NHBE cultures 24 hours after 30 minutes exposure to CS and stained with toluidine blue. [A] NHBE cultures treated with a 1:50 CS; dedifferentiation and cell death, highlighting a hypertrophic basal cell. [B] NHBE cultures treated with 1:30 CS; total destruction rendering a monolayer of very damaged basal cells. [C] NHBE cultures treated with 1:20 CS; all areas sectioned and stained revealed no cells remaining on the membrane (highlighted).

5.4.5.3 SCANNING ELECTRON MICROSCOPY

Control NHBE cultures (4h), exhibited normal surface topography (Figure 5.19[A]). The 1:50-4h CS treated cultures revealed no real disruption to the surface integrity. Dedifferentiation was observed, most cells were only covered in microvilli, with the loss of numerous ciliated cells (Figure 5.19[B]). Focal damage was observed in response to the 1:20-4h treatment. Some areas were similar to 1:50-4h treated cultures, with less microvilli and cellular delineation (Figure 5.19[C]). Other areas displayed more damage to the cells and epithelial integrity (Figure 5.19[D]). These areas of increased damage had a compromised epithelial barrier, with detaching, dedifferentiated cells with a ruffled cell membrane, the insert membrane was also visible (Figure 5.19[D]).

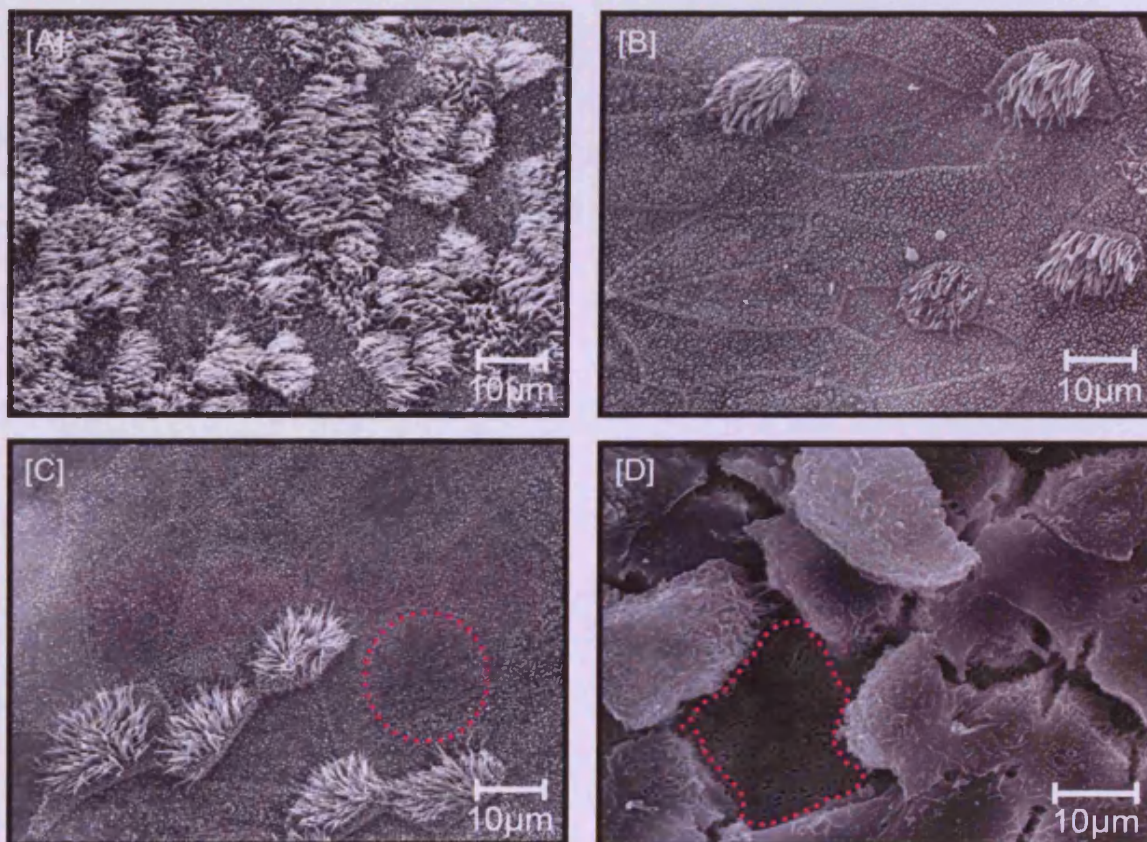


Figure 5.19 SEM images of NHBE cultures 4 hours after 30 minutes exposure to CS. [A] Control cultures; air exposed. [B] NHBE cultures treated with 1:50 CS; dedifferentiation and cilia loss. [C] NHBE cultures treated with 1:20 CS; less damaged area, dedifferentiation, cilia loss, highlighted area demonstrating microvillus loss. [D] NHBE cultures treated with 1:20 CS; more damaged area, loss of barrier, dedifferentiated cells, insert membrane visible (highlighted).

The 24 hour control NHBE cultures (left in the hood during exposure, RT), exhibited normal surface topography (Figure 5.20[A]). The surface of cells after 1:50-24h treatment had a pitted/retracted appearance. The cilia present were also very sunken into the surface and appeared to stick to or merge with neighbouring cilia (Figure 5.20[B]). The epithelial integrity of 1:30-24h cultures was severely compromised with the vast majority of cells, detaching, fragmenting and blebbing (Figure 5.20[C]). Extreme damage and almost complete epithelial shedding was observed after 1:20-24h treatment. In the areas where cells were located, they were either present as individual cells sparsely scattered on the membrane or as a small cluster of cells forming part of an epithelial sheet. The majority of these cells appeared to be dedifferentiated and undergoing cell death (Figure 5.20[D]).

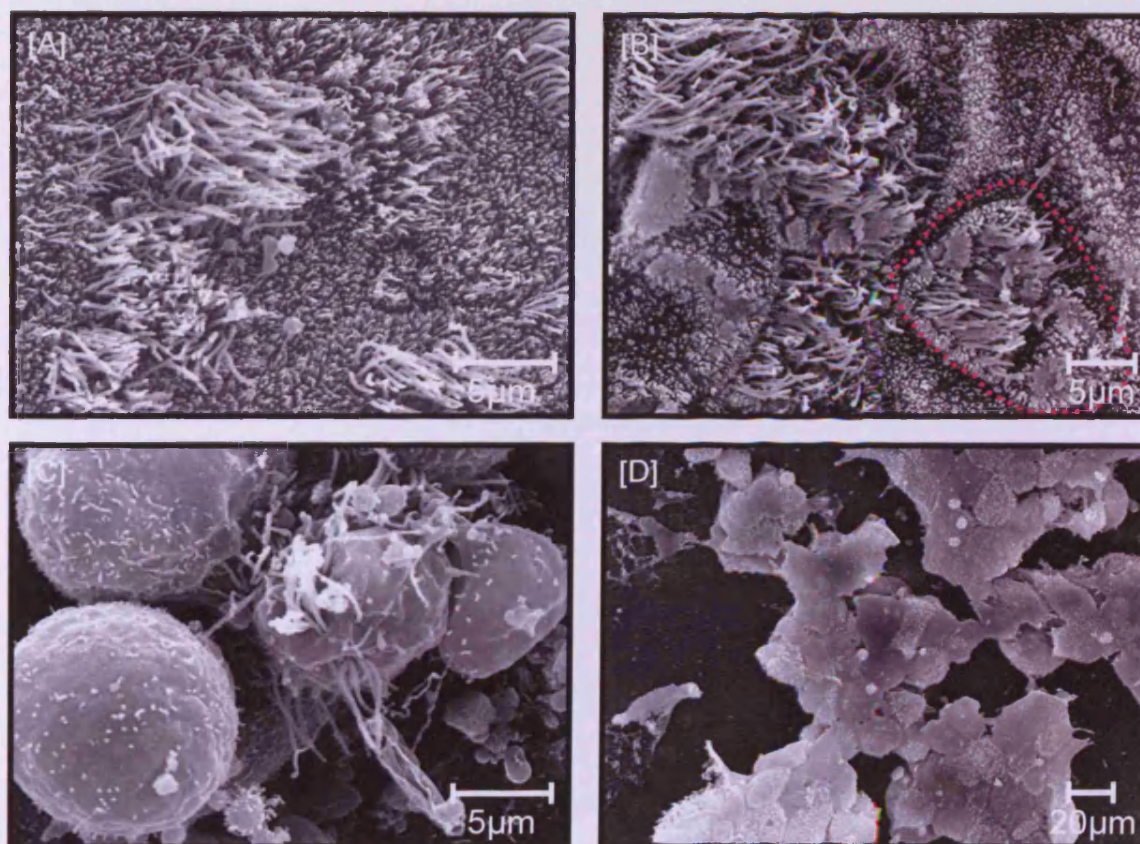


Figure 5.20 SEM images of NHBE cultures 24 hours after 30 minutes exposure to CS. [A] Control cultures; air exposed. [B] NHBE cultures treated with 1:50 CS; pitted surface, dotted area displays clumped and sunken cilia. [C] NHBE cultures treated with 1:30 CS; major destruction, numerous detached, undifferentiated and dying cells. [D] NHBE cultures treated with 1:20 CS; cells were lacking from the majority of the insert, with a few clusters of highly-damaged cells remaining.

5.4.6 NHBE CYTOKINE RESPONSE TO LIPOPOLYSACCHARIDE

Thirty seven (out of 42) cytokines tested displayed a 1.5-fold change or more in response to at least one of the LPS treatments (Figure 5.21 and 5.22). NHBE cultures treated with the TD₅ (24 hours) dose exhibited increased expression of 6 and decreased expression of 17 cytokines. In the TD₂₀ dosed cultures, the 4 hours LPS challenge induced 11 and reduced 1 cytokine expression. In the culture treated with TD₂₀ dose for 24 hours, 9 cytokines had increased and 14 decreased their expression.

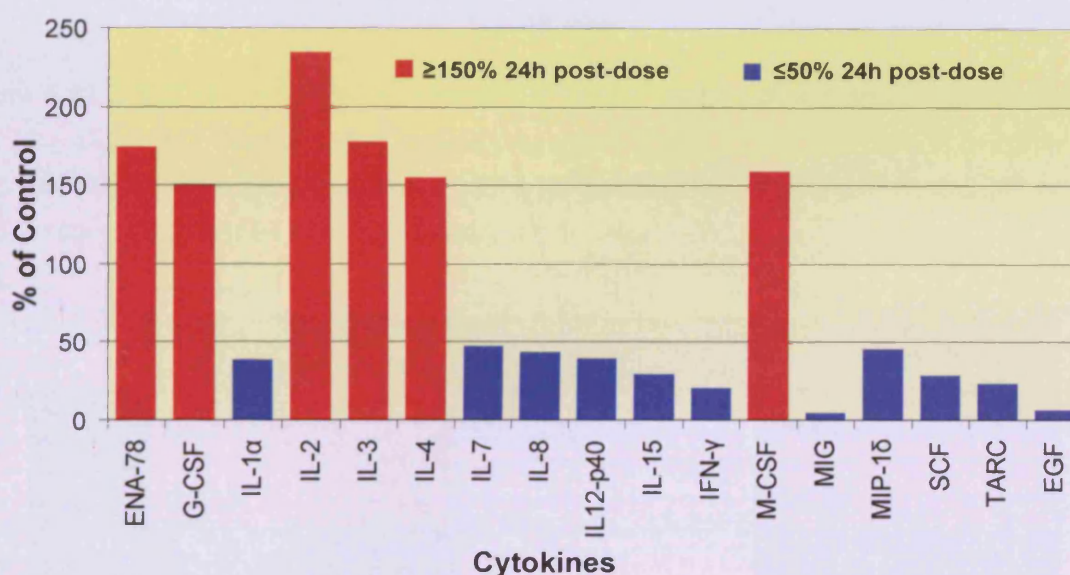


Figure 5.21 Graph displaying major cytokine changes in NHBE cultures after 24 hours incubation with the TD₅ (0.1mg/ml) dose of LPS. Cytokine expression above 150% of control (■) or below 150% of control (■) were displayed, $n = 1$.

A number of correlations were observed between different LPS treatments (Table 5.4). ENA-78 and G-CSF were up-regulated and SCF down-regulated in both doses after 24 hours (Group 1). IL-1 α and IFN- γ decreased expression with the TD₅ dose, but increased after both TD₂₀ doses (Group 2). IL-1 α , IL-1 β and IFN- γ all increased in response to the TD₂₀ dose after 4 hours and slightly more after 24 hours (Group 2 and 3). IL-5, IL-6, RANTES and TPO were all upregulated above the 1.5-fold threshold level after the TD₂₀-4 hour dose only (Group 4).

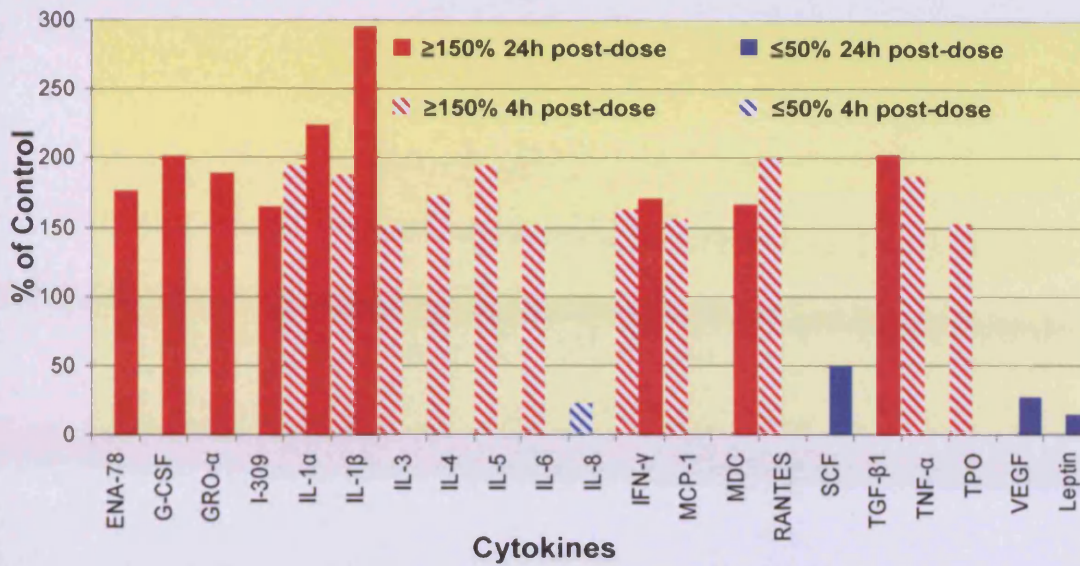


Figure 5.22 Graph of major cytokine changes in NHBE cultures after 4 and 24 hours incubation with TD₂₀ (0.5mg/ml) dose of LPS. Cytokine expression above 150% of control (▨) or below 150% of control (▩) after 4 hours incubation. Cytokine expression above 150% of control (■) or below 150% of control (■) after 24 hours incubation, n = 1.

	TD ₅ -24h	TD ₂₀ -4h	TD ₂₀ -24h
1	ENA-78	---	ENA-78
	G-CSF	---	G-CSF
	SCF	---	SCF
2	IL-1 α	IL-1 α	IL-1 α
	IFN-γ	IFN-γ	IFN-γ
3	---	IL-1β	IL-1β
4	---	IL-5	---
	---	IL-6	---
	---	RANTES	---
	---	TPO	---

Table 5.4 Correlations between cytokine changes after treatment with LPS. Red boxes indicated increased expression ≥1.5-fold, blue boxes indicated decrease in expression ≤1.5-fold.

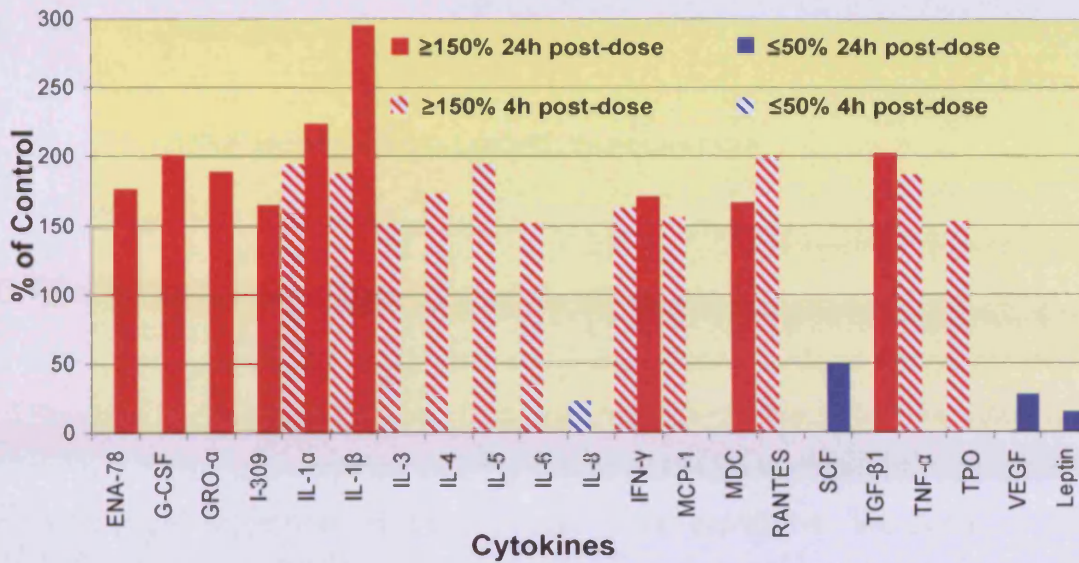


Figure 5.22 Graph of major cytokine changes in NHBE cultures after 4 and 24 hours incubation with TD₂₀ (0.5mg/ml) dose of LPS. Cytokine expression above 150% of control (▨) or below 150% of control (▩) after 4 hours incubation. Cytokine expression above 150% of control (■) or below 150% of control (■) after 24 hours incubation, n = 1.

	TD ₅ -24h	TD ₂₀ -4h	TD ₂₀ -24h
1	ENA-78	---	ENA-78
	G-CSF	---	G-CSF
	SCF	---	SCF
2	IL-1 α	IL-1 α	IL-1 α
	IFN-γ	IFN-γ	IFN-γ
3	---	IL-1β	IL-1β
4	---	IL-5	---
	---	IL-6	---
	---	RANTES	---
	---	TPO	---

Table 5.4 Correlations between cytokine changes after treatment with LPS. Red boxes indicated increased expression ≥1.5-fold, blue boxes indicated decrease in expression ≤1.5-fold.

5.5 DISCUSSION

5.5.1 NHBE RESPONSE TO LIPOPOLYSACCHARIDE

5.5.1.1 CULTURE VIABILITY AND TRANS-EPITHELIAL ELECTRICAL RESISTANCE

The ATP assay produced a biphasic response over the dose range tested, with the TD₅ dose (0.1mg/ml) obtained from the initial decrease in culture viability. The subsequent increase in culture viability (up to 120%) was thought to be part of an early-protective response of the culture. This protective increase in culture viability could be due to numerous reasons, including goblet cell hyperplasia (Harris *et al.*, 2007), an increase in glycolysis (Spolarics and Spitzer, 1993) and cellular hypertrophy (Kumar *et al.*, 2010). Higher concentrations of LPS over-rode these early-protective responses, resulting in a decrease in culture viability, with the TD₂₀ dose being achieved at 0.5mg/ml LPS, to a TD₅₀ at 1mg/ml. The LPS dose range used appeared high when compared to monolayer data (A549; 12 fold; Tang *et al.*, 2006); which may be due to a variety of reasons. Firstly, in order to achieve an adequate response to LPS in 24 hours. Secondly, the toxic effect of endotoxins is not mediated by direct killing of host cells or inhibition of cellular functions (Rietschel *et al.*, 1994). Thirdly, the human airway epithelium has been shown to be hyporesponsive to LPS, due to a low MD-2 expression in primary cultures (Jia *et al.*, 2004).

Culture integrity was evaluated by monitoring the TEER, which decreased in response to increasing LPS concentrations. The TEER readings did not increase above control readings (as did the ATP activity), but appeared to mimic the ATP response during the period of increased culture viability. This may indicate either that disruption of epithelial junctions in response to LPS plateaued at certain concentrations or that cellular hypertrophy and/or hyperplasia counteracted the decline in TEER readings from junctional disruption. In response to the TD₅ dose there was a significant decline in TEER (55% of controls), with the TD₂₀ dose yielding a TEER of only 4% of the control; at this level of resistance epithelial integrity was deemed to be negligible. This decrease in culture integrity in response to increasing concentrations of LPS would suggest that the cellular

junctions were being corrupted, with tight junctions known to open in response to LPS (Eutamene *et al.*, 2005). However, this disruption or detachment of epithelial cell contacts could be part of a protective and regeneration response, with cells detaching in order to migrate to areas of increased damage and restore the epithelial barrier (Park *et al.*, 2006).

5.5.1.2 MORPHOLOGICAL CHANGES

Morphological assessment of NHBE cell cultures treated with a TD₅ dose of LPS revealed that the basal cells were the most severely affected cell type. Many were shrunken in appearance and displayed detachment of cell-cell contacts, features suggestive of apoptosis (Elmore, 2007). However, some basal cells appeared to be migrating to the columnar layer, i.e. becoming intermediate cells. TEER values were low at this dose, indicating that cell junctions were compromised, enhancing the basal cells exposure to LPS (and inflammatory mediators; Han *et al.*, 2004). It is therefore presumed that, basal cell demise/death contributed to the corresponding drop in culture viability. In addition to basal cell damage, there was a shift in the epithelial phenotype, denoted by increased mucus producing cells leading to excess apical mucin. Mucin hypersecretion is a well known protective response to lung injury (Burgel and Nadel, 2004), but the exact nature of this response is not always known. The replacement of many non-mucus with mucus cells was probably a combination of goblet cell hyperplasia (Toward and Broadley, 2002), basal cells differentiating into goblet cells and transdifferentiation of Clara and ciliated cells (Jeffery and Li, 1997; Evans *et al.*, 2009; Park *et al.*, 2006). The transdifferentiation of Clara and ciliated cells was likely to account for the majority of 'new' mucin-secreting epithelial cells observed and are therefore,, not 'true' goblet cells. In response to injury, Clara and ciliated cells are known to become Clara-mucus and ciliated-secretory cells, with each retaining some characteristics of their original cell type, whilst incorporating mucus producing characteristics (Jeffery and Li, 1997). Histochemical and immunohistochemical techniques to detect specific cell types may shed light on the origin or dual nature of these transdifferentiated cells. Additionally, it is unknown whether the mucin secreted by these pseudo-goblet cells alters the physiochemical properties of the mucous layer, and if they do, is this change advantageous?

Topographically, NHBE cultures treated with the TD₅ dose appeared similar to control cultures, with an intact apical surface speckled with microvilli and cilia. There was evidence of dedifferentiation, with less ciliated cells than expected (control and TD₅ cultures). These findings reinforced previous observations that a high dose of LPS could disrupt epithelial junctions without causing significant cell death, thereby allowing preferential damage to the basal cells.

In response to the TD₂₀ dose of LPS, there was loss of cell-cell contacts, with large inter-cellular gaps observed. Numerous cells, at all levels within the epithelium appeared shrunken with large nucleus-to-cytoplasmic ratios or indeed no discernable nucleus; all features indicative of cell death (Elmore, 2007). Large areas of degenerative material could be observed, which was thought to be reticular fibre or other ECM components (Fueki *et al.*, 2009), further histological staining would be necessary to confirm this.

The NHBE cultures surface, following the TD₂₀ dose, demonstrated focal damage, with some areas exhibiting normal surface topography. Zones of intermediate regions displayed cells detached from their neighbours, which were spherical in appearance and had numerous protruding cilia, with other cells bulging apically, as if beginning to detach. Areas of severe damage revealed multiple cell layers of unattached, cilia protruding, cells. These regions of disrupted apical surface would cause the negligible TEER values exhibited at this dose. The reason for the detaching cells could be 2-fold, firstly, these cells were undergoing cell death and were detaching for this reason. Secondly, that these ciliated cells were detaching in order to migrate to areas of severe damage, where the epithelium had been completely denuded and were attempting to regenerate the epithelium in this region. It has been documented that ciliated cells that detach from explant cultures dedifferentiate, become squamous and contribute to the formation of a mature epithelium (Wallace *et al.*, 1994).

5.5.1.3 CYTOKINE CHANGES

Only one CPT (LPS) was taken forward in an experimental trial to characterise the cytokine responses of the NHBE model. The NHBE cultures response to

differing LPS doses provided an insight only into the cytokine and possible subsequent immune response and was therefore, not conclusive. This is mainly due to the fact that the NHBE culture consists of cells of the bronchial epithelium only and does not involve any immune cells that could be attracted in response to cytokines produced by the epithelium and in turn secrete their own mediators that could change the cytokine profile observed. Another limitation is that the array used only detects 42 and not all possible cytokines; therefore any conclusions may only be made on the changes observed. Additionally, this experiment was only performed on one insert, from one donor and without sufficient 'n' numbers is inconclusive.

In light of the above limitations and the large number of cytokines that have been altered, only certain cytokines and groups thereof, were investigated in more detail. The first of these groups involved the cytokines capable of initiating a T_H1 or a T_H2 immune response (Table 1.3). IL-12 is the major cytokine involved in the activation of a T_H1 response, whilst IL-4 in the activation of a T_H2 response (Liu, 2002). From our results, the response to the TD_5 dose was a reduced expression of IL-12, with an increased expression of IL-4. Four hours after the TD_{20} dose, IL-4 was increased. In response to both TD_{20} doses (4 and 24 hour exposures), IFN- γ (an important TH_1 cytokine) was increased. IFN- γ was also reduced after the TD_5 dose. This data suggested that the 'low' LPS dose produced a T_H2 response and the 'high' LPS dose resulted in the T_H1 response; a documented response in hyposensitised individuals (Singh and Schwartz, 2005; Kim *et al.*, 2007). Morphologically, a T_H2 response leads to chronic inflammation, goblet cell hyperplasia and hypersecretion and fibrotic repair, which can eventually result in COPD (Liu, 2002; Tulić *et al.*, 2000). Semi-thin sections of the TD_5 dose, thought to be initiating a T_H2 response also displayed evidence of increased mucin producing cells.

It was believed that only high doses of LPS cause the activation of an adaptive immune response in normal individuals, this response would be presented as a T_H1 response. Whilst, in asthmatic/allergic (i.e. hypersensitised) individuals a T_H2 response is induced and thought to be the common response to inhaled antigens, even to low doses of LPS (Lui, 2002). Non-asthmatic individuals can also suffer

from a T_H2 type response, in tobacco smokers (Singh and Schwartz, 2005) and occupational exposure to high levels of LPS ("Monday asthma"; Liu, 2002). However, there is growing evidence that in asthmatic and allergic individuals, the immune response launched is based on the dose of LPS, with a low dose initiating a T_H2 response and a high dose a T_H1 response (Singh and Schwartz, 2005; Kim *et al.*, 2007).

Four groups of cytokines displayed interesting changes in response to LPS (Table 5.5). Group 1; ENA-78, G-CSF (up-regulated) and SCF (down-regulated) changed in both TD_5 and TD_{20} exposures after 24 hours. These could serve as general indicators/mediators of injury (at this time only in response to LPS), which persisted 24 hours after initial infection. Group 2; IL-1 α and IFN- γ displayed a decrease in expression with the TD_5 dose, but an increase after both TD_{20} doses, with a slight increase from 4 to 24 hours. These cytokines could be helpful markers in differentiating low level injury compared to severe injury. Group 3; IL-1 β displayed an increase in expression in both TD_{20} doses, which in conjunction with Group 2, could serve as possible indicators of more severe injury. Group 4; IL-5, IL-6, RANTES and TPO, were all up-regulated in the 4 hours TD_{20} dose, but no others, therefore, these cytokines have the potential as early-indicators of injury within the bronchial epithelium.

One advantage that the NHBE model possessed was the fact that the culture consisted only of the cells of the bronchial epithelium. This was advantageous since initial products from the epithelium itself, in response to pulmonary toxins, could be detected before they become masked by cytokines secreted by attracted immune cells. This may help to identify 'early-markers of injury', as well as, 'cellular targets' for new therapeutic drugs for diseases associated with an over-active immune response. The obvious disadvantage to this system is that it only accounts for the cells of the bronchial epithelium, thereby eliminating the larger, downstream response produced by inflammatory cells.

5.5.2 NHBE RESPONSE TO CADMIUM

5.5.2.1 CULTURE VIABILITY AND TRANS-EPITHELIAL ELECTRICAL RESISTANCE

The ATP assay displayed a biphasic response over the dose range, with the TD₅ dose (0.05mM) obtained from the initial decrease in culture viability. The subsequent increase in culture viability (up to 110%) was thought to be part of an early-protective response of the culture. This protective increase could be due to hypertrophy and/or an increase in glycolysis, both of which are known responses to cadmium (Shin *et al.*, 2003; Waalkes, 2003). Higher concentrations over-rode these early-protective responses, resulting in decreased culture viability, with the TD₂₀ dose obtained at 0.34mM, down to 35% of controls at 0.5mM.

The TEER of cultures to CdCl gave a dose response, with increasing concentrations resulting in decreasing TEER. There was a significant drop in TEER to 40% in response to the TD₅ dose, with the decrease in TEER after this point being more gradual, until the TD₂₀ dose. At the TD₂₀ dose, the TEER was only 2% of the control values and deemed to be negligible. Higher doses of CdCl did not have any effect on the TEER values, which remained extremely low (0 – 2%). This loss in culture integrity would suggest that CdCl was eliciting its effects on the cellular junctions. Cadmium has been shown to selectively damage cell-cell junctions in many epithelial cells, including the lung, through initial disruption of E-cadherin adherens junctions. This initial damage to epithelial adherens junctions could in time result in subsequent intracellular accumulation of cadmium which would cause the separation of tight junctions and result in further cell damage and eventually cell death (Prozialeck, 2000; Pearson and Prozialeck, 2001; Pearson *et al.*, 2003).

5.5.2.2 MORPHOLOGICAL CHANGES

Distinct morphological changes were observed between NHBE cultures treated with both the TD₅ and TD₂₀ doses of CdCl. In response to the TD₅ dose, the cultures had undergone mild degeneration, with basal cell squamation and hypertrophy, columnar cuboidalisation and dedifferentiation of goblet and Clara

cells. Numerous cells, of all types appeared to suffer from the cytotoxic effects of CdCl₂, with cell shrinkage and vacuolisation apparent throughout. As mentioned earlier, cadmium is known to affect cell-cell junctions causing the cells to detach and become rounded (Prozialeck, 2000). This effect was observed more significantly on ciliated cells at the TD₅ dose, with numerous ciliated cells balled-up and detached from the epithelium. The reason that the ciliated cells were affected first could be due to the fact that their junctions have been preferentially disrupted (which should be the same for all cell types) but may be more due to the fact that CdCl₂ is known to cause ciliostasis (Gabridge and Meccoli, 1982) and this is probably due to inhibition of mitochondrial ATP production (Kisling *et al.*, 1987). This inhibition of mitochondrial ATP production may also be the reason that Clara and goblet cells appeared to have dedifferentiated. However, a relatively small dose of cadmium is known to be highly toxic to Clara cells and may be the reason for their early disappearance (Låg *et al.*, 2005).

Semi-thin sections of NHBE cultures revealed areas of severe damage, much more than would be expected at a TD₂₀ dose. The epithelium presented as an almost confluent monolayer of cells, many of which displayed signs of cell death. SEM observations at this dose revealed that the semi-thin section was representative of an area of severe focal damage and not representative of the whole culture; hence the utility of using multiple microscope techniques. Surface analysis revealed that most of the culture had a dedifferentiated surface, with distinct lack of ciliated cells and numerous cells protruding and detaching from the surface; many of which were undergoing cell death. There were also numerous areas of severe focal damage, containing detached cells undergoing cell death and covered in a strange stringy coating, which was thought to be cell or ECM debris.

5.5.3 NHBE RESPONSE TO PARAQUAT

5.5.3.1 CULTURE VIABILITY AND TRANS-EPITHELIAL ELECTRICAL RESISTANCE

The ATP assay displayed a gradual decrease in culture viability with increasing Pq concentrations. The TD₅ dose was deemed to be 75µM and the TD₂₀ dose to

be 750 μ M. The culture viability decreased down to around 65% of controls by 1500 μ M. Pq concentrations required to have the same effect on NHBE cultures was roughly 15 fold higher than monolayer (A549) and 1.5 fold higher than BEAS-2B cell line (Song *et al.*, 2006).

TEER of cultures to different concentrations of Pq yielded a biphasic response. Initial low doses (100 and 300 μ M) resulted in TEER higher than controls and subsequent higher doses of Pq resulted in total obliteration of TEER measurements. At the TD₅ dose the projected TEER would be around 115%, whilst the TD₂₀ dose resulted in a TEER of only around 9%. Pq concentrations \geq 450 μ M resulted in negligible TEER readings. The initial increase in TEER readings was possibly part of an early-protective response with the increase likely to be caused by tightening of cellular junctions, stratification of the epithelium, mucus hypersecretion, cellular hypertrophy or hyperplasia. However, these TEER increasing factors need to balance with a slight loss in culture ATP levels. Wang and co-workers (1992) pointed to the mitochondria as the initial toxic site of Pq and Clara cells are known to be particularly sensitive to Pq toxicity (Masek and Richards, 1990; Smith *et al.*, 1990). Therefore, as long as these losses in ATP content were larger than any subsequent increase caused by the above TEER raising mechanisms, this result could be achieved.

5.5.3.2 MORPHOLOGICAL CHANGES

In response to the TD₅ dose, the cultures had changed from a pseudo-stratified epithelium to a cuboidal, stratified epithelium, with basal cells hypertrophic and squamated; all known responses to Pq (Clark *et al.*, 1966; Kelly *et al.*, 1978). There was evidence for ciliated cell loss and appearance of cytoplasmic vacuoles, which may be due to the observations of Wang and colleagues (1992), that the mitochondria were the initial site for Pq toxicity. There was an increase in secreting cells, however, due to cellular cuboidalisation, it was hard to determine if these were of goblet or Clara phenotype; CC10 and PAS staining (Chapter 4) could confirm this. Large inter-cellular gaps along with cytoplasmic vacuoles indicated that there was a degree of cell death. All of the morphological

observations could account for an increase in TEER and slight decrease in culture viability at this dose.

There were significant morphological changes in response to the TD₂₀ dose, with the cuboidal, stratified epithelium becoming a cuboidal monolayer, as observed in mice by Popenoe (1979). The surface revealed some dedifferentiation, loss of microvilli and some remaining ciliated cells. There were also regions of disrupted epithelium, cellular detachment and blebbing of apoptotic/necrotic cells (Mullinger and Johnson, 1976; Wyllie *et al.*, 1980). This could account for the drop in TEER values to barely negligible levels.

5.5.4 NHBE RESPONSE TO AMIODARONE

5.5.4.1 CULTURE VIABILITY AND TRANS-EPITHELIAL ELECTRICAL RESISTANCE

The ATP assay produced a biphasic response over the dose range, with the TD₅ dose (300µg/ml) obtained from the initial decrease in culture viability. The subsequent increase only returned to control values and not above (at 500µg/ml), and was thought to be a slight early-protective response. As this protective increase did not increase culture viability above control values, was unlikely to be caused by extensive hypertrophy or hyperplasia. Although, they could be present in a subtle way, with an increase in glycolysis likely. Higher concentrations overrode these responses, resulting in decreased culture viability, with the TD₂₀ dose obtained at 850µg/ml and further culture demise to 75% (1,000µg/ml).

Culture integrity (TEER), like the ATP profile displayed a slight biphasic response, with TEER readings not rising above controls. At 200µg/ml, the TEER values had decreased to 75%, yet by the TD₅ dose (300µg/ml) the TEER readings had returned to control values, that may be due to the tightening of cellular junctions. Subsequent TEER readings gradually declined as the concentration of Am increased to 700µg/ml, but, above this, there was a much sharper decrease in TEER measurements to 50% at 1,00µg/ml. The TEER and therefore, junctional and epithelial integrity was not as severely affected in response to Am as it was to the other CPTs. This may indicate that Am does not specifically affect the cellular

junctions and probably affected the basal cells of the bronchial epithelium more severely without causing too much disruption to the surface barrier.

5.5.4.2 MORPHOLOGICAL CHANGES

There were more significant morphological changes observed in semi-thin sections than from the surface topography. The TD₅ dosed sections revealed a degree of dedifferentiation, loss of cilia and basal cell squamation and hypertrophy. Surface analysis revealed no significant change from control cultures, indicating that the epithelial surface and apical junctions were intact (correlating with TEER data).

The TD₂₀ dose revealed further degeneration and dedifferentiation of the epithelium. Basal cells appeared to be the most severely affected, with evidence of basophilia (Wyllie *et al.*, 1980). There was also evidence of numerous darkly stained intra-cytoplasmic inclusions, which are known to accumulate in bronchial epithelial cells in response to Am (Colgan and Simon, 1984). Surface topography revealed some disruption of the epithelial barrier, with a few holes present, but on the whole the surface remained relatively normal. Higher magnification revealed surface dedifferentiation and cells were possibly regenerating, with the presence of what may be immature cilia and/or microvilli.

5.5.5 NHBE RESPONSE TO CIGARETTE SMOKE

5.5.5.1 CULTURE VIABILITY AND TRANS-EPITHELIAL ELECTRICAL RESISTANCE

Culture viability was decreased in response to both concentrations 4 hours after recovery, with 82% for 1:50-4h and 54% for 1:20-4h. In addition to these two dilutions of CS, a 1:30 dilution was also utilised and all three monitored 24 hours after exposure. The viability of NHBE cultures 24 hours after exposure were severely damaged, with 60% for 1:50-24h, 32% for 1:30-24h and only 10% for 1:20-24h. This response appeared severe, however, cultures did undergo continuous exposure to CS for 30 minutes, which was undertaken in order to produce a long-term effect of CS exposure. CS and its constituents are known to

cause apoptosis and necrosis of bronchial epithelial cells (Domagala-Kulwik, 2008; Izard and Libermann, 1978; Parsanejad *et al.*, 2008).

Early, low-dose response (1:50-4h), resulted in increased TEER (~125%), even though the culture viability was reduced almost to a TD₂₀. This again demonstrated the NHBE models early-protective response to toxicants and would be indicative of a tightening epithelial tight junctions and/or an increase in glycolysis along with specific damage to basal cells. This protective mechanism was over-rode in response to the higher dose (54% at 1:20-4h), as well as 24 hours later (25% at 1:50-24h). Both the 1:30-24h and 1:20-24h dilutions resulted in negligible TEER readings (both around 5% of controls), suggesting that epithelial integrity had been compromised. The decrease in TEER of the bronchial epithelium is a known response to CS, with loss of desmosomes and a decrease in ZO-1 and Claudin-1 genes known to occur (Frasca *et al.*, 1968; Glader *et al.*, 2006; Maunders *et al.*, 2007).

5.5.5.2 MORPHOLOGICAL CHANGES

Significant morphological changes were observed in response to CS. In response to the 1:50-4h dose the most striking change was exhibited in the total separation of the basal cells from the columnar cells and their detachment from the insert membrane. With loss of desmosomes known to occur in response to CS (Frasca *et al.*, 1968), this had been exaggerated due to damage caused during tissue processing. There was evidence of dedifferentiation, cilia loss, mucin hypersecretion, basal cell hypertrophy, as well as cell death; all known in response to CS (Domagala-Kulwick, 2008; Parsanejad *et al.*, 2008; van der Toorn *et al.*, 2007). Surface topography revealed loss of ciliated cells and dedifferentiation, with most cells covered in microvilli only. There was an increase in damage by the 1:20-4h concentration, with the epithelium regressing to a monolayer phenotype, with numerous inter- and intra-cellular gaps/vacuoles, indicative of cell death (Wyllie *et al.*, 1980). SEM images displayed evidence of focal damage in response to the 1:20-4h dose. Areas of minor damage appeared similar to the lower dose, with surface dedifferentiation apparent, fewer ciliated cells and there appeared to be loss of the microvillus covering. The areas of more

severe damage displayed detached, undifferentiated cells, with the insert membrane visible in places.

Cultures exposed to 1:50-24h CS displayed degeneration, dedifferentiation, cell death and basal cell hypertrophy. The culture surface was pitted with cells appeared to have sunken, probably due to a significant amount of cell loss (40% loss). Cilia seemed to be retracting into the cell itself, which may infer the initiation of transdifferentiation of ciliated cells (Park *et al.*, 2006). Additionally, some cilia appeared to have clumped together, which may be part of the re-absorption of cilia or may be due to the combination of ciliostasis (Izard and Libermann, 1978; Romet-Haddad *et al.*, 1992) and acidic mucus (Rogers and Jeffery, 1986; Izard and Libermann, 1978). Toluidine blue sections of the 1:30-24h dose revealed extensive destruction of the epithelium, with a monolayer of undifferentiated, basophilic, dying cells remaining. SEM analysis confirmed these observations with the presence of undifferentiated cells and numerous cells undergoing cell death and an abundance of cellular debris (Mullinger and Johnson, 1976). The ATP reading of cultures was 10% of control values, revealed very few remaining cells at the 1:20-24h exposure. This was highlighted in semi-thin sections where no cells were discovered in any sections. This was confirmed by SEM with most of the insert membrane devoid of cells. There were only a few areas where solitary or small sheets of cells remained.

5.6 CONCLUSIONS

The NHBE model was exposed to a number of CPT in order to elucidate mechanisms of injury within the NHBE construct. In this manner, the model could not only be validated in terms of response to each toxicant as comparable to the *in vivo* situation, but, further analysis may elucidate cell/bronchial specific responses to each toxicant. This, in turn, may provide new targets for pulmonary drugs. A select panel of 5 toxins were chosen for their different toxic properties, in order to demonstrate a more complete view of defence, injury and repair mechanisms within the NHBE model.

Naturally, the NHBE model displayed similarities in its response to CPTs, as there were a finite number of changes possible in such a closed or 'static' system of defined phenotype. However, in spite of this, the model appeared to reproduce toxicant-specific responses, often characteristic of the changes previously observed *in vivo* and *in vitro*.

Many of the compounds elicited an early-protective response with either a biphasic response of the ATP assay, TEER measurements or both. This indicated that in response to lower doses of some toxicants, the NHBE model can mount a protective response, which could in the future, be utilised to produce a 'disease' phenotype for testing 'new' pulmonary drugs.

The morphologic changes associated with CPT challenge involved numerous general responses (mucin hypersecretion, dedifferentiation, basal cell squamation and hypertrophy), as well as some toxicant specific alterations (e.g. cuboidal, stratification of the epithelium in response to Pq). Indicating that the NHBE model was relatively sensitive to different challenges, highlighting its potential as an *in vitro* model reflective of *in vivo* toxicity.

The cytokine expression profiles for LPS enabled a brief glimpse into the initial cytokine responses of the bronchial epithelium without the influence of other immune cells. This information may, in turn, permit the identification of markers of injury and/or target sites for pulmonary drugs.

The exposure of the NHBE model to a selection of CPTs done in this chapter revealed its potential as an investigative system in respiratory toxicology and pharmacology.

CHAPTER 6:

BLIND-EXPOSURE OF NHBE MODEL TO AZ COMPOUNDS

6.1 INTRODUCTION

Exposure of the NHBE model to CPTs (Chapter 5) was performed to ensure that the model responded in the appropriate manner to these established toxicants. Further validation of the NHBE model as a viable *in vitro* alternative to animal testing, could be achieved by conducting blind-exposure to a number of AZ candidate respiratory compounds. The irritancy response was then compared to that obtained from AZ *in vivo* (rat), in-house testing and physicochemical data (supplied by AZ).

Biochemical (ATP and Bradford assays and TEER) and morphological (LM) analysis of irritancy was performed after blind-exposure of the NHBE model to AZ candidate respiratory compounds. Comparison of the *in vitro* irritancy data with corresponding *in vivo* data would be utilised to validate the NHBE model as a robust predictor of *in vivo* irritancy in respiratory toxicology and pharmacology, enabling Reduction, Refinement and Replacement of animals in this sense (3Rs principles: NC3R, 2010).

Certain trends in the ability of compounds to cause irritancy may be elucidated from their physicochemical properties. In 1997, Lipinski and co-workers analysed numerous orally administered drugs approved into Phase II trials in order to determine certain physicochemical properties that would suggest poor absorption and permeability. They devised the 'rule of 5', which stated that, poor absorption or permeability was more likely when: molecular weight >500Da; hydrogen bond donors >5; hydrogen bond acceptors >10; an octanol-water partition coefficient (clogP)>5. The 'Lipinski Score' denotes how many of these rules have been breached.

COPD currently affects an estimated 210 million people worldwide (WHO, 2009) and current, available treatments have only a limited effect on inflammation and do not treat chronic symptoms or disease progression. Therefore, the AZ candidate respiratory drugs developed and tested in this chapter are inhibitors of three key pathways involved in driving COPD; p38, kappa-B kinase-2 (IKK2) and phosphodiesterase-4 (PDE4) (Barnes, 2006; Seemungal *et al.*, 2008).

The p38 pathway can be activated in the COPD lung by several stimuli, including tobacco smoke, infection and oxidative stress (Newton and Holden, 2006; Renda *et al.*, 2008). Activation of the p38 pathway within the lung can cause inflammatory cell migration and activation, as well as, pro-inflammatory mediator release. All of which have been implicated in the development and exacerbation of COPD (Chung, 2001).

The inhibition of the IKK2 pathway is expected to reduce mucus secretion, cell death, acidic conditions and influx and activation of neutrophils and mononuclear cells. All of which are major pathological consequences of COPD, contributing to disease severity and progression (Barnes, 2006).

PDE4, a cAMP specific PDE, located predominantly within inflammatory cells (neutrophils, macrophages and lymphocytes), fibroblasts and airway smooth muscle, which are present in COPD airways (Boswell-Smith and Spina, 2007). All current oral PDE4 inhibitors are associated with target-related side-effects. The development of inhaled PDE4 inhibitors are hoped to reduce systemic exposure and hence, side-effects of oral PDE4 inhibitors (Boswell-Smith and Spina, 2007).

6.2 MATERIALS AND STOCK SOLUTIONS

6.2.1 MATERIALS

MATERIALS	SUPPLIER
AZ1 – 15 Compounds; powder AZ25 – 37 Compounds; powder	AstraZeneca R&D, Loughborough, UK

Table 6.1 Table of materials used and their suppliers.

6.2.2 STOCK SOLUTIONS

SOLUTIONS	SUPPLIER
Dimethyl Sulfoxide (DMSO)	Sigma, Dorset, UK

Table 6.2 Table of stock solutions used and their suppliers.

6.3 METHODS

6.3.1 DOSING

NHBE cells grown at an ALI (Section 2.3.1) were dosed when cultures were between Days 27 – 33. TEERs were checked prior to dosing to ensure that they were above $1,500\Omega$ ($\sim 4,550\Omega\cdot\text{cm}^2$). All AZ compounds (dry powder) were dissolved in dimethyl sulfoxide (DMSO) overnight (dark, RT) on a shaker, to give a 100mM stock solution before further dilution (in ALI media) and dosing.

AZ1 – 10 were the initial compounds tested and stock solutions (100 μM in DMSO) were diluted in ALI media to produce the dose range: 1, 3, 10, 30 and 100 μM in 0.1% DMSO. DMSO (0.1%) was used as the control solution. Each dose (50 μl) was applied apically to NHBE cultures ($n = 3$). After incubation with the AZ compound or 0.1% DMSO (24 hours), the TEER was recorded on each NHBE culture insert (Section 6.3.2) and the PBS used in the TEER reading kept for future analysis of protein content (Bradford assay; Section 6.3.4). That same insert was then used to assess culture viability (ATP assay; Section 6.3.3). All doses ($n = 2$) were assessed for morphological changes (Section 6.3.5). Following this, it was deemed that this dose range was too small and AZ1 – 10 were all re-dosed at 400 μM in 0.4% DMSO and ALI media (0.4% DMSO used as control) and assessed for culture viability and TEER.

Stock solutions (100mM in DMSO) of AZ11 – 15 were diluted in ALI media to produce the dose range: 10, 30, 100 μM in 0.1% DMSO (0.1% DMSO used as control); 400 μM in 0.4% DMSO (0.4% DMSO used as control); 800 μM in 0.8% DMSO (0.8% DMSO used as control); 1000 μM in 1% DMSO (1% DMSO used as control). Each dose (50 μl) was applied apically to NHBE cultures ($n = 3$). After incubation with AZ compound or relevant DMSO control (24 hours), the TEER was recorded on each NHBE culture insert (Section 6.3.2) and the PBS used in the TEER reading kept for future analysis on protein content (Section 6.3.4). That same insert was then used to assess culture viability (Section 6.3.3). Cultures treated with 10, 100 and 400 μM doses of each AZ compound ($n = 2$) were assessed for morphological changes (Section 6.3.5).

Stock solutions (100mM in DMSO) of AZ25 – 37 were diluted in ALI media to produce the dose range: 100µM in 0.1% DMSO (0.1% DMSO used as control); 400µM in 0.4% DMSO (0.4% DMSO used as control); 800µM in 0.8% DMSO (0.8% DMSO used as control). Each dose (50µl) was applied apically to NHBE cultures ($n = 3$). After incubation with AZ compound or relevant DMSO control (24 hours), the TEER was recorded (Section 6.3.2) and the PBS used in the TEER reading kept for future analysis on protein content (Section 6.3.4). That same insert was then used to assess culture viability (Section 6.3.3). There was not enough culture inserts from that donor to do the corresponding morphological assessment, therefore, this was not done with AZ25 – 37.

All culture viability (ATP assay), TEER and apical protein content (Bradford assay) was presented as a percentage of the relevant controls. Irritancy was generally revealed at 100µM or 400µM (if less irritant), based on this these were the two concentrations focused on in this chapter.

6.3.2 TRANS-EPITHELIAL ELECTRICAL RESISTANCE

The TEER of NHBE cultures, immediately prior to- and 24 hours post-dosing was established using the method previously described (Section 2.3.3).

6.3.3 ATP ASSAY

NHBE inserts that had been dosed and had their TEER measured were then placed in an empty well (24 well-plate) prior to performing the ATP assay, method previously described (Section 5.3.3).

6.3.4 BRADFORD ASSAY

The PBS (150µl) added apically to the dosed cultures for measuring the TEER was removed and assessed for protein content via the Bradford assay, method previously described (Section 2.3.4).

6.3.5 LIGHT MICROSCOPY: TOLUIDINE BLUE

Inserts dosed with AZ1, 3 – 6 compounds and carrier solution (DMSO controls) for 24 hours were prepared for semi-thin sectioning and staining with toluidine blue and images taken (Section 3.3.1). NHBE inserts dosed with AZ2, 7 – 15 compounds and carrier solutions (DMSO controls) for 24 hours were prepared for semi-thin sectioning as before (Section 3.3.1.1 – 3.3.1.5), with sectioning, toluidine blue staining and images taken by Dr. Sarah Bolton (AstraZeneca R&D, Loughborough, UK). Images were captured using the Zeiss Axioskop 2 microscope (Carl Zeiss Ltd., Hertfordshire, UK), with a Leica DFC320 camera, using Leica DFC Twain Acquire software (Leica Ltd., Milton Keynes, UK) and Adobe Photoshop CS3 (Adobe Systems Incorporated, 2010).

6.3.6 CORRELATION OF *IN VITRO* DATA WITH *IN VIVO* STUDIES

Compound information and correlative *in vivo* data (where possible) was provided by Dr. Victor Oreffo (AstraZeneca R&D, Loughborough, UK). Due to the confidential nature of the work *in vivo* dosing methods, morphology analysis and concentrations of compounds used were not released.

6.4 RESULTS

6.4.1 PHYSICOCHEMICAL PROPERTIES OF THE AZ COMPOUNDS

Physicochemical properties of the AZ candidate respiratory compounds were provided by the industrial sponsor AZ (Table 6.3) after completion and analysis of testing in the NHBE model. These properties were believed to influence the irritancy potential and as such, were indicative of drug absorption/permeability *in vivo* (Hughes *et al.*, 2008; Lipinski *et al.*, 1997; Tronde *et al.*, 2003; Waring, 2009).

GROUP ^a	AZ ^b	ION CLASS ^c	MWT ^d	PSA ^e	cLogP ^f	LogD ^g	LIPINSKI SCORE ^h
p38	1	B	527.67	79	6.87	5.34	2
	2	B	577.72	85	7.46	4.92	2
	3	N	340.33	43	3.08	3.60	0
	4	B	572.70	94	3.10	3.00	1
	5	B	592.14	111	4.10	1.21	1
	6	B	431.54	64	3.16	-0.01	0
IKK2	7	ND	ND	ND	ND	ND	ND
	8	B	346.41	130	1.26	-0.56	1
	9	B	346.41	130	1.26	-0.56	1
	10	B	360.44	130	1.28	-0.31	1
PDE4	11	B	681.83	107	6.36	1.15	2
	12	B	703.82	106	6.03	1.38	3
	13	B	690.75	107	6.55	0.68	3
	14	ND	ND	ND	ND	ND	ND
	15	B	690.75	107	6.55	0.68	3
	25	B	681.85	115	5.59	3.41	2
	26	B	707.89	112	6.56	3.09	2
	27	B	755.96	121	5.99	3.15	3
	28	Z	764.94	134	7.16	4.14	3
	29	B	693.86	101	4.95	3.49	1
	30	B	656.82	111	5.87	3.01	2
	31	B	681.85	115	5.59	3.41	2
	32	B	704.85	125	5.60	3.09	3
	33	B	700.88	134	5.20	3.14	2
	34	N	518.59	136	3.80	2.64	1
	35	A	499.49	108	5.27	5.10	1
	36	B	667.83	115	5.07	2.97	2
37	B	477.51	76	5.87	2.68	1	

Table 6.3 Physicochemical properties of the AZ compounds tested. ^a Pathway targeted by the compound. ^b AZ candidate drug number. ^c Ion class of the molecule; A = acid, B = base, N = neutral, Z = zwitterion. ^d Molecular weight (Da), red text = >500Da. ^e Polar Surface Area (PSA; Å²). ^f cLogP, red text = >5. ^g ACD LogD at pH 7.4. ^h Number of violations of Lipinski's rule of 5. ND = not determined.

6.4.2 BIOCHEMICAL IRRITANCY OF AZ COMPOUNDS

NHBE cultures were exposed to a variety of AZ compounds at many different concentrations. The whole panel of AZ compounds were exposed to both the 100µM and 400µM doses, with biochemical irritancy (*in vitro*) revealed at these concentrations, the results were therefore focused on these concentrations.

The culture viability (ATP assay), TEER and apical protein content (Bradford assay) were all displayed as a percentage of the relevant controls. Generally, the AZ compounds displayed 3 main responses at this biochemical level: 1) no irritancy; 2) possible irritancy; and 3) irritancy. These three main responses have been demonstrated graphically with AZ14, AZ9 and AZ28, respectively (Figure 6.1).

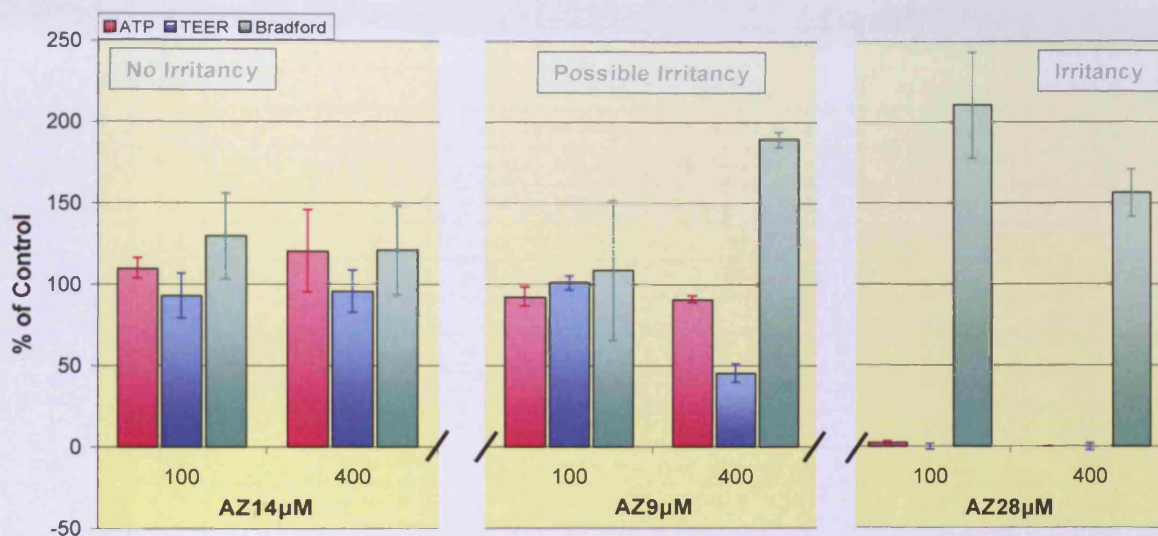


Figure 6.1 Graph displaying the three main biochemical responses of the NHBE culture to AZ compounds 24 hours after treatment. AZ14; no irritancy. AZ9; possible irritancy. AZ28; irritancy. ATP (■), TEER (■) and Bradford (■) values displayed as percentage of relevant control values. Standard Deviation was shown for ATP (I), TEER (I) and Bradford (I), $n = 3$.

The biochemical response (ATP assay, TEER and apical protein) of NHBE cultures to AZ compounds was graded and biochemical irritancy decided. This was then compared to *in vivo* morphological irritancy (Table 6.4). Morphological irritancy (*in vivo*) was given post-*in vitro* dosing and analysis. Changes to ATP and TEER values, as a percentage of controls were graded as follows: +/- = change of 20 – 49%; ++/-- = change of 50 – 79%; +++/--- = change $\geq 80\%$. Apical protein content often increased above 100% of control values and were therefore graded: +/- = change of 40 – 69%; ++/-- = change of 70 – 79%; +++/--- = change $\geq 100\%$.

GROUP ^a	AZ ^b	ATP ^c		TEER ^c		BRADFORD ^d		IRRITANT?	
		100µM	400µM	100µM	400µM	100µM	400µM	IN VITRO ^e	IN VIVO ^f
p38	1				--			No/POSS	MILD
	2		-		+	+		No/POSS	YES
	3			-	-	+		No/POSS	YES
	4		-	-	+			No/POSS	YES
	5	-	-	-	--	+		POSS	NO
	6				+++			No/POSS	NO
IKK2	7	-	-	++	-		+	POSS	ND
	8		-					No/POSS	NO
	9				--		++	POSS	YES
	10			+	+++	+		POSS	YES
PDE4	11	+	----	-	----	++	+++	YES	YES
	12		+	-	--	++		YES*	YES
	13	+	----	--	----	+++	+++	YES	YES
	14		+		-			No/POSS	ND
	15	-	----	--	----		++	YES	YES
	25	-	----		----	++	+++	YES	POSS [†]
	26	-	----	++	----	++	+++	YES	ND
	27	-	----		----		+++	YES	YES
	28	----	----	----	----	+++	+	YES	NO
	29	-	----		----	++	+++	YES	ND
	30	-	----		----	++	++	YES	YES
	31		----	+	----		+++	YES	ND
	32		----		----		+++	YES	ND
	33	-	----	-	----		+++	YES	ND
	34			-	-			No/POSS	NO
	35				-			No/POSS	NO
	36	-	----		----	+++	+++	YES	ND
37		-	--	--			YES*	YES	

Table 6.4 Biochemical response of the NHBE culture to AZ compounds 24 hours after treatment.

^a Pathway targeted by the compound. ^b AZ candidate drug number. ^c Change in ATP assay or TEER compared to controls: +/- = change of 20 – 49%; +/+- = change of 50 – 79%; +++/--- = change ≥80%. ^d Change in apical protein content compared to controls: +/- = change of 40 – 69%; +/+- = change of 70 – 99%; +++/--- = change ≥100%. ^e Irritancy based on biochemistry *in vitro* (NHBE) ^f Irritancy based on morphology *in vivo*. Poss = possibly, ND = not determined. * AZ compound was highly toxic at 800µM. [†] Inflammatory response only.

Biochemical irritancy analysis revealed that 10 of the AZ compounds (all targeting the PDE4 pathway), deemed irritant *in vitro* had corresponding *in vivo* data. Out of these 10, 7 were irritant, 1 was possibly irritant and 2 displayed no irritancy *in vivo* (morphological assessment) (Table 6.4).

6.4.3 MORPHOLOGICAL ANALYSIS OF AZ COMPOUNDS

Due to blind-testing and large numbers of AZ compounds, morphological analysis was only performed on doses up to, 100 μ M for AZ1 – 10, 400 μ M for AZ10 – 15 and none on AZ25 – 37.

Morphologic analysis of NHBE cultures treated with various AZ compounds would enable distinction between compounds that weren't deemed irritant at the biochemical level. The four main morphological responses to AZ compounds were: 1) no irritancy; 2) no/possible irritancy at the biochemical level, which revealed irritancy at the morphological level; 3) irritant *in vitro* but not irritant *in vivo*; 4) irritant at both biochemical and morphological levels (Figure 6.2).

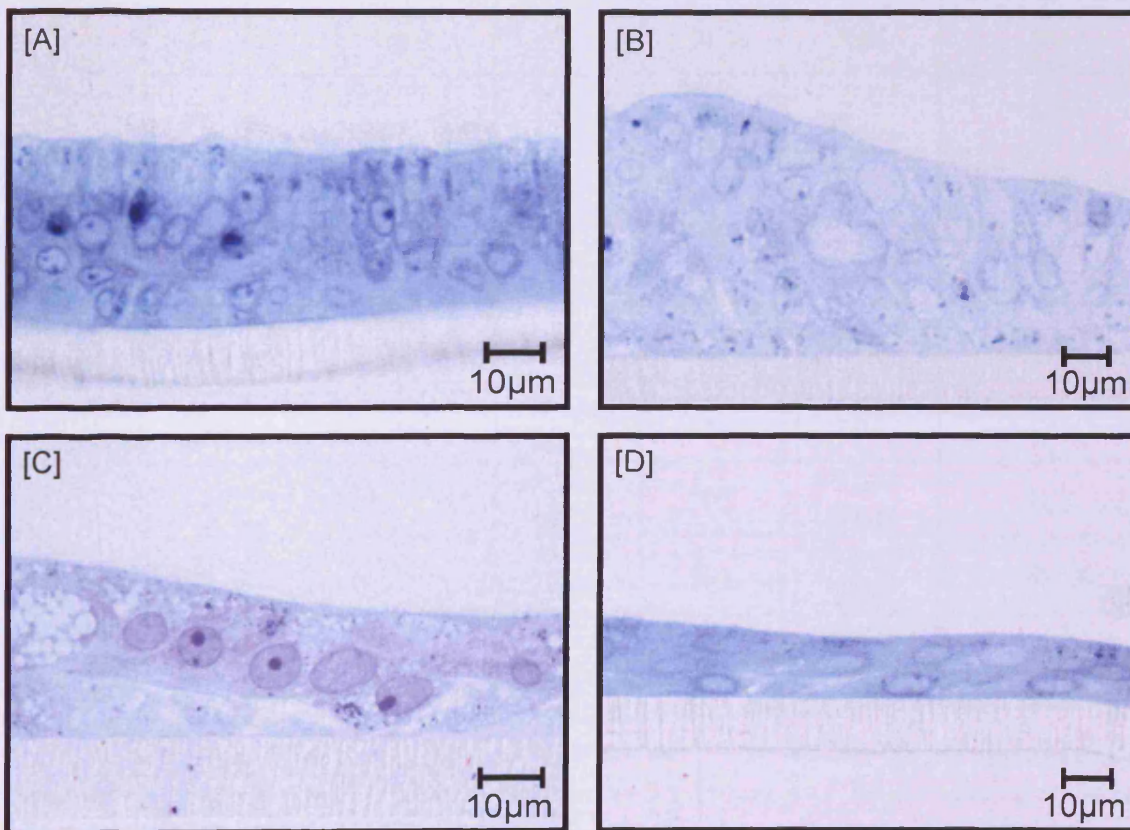


Figure 6.2 LM images of NHBE main responses to AZ compounds, stained with toluidine blue. [A] AZ compound deemed not irritant (biochemically), confirmed morphologically; NHBE culture treated with AZ8 (100 μ M). [B] Not/possible irritant AZ compound (biochemically), mild irritant morphologically; NHBE culture treated with AZ10 (100 μ M). [C] AZ compound deemed not irritant *in vivo*, but irritant morphologically *in vitro*; NHBE culture treated with AZ1 (100 μ M). [D] Irritant AZ compound (biochemically), confirmed morphologically; NHBE culture treated with AZ13 (100 μ M).

AZ compounds that were deemed not irritant at the biochemical level (Table 6.4). underwent morphological analysis in order to confirm/dispel irritancy potential *in vitro*. This was compared to *in vivo* irritancy data (morphology) and correlations determined (Table 6.5).

GROUP ^a	AZ ^b	BIOCHEMICAL IRRITANT <i>IN VITRO</i> ^c	MORPHOLOGY – IRRITANT? ^d		IRRITANT <i>IN VITRO</i>	<i>IN VIVO</i> – <i>IN VITRO</i> CORRELATION
			<i>IN VITRO</i>	<i>IN VIVO</i>		
p38	1	No/ POSS	YES/ MILD	MILD	YES/ MILD	YES
	2	No/ POSS	NO*	YES	POSS	POSS
	3	No/ POSS	NO*	YES	POSS	POSS
	4	No/ POSS	YES/ MILD	YES	YES/ MILD	YES
	5	POSS	YES	NO	YES	NO
	6	No/ POSS	YES/ MILD	NO	YES/ MILD	NO
IKK2	7	POSS	NO*	ND	POSS	ND
	8	No	NO*	No	POSS	POSS
	9	POSS	NO*	YES [†]	POSS	POSS
	10	POSS	YES/ MILD*	YES	YES	YES
PDE4	14	No	YES/ MILD*	ND	YES/ MILD	ND
	34	No	ND	No	POSS/ NO [#]	POSS
	35	No	ND	No	POSS/ NO [#]	POSS

Table 6.5 Table correlating *in vitro* and *in vivo* responses to AZ compounds deemed not/possible irritant at the biochemical level ^a Pathway targeted by the compound. ^b AZ candidate drug number. ^c Biochemical irritancy, *in vitro*, determined from Table 6.5. ^d Compound irritancy based on morphology. Poss = possibly, ND = not determined. * = Morphology only done at 100µM, where compound was not biochemically toxic. [†] = Irritant via an inflammatory response. [#] Not deemed toxic at 800µM.

Irritancy analysis of AZ compounds that were deemed not/possibly irritant biochemically *in vitro* were checked for morphological signs of irritancy. From

these 11 had corresponding *in vitro* and *in vivo* data; 3 correlated, 2 did not and 6 possibly did. Out of the 6 possible irritants, 3 were irritant and 3 displayed no irritancy *in vivo*.

6.5 DISCUSSION

The main purpose of exposing the NHBE model to unknown AZ compounds was to validate the model's efficiency at predicting irritancy outcomes *in vitro* which maybe predictive of the *in vivo* situation. Additionally, comparison of physicochemical properties of the AZ compounds with their irritancy potential *in vitro* and *in vivo* may reveal those characteristics which should be avoided or targeted when designing new respiratory drugs. The above was not as easily determined due to the nature of the work, that is, with the dose ranges and selection of compounds/doses to be used for morphological work often controlled by the industrial sponsor (AZ).

The initial concentration range utilised failed to highlight possible compound irritancy, until a 400µM spot-test ($n = 3$) with biochemical characterisation undertaken. This higher dose proved to be a more accurate predictor of biochemical irritancy. Following this, the dose range for subsequent compounds (AZ11 – 15, 25 – 37) was scaled-up along with corresponding morphology. This resulted in gaps in the data set, which may have been useful and should therefore, be incorporated into any future experiments. Additional gaps in the data set were due to not all of the AZ compounds tested *in vitro* being tested *in vivo* or their physicochemical properties determined.

Biochemical irritancy testing revealed that 15 AZ compounds (all targeting the PDE4 pathway of which there were 17) were deemed irritant in the NHBE system. The physicochemical properties of the PDE4 inhibitor group were mainly basic, of high molecular weight, lipophilic and had Lipinski scores of 2 or 3. Based on these parameters it was unsurprising that many of them were irritant. From the 15 irritant PDE4 compounds, 10 had been tested *in vivo*, of which, 7 were considered irritant *in vivo*. One of which displayed no irritancy with a nasal spot-test, but showed evidence of an inflammatory response in the rat. The other

compound (AZ28) was determined as not irritant *in vivo* (rat), however, from the biochemical data (*in vitro*) collected, AZ28 was the most irritant compound tested. Unfortunately, no morphological evaluation was performed on this compound in the NHBE system. The NHBE response to AZ28 may either reflect the true response (i.e. human *in vivo*) or it may represent a false-positive. Based on physicochemical properties alone the likely-hood of AZ28 being a poor candidate, promiscuous drug, was high (Leeson and Springthorpe, 2007; Lipinski *et al.*, 1997; Ritchie *et al.*, 2009). AZ28 is a zwitterion of high molecular weight (764.94Da), high clogP (7.16), logD (4.14) and having a Lipinski score of 3. Further continuation of this drug into dog and human trials may reveal the correct response and possible validation of the NHBE system to detect irritant compounds prior to *in vivo* work being implemented. Numerous drugs are known to fail at Phase II and III clinical trials due to preliminary testing being undertaken in inappropriate systems (Kola and Landis, 2004), the possibility that AZ28 fails at these stages is likely based on irritancy in the NHBE system and its physicochemical properties. Equally, the deduction of AZ28 as an irritant may be a false-positive due to limitations in the *in vitro* system. These limitations include: 1) bronchial epithelium only; 2) ballistic properties of the aerosol and particle size distribution lost; 3) no inflammatory cells and therefore, phagocytosis; and 4) possible dissolution in the lung lining fluid *in vivo*.

All compounds that were classed as being irritant, at the biochemical level (NHBE), displayed evidence of irritancy in corresponding morphological analysis (where undertaken). Therefore, it was decided to look closer at the morphology of those AZ compounds that were deemed not/possible irritants at the biochemical level. This was done not only to gain a more detailed view of what changes may have occurred but to ensure that the biochemical response did not produce false-negatives. This could occur if the compound caused a multicellular event (i.e. hypertrophy or hyperplasia) within the NHBE model.

From the 13 AZ compounds that suggested no/possible irritancy at the biochemical level, 11 had corresponding *in vitro* and *in vivo* data; 3 correlated, 2 did not and 6 possibly did. AZ5 and AZ6 (p38 inhibitors) displayed irritancy in the NHBE system but not *in vivo* (rat only); further investigation would confirm the

true response. AZ5 was not phospholipidotic, but basic, with a high molecular weight (592.14Da) and a Lipinski score of 1. It was therefore probable that this was a false-positive result by the NHBE system. AZ6 had a Lipinski score of 0, indicating that it was unlikely to be an irritant. However, according to Hughes and colleagues (2008) any compound which had a clogP >3 and a polar surface area (PSA) <75Å² (as AZ6 is) was 2.5 times more likely to be toxic than clean.

Of the 6 compounds that were possible irritants, 3 were deemed irritant and 3 not *in vivo*. It would be expected that the 3 AZ compounds that were deemed irritant *in vivo* (AZ2, 3 and 9) would demonstrate irritancy *in vitro*, with morphology undertaken at the 400µM doses of these compounds. The only reason they were deemed 'possible' irritants, as opposed to irritants, was due to the fact that morphological analysis, at 100µM displayed no irritancy. However, all of these compounds did not display biochemical evidence of irritancy until 400µM and morphological analysis at this dose may clarify whether these compounds were irritant *in vitro*.

The 3 compounds that were not irritant *in vivo* were AZ8 (IKK2 parent compound), 35 (PDE4) and 35 (PDE4). AZ8 did not display biochemical irritancy until 400µM, where no corresponding morphology was undertaken, further investigation would be required to determine its true irritancy. AZ34 and AZ35 did not have any *in vitro* morphology information (due to lack of inserts at the time), but did not display biochemical signs of irritancy even at 800µM. This suggested that they were not irritants *in vitro*, but this was not confirmed. Both of these compounds are currently in Phase II clinical trials and as yet, have not displayed evidence of irritancy. Both of these compounds were from the PDE4 inhibitor group, but displayed some physicochemical differences to the other compounds in this group, which were mainly basic, of high molecular weight and phospholipidotic. AZ34 was a neutral molecule, with a slightly high molecular weight (518.59Da), but was not phospholipidotic, whilst AZ35 was an acidic molecule, that was slightly phospholipidotic (clogP: 5.27 and logD(7.4): 5.10). This indicated that when searching for a candidate drug that inhibits PDE4 a neutral or acidic molecule with a low Lipinski score (both = 1) may provide the best candidate.

In the development of IKK2 candidate compounds, AZ8 was optimised for further evaluation. In the process of optimising the compound for dry powder inhalation studies, a salt form was required to achieve compound delivery as a dry powder. When AZ8 delivered as a succinate salt, was subsequently shown to be irritant *in vivo*. *In vitro* analysis of AZ7 (succinic acid) indicated the salt itself was an irritant to the epithelium. AZ8, the parent compound, was found not to be irritant to NHBE cells *in vitro* in agreement with findings observed *in vivo*. An alternative compound, AZ10, was also evaluated, however, the parent compound proved to be both irritant *in vivo* and *in vitro*. The limited IKK2 compound set evaluated, demonstrated that the order of cytotoxic injury to the ALI culture agreed with the severity of irritancy seen *in vivo*. The irritancy severity could be ranked as follows: IKK2 drug1 succinate succinic acid (AZ79)>>IKK2 drug 2 (AZ10)>>IKK2 drug1 parent (AZ8) > control (AZ1).

With respect to the p38 group (AZ1 – 6) and IKK2 group (AZ7 – 10) of compounds, an insufficient compound set was available to ascertain clear physicochemical properties that were associated with irritancy. A larger screen of compounds with an increase in the variety of the physicochemical parameters assessed may reveal more promising candidate respiratory drugs with an indication of which parameters confer irritancy with these targets.

6.6 CONCLUSIONS

Correlation between the NHBE *in vitro* model and *in vivo* rat model, based on this work, where a correlation was a clear yes or no was 76.9%. If all the possible correlations did correspond this would increase to 85%. However, this is only based on a limited study utilising a small set of compounds and more analysis would be required to confirm the accuracy of the NHBE model at predicting the *in vivo* rat response and if this has any correlation with the human *in vivo* response.

There is a high attrition rate of new compounds at Phase II and III of clinical trials (Kola and Landis, 2004). It is many researchers belief that this is mainly due to inadequate or inappropriate screening prior to these phases (Matsuda *et al.*,

2009; May *et al.*, 2009). One issue is that the animal system tested is not an accurate enough reflection of the human *in vivo* situation; another is due to toxicity to organs/systems not directly associated with the compound (off-target toxicity). In light of this, the NHBE culture system may be utilised as part of candidate respiratory drug screening protocols. However, as the candidate respiratory drugs utilised in this chapter (with the exception of AZ34 and 35) have not been tested in humans, the accuracy of the NHBE *in vitro* model to determine human *in vivo* irritancy has not been established. Continuation of the comparison of candidate respiratory drugs throughout their pre-clinical and clinical screening processes with the NHBE model may shed light on the accuracy of the *in vitro* model at predicting human *in vivo* outcomes. For instance, the monitoring of compounds such as AZ28 (highly irritant *in vitro* [NHBE], but not *in vivo* [rat]), during future clinical trials, may provide us with the answer to whether the NHBE model could determine human respiratory irritancy *in vivo*.

Therefore, in the future, the use of the NHBE culture system in the screening of candidate respiratory drugs could possibly be beneficial by 1) potentially reducing attrition rates in Phase II and III of clinical trials; and 2) reducing the number of compounds tested in animals. However, more work is needed in order to determine these potential benefits and is only speculative at this phase.

CHAPTER 7:

GENERAL DISCUSSION

7.1 OVERVIEW

The overall objective of this research project was to utilise NHBE cells in creating an *in vitro* model of the human bronchial epithelium as a toxicological testing tool. In order to validate the NHBE model as a suitable alternative, extensive biochemical, morphological and toxicological analysis was essential. In this way, it was ensured that the NHBE model not only resembled the *in vivo* bronchial epithelium, but that it responded to toxic challenges in a similar manner.

The bronchial epithelium provides one of the initial lines of defence to inhaled substances, including inert, non-pathogenic and xenobiotic particles, pathogenic organisms and toxic/inert gases (Berne *et al.*, 2004; Gerritsen, 2000; Korpáš and Honda, 1996; Nicod, 1999), making it an ideal region to study the toxicological consequences of inhaled substances. In addition to this, numerous pulmonary diseases, such as COPD and asthma, cause severe damage/alterations to the bronchial epithelium (Puchelle *et al.*, 2006; Trautman *et al.*, 2005; White and Dorscheid, 2002). In order to better understand the impact of inhaled substances, disease mechanisms and to accurately test potential new drugs, within the context of the respiratory epithelium, an adequate human-like model system was required.

The first hypothesis proposed that ***“primary normal human bronchial epithelial (NHBE) cells can be cultured at an air-liquid interface in order to create a fully-differentiated bronchial epithelium of muco-ciliary phenotype containing basal, intermediate, Clara, serous, goblet and ciliated cells”***. This was confirmed through extensive biochemical and morphological analysis, as well as histochemical and immunohistochemical identification of specific cell/epithelial markers. The mature NHBE model (Days 27 – 33) displayed a pseudo-stratified, fully-differentiated, muco-ciliary epithelium characteristic of the human *in vivo* bronchial epithelium (Breeze and Wheeldon, 1977; Rhodin, 1959). In addition to the basic morphology of the model, major bronchial-specific cell types were identified on more than one level. Basal cells were identified via their location (LM and TEM; Baldwin, 1994) and selective positive staining of CK 5/6 and p63 in the mature epithelium (Stosiek *et al.*, 1992; Yang *et al.*, 1998). Goblet cells were

confirmed from their characteristic 'goblet' shape (LM and TEM; Rogers 2003), secretion of mucin (SEM, visually [visco-elastic fluid] and positive Bradford assay), as well as histochemical staining by PAS (Zugibe, 1970). Ciliated cells were distinguishable by the numerous cilia protruding from their surface (LM, TEM and SEM; Breeze and Wheldon, 1977), with cilia verified at the TEM level by the electron-dense striations caused by the microtubules, the classical "9+2" axoneme on transverse sections and the anchoring basal bodies, surrounded by mitochondria (Hasleton and Curry, 1996). Clara cells were identified morphologically (LM [semi-thin sections] and TEM; Boers *et al.*, 1999) and via expression of the Clara cell specific marker, CC10 (Singh and Katyal, 1997). The additional presence of Clara cells identified the NHBE model as a bronchial, not a tracheobronchial model, with this potentially indicating that the NHBE model contained important P450 metabolising enzymes (not investigated in this research project; Boyd, 1977). The presence of cellular junctions were established biochemically (TEER; Gardener *et al.*, 1997) and the tripartite junctional conformation (tight junction, adherens junction and desmosome), determined visually (TEM; Farquar and Palade, 1963). The detection of three major tight junction proteins, ZO-1, occludin and claudin-1 were ascertained within the model. All of the above parameters stabilised during the maturation of the model to generate a static, *in vitro* model of the human bronchial epithelium between Days 27 – 33.

The hypothesis for Chapter 5 postulated that ***"when challenged with classical pulmonary toxins the NHBE model would respond with general and toxicant specific responses"*** and the second main hypothesis inferred that ***"the NHBE cell model will predict drug irritancy outcomes for rat in vivo airway exposures"***. Exposure of the NHBE model to classical pulmonary toxins (CPT) revealed that the model was sensitive to these known CPTs. The NHBE model produced some general characteristic morphological changes, such as, mucin hypersecretion, dedifferentiation, squamation, hypertrophy and cell death. In addition, the NHBE model also produced some toxicant-specific responses: 1) LPS – goblet cell hyperplasia, hypersecretion and disruption of cellular junctions (Euramene *et al.*, 2005; Lui, 2002; Tulić *et al.*, 2000); 2) CdCl – disruption to cellular junctions (probably E-cadherin based), highly cytotoxic to Clara cells and

loss of ciliated cells (most likely due to mitochondrial toxicity; Gabridge and Meccoli, 1982; Kisling *et al.*, 1987; Låg *et al.*, 2005); 3) Pq – alteration to cuboidal stratified epithelium with squamated basal cells in response to lower doses and deterioration to cuboidal monolayer at higher doses (Clark *et al.*, 1966; Kelly *et al.*, 1978; Popenoe, 1979); 4) Am – presence of electron-dense, intra-cytoplasmic inclusions (Colgan *et al.*, 1984); 5) CS – dedifferentiation, cell death, cilia loss, mucin hypersecretion and basal cell hypertrophy (Domagala-Kulwick, 2008; Parsanejad *et al.*, 2008; van der Toorn *et al.*, 2007). The NHBE model demonstrated the ability to alter its cytokine profile in response to LPS; a useful tool when studying toxicological consequences. The NHBE model also underwent blind-exposure to AZ candidate respiratory drugs, subsequent toxicological analysis and corresponding *in vivo* exposures performed. Overall, the NHBE model had a ~76.9 – 85% correlation with rat *in vivo* toxicity.

7.2 CONCLUSIONS

In conclusion, the use of NHBE cells to create a fully-differentiated model of the human respiratory epithelium and determine its validity as a possible *in vitro* model predictive of *in vivo* toxicity, resulted in numerous observations and these have been discussed below.

Key deductions from initial NHBE model development:

- Correct culturing of NHBE cells in non-collagen coated flasks and seeding at Passage 3 into Millipore® cell culture inserts, produced around 300 inserts from one donor cryovial (~500,000 cells), improving cost effectiveness greatly over the Richter method (i.e. 60 inserts form one cryovial)
- The formation of tight junctions, measured by TEER, resulted in similar profiles from 3 different donors, demonstrating lack of donor variability in this aspect

- The development of the NHBE epithelium mimicked the re-epithelialisation of a COPD patients bronchial airway

Key deductions from fully-developed NHBE model:

- LM and TEM observations over the models morphogenesis revealed the production of a well-differentiated, pseudo-stratified epithelium of muco-ciliary phenotype similar to the human *in vivo* situation
- Morphological, histochemical and immunohistochemical analysis confirmed the presence of basal, intermediate, Clara, goblet and ciliated cells within the NHBE model as is in the human bronchial epithelium
- TEM accurately determined the presence of cilia from their length, electron-dense striations, characteristic “9+2” axoneme structure and anchoring basal bodies
- SEM enabled surface topography analysis of the muco-ciliary phenotype as well as whole culture overviews (useful in determining focal or severe damage)
- Extensive characterisation, biochemically, morphologically as well as the relative cell numbers of each specific cell type within the NHBE model may prove a useful tool when monitoring toxicological response
- The NHBE model was stable in all monitored parameters from Days 27 – 33 and this, should therefore, be the toxicological dosing window

Key deductions from exposure to classical pulmonary toxicants:

- The NHBE model displayed numerous general defence/irritancy responses to CPTs (such as goblet cell hyperplasia), which may be useful in creating ‘disease’ models of the bronchial epithelium

- Toxicant-specific responses were also noted in response to the CPTs, indicating that the model was sensitive to at least some of the specific mechanisms of action of each individual pulmonary toxicant
- Cytokines are produced by the NHBE model and their expression profile was altered in response to LPS and would therefore, probably alter in response to other irritants/drugs
- A closed system of defined phenotype, such as this enabled the initial response of the bronchial epithelium to be elucidated, prior to masking by incoming inflammatory cells, thereby, identifying initial changes and possible new therapeutic targets

Key deductions from AZ candidate respiratory drug testing:

- Biochemical analysis (TEER and ATP assay) alone was, occasionally, insufficient in attempting to determine irritancy
- Complimentary morphological analysis revealed false-negatives from biochemical irritancy assessment, which occurred when the response was a multicellular event
- The NHBE model predicted the *in vivo* (rat) toxicological response relatively accurately, with a 76.9 – 85% correlation, indicating it was a suitable alternative to *in vivo* (rat) testing

7.3 FUTURE WORK

7.3.1 GENERAL NHBE PARAMETERS

With respect to the establishment of the NHBE model for use in toxicological testing, the method is well-characterised, with the dosing window between Days 27 – 33. However, the use of biochemical, morphological, histochemical and immunohistochemical characterisations, employed to determine this dosing window, may be implemented on Days 25, 26, 34 and 35, in order to potentially broaden this window.

The Bradford assay was a useful tool in assessing the protein content of apical secretions; it does not however, specifically identify mucin. One particular alternative could be the lectin-based mucin assay, which used a modified standard 'sandwich' immunoassay to more accurately determine and quantify mucin production (Jackson *et al.*, 2002).

The identification of the tight junction proteins, ZO-1, occludin and claudin-1 was deemed successful. One highlighted problem was that human lung cells (*in vivo*) express claudin-1, -3, -5, -7 and -8 (Coyne *et al.*, 2003; Morita *et al.*, 1999) and that human primary cultures (*in vitro*) only contain claudin-1 and -4 (Coyne *et al.*, 2003). Further examination of the different claudin family members, possibly via immunohistochemistry, could determine if this is indeed the case within the NHBE model.

The fact that the NHBE model contained Clara cells suggested that it possessed potential P450 activity. As P450 expression is relatively low in the lung, the most reliable method to assess this would be quantitative real-time RT-PCR of specific CYP family members, known to be expressed in the human bronchial epithelium *in vivo* (Castell *et al.*, 2005).

7.3.2 TOXICOLOGICAL EXPOSURE

In continuation of the work on CPTs, further analysis could be undertaken on the specific response of the NHBE model to each CPT. Specific cell types and their profile alteration, could be monitored through use of the histochemical and immunohistochemical procedures utilised in Chapter 4. This would identify an increase in and specific toxicity of, any particular cell type. Additionally, transdifferentiating cells, such as, ciliated-secretory or Clara-mucous cells may be detected (Jeffery and Li, 1997). The monitoring of cell junction proteins may enlighten the specific junctional interactions/interference that individual toxins may have, such as E-cadherin in CdCl treated cultures (Prozialeck, 2000) or desmosomes in response to CS (Frasca *et al.*, 1968).

Cytokine changes in response to LPS were interesting, but were only achieved for $n = 1$ insert for each treatment and therefore, could only be interpreted with caution. The completion of this experiment, with sufficient ' n ' numbers would give more weight to the conclusions drawn. The monitoring of cytokine production after exposure to other pulmonary toxins may also give a great insight into the bronchial epithelium cytokine response and due to the confined nature of the system may reveal new therapeutic targets.

Blind-exposure of the NHBE model to AZ candidate respiratory drugs demonstrated a relatively high level of accuracy in predicting the *in vivo* animal (rat) response. Further feedback on those AZ compounds continued to the next stage in the screening procedure (especially those which were deemed non-irritant *in vivo* but irritant *in vitro*), may provide essential information on the validation of the NHBE model as an accurate predictor of human *in vivo* respiratory toxicity.

7.3.3 FUTURE DIRECTIONS

The development of this model as a toxicological and pharmacological tool could be pushed well beyond the scope of this research project. The model could be adapted further, with the co-culture of fibroblasts, dendritic cells, T-cells, or even

a combination of these cell types. This would enable researchers to create ever-more complicated models, which would more accurately reflect the human *in vivo* situation.

The co-culture of the NHBE cells with fibroblasts to create a 'full-thickness' model could be utilised in a scratch-wound assay. This could enable the normal and fibrotic (disease) repair mechanisms to be elucidated, with the potential to create new therapeutic agents to minimise or prevent fibrosis within the bronchial epithelium.

In addition to this, the model may be manipulated, for instance to a goblet cell hyperplasia mode, thereby, creating potential 'disease' models. These 'disease' models could allow further understanding of disease mechanisms within the bronchial epithelium and allow the effective testing of new therapeutic agents in retarding/reversing the disease phenotype.

7.4 ULTIMATE CONCLUSION

The ultimate conclusion from this research project was that the NHBE cells could be cultured at an air-liquid interface to provide a suitable *in vitro* model of the human respiratory epithelium, which may be predictive of human *in vivo* toxicology. This model (under current characterisation parameters) may be utilised for toxicological testing during Days 27 – 33.

REFERENCES:

- Adler, K. B. and Li, Y.** (2001). Airway Epithelium Mucus: Intracellular Signaling Pathways for Gene Expression and Secretion. *American Journal of Respiratory Cellular and Molecular Biology*. **25**: 397-400.
- Adler, K. B., Schwartz, J. E., Whitcutt, M. J. and Wu, R.** (1987). A New Chamber System for Maintaining Differentiated Guinea Pig Respiratory Epithelial Cells between Air and Liquid Phases. *BioTechniques*. **5**(5): 462-466.
- Agius, L.** (1987). Human Liver *in vitro* Techniques for Metabolic Studies. *Bailliere's Clinical Endocrinology and Metabolism*. **1**(4): 999-1021.
- Alberts, B., Johnson, A., Lewis, J., Raff, M., Roberts, K. and Walter, P.** (2002). *Molecular Biology of the Cell*. 4th ed. Garland Publishing Inc., London, UK.
- Anderson, J. M., Stevenson, B. R., Jesaitis, L. A., Goodenough, D. A. and Mooseker, M. S.** (1988). Characterization of ZO-1, a Protein Component of the Tight Junction from Mouse Liver and Madin-Darby Canine Kidney Cells. *The Journal of Cell Biology*. **106**: 1141-1149.
- ATSDR** (1999). Cadmium, CAS# 7440-43-9. <http://www.atsdr.cdc.gov/tfacts5.pdf>
- Ayers, M. M. and Jeffery, P. K.** (1988). Proliferation and Differentiation in Mammalian Airway Epithelium. *European Respiratory Journal*. **1**: 58-80.
- Balda, M. S., Whitney, J. A., Flores, C., González, S., Cereijido, M. and Matter, K.** (1996). Functional Dissociation of Paracellular Permeability and Transepithelial Electrical Resistance and Disruption of the Apico-Basolateral Intermembrane Diffusion Barrier by Expression of a Mutant Tight Junction Membrane Protein. *The Journal of Cell Biology*. **134**(4): 1031-1049.
- Baldwin, F.** (1994). Basal Cells in Human Bronchial Epithelium. *The Anatomical Records*. **238**: 360-367.
- Balharry, D., Sexton, K. and BéruBé, K. A.** (2008). An *in vitro* Approach to Assess the Toxicity of Inhaled Tobacco Smoke Components: Nicotine, Cadmium, Formaldehyde and Urethane. *Toxicology*. **244**: 66-76.
- Bals, R., Gamarra, F., Kaps, A., Grundler, S., Huber, R. M. and Welsch, U.** (1998). Secretory Cell Types and Cell Proliferation of Human Bronchial Epithelial Cells in an Organ-Culture System. *Cell and Tissue Research*. **293**: 573-577.

Baraldo, S., Oliani, K. L., Turato, G., Zuin, R. and Saetta, M. (2007). The Role of Lymphocytes in the Pathogenesis of Asthma and COPD. *Current Medicinal Chemistry*. **14**: 2250-2256.

Bargout, R., Jankov, A., Dincer, E., Wang, R., Komodromos, T., Ibarra-Sunga, O., Filippatos, G. and Uhal, B. D. (2000). Amiodarone Induces Apoptosis of Human and Rat Alveolar Cells In Vitro. *American Journal of Physiology- Lung Cellular and Molecular Physiology*. **278**: L1039-L1044.

Barnes, P. J. (2006). Novel Signal Transduction Modulators for the Treatment of Airway Diseases. *Pharmacology and Therapeutics*. **109**: 238-245.

Becker, M. N., Diamond, G., Verghese, M. W. and Randell, S. H. (2000). CD14-Dependent Lipopolysaccharide-Induced β -Defensin-2 Expression in Human Tracheobronchial Epithelium. *The Journal of Biological Chemistry*. **275**(38): 29731-29736.

Bernard, A. M., Roels, H. A., Buchet, J-P. and Lauwerys, R. R. (1994). Serum Clara Cell Protein: An Indicator of Bronchial Cell Dysfunction Caused by Tobacco Smoking. *Environmental Research*. **66**: 96-104.

Berne, R. M., Levy, M. N., Koeppen, B. M. and Stanton, A. (2004). *Physiology*. 5th ed. Mosby, St. Louis, Missouri, USA.

BéruBé, K., Aufderheide, M., Breheny, D., Clothier, R., Combes, R., Duffin, R., Forbes, B., Gaça, M., Gray, A., Hall, I., Kelly, M., Lethem, M., Liebsch, M., Merolla, L., Morin, JP., Seagrave, J., Swartz, MA., Tetley, TD. and Umachandran, M. (2009). In vitro Models of Inhalation Toxicity and Disease: The Report of a FRAME Workshop. *Alternatives to Laboratory Animals: ALTA*. **37**(1): 89-141.

Boers, J. E., Ambergen, A. W. and Thunnissen, F. B. J. M. (1998). Number and Proliferation of Basal and Parabasal Cells in Normal Human Airway Epithelium. *American Journal of Respiratory and Critical Care Medicine*. **157**: 2000-2006.

Boers, J. E., Ambergen, A. W. and Thunnissen, F. B. J. M. (1999). Number and Proliferation of Clara Cells in Normal Human Airway Epithelium. *American Journal of Respiratory and Critical Care Medicine*. **150**: 1585-1591.

Bolt, M. W., Card, J. W., Racz, W. J., Brien, J. F. and Massey, T. E. (2001). Disruption of Mitochondrial Function and Cellular ATP Levels by Amiodarone and N-Desethylamiodarone in Initiation of Amiodarone-Induced Pulmonary Cytotoxicity. *The Journal of Pharmacology and Experimental Therapeutics*. **298**(3): 1280-1289.

- Basbaum, C. B., Jany, B. and Finkbeiner, W. E.** (1990). The Serous Cell. *Annual Review of Physiology*. **52**: 97-113.
- Boswell-Smith, V. and Spina, D.** (2007). PDE4 Inhibitors as Potential Therapeutic Agents in the Treatment of COPD-focus on Roflumilast. *International Journal of COPD*. **2**(2): 121-129.
- Boucher, R. C.** (2003). Regulation of Airway Surface Liquid Volume by Human Airway Epithelia. *Pflügers Archiv European Journal of Physiology*. **445**: 495-498.
- Boyd, M. R.** (1977). Evidence for the Clara Cell as a Site for Cytochrome P450-Dependent Mixed-Function Oxidase Activity in Lung. *Nature*. **269**: 713-715.
- Boyle, P. and Levin, B.** (2008). *World Cancer Report 2008*. WHO Press, Geneva, Switzerland.
- Boyton, R. J. and Openshaw, P. J.** (2002). Pulmonary Defences to Acute Respiratory Infection. *British Medical Bulletin*. **61**: 1-12.
- Breeze, R. G. and Wheeldon, E. B.** (1977). The Cells of the Pulmonary Airways. *American Review of Respiratory Disease*. **116**: 705-777.
- Brody, A. R.** (1984). Inhaled Particles in Human Disease and Animal Models: Use of Electron Beam Instrumentation. *Environmental Health Perspectives*. **56**: 149-162.
- Brody, A. R., Hook, G. E., Cameron, G. S., Jetten, A. M., Butterick, C. J. and Netteshiem, P.** (1987). The Differentiation Capacity of Clara Cells Isolated from the Lungs of Rabbits. *Laboratory Investigation*. **57**(2): 219-229.
- Burge, P. S.** (1994). Occupation and Chronic Obstructive Pulmonary Disease (COPD). *European Respiratory Journal*. **7**: 1032-1034.
- Burgel, P-R. and Nadel, J. A.** (2004). Roles of Epidermal Growth Factor Receptor Activation in Epithelial Cell Repair and Mucin Production in Airway Epithelium. *Thorax*. **59**: 669-996.
- Burnett, D.** (1986). Immunoglobulins in the Lung. *Thorax*. **41**: 337-344.
- Camus, P., Fanton, A., Bonniaud, P., Camus, C. and Foucher, P.** (2004). Interstitial Lung Disease Induced by Drugs and Radiation. *Respiration*. **71**: 301-326.

- Card, J. W., Racz, W. J., Brien, J. F. and Massey, T. E.** (2003). Attenuation of Amiodarone-Induced Pulmonary Fibrosis by Vitamin E is Associated with Suppression of Transforming Growth Factor- β_1 Gene Expression but not Prevention of Mitochondrial Dysfunction. *The Journal of Pharmacology and Experimental Therapeutics*. **304**(1): 277-283.
- Cappelletti, G., Maggioni, M. G. and Maci, R.** (1998). Apoptosis in Human Lung Epithelial Cells: Triggering by Paraquat and Modulation by Antioxidants. *Cell Biology International*. **22**(9): 671-678.
- Casartelli, A., Bonato, M., Cristofori, P., Crivellente, F., dal Negro, G., Masotto, I., Mutinelli, C., Valko, K. and Bonfante, V.** (2003). A Cell-Based Approach for the Early Assessment of the Phospholipidogenic Potential in Pharmaceutical Research and Drug Development. *Cell Biology and Toxicology*. **19**: 161-176.
- Castell, J. V., Donato, M. T. and Gomez-Lechon, M. J.** (2005). Metabolism and Bioactivation of Toxicants in the Lung. The *In Vitro* Cellular Approach. *Experimental and Toxicologic Pathology*. **57**: 189–204.
- Chiba, H., Osanai, M., Murata, M., Kojima, T., and Sawada, N.** (2008). Transmembrane Proteins of Tight Junctions. *Biochimica et Biophysica Acta*. **1778**: 588-600.
- Chilvers, M. A. and O'Callaghan, C.** (2000). Local Mucociliary Defence Mechanisms. *Paediatric Respiratory Reviews*. **1**: 27-34.
- Choi, I-S., Kim, B-S., Cho, K-S., Park, J-C., Jang, M-H., Shin, M-C., Jung, S-B., Chung, J-H. and Kim, C-J.** (2002). Amiodarone Induces Apoptosis in L-132 Human Lung Epithelial Cell Line. *Toxicology Letters*. **132**: 47-55.
- Chu, C-H., Liu, D. D., Hsu, Y., Lee, K. and Chen, H.** (2007). Propofol Exerts Protective Effects on the Acute Lung Injury Induced by Endotoxin in Rats. *Pulmonary Pharmacology & Therapeutics*. **20**: 503–512.
- Chu, P. G. and Weiss, L. M.** (2002). Keratin Expression in Human Tissues and Neoplasms. *Histopathology*. **40**: 403-439.
- Chung, K. F.** (2001). Cytokines in Chronic Obstructive Pulmonary Disease. *European Respiratory Journal*. **18**(Suppl. 34): 50s–59s.
- Clark, D. G., McElligott, T. F. and Hurst, E. W.** (1966). The Toxicity of Paraquat. *British Journal of Industrial Medicine*. **23**: 126-132.

- Claude, P. C.** (1978). Morphological Factors Influencing Transepithelial Permeability: a Model for Resistance of the Cannula Occludens. *The Journal of Membrane Biology*. **39**: 219-323.
- Cole, A. M. and Waring, A. J.** (2002). The Role of Defensins in Lung Biology and Therapy. *American Journal of Respiratory Medicine*. **1**(4): 249-259.
- Colgan, T. and Simon, G. T.** (1984). Amiodarone Pulmonary Toxicity. *Ultrastructural Pathology*. **6**: 199-207.
- Coyne, C. B., Gambling, T. M., Boucher, R. C., Carson, J. L. and Johnson, L. G.** (2003). Role of Claudin Interactions in Airway Tight Junctional Permeability. *American Journal of Physiology-Lung Cellular and Molecular Physiology*. **285**: L1166-L1178.
- Croute, F., Beau, B., Arrabit, C., Gaubin, Y., Delmas, F., Murat, J-C. and Soleilhavoup, J-P.** (2000). Pattern of Stress Protein Expression in Human Lung Cell-Line A549 after Short- or Long-Term Exposure to Cadmium. *Environmental Health Perspectives*. **108**(1): 55-60.
- Dalvie, M. A., White, N., Raine, R., Myers, J. E., London, L., Thompson, M. and Christiani, D. C.** (1999). Long-Term Respiratory Health Effects of the Herbicide, Paraquat, among Workers in the Western Cape. *Occupational and Environmental Medicine*. **56**: 391-396.
- Devereux, T. R.** (1984). Alveolar Type II and Clara Cells: Isolation and Xenobiotic Metabolism. *Environmental Health Perspectives*. **56**: 95-101.
- Doherty, M. M., Liu, J., Randell, S. H., Carter, C. A., Davis, C. W., Nettekheim, P. and Ferriola, P. C.** (1995). Phenotype and Differentiation Potential of a Novel Rat Tracheal Epithelial Cell Line. *American Journal of Respiratory Cell and Molecular Biology* **12**(4): 385-395.
- Domagala-Kulawik, J.** (2008). Effects of Cigarette Smoke on the Lung and Systemic Immunity. *Journal of Applied Physiology and Pharmacology*. **59**(Suppl 6): 19-34.
- Duncan, D. and Hild, W.** (1960). Mitochondrial Alterations in Cultures of the Central Nervous System as Observed with the Electron Microscope. *Cell and Tissue Research*. **51**: 123-135.
- Dytham, C.** (2003). *Choosing and using Statistics: A Biologist's Guide*. **2nd ed.** Blackwell Publishing, Oxford, UK.
- Eggleton, P. and Reid, K. B. M.** (1999). Lung Surfactant Proteins Involved in Innate Immunity. *Current Opinion in Immunology*. **11**: 28-33.

- Ehrhardt, C., Kneuer, C., Laue, M., Schaefer, U. F., Kim, K-J. and Lehr, C-M.** (2003). 16HBE14o- Human Bronchial Epithelial Cell Layers Express P-Glycoprotein, Lung Resistance-Related Protein, and Caveolin-1. *Pharmaceutical Research*. **20**(4): 545-551.
- Eisenbarth, S. C., Piggott, D. A., Huleatt, J. W., Visintin, I., Herrick, C. A. and Bottomly, K.** (2002). Lipopolysaccharide-Enhanced, Toll-Like Receptor 4-Dependent T Helper Cell Type 2 Responses to Inhaled Antigen. *Journal of Experimental Medicine*. **196**(12): 1645-1651.
- Elbert, K. J., Schäfer, U. F., Schäfers, H-J., Kim K-J., Lee, V. H. L. and Lehr C-M.** (1999). Monolayers of Human Alveolar Epithelial Cells in Primary Culture for Pulmonary Absorption and Transport Studies. *Pharmaceutical Research*. **16**(5): 601-608.
- Elmore, S.** (2007). Apoptosis: A Review of Programmed Cell Death. *Toxicologic Pathology*. **35**: 495-516.
- Engelhardt, J. F., Allen, E. D. and Wilson, J. M.** (1991). Reconstitution of Tracheal Grafts with a Genetically Modified Epithelium. *Proceedings of the National Academy of Science USA*. **88**: 11192-11196.
- EU Directive 76/768/EEC.** (2003), Directive 2003/15/EC of the European Parliament and of the Council of 27 February 2003, *Official Journal of the European Union*. **L66**: 26-35.
- Eutamene, H., Theodorou, V., Schmidlin, F., Tondereau, V., Garcia-Villar, R., Salvador-Cartier, C., Chovet, M., Bertrand, C. and Bueno, L.** (2005). LPS-Induced Lung Inflammation is linked to Increased Epithelial Permeability: Role of MLCK. *European Respiratory Journal*. **25**: 789-796.
- Evans, C. M., Kim, K., Tuvim, M. J. and Dickey, B. F.** (2009). Mucus Hypersecretion on Asthma: Causes and Effects. *Current Opinions in Pulmonary Medicine*. **15**(1): 4-11.
- Fanning, A. S., Jameson, B. J., Jesaitis, L. A. and Anderson, J. A.** (1998). The Tight Junction Protein ZO-1 Establishes a Link between the Transmembrane Protein Occludin and the Actin Cytoskeleton. *The Journal of Biological Chemistry*. **273**(45): 29745-29753.
- Farquhar, M. G. and Palade, G. E.** (1963). Junctional Complexes in Various Epithelia. *Journal of Cell Biology*. **17**: 375-412.

Fiala, E. S., Sohn, O. S., Wang, C-X., Seibert, E., Tsurutani, J., Dennis, P. A., El-Bayoumy, K., Sodum, R. S., Desai, D., Reinhardt, J. and Aliaga, C. (2005). Induction of Preneoplastic Lung Lesions in Guinea Pigs by Cigarette Smoke Inhalation and their Exacerbation by High Dietary Levels of Vitamins C and E. *Carcinogenesis*. **26**(3): 605-612.

Florea, B. I., Cassara, M. L., Junginger, H. E. and Borchard, G. (2003). Drug Transport and Metabolism Characteristics of the Human Airway Epithelial Cell Line Calu-3. *Journal of Controlled Release*. **87**: 131-138.

Forbes, B. (2000). Human Airway Epithelial Cell Lines for In Vitro Drug Transport and Metabolism Studies. *Pharmaceutical Science and Technology Today*. **3**(1): 18-27.

Foster, K. A. (1998). Characterization of the A549 Cell Line as a Type II Pulmonary Epithelial Cell Model for Drug Metabolism. *Experimental Cell Research*. **243**: 359-366.

Foster, K. A., Oster, C. G., Mayer, M. M., Avery, M. L. and Audus, K. L. (2000). Characterization of the Calu-3 Cell Line as a Tool to Screen Pulmonary Drug Delivery. *International Journal of Pharmaceutics*. **208**: 1-11.

Fox, S. I. (2004). *Human Physiology*. 8th ed. McGraw-Hill, New York, USA.

FRAME. (2010). <http://www.frame.org.uk>.

Franke, W. W., Schmid, E., Wellsteed, J., Grund, C., Gigi, O. and Geiger, B. (1983). Change of Cytokeratin Filament Organization during the Cell Cycle: Selective Masking of an Immunologic Determinant in Interphase PtK2 Cells. *The Journal of Cell Biology*. **97**: 1255-1260.

Frasca, J. M., Auerbach, O., Parks, V. R. and Jamieson, J. D. (1968). Electron Microscopic Observations of the Bronchial Epithelium of Dogs: II Smoking Dogs. *Experimental and Molecular Pathology*. **9**: 380-399.

Freshney, R. I. (2005). *Culture of Animal Cells: A Manual of Basic Techniques*. 5th ed. Wiley, New Jersey, USA.

Fueki, N., Sagara, H., Fueki, M., Hashii, A., Ota, M., Okada, T., Sugiyama, K., Akimoto, K., Makino, S. and Fukuada, T. (2009). Collagen Production from Activated Epithelial Cells Regulate Airway Remodeling. *American Journal of Respiratory and Critical Care Medicine*. **179**: A2754. (Abstract Only)

- Furuse, M., Hirase, T., Itoh, M., Nagafuchi, A., Yonemura, S., Tsukita, S., and Tsukita, S.** (1993). Occludin: A Novel Integral Membrane Protein Localizing at Tight Junctions. *The Journal of Cell Biology*. **123**(6): 1777-1788.
- Furuse, M., Itoh, M., Hirase, T., Nagafuchi, A., Yonemura, S., Tsukita, S. and Tsukita, S.** (1994). Direct Association of Occludin with ZO-1 and its Possible Involvement in the Localization of Occludin at Tight Junctions. *The Journal of Cell Biology*. **6**(1): 1617-1626.
- Furuse, M., Fujita, K., Hiitagi, T., Fujimoto, K. and Tsukita, S.** (1998). Claudin-1 and -2: Novel Integral Membrane Proteins Localizing at Tight Junctions with No Sequence Similarity to Occludin. *The Journal of Cell Biology*. **171**(7): 1539-1550.
- Gabridge, M. G. and Meccoli, R. A.** (1982). Cytotoxicity and Ciliostasis in Tracheal Explants Exposed to Cadmium Salts. *Environmental Health Perspectives*. **44**: 189-196.
- Gardner, D. E.** (2006). *Toxicology of the Lung*. **4th ed.** Taylor & Francis, London, UK.
- Gardner, T. W., Lieth, E., Khin, S. A., Barber, A. J., Bonsall, D., Leshner, T., Rice, K. and Brennan, Jr. W. A.** (1997). Astrocytes Increase Barrier Properties and ZO-1 Expression in Retinal Vascular Endothelial Cells. *Investigative Ophthalmology & Visual Science*. **38**(11): 2423-2427.
- Gerritsen, J.** (2000). Host Defence Mechanisms of the Respiratory System. *Paediatric Respiratory Reviews*. **1**: 128-134.
- Garrod, D. and Chidgey, M.** (2008). Desmosome Structure, Composition and Function. *Biochimica et Biophysica Acta*. **1778**: 527-587.
- Glader, P., Möller, S., Lilja, J., Wieslander, E., Löfdahl, C-G. and von Wachenfeldt, K.** (2006). Cigarette Smoke Extract Modulates Respiratory defence Mechanisms through Effects on T-Cells and Airway Epithelial Cells. *Respiratory Medicine*. **100**: 818-827.
- Godfrey, R. W. A.** (1997). Human Airway Epithelial Tight Junctions. *Microscopy Research and Technique*. **38**: 488-499.
- Goldman, R. D. and Steinert, P. M.** (1990). Cellular and Molecular Biology of Intermediate Filaments. **1st ed.** Plenum Press, New York, USA.
- Gordon, S. B. and Read, R. C.** (2002). Macrophage Defences against Respiratory Tract Infections. *British Medical Bulletin*. **61**: 45-61.

- Grainger, C. I., Greenwell, L. L., Lockley, D. J., Martin, G. P. and Forbes, B.** (2006). Culture of Calu-3 Cells at the Air Interface Provides a Representative Model of the Airway Epithelial Barrier. *Pharmaceutical Research*. **23**(7): 1482-1490.
- Gram, T. E., Okine, L.K. and Gram, R. A.** (1986). The Metabolism of Xenobiotics by Certain Extrahepatic Organs and its Relation to Toxicity. *Annual Review of Pharmacology and Toxicology*. **26**: 259-291.
- Gray, T. E., Guzman, K., Davis, C. W., Abdullah, L. H. and Nettesheim, P.** (1996). Mucociliary Differentiation of Serially Passaged Normal Human Tracheobronchial Epithelial Cells. *American Journal of Respiratory Cell and Molecular Biology* **14**(1): 104-112.
- Gray, T., Nettesheim, P., Loftin, C., Koo, J-S., Bonner, J., Peddada, S. and Langenbach, R.** (2004). Interleukin-1 β -Induced Mucin Production in Human Airway Epithelium is Mediated by Cyclooxygenase-2, prostaglandin E₂ Receptors, and Cyclic AMP-Protein Kinase A Signaling. *Molecular Pharmacology*. **66**(2): 337-346.
- Gruenert, D. C., Basbaum, C. B., Welsh, M. J., Li, M., Finkbeiner, W. E., and Nadel, J. A.** (1988). Characterization of Human Tracheal Epithelial Cells Transformed by an Origin-Defective Simian Virus 40. *Proceedings of the National Academy of Science*. **85**: 5951-5955.
- Guillemot, I., Paschoud, S., Pulimeno, P., Foglia, A., and Citi, S.** (2008). The Cytoplasmic Plaques of Tight Junctions: A scaffolding and Signalling Centre. *Biochimica et Biophysica Acta*. **1778**: 601-613.
- Han, X., Fink, M. P., Uchiyama, T., and Delude, R. L.** (2004). Increased iNOS Activity is Essential for the Development of Pulmonary Epithelial Tight Junction Dysfunction in Endotoxemic Mice. *American Journal of Physiology: Lung Cellular and Molecular Physiology*. **286**: L259-L267,
- Harris, J. F., Aden, J., Lyons, C.R. and Tesfaigzi, Y.** (2007). Resolution of LPS-Induced Airway Inflammation and Goblet Cell Hyperplasia is Independent of IL-18. *Respiratory Research*. **8**(1): 24.
- Hasleton, P. S. and Curry, A.** (1996). *Anatomy of the Lung, Spencer's Pathology of the Lung*. 5th ed. McGraw-Hill, New York, USA.
- Hecht, S. S.** (1999). Tobacco Smoke Carcinogens and Lung Cancer. *Journal of the National Cancer Institute*. **91**(14): 1194-1210.

Hill, E. M., Eling, T. and Nettesheim, P. (1998). Differentiation Dependency of Eicosanoid Enzyme Expression in Human Tracheobronchial Epithelial Cells. *Toxicological Letters*. **96**(97): 239-244.

Holtzman, M. J. (2001). Immunity, Inflammation, and Remodelling in the Airway Epithelial Barrier: Epithelial-Viral-Allergic Paradigm. *Physiological Review*. **82**: 19-46.

Housley, D. G., BéruBé, K. A., Jones, T. P., Anderson, S., Pooley, F. and Richards, R. J. (2002). Pulmonary Epithelial Response in the Rat Lung to Instilled Montserrat Respirable Dusts and their Major Mineral Components. *Occupational and Environmental Medicine*. **59**: 466-472.

Hughes, J. D., Blagg, J., Price, D. A., Bailey, S., DeCrescenzo, G. A., Devraj, R. V., Ellsworth, E., Fobian, Y. M., Gibbs, M. E., Gilles, R. W., Greene, N., Huang, E., Krieger-Burke, T., Loesel, J., Wager, T., Whiteley, L. and Zhang, Y. (2008). Physicochemical Drug Properties Associated with In Vivo Toxicological Outcomes. *Bioorganic & Medicinal Chemistry Letters*. **18**: 4872-4875.

Hukkanen, J., Lassila, A., Päivärinta, K., Valanne, S., Sarpo, S., Hakkola, J., Pelkonen, O. and Raunio, H. (2000). Induction and Regulation of Xenobiotic-Metabolising Cytochrome P450s in the Human A549 Lung Adenocarcinoma Cell Line. *American Journal of Respiration Cellular Molecular Biology*. **22**: 360-366.

Humphrey, E. W., Ewing, S. L., Wrigley, J. V., Northrup III, W. F., Kersten, T. E., Mayer, J. E. and Varco, R. L. (1981). The Production of Malignant Tumors of the Lung and Pleura in Dogs from Intratracheal Asbestos Instillation and Cigarette Smoking. *Cancer*. **47**: 1994-1999.

IARC. (1997). Beryllium, Cadmium, Mercury and Exposures in the Glass Manufacturing Industry. *IARC Monographs on the Evaluation of Carcinogenic Risks to Humans*. **58**.

IARC. (2004). Tobacco Smoke and Involuntary Smoking. *IARC Monographs on the Evaluation of Carcinogenic Risks to Humans*. **83**.

Innes, A. L., Woodruff, P. G., Ferrando, R. E., Donnelly, S., Dolganov, G. M., Lazarus, S. C. and Fahy, J. V. (2006). Epithelial Mucin Stores are Increased in the Large Airways of Smokers with Airflow Obstruction. *Chest*. **130**(4): 1102-1108.

Inyama, Y., Hook, G. E. R., Brody, A. R., Cameron, G. S., Jetten, A. M., Gilmore, L. B., Gray, T. and Nettesheim, P. (1988). The Differentiation Potential of Tracheal Basal Cells. *Laboratory Investigation*. **25**: 706-717.

- Itoh, M., Furuse, M., Morita, K., Kubota, K. and Saitou, M.** (1999). Direct Binding of Three Tight Junction-Associated MAGUKs, ZO-1, ZO-2, and ZO-3, with the COOH Termini of Claudins. *The Journal of Cell Biology*. **147**(6): 1351-1363.
- Izard, C. and Libermann, C.** (1978). Acrolein. *Mutation Research*. **47**: 115-138.
- Jackson, A., Kemp, P., Giddings, J. and Sugar, R.** (2002). Development and Validation of a Lectin-Based Assay for the Quantitation of Rat Respiratory Mucin. *Novartis Foundation Symposium*. Vol **248**: 94-110.
- Janeway, C. A., Travers, P., Walport, M. and Shlomchik, M.** (2005). *Immunobiology: The Immune System in Health and Disease*. 6th ed. Garland Science, London, UK.
- Jeffery, P. K. and Li, D.** (1997). Airway Mucosa: Secretory Cells, Mucus and Mucin Genes. *European Respiratory Journal*. **10**: 1655-1662.
- Jeffery, P. K. and Reid, L.** (1975). New Observations of Rat Airway Epithelium: a Quantitative and Electron Microscopic Study. *Journal of Anatomy*. **120**(2): 295-320.
- Jerome, H. E.** (1996). Chronic Interleukin-2 Treatment in Awake Sheep Causes Minimal or No Injury to the Lung Microvascular Barrier. *Journal of Applied Physiology*. **81**: 1730-1738.
- Jia, H. P., Kline, J. N., Penisten, A., Apicella, M. A., Giannini, T. L., Weiss, J. and McCray, P. B.** (2004). Endotoxin Responsiveness of Human Airway Epithelia is limited by Low Expression of MD-2. *American Journal of Physiology: Lung Cellular and Molecular Physiology*. **287**: L428-L437.
- Kaartinen, L., Nettekheim, P., Adler, K. B. and Randell, S. H.** (1993). Rat Tracheal Epithelial Cell Differentiation *in vitro*. *In Vitro Cellular and Developmental Biology - Animal* **29**(6): 481-492.
- Karp, G.** (2005). *Cell and Molecular Biology: Concepts and Experiments*. John Wiley Sons, Inc., USA.
- Kelly, D. F., Morgan, D. G., Darke, P. G. G., Gibbs, C. Pearson, H. and Weaver, B. M. Q.** (1978). Pathology of Acute Respiratory Distress in the Dog Associated with Paraquat Poisoning. *Journal of Comparative Pathology*. **88**: 275-294.

- Ke, Y., Gerwin, B. I., Ruskie, S. E., Pfeifer, A. M., Harris, C. C. and Lechner, J. F.** (1990). Cell Density Governs the Ability of Human Bronchial Epithelial Cells to Recognise Serum and Transforming Growth Factor Beta-1 as Squamous Differentiation-Inducing Agents. *American Journal of Pathology*. **137**(4): 833-843.
- Khair, O. A., Davies, R. J. and Devalia, J. L.** (1996). Bacterial-Induced Release of Inflammatory Mediators by Bronchial Epithelial Cells. *European Respiratory Journal*. **9**: 1913-1922.
- Kim, K. C., McCracken, K., Lee, B. C., Shin, C. Y., Jo, M J., Lee, C. J. and Ko, K. H.** (1997). Airway Goblet Cell Mucin: its Structure and Regulation of Secretion. *European Respiratory Journal*. **10**: 2644-2649.
- Kim, Y-K., Oh, S-Y., Jeon, S. G., Park, H-W., Lee, S-Y., Chun, E-Y., Bang, B., Lee, H-S., Oh, M-H., Kim, Y-S., Kim, J-H., Gho, Y. S., Cho, S-H., Min, K-U., Kim, Y-Y. and Zhu, Z.** (2007). Airway Exposure Levels of Lipopolysaccharide Determine Type 1 versus Type 2 Experimental Asthma. *Journal of Immunology*. **178**(8): 5375-5382.
- Kisling, G. M., Kopp, S. J., Paulson, D. J., Hawley, P. L. and Tow, J. P.** (1987). Inhibition of Rat Heart Mitochondrial Respiration by Cadmium Chloride. *Toxicology and Applied Pharmacology*. **89**: 295-304.
- Kola, I. and Landis, J.** (2004). Can the Pharmaceutical Industry Reduce Attrition Rates? *Nature Reviews: Drug Discovery*. **3**: 711-715.
- Kondo, M., Finkbeiner, W. E. and Widdicombe, J. H.** (1993). Cultures of Bovine Tracheal Epithelium with Differentiated Ultrastructure and Ion Transport. *In Vitro Cellular and Developmental Biology - Animal*. **29** (1): 19-24.
- Korpáš, J. and Honda, Y.** (1996). Aspects of Airway Defence Mechanisms *Pathophysiology*. **3**: 81-86.
- Kreyling, W. G., Dietl, F., Neuner, M. and Rosenbruch, M.** (1992). Retained Particle Burden in the Lungs of Monkeys after Chronic Quartz Dust Exposure. *Journal of Aerosol Science*. **23**(Sup. 1): S507-S510.
- Kroegel, C., Virchow Jr, J. C., Luttmann, W., Walker, C. and Warner, J. A.** (1994). Pulmonary Immune Cells in Health and Disease: The Eosinophil Leucocyte (Part I). *European Respiratory Journal*. **7**: 519-543.

- Kumar, V., Abbas, A. K., Fausto, N. and Aster, J. C.** (2010). *Robbins and Cotran: Pathologic Basis of Disease*. 8th ed. Saunders Elsevier, Philadelphia, USA.
- Kuo, M-L., Lee, K-C., Lin, J-K. and Huang, T. S.** (1995). Pronounced Activation of Protein Kinase C, Ornithine Decarboxylase and *c-jun* Proto-Oncogene by Paraquat-Generated Active Oxygen Species in WI-38 Human Lung Cells. *Biochimica et Biophysica Acta*. **1268**: 229-236.
- Låg, M., Refsnes, M., Lilleaas, E. M., Holme, J. A., Becher, R. and Schwarze, P. E.** (2005). Role of Mitogen Activated Protein Kinases and Protein Kinase C in Cadmium-Induced Apoptosis of Primary Epithelial Lung Cells. *Toxicology*. **211**: 253-264.
- Lantelme, E., Luca, O., Paola, P., Valentina, T., Mario, D. M., Antonio, A., Stefania, M. and Claudia, G.** (2008). An *In Vitro* Model of T Cell Receptor Revision in Mature Human CD8⁺ T Cells. *Molecular Immunology*. **45**: 328-337.
- Lechner, J. F., McClendon, I. A., LaVeck, M. A., Shamsuddin A. M. and Harris, C. C.** (1983). Differential Control by Platelet Factors of Squamous Differentiation in Normal and Malignant Human Bronchial Epithelial Cells. *Cancer Research*. **43**: 5915-5921.
- Lee, C. M., Carpenter, F., Coaker, T. and Kealey, T.** (1986). The Primary Culture of Epithelia from the Secretory Coil and Collecting Duct of Normal and Cystic Fibrotic Eccrine Sweat Glands. *Journal of Cell Science*. **83**: 103-118.
- Leeder, R. G., Rafeiro, E., Brien, J. F., Mandin, C. C. and Massey, T. E.** (1996). Evaluation of Reactive Oxygen Species Involvement in Amiodarone Pulmonary Toxicity In Vivo and In Vitro. *Journal of Biochemical Toxicology*. **11**(3): 147-160.
- Leeson, P. D. and Springthorpe, B.** (2007). The Influence of Drug-Like Concepts on Decision-Making in Medicinal Chemistry. *Nature Reviews: Drug Discovery*. **6**: 881-890.
- Leong, B. K. J., Coombs, J. K. Sabaitis, C. P. Rop, D. A. and Aaron, C. S.** (1998). Quantitative Morphometric Analysis of Pulmonary Deposition of Aerosol Particles Inhaled via Intratracheal Nebulization, Intratracheal Instillation or Nose-only Inhalation in Rats. *Journal of Applied Toxicology*. **18**: 149-160.
- Levitzky, M. G.** (2003). *Pulmonary Physiology*. 6th ed. New York: McGraw-Hill, New York, USA.
- Lin, S., Walker, J., Xu, L., Gozal, D. and Yu, J.** (2007). Behaviours of Pulmonary Sensory Receptors during Development of Acute Lung Injury in the Rabbit. *Experimental Physiology*. **92**(4): 749-755.

Lipinski, C. A., Lombardo, F., Dominy, B. W., and Feeney, P. J. (1997). Experimental and Computational Approaches to Estimate Solubility and Permeability in Drug Discovery and Development Settings. *Advanced Drug Delivery Reviews*. **23**: 3-25.

Liu, A. H. (2002). Endotoxin Exposure in Allergy and Asthma: Reconciling a Paradox. *Current Reviews of Allergy and Clinical Immunology*. **109**(3): 379-392.

Lodish, H., Berk, A., Zipursky, S. L., Matsudaira, P., Baltimore, D. and Darnell, J. (2001). *Molecular Cell Biology*. 4th ed. Freeman, New York, USA.

Madara, J. L. (1987). Intestinal Absorptive Cell Tight Junctions are linked to Cytoskeleton. *American Journal of Physiology - Cell Physiology*. **22**: C171-C175.

Marrs, T. C. and Adjei, A. (2003). Paraquat. *Joint Meeting on Pesticide Residue*. 203-266. http://whqlibdoc.who.int/publications/2004/924166519X_paraquat.pdf.

Martin, W. R., Brown, C., Zhang, Y. J. and Wu, R. (1991). Growth and Differentiation of Primary Tracheal Epithelial Cells in Culture: Regulation by Extracellular Calcium. *Journal of Cellular Physiology*. **147**: 138-148.

Martins, M. de F. and Abairos, V. (2002). Glycocalyx of Lung Epithelial Cells. *International Review of Cytology*. **216**: 131-173.

Masek, L., and Richards, R. J. (1990). Interactions between Paraquat, Endogenous Lung Amines' Antioxidants and Isolated Mouse Clara Cells. *Toxicology*. **63**: 315-326.

Matsuda, S., Hisama, M., Shibayama, H., Itou, N. and Iwaki, M. (2009). Application of the Reconstructed Rabbit Corneal Epithelium Model to Assess the *in vitro* Eye Irritancy Test of Chemicals. *The Pharmaceutical Society of Japan*. **129**(9): 1113-1120.

MatTek. (2008). <http://www.mattek.com/pages/products/epi-airway>.

Maunder, H., Patwardhan, S., Phillips, J., Clack, A. and Richter, A. (2007). Human Bronchial Epithelial Cell Transcriptome: Gene Expression Changes Following Acute Exposure to Whole Cigarette Smoke In Vitro. *American Journal of Physiology - Lung Cellular and Molecular Physiology*. **292**: L1248-L1256.

Mautz, W. J. (2003). Exercising Animal Models in Inhalation Toxicology: Interactions with Ozone and Formaldehyde. *Environmental Research*. **92**: 14-26.

- May, J. E., Xu, J., Morse, H. R., Avent, N. D. and Donaldson, C.** (2009). Toxicity Testing: the search for an *in vitro* Alternative to Animal Testing. *British Journal of Biomedical Science*. **66**(3): 160-165.
- McCarthy, K. M., Skare, I. B., Stankewich, M. C., Furuse, M., Tsukita, S., Rogers, R. A., Lynch, R. D. and Schneeberger, E. E.** (1996). Occludin is a Functional Component of the Tight Junction. *Journal of Cell Science*. **109**: 2287-2298.
- Méplan, C., Mann, K. and Hinaut, P.** (1999). Cadmium Induces Conformational Modifications of Wild-Type p53 and Suppresses p53 Response to DNA Damage in Cultured Cells. *The Journal of Biological Chemistry*. **274**(44): 31663-31670.
- Microbiology and Immunology Online.** (2007)
http://pathmicro.med.sc.edu/fox/cell_envelope.html
- Miller, F. J., Graham, J. A. and Gardner, D. E.** (1983). The Changing Role of Animal Toxicology in Support of Regulatory Decisions. *Environmental Health Perspectives*. **52**: 169-176.
- Miyoshi, J. and Takai, Y.** (2008). Structural and Functional Associations of Apical Junctions with Cytoskeleton. *Biochimica et Biophysica Acta*. **1778**: 670-691.
- MRC.** (1957). Tobacco Smoking and Cancer of the Lung. *British Medical Journal*. **29**: 1523-1524
- Mochizuki, H., Morikawa, A., Tokuyama, K., Kuroume, T. and Chao, A. C.** (1994). The Effect of Non-Steroidal Anti-Inflammatory Drugs on the Electrical Properties of Cultured Dog Tracheal Epithelial Cells. *European Journal of Pharmacology*. **252**: 183-188.
- Moll, R., Franke, W. W. and Schiller, D. L.** (1982). The Catalogue of Human Cytokeratins: Patterns of Expression in Normal Epithelia, Tumors and Cultured Cells. *Cell*. **31**: 11-24.
- Moore, B. B.** (2001). Role of T- and B-lymphocytes in Pulmonary Host Defences. *European Respiratory Journal*. **18**: 846-856.
- Morita, K., Furuse, M., Fujimoto, K. and Tsukita, S.** (1999). Claudin Multigene Family Encoding Four-Transmembrane Domain Protein Components of Tight Junction Strands. *Proceedings of the National Academy of Science USA*. **96**: 511-516.
- Mullinger, A. M. and Johnson, R. T.** (1976). Perturbation of Mammalian Cell Division: III The Topography and Kinetics of Extrusion Subdivision. *Journal of Cell Science*. **22**(2): 243-285.

Nakata, Y. and Dahms, T. E. (2000). Triolein Increases Microvascular Permeability in Isolated Perfused Rabbit Lungs: Role of Neutrophils. *The Journal of TRAUMA® Injury, Infection, and Critical Care*. **49**: 320 –326.

NC3R. (2010). <http://www.nc3rs.org.uk>.

Nelson, W.G. and Sun, T-T. (1983) The 50- and for Stratified 58-kdalton Squamous Keratin Classes as Molecular Markers Epithelia: Cell Culture Studies. *The Journal of Cell Biology*. **97**: 244-251.

Neudeck, H., Oei, S. L., Steimer, B., Hopp, H. and Graf, R. (1997). Binding of Antibodies Against High and Low Molecular Weight Cytokeratin Proteins in the Human Placenta with Special Reference to Infarcts, Proliferation and Differentiation Processes. *Histochemical Journal*. **29**: 419-430.

Newton, R. and Holden, N. S. (2006). New Aspects of p38 Mitogen Activated Protein Kinase (MAPK) Biology in Lung Inflammation. *Drug Discovery Today: Disease Mechanisms*. **3**(1): 53-61.

Nicod, L. P. (1999). Pulmonary Defence Mechanisms. *Respiration*. **66**: 2-11.

Nicod, L. P. (2005). Lung Defences: an Overview. *European Respiratory Review*. **14**(95): 45-50.

Nicolescu, A. C., Comeau, J. L., Hill, B. C., Bedard, L. L., Takahashi, T., Brien, J. F., Racz, W. J. and Massey, T. E. (2007). Aryl Radical Involvement in Amiodarone-Induced Pulmonary Toxicity: Investigation of Protection by Spin-Trapping Nitrones. *Toxicology and Applied Pharmacology*. **220**: 60-71.

Niemeier, R. W. (1984). The Isolated Perfused Lung. *Environmental Health Perspectives*. **56**: 35-41.

Niessen, C. M. and Gottardi, C. J. (2008). Molecular Components of the Adherens Junction. *Biochimica et Biophysica Acta*. **1778**: 562-571.

O'Grady, N. P., Preas, H. L., Pugin, J., Fiuza, C., Tropea, M., Reds, D., Banks, S. M. and Suffredini, A. F. (2001). Local Inflammatory Responses Following Bronchial Endotoxin Instillation in Humans. *American Journal of Respiratory and Critical Care Medicine*. **163**: 1591-1598.

Paris, L., Tonutti, L., Vannini, C. and Bazzoni, G. (2008). Structural Organization of the Tight Junctions. *Biochimica et Biophysica Acta*. **1778**: 646-659.

- Park, K-S., Wells, J. M., Zorn, A. M., Wert, S. E., Laubach, V. E., Fernandez, L. G. and Whitsett, J. A.** (2006) Transdifferentiation of Ciliated Cells during Repair of the Respiratory Epithelium. *American Journal of Respiratory Cell and Molecular Biology*. **34**: 151-157.
- Parker, J. C., Tsien, C. I., Gingras, C. and Freeman, C. R.** (1999). High Airway Pressure Stress Induces Cytokine Release from Perfused Mouse Lungs. *American Society of Mechanical Engineers, Bioengineering Division (Publication) BED* **42**: 427-428.
- Parsanejad, R., Fields, W. R., Morgan, W. T., Bombick, B. R. and Doolittle, D. J.** (2008). The Time Course of Expression of genes Involved in Specific Pathways in Normal Human Bronchial Epithelial Cells Following Exposure to Cigarette Smoke. *Experimental Lung Research*. **34**: 513-530.
- Pasternak, A. S. and Miller, W. M.** (1995). Measurement of Trans-Epithelial Electrical Resistance in Perfusion: Potential Application for In Vitro Ocular Toxicity Testing. *Biotechnology and Bioengineering*. **50**(5): 568-579.
- Peão, M. N. D., Águas, A. P., de Sá, C. M. and Grande, N. R.** (1993). Anatomy of Clara Cell Secretion: Surface Changes Observed by Scanning Electron Microscopy. **183**: 377-388.
- Pearson, C. A., Lamar, P. C. and Prozialeck, W. C.** (2003). Effects of Cadmium on E-Cadherin and VE-Cadherin in Mouse Lung. *Life Sciences*. **72** : 1303-1320.
- Pearson, C. A. and Prozialeck, W. C.** (2001). E-Cadherin, β -Catenin and Cadmium Carcinogenesis. *Medical Hypotheses*. **56**(5) : 573-581.
- Petitjean, A., Ruptier, C., Tribollet, V., Hautefeuille, A., Chardon, F., Cavard, C., Puisieux, A., Hainaut, P. and Caron de Fromentel, C.** (2008). Properties of the Six Isoforms of p63: p53-like Regulation in Response to Genotoxic Stress and Cross-Talk with Δ Np73. *Carcinogenesis*. **29**(2): 273-281.
- Pingoud, A., Urbanke, C., Hoggette, J. and Jeltsch, A.** (2002). *Biochemical Methods: A Concise Guide for Students and Researchers*. Wiley-VCH Chp 5: 155-160.
- Popenoe, D.** (1979). Effects of Paraquat Aerosol on Mouse Lung. *Archives of Pathology and Laboratory Medicine*. **103**: 331-334.
- Presland, R. B. and Dale, B. A.** (2000). Epithelial Structural Proteins of the Skin and Oral Cavity: Function in Health and Disease. *Critical Reviews in Oral Biology and Medicine*. **11**(4): 383-408.

- Presland, R. B. and Jurevic, R. J.** (2002). Making Sense of the Epithelial Barrier: what Molecular Biology and Genetics tell us About the Functions of Oral Mucosal and Epidermal Tissues. *Journal of Dental Education*. **66**(4): 564-574.
- Prozialeck, W. C.** (2000). Evidence that E-Cadherin may be a Target for Cadmium Toxicity in Epithelial Cells. *Toxicology and Applied Pharmacology*. **164**: 231-249.
- PubChem.** (2007a) - Paraquat
<http://pubchem.ncbi.nlm.nih.gov/summary/summary.cgi?cid=16218602>
- PubChem.** (2007b) - Amiodarone
<http://pubchem.ncbi.nlm.nih.gov/summary/summary.cgi?cid=2157>
- Puchelle, E., Zahm, J-M., Tournier, J-M. and Coraux, C.** (2006) Airway Epithelial Repair, Regeneration, and Remodeling after Injury in Chronic Obstructive Pulmonary Disease. *Proceedings of the American Thoracic Society*. **3**: 726-733.
- Rajasekaran, A. K., Hojo, M., Huima, T. and Rodriguez-Boulan, E.** (1996). Catenins and Zonula Occludens-1 form a Complex during Early Stages in Assembly of Tight Junctions. *The Journal of Cell Biology*. **132**: 451-463.
- Randell, S. H., Liu, J. Y., Ferriola, P. C., Kaartinen, L., Doherty, M. M., Davis, C. W. and Nettekheim, P.** (1996). Mucin Production by SPOC1 Cells - an Immortalized Rat Tracheal Epithelial Cell Line. *American Journal of Respiratory Cell and Molecular Biology* **14**(2): 146-154.
- Reed, C. E. and Milton, D. K.** (2001). Endotoxin-Stimulated Innate Immunity: A Contribution Factor for Asthma. *Journal of Allergy and Clinical Immunology*. **108**(2): 157-166.
- Renda, T., Baraldo, S., Pelaia, G., Bazzan, E., Turato, G., Papi, A., Maestrelli, P., Maselli, R., Vatrella, A., Fabbri, L. M. Zuin, R., Marsico, S. A. and Saetta, M.** (2008). Increased Activation of p38 MAPK in COPD. *European Respiratory Journal*. **31**: 62-69.
- Rhodin, J.** (1959). Ultrastructure of the Tracheal Ciliated Mucosa in Rat and Man. *Annals of Otolaryngology, Rhinology & Laryngology*. **68**: 964-974.
- Rhodin, J. A. G.** (1966). The Ciliated Cell: Ultrastructure and Function of the Human Tracheal Mucosa. *The American Review of Respiratory Disease*. **93**(3): 1-15.
- Richter, A.** (R & D Centre Reagents Park Road, Millbrook, Southampton UK) (2005). Meeting with members of LPRG on September 27, 2005.

- Rietschel, E. T., Kirikae, T., Schade, F. U., Mamat, U., Schmidt, G., Loppnow, H., Ulmer, A. J., Zahringer, U., Seydel, U. and Di Padova, F.** (1994). Bacterial Endotoxin: Molecular Relationships of Structure to Activity and Function. *Federation of American Societies for Experimental Biology*. **8**: 217-225.
- Rimar, S. and Gillis, C. N.** (1995). Site of Pulmonary Vasodilation by Inhaled Nitric Oxide in the Perfused Lung. *Journal of Applied Physiology*. **78**(5): 1745-1749
- Ritchie, T. J., Luscombe, C. N. and Macdonald, S. J. F.** (2009). Analysis of the Calculated Physicochemical Properties of Respiratory Drugs: Can we Design for Inhaled Drugs Yet? *Journal of Chemical Information and Modeling*. **49**: 1025-1032.
- Rogan, M. P., Geraghty, P., Greene, C. M., O'Neill, S. J., Taggart, C. C. and McElvaney, N. G.** (2006). Antimicrobial Proteins and Polypeptides in Pulmonary Innate Defence. *Respiratory Research*. **7**: 29-40.
- Rogers, D. F.** (1994). Airway Goblet Cells: Responsive and Adaptable Front-Line Defenders. *European Respiratory Journal*. **7**: 1690-1706.
- Rogers, D. F.** (2003). The Airway Goblet Cell. *The International Journal of Biochemistry and Cell Biology*. **35**: 1-6.
- Rogers, D. F. and Jeffery, P. K.** (1986). Inhibition by Oral N-Acetylcysteine of Cigarette Smoke-Induced "Bronchitis" in the Rat. *Experimental Lung Research*. **10**(3): 267-283.
- Roguet, R. and Schaefer, H.** (1997). Overview of *in vitro* Cell Culture Technologies and Pharmaco-Toxicological Applications. *Toxicology In Vitro* **11**(5): 591-599.
- Romet-Haddad, S., Marano, F., Blanquart, C. and Baeza-Squiban, A.** (1992). Tracheal Epithelium in Culture: A Model for Toxicity Testing of Inhaled Molecules. *Cell Biology and Toxicology*. **8**(3): 141-150.
- Rose, M. C. and Voynow, J. A.** (2006). Respiratory Tract Mucin Genes and Mucin Glycoproteins in Health and Disease. *Physiology Reviews*. **86**: 245-278.
- Sakagami, M.** (2006). In Vivo, In Vitro and Ex Vivo Models to Assess Pulmonary Absorption and Disposition of Inhaled Therapeutics for System Delivery. *Advanced Drug Delivery Reviews*. **58**: 1030-1060.

- Salvi, S. and Holgate, S. T.** (1999). Could the Airway Epithelium Play an Important Role in Mucosal Immunoglobulin A Production?. *Clinical and Experimental Allergy*. **29**: 1597-1605.
- Samet, J. M. and Cheng, P-W.** (1994). The Role of Airway Mucus in Pulmonary Toxicology. *Environmental Health Perspectives*. **102**(Supp. 2): 89-103.
- Satir, P.** (1989). The Role of Axonemal Components in Ciliary Motility. *Comparative Biochemistry and Physiology – Part A: Physiology*. **94**(2): 351-357.
- Seemungal, T., Sykes, A. and the ICEAD Contributors.** (2008). Recent Advances in Exacerbations of COPD. *Thorax*. **63**: 850-852.
- Schlesinger, R. B.** (1985). Comparative Deposition of Inhaled Aerosols in Experimental Animals and Humans: A Review. *Journal of Toxicology and Environmental Health*. **15**: 197-214.
- Schulz, C., Farkas, L., Wolf, K., Krätzel, K., Eissner, G. and Pfeifer, M.** (2002). Differences in LPS-Induced Activation of Bronchial Epithelial Cells (BEAS-2B) and Type II-Like Pneumocytes (A-549). *Scandinavian Journal of Immunology*. **56**: 294-302.
- Seagrave, J-C., McDonald, J. D. and Mauderly, J. L.** (2005). In Vitro Versus In Vivo Exposure to Combustion Emissions. *Experimental and Toxicologic Pathology*. **57**: 233-238.
- Shier, D., Butler, J. L. and Lewis, R.** (2004). *Hole's Human Anatomy and Physiology*. **10th** ed. McGraw-Hill, New York, USA.
- Simon, L. M., Robin, E. D. and Theodore, J.** (1981). Differences in Oxygen-Dependent Regulation of Enzymes between Tumor and Normal Cell Systems in Culture. *Journal of Cellular Physiology*. **108**: 393-400.
- Singh, G. and Katyal, S. L.** (1997). Clara Cells and Clara Cell 10 kD Protein (CC10). *American Journal of Respiratory Cell and Molecular Biology*. **17**: 141-143.
- Singh, G. and Katyal, S. L.** (2000). Clara Cell Proteins. *Annals of the New York Academy of Sciences*. **923**: 43-57.
- Singh, J. and Schwartz, D. A.** (2005). Endotoxin and the Lung: Insight into the Host-Environment Interaction. *Journal of Allergy and Clinical Immunology*. **115**(2): 330-333.

- Singh, P. K., Jia, H. P., Wiles, K., Hesselberth, J., Liu, L., Conway, B-A. D., Greenberg, E. P., Valore, E. V., Welsh, M. J., Ganz, T. and Tack, B. F.** (1998). Production of β -defensins by Human Airway Epithelia. *Proceedings of the National Academy of Science, USA*. **95**: 14961-14966.
- Shin, H-J., Park, K-K., Lee, B-H., Moon, C-K. and Lee, M-O.** (2003). Identification of Genes that are Induced after Cadmium Exposure by Suppression Subtractive Hybridization. *Toxicology*. **191**: 121-131.
- Smith, L. L., Lewis, C. P. L., Wyatt, I. and Cohen, G. M.** (1990). The Importance of Epithelial Uptake Systems in Lung Toxicity. *Environmental Health Perspectives*. **85**: 25-30.
- Song, T. H., Yang, J. Y., Jeong, I. K., Park, J. S., Jee, Y. K., Kim, Y. S. and Lee, K. Y.** (2006). Paraquat-Induced Apoptotic Cell Death in Lung Epithelial Cells. *Tuberculosis and Respiratory Disease*. **61**(4): 366-373. (Abstract Only).
- Sopori, M.** (2002). Effects of Cigarette Smoke on the Immune System. *Nature Reviews – Immunology*. **2**: 372-377.
- Sorokin, S. P.** (1968). Reconstruction of Centriole Formation and Ciliogenesis in Mammalian Lungs. *Journal of Cell Science*. **3**: 207-230.
- Steinhorn, R. H., Gordon, J. B. and Tod, M. L.** (2000). Site-Specific Effect of Guanosine 3',5'-Cyclic Monophosphate Phosphodiesterase Inhibition in Isolated Lamb Lungs. *Critical Care Medicine* **28**(2): 490-495.
- Spolarics, Z. and Spitzer, J. J.** (1993). Augmented Glucose use and Pentose Cycle Activity in Hepatic Endothelial Cells after *In Vivo* Endotoxemia. *Hepatology*. **17**(4): 615-620.
- Stevens, A. and Lowe, J.** (2005). *Human Histology*. 3rd ed. Elsevier Mosby, London, UK.
- Stevenson, B. R., Siliciano, J. D., Mooseker, M. S. and Goodnough, D. A.** (1986). Identification of ZO-1: A High Molecular Weight Polypeptide Associated with the Tight Junction (Zonula Occludens) in a Variety of Epithelia. *The Journal of Cell Biology*. **103**: 755-766.
- Stuart, B. O.** (1984). Deposition and Clearance of Inhaled Particles. *Environmental Health Perspectives*. **55**: 369-390.

- Stosiek, P., Kasper, M. and Moll, R.** (1992). Changes in Cytokeratin Expression Accompany Squamous Metaplasia of the Human Respiratory Epithelium. *Virchows Archiv A – Pathological Anatomy and Histopathology*. **421**: 133-141.
- Sun, T-T., Shih, C. and Green, H.** (1979). Keratin Cytoskeletons in Epithelial Cells of Internal Organs. *Proceedings of the National Academy of Science USA*. **76**(6): 2813-2817.
- Suntres, Z. E.** (2002). Role of Antioxidants in Paraquat Toxicity. *Toxicology*. **180**: 65-77.
- Takahashi, T., Takahashi, Y. and Nio, M.** (1994). Remodelling of the Alveolar Structure in the Paraquat Lung of Humans: A Morphometric Study. *Human Pathology*. **25**(7): 702-708.
- Takeyama, K., Jung, B., Shim, J. J., Burgel, P-R., Dao-Pick, T., Ueki, I. F., Protin, U., Kroschel, P. and Nadel, J. A.** (2001). Activation of Epidermal Growth Factor Receptors is Responsible for Mucin Synthesis Induced by Cigarette Smoke. *American Journal of Physiology - Lung Cellular and Molecular Physiology*. **280**: L165-L172.
- Terzaghi, M., Nettesheim, P. and Williams, M. L.** (1978). Repopulation of Denuded Tracheal Grafts with Normal, Preneoplastic, and Neoplastic Epithelial Cell Populations. *Cancer Research*. **38**: 4546-4553.
- Thomas, L. H. and Howard, C. J.** (1974). Effect of Mycoplasma Dispar, Mycoplasma Bovirhinis, Acholeplasma Laidlawii and T Mycoplasmas on Explant Cultures of Bovine Trachea. *Journal of Comparative Pathology*. **84**(2): 193-201.
- Thomassen, D. G., Nettesheim, P.** (1990). *Biology, Toxicology, and Carcinogenesis of Respiratory Epithelium*. Hemisphere Publishing Corporation, London, UK.
- Thompson, A. B., Robbins, R. A., Romberger, D. J., Sisson, J. H., Spurzem J. R., Teschler, H. and Rennard, S. I.** (1995). Immunological Functions of the Pulmonary Epithelium. *European Respiratory Journal*. **8**: 127-149.
- Trivier, J. M., Ommery, N. and Lhermitte, M.** (1997). Antioxidant Defence Capacity Modulation of Two Human Cell Lines by Amiodarone and Desethylamiodarone. *Toxicology in Vitro*. **11**: 209-216.
- Trautman, A., Krüger, K., Akdis, M., Müller-Wening, D., Akkaya, A., Bröcker, E-B., Blasser, K. and Akdis, C. A.** (2005). Apoptosis and Loss of Adhesion of Bronchial Epithelial Cells in Asthma. *International Archives of Allergy and Immunology*. **138**: 142–150.

- Tronde, A., Nordén, B., Marchner, H., Wendel, A-K., Lennernäs, H. and Bengtsson, U. H.** (2003). Pulmonary Absorption Rate and Bioavailability of Drugs In Vivo in Rats: Structure-Absorption Relationships and Physicochemical Profiling of Inhaled Drugs. *Journal of Pharmaceutical Sciences*. **92**(6): 1216-1233.
- Tosi, M. F.** (2005). Innate Immune Responses to Infection. *Journal of Allergy and Clinical Immunology*. **116**(2): 241-249.
- Toward, T. J. and Broadley, K. J.** (2002). Goblet Cell Hyperplasia, Airway Function, and Leukocyte Infiltration after Chronic Lipopolysaccharide Exposure in Conscious Guinea Pigs: Effects of Rolipram and Dexamethasone. *The Journal of Pharmacology and Experimental Therapeutics*. **302**(2): 814-821.
- Tulić, M. K., Wale, J. L., Holt, P. G. and Sly, P. D.** (2000). Modification of the Inflammatory Response to Allergen Challenge after Exposure to Bacterial Lipopolysaccharide. *American Journal of Respiratory Cellular and Molecular Biology*. **22**:604-612.
- Turksen, K. and Troy, T-C.** (2004). Barriers Built on Claudins. *Journal of Cell Science*. **117**: 2435-2447.
- Van der Toorn, M., Slebos, D-J., de Bruin, H. G. Leuvenink, H. G., Bakker, S. J. L., Gans, R. O. B., Koëter, G. H., van Oosterhout, A. J. M. and Kauffman, H. F.** (2007). Cigarette Smoke-Induced Blockade of the Mitochondrial Respiratory Chain Switches Lung Epithelial Cell Apoptosis into Necrosis. *American Journal of Physiology - Lung Cellular and Molecular Physiology*. **292**: L1211-L1218.
- Voynow, J. A., Fischer, B. M., Roberts, B. C. and Proia, A. D.** (2005). Basal-like Cells Constitute the Proliferating Cell Population in Cystic Fibrosis Airways. *American Journal of Respiratory and Critical Care Medicine*. **172**:1013-1018.
- Waalkes, M. P.** (2000). Cadmium Carcinogenesis in Review. *Journal of Inorganic Biochemistry*. **79**: 241-244.
- Waalkes, M. P.** (2003). Cadmium Carcinogenesis. *Mutation Research*. **533**: 107-120.
- Wagner, M. Hermanns, I., Bittinger, F. and Kirkpatrick, C. J.** (1999). Induction of Stress Proteins in Human Endothelial Cells by Heavy Metal Ions and Heat Shock. *American Journal of Physiology - Lung Cellular and Molecular Physiology*. **277**: 1026-1033.

- Wallace, P., Kennedy, J. R. and Mendicino, J.** (1994). Transdifferentiation of Outgrowth Cells and Cultured Epithelial Cells from Swine Trachea. . *In Vitro Cellular and Developmental Biology - Animal*. **30**: 168-180.
- Wan, H., Winton, H. L., Soeller, C., Stewart, G. A., Thompson, P. J., Gruenert, D. C., Cannell, M. B., Garrod, D. R. and Robinson, C.** (2000). Tight Junction Properties of the Immortalized Human Bronchial Epithelial Cell Lines Calu-3 and 16HBE14o-. Tight junction properties of the immortalized human bronchial epithelial cell lines Calu-3 and 16HBE14o. *European Respiratory Journal*. **15**: 1058–1068.
- Wang, B. Y., Gil, J., Kaufman, D., Gan, L., Kohtz, S. D. and Burstein, D. E.** (2002). p63 in Pulmonary Epithelium, Pulmonary Squamous Neoplasms, and Other Pulmonary Tumors. *Human Pathology*. **33**(9): 921-926.
- Wang, G-Y., Hirai, K-I. and Shimada, H.** (1992). Mitochondrial Breakage Induced by the Herbicide Paraquat in Cultured Human Lung Cells. *Journal of Electron Microscopy*. **41**:181-184.
- Wang, Z. and Zhang, Q.** (2004). Transport of Proteins and Peptides Across Human Cultured Alveolar A549 Cell Monolayer. *International Journal of Pharmaceutics*. **269**:451-456.
- Waring, M. J.** (2009). Defining Optimum Lipophilicity and Molecular Weight Ranges for Drug Candidates – Molecular Weight Dependent Lower logD Limits Based on Permeability. *Bioorganic & Medicinal Chemistry Letters*. **19**: 2844-2851.
- Warner, J. A. and Kroegel, C.** (1994). Pulmonary Immune Cells in Health and Disease: Mast Cells and Basophils. *European Respiratory Journal*. **7**:1326-1341.
- Watson, T. M., Reynolds, S. D., Mango, G. W., Boe, I-M., Lund, J. and Stripp, B. R.** (2001). Altered Lung Gene Expression in CCSP-null Mice Suggests Immunoregulatory Roles for Clara Cells. *American Journal of Physiology. Lung Cellular and Molecular Physiology*. **281**:L1523-L1530.
- Welsh, M. J.** (1985). Ion Transport by Primary Cultures of Canine Tracheal Epithelium: Methodology, Morphology, and Electrophysiology. *The Journal of Membrane Biology*. **88**: 149-163.
- West, J.** (2003). *Pulmonary Pathophysiology: The Essentials*. **6th ed.** Lippincott Williams & Wilkins, Baltimore and Philadelphia, USA.

Westmoreland, C., Walker, T., Matthews, J. and Murdock, J. (1999). Preliminary Investigations into the Use of a Human Bronchial Cell Line (16HBE14o-) to Screen for Respiratory Toxins In Vitro. *Toxicology in Vitro*. **13**: 761-764.

White, S. R. and Dorscheid, D. R. (2002) Corticosteroid-Induced Apoptosis of Airway Epithelium: A Potential Mechanism for Chronic Airway Epithelial Damage in Asthma. *Chest*. **122**: 278-284.

WHO. (2000) http://www.euro.who.int/document/aig/6_3cadmium.pdf

WHO. (2009) <http://www.who.int/mediacentre/factsheets/fs315/en/index.html>

WHO. (2010a) http://www.who.int/tobacco/health_priority/en/index.html

WHO. (2010b) <http://www.who.int/tobacco/en/atlas9.pdf>;

Widdicombe, J. H. (2002). Regulation of the Depth and Composition of Airway Surface Liquid. *Journal of Anatomy*. **201**:313-318.

Willey, J. C., Grafstrom, R. C., Moser Jr., C. E., Ozanne, C., Sundqvist, K. and Harris, C. C. (1987). Biochemical and Morphological Effects of Cigarette Smoke Condensate and its Fractions on Normal Human Bronchial Epithelial Cells In Vitro. *Cancer Research*. **47**: 2045-2049.

Wong, H. R. and Shanley, T. P. (2001). *Molecular Biology of Acute Lung Injury*. Kluwer Academic Publishers, London, UK.

Wright, J. R. (2005). Immunoregulatory Functions of Surfactant Proteins. *Nature Reviews: Immunology*. **5**: 58-58.

Wu, R., Sato, G. H. and Whitcutt, M. J. (1986). Developing Differentiated Epithelial Cell Cultures: Airway Epithelial Cells. *Fundamental and Applied Toxicology*. **6**: 580-590.

Wyllie, A. H., Kerr, J. F. R. and Currie, A. R. (1980). Cell Death: The Significance of Apoptosis. *International Review of Cytology*. **68**: 251-306.

Xu, Y., Kobayashi, T., Cui, X., Ohta, K., Kabata, C. and Tashiro, K. (2004). Lung Volumes and Alveolar Expansion Pattern in Immature Rabbits Treated with Serum-Diluted Surfactant. *Journal of Applied Physiology*. **97**: 1408-1413.

- Yamane, K. and Kawata, M.** (1999). Catecholamine Release from Isolated Guinea Pig Lungs during Sympathetic Stimulation with varied Ventilation and Perfusion. *Experimental Animals*. **48**(2): 65-72.
- Yamaya, M., Finkbeiner, W. E., Chun, S. Y. and Widdicombe, J. H.** (1992). Differentiated Structure and Function of Cultures from Human Tracheal Epithelium. *American Journal of Physiology - Lung Cellular and Molecular Physiology*. **6**: L713-L724.
- Yang, A., Kaghad, M., Wang, Y., Gillette, E., Fleming, M. D., Dötsch, V., Andrews, N. C., Caput, D. and McKeon, F.** (1998). p63, a p53 Homolog at 3q27-29, Encodes Multiple Products with Transactivating, Death-Inducing, and Dominant-Negative Activities. *Molecular Cell*. **2**: 305-316.
- Yang, A., Schweitzer, R., Sun, D., Kaghad, M., Walker, N., Bronsonk, R. T., Tabin, C., Sharpe, A., Caput, D., Crum, C. and McKeon, F.** (1999). p63 is Essential for Regenerative Proliferation in Limb, Craniofacial and Epithelial Development. *Nature*. **398**: 714-718.
- Young, B. and Heath, J. W.** (2000). *Wheater's Functional Histology: a Text and Colour Atlas*. 4th ed. Churchill Livingstone, London, UK.
- Zalups, R. K. and Ahmad, S.** (2003). Molecular Handling of Cadmium in Transporting Epithelia. *Toxicology and Applied Pharmacology*. **186**: 163-188.
- Zugibe, F. T.** (1970). Positive Periodic Acid-Schiff Staining of Acid Mucopolysaccharides. *Histochemical Journal*. **2**: 191-197.

